APPLICATION OF FUZZY LOGIC BASED COASTAL VULNERABILITY MODEL IN COASTAL CULTURAL HERITAGE SITES IN TURKEY

A THESIS SUBMITTED TO
THE GRADUATE SCHOOL OF NATURAL AND APPLIED SCIENCES
OF
MIDDLE EAST TECHNICAL UNIVERSITY

BY

AKDENİZ İNCE

IN PARTIAL FULFILLMENT OF THE REQUIREMENTS
FOR
THE DEGREE OF MASTER OF SCIENCE
IN
CIVIL ENGINEERING

DECEMBER 2024

Approval of the thesis: Civil Engineering Department

APPLICATION OF FUZZY LOGIC BASED COASTAL VULNERABILITY MODEL IN COASTAL CULTURAL HERITAGE SITES IN TURKEY

submitted by **AKDENİZ İNCE** in partial fulfillment of the requirements for the degree of **Master of Science** i**n Civil Engineering, Middle East Technical University** by,

Prof. Dr. Naci Emre Altun
Dean, **Graduate School of Natural and Applied Sciences** _____

Prof. Dr. Erdem Canbay
Head of the Department, **Civil Engineering** _____

Assist. Prof. Dr. Gülizar Özyurt Tarakcıoğlu
Supervisor, **Civil Engineering, METU** _____

Prof. Dr. Ayşen Ergin
Co-Supervisor, **Civil Engineering, METU** _____

Examining Committee Members:

Prof. Dr. Mehmet Lütfi Süzen
Geological Engineering, METU _____

Assist. Prof. Dr. Gülizar Özyurt Tarakcıoğlu
Civil Engineering, METU _____

Assist. Prof. Dr. Cüneyt Baykal
Civil Engineering, METU _____

Assist. Prof. Dr. Hasan Gökhan Güler
Civil Engineering, METU _____

Assist. Prof. Dr. Doğan Kısacık
Civil Engineering, İYTE _____

Date: 02.12.2024

I hereby declare that all information in this document has been obtained and presented in accordance with academic rules and ethical conduct. I also declare that, as required by these rules and conduct, I have fully cited and referenced all material and results that are not original to this work.

Name Last name : Akdeniz İnce

Signature :

ABSTRACT

APPLICATION OF FUZZY LOGIC BASED COASTAL VULNERABILITY MODEL IN COASTAL CULTURAL HERITAGE SITES IN TURKEY

İnce, Akdeniz
Master of Science, Civil Engineering
Supervisor: Assist. Prof. Dr. Gülizar Özyurt Tarakcıoğlu
Co-Supervisor: Prof. Dr. Ayşen Ergin

December 2024, 244 pages

Coastal vulnerability assessment is a key factor in achieving the sustainable development of coastal areas and helps decision-makers prepare or adapt their coastal management plans. These plans are essential for countries such as Türkiye, which has 8,333 km of shoreline length, along which many coastal cultural heritage areas and natural conservation zones are located. These areas are very valuable for Türkiye in economic and social terms; however, they are also susceptible to sea-level rise. Therefore, in this study, the Fuzzy Coastal Vulnerability Assessment Model (FCVAM) was utilized to determine the Coastal Vulnerability Index (CVI) along the shoreline projection of 1,176 coastal cultural heritage sites and 1,171 natural conservation zones, focusing on coastal erosion, inundation, and coastal flooding due to storm surge, by considering pathways defined in the IPCC 6th Assessment Report (2023). The results of all scenarios are provided, whereas, for the SSP2-4.5 and SSP5-8.5 scenarios, an in-depth comparison and discussion are presented, highlighting the key factors that drive changes in vulnerability for both cultural heritage sites and natural protection zones. In the case of SSP2-4.5, when global FCVAM limits are considered, the most vulnerable class observed was "Moderate," while the most common one was "Low" vulnerability. On the other hand, localization

of results by redefining class limits concerning Natural Jenks Breaks shows that 11.6% of natural conservation zones and 16.1% of cultural heritage sites in Türkiye are highly vulnerable to the impacts of sea-level rise relative to all studied shorelines. The model was then run for SSP5-8.5 conditions to observe how impact scores and CVI would be affected. The highest number of class changes were observed in the erosion module, while the inundation module demonstrated the most severe vulnerability class shifts. However, despite increases in CVI and impact scores, the most common and most vulnerable class—other than one highly vulnerable cultural heritage site—did not change. Regarding localized results, 18.4% of natural conservation zones and 20.7% of cultural heritage sites are highly vulnerable. On a regional scale, for both pathways, since most of the natural conservation zones and cultural heritage sites are located in the Aegean Region, the highest number of least and most vulnerable shores are within this region.

Keywords: Coastal Vulnerability Assessment, Fuzzy Logic, Sea Level Rise, Coastal Cultural Heritage Sites, Natural Conservation Zones.

ÖZ

TÜRKİYEDEKİ KIYI KÜLTÜREL MİRAS ALANLARINDA BULANIK MANTIK TABANLI KIYI KIRILGANLIK MODELİNİN UYGULANMASI

İnce, Akdeniz
Yüksek Lisans, İnşaat Mühendisliği
Tez Yöneticisi: Assist. Prof. Dr. Gülizar Özyurt Tarakcıoğlu
Ortak Tez Yöneticisi: Prof. Dr. Ayşen Ergin

Aralık 2024, 244 sayfa

Kıyı kırılganlığının değerlendirilmesi, kıyı alanlarının sürdürülebilir kalkınmasını sağlamak için önemli bir faktördür ve karar alıcıların kıyı yönetim planlarını hazırlamaları veya uyarlamaları için yardımcı olur. Bu planlar, Türkiye gibi, 8.333 km kıyı uzunluğuna sahip olan ve bu kıyılarda birçok kıyı kültürel miras alanı ve doğal koruma bölgesi bulunan ülkeler için özellikle önemlidir, çünkü bu alanlar Türkiye için ekonomik ve sosyal açıdan çok değerli olmakla birlikte, deniz seviyesi yükselmesine karşı kırılgandırlar. Bu nedenle, bu çalışmada, IPCC 6. Değerlendirme Raporu'nda (2023) tanımlanan yollar dikkate alınarak, kıyı erozyonu, kalıcı taşkın ve fırtına kabarması nedeniyle oluşan su baskını üzerinde odaklanarak, 1.176 kıyı kültürel miras alanı ve 1.171 doğal koruma bölgesinin kıyı kırılganlık indeksi (KKİ) belirlemek için Bulanık Mantık Kıyı Kırılganlık Modeli (FCVAM) kullanılmıştır. Böylece, tüm senaryolara ait sonuçlar hesaplanmış olup, SSP2-4.5 ve SSP5-8.5 senaryoları için derinlemesine bir karşılaştırma ve tartışma sunulmuş, her iki senaryo için kültürel miras alanları ve doğal koruma bölgelerindeki kırılganlık değişikliklerini tetikleyen anahtar faktörler vurgulanmıştır. SSP2-4.5 senaryosunda, küresel FCVAM sınırları göz önünde bulundurulduğunda, en kırılgan sınıf "Orta"

olarak gözlemlenirken, en yaygın sınıf "Düşük" kırılganlık olmuştur. Öte yandan, sonuçların Doğal Jenks Kırılma sınırlarına göre yeniden sınıflandırılması, Türkiye'deki doğal koruma alanlarının %11.6'sı ve kültürel miras alanlarının %16.1'inin deniz seviyesi yükselmesinin etkilerine karşı yüksek kırılganlığa sahip olduğunu göstermektedir. Model, ardından SSP5-8.5 koşulları için çalıştırılmış ve etki puanları ve KKİ'nın nasıl etkileneceği gözlemlenmiştir. En fazla sınıf değişikliği erozyon modülünde gözlemlenirken, kalıcı taşkın modülü en şiddetli kırılganlık sınıfı değişimlerini göstermiştir. Ancak, KKİ ve etki puanlarındaki artışlara rağmen, en yaygın ve en kırılgan sınıf—bir yüksek kırılganlık kültürel miras alanı hariç—değişmemiştir. Lokalize edilmiş sonuçlar incelendiğinde, doğal koruma alanlarının %18.4'ü ve kültürel miras alanlarının %20.7'si yüksek derecede kırılgandır. Bölgesel ölçekte, her iki yol için de, çoğu doğal koruma alanı ve kültürel miras alanı Ege Bölgesi'nde yer aldığı için, en az ve en çok kırılgan kıyıların en yüksek sayıda olduğu bölge bu bölgedir.

Anahtar Kelimeler: Kıyı Kırılganlık Değerlendirmesi, Bulanık Mantık, Deniz Seviyesi Yükselmesi, Kıyı Kültürel Miras Alanları, Kıyı Doğal Koruma Alanları

To All Shorelines That Have Been Assessed and Those Yet to Be Assessed,

ACKNOWLEDGMENTS

I would like to express my deepest gratitude to my supervisor, Assist. Prof. Dr. Gülizar Özyurt Tarakcıoğlu and my co-supervisor, Prof. Dr. Ayşen Ergin, for their invaluable guidance, advice, constructive criticism, encouragement, and insightful feedback throughout the research process. Their expertise and continuous support have been essential to completing this work.

Special thanks are due to Mr. Arif Çağatay Uysal and Ms. İremnaz Kösem for their technical assistance, as well as to the K5 – Coastal and Ocean Research Laboratory for providing the resources and environment necessary for this study.

I would also like to extend my heartfelt gratitude to my family: to my parents for their unwavering love, patience, and belief in me, and to my brother for his constant support and encouragement. Without their support, this journey would not have been possible.

Finally, I acknowledge the funding support from the Scientific and Technological Research Council of Turkey (TÜBİTAK) under project number TUBİTAK 122M613.

TABLE OF CONTENTS

ABSTRACT v

ÖZ vii

ACKNOWLEDGMENTS x

TABLE OF CONTENTS xi

LIST OF TABLES xiv

LIST OF FIGURES xix

LIST OF ABBREVIATIONS xxxi

1 INTRODUCTION 1

1.1 Objective of the Study 2

1.2 Outline of the Thesis 3

2 LITERATURE REVIEW 5

2.1 Global Climate Change 6

2.2 Coastal Vulnerability 10

2.3 Coastal Vulnerability Index and Global Assessments 11

2.4 CVI Applications Along Turkish Coasts 16

2.5 Assessment Approaches and Socioeconomic Data Limitations 18

3 METHODOLOGY 21

3.1 Fuzzy Coastal Vulnerability Assessment Model 21

3.1.1 Parameter Changes 27

3.1.2 MATLAB to Python Conversion 29

3.2 Example Study Case 32

3.3 Jenks Natural Breaks 37

4 DATASETS & PRE-PROCESSING 39
4.1 Studied Shorelines 39
4.2 Model Input Parameters 40
4.2.1 Rate of Sea Level Rise 40
4.2.2 Geomorphology 43
4.2.3 Beach Slope 47
4.2.4 Annual Mean Wave Height 49
4.2.5 Sediment Budget 51
4.2.6 Extreme Sea Level 52
4.2.7 Tidal Range 54
4.2.8 River Flow Regulation 55
4.2.9 Engineered Frontage and Coastal Protection Structure 59
4.2.10 Natural Protection Degradation 62
5 RESULTS & DISCUSSIONS 65
5.1 FCVAM Application Results 65
5.2 Natural Conservation Zones 66
5.2.1 Human Impact Scores 66
5.2.2 AR6 SSP2 – 4.5 Physical Impact Scores 69
5.2.3 AR6 SSP5 – 8.5 Physical Impact Scores 86
5.3 Coastal Cultural Heritage Sites 107
5.3.1 Human Impact Scores 107
5.3.2 AR6 SSP2-4.5 Physical Impact Scores 110
5.3.3 AR6 SSP5-8.5 Physical Impact Scores 127
5.4 Discussions 147

5.4.1 Impact Score Distribution Behavior 147
5.4.2 Vulnerability Distribution of SSP1-1.9, SSP1-2.6, SSP3-7.0.....158
5.4.3 Result Comparison of FCVAM with Other Assessment 159
6 CONCLUSION.....163
REFERENCES 169
7 APPENDICES 177
A. Natural Conservation Zones SSP1-1.9.....177
B. Natural Conservation Zones SSP1-2.6.....188
C. Natural Conservation Zones SSP3-7.0.....199
D. Cultural Heritage Sites SSP1-1.9.....210
E. Cultural Heritage Sites SSP1-2.6.....221
F. Cultural Heritage Sites SSP3-7.0.....232
G. Cultural Heritage Site SSP2-4.5 & SSP5-8.5 Scatter Diagrams.....243

LIST OF TABLES

TABLES

Table 2.1 Long-Term Potential Global Average Temperature Increases.....7
Table 2.2 Ranking of Coastal Vulnerability Index (Thieler et al.,2000).....13
Table 2.3 Barcelona Shoreline CVI Distribution (Koroglu et al., 2019) 15
Table 3.1 Input Parameters and Affected Vulnerabilities of Compact FCVAM 26
Table 3.2 CVI Classes and Class Limits 26
Table 3.3 Parameter Weight Comparison 27
Table 3.4 FCVAM Inputs of Current and High Usage Scenario 33
Table 3.5 Results of Current and High Usage Scenario.....36
Table 4.1 SSP1-1.9 RSLR Input Distribution Over Shoreline Types 41
Table 4.2 SSP1-2.6 RSLR Input Distribution Over Shoreline Types 41
Table 4.3 SSP2-4.5 RSLR Input Distribution Over Shoreline Types 42
Table 4.4 SSP3-7.0 RSLR Input Distribution Over Shoreline Types 42
Table 4.5 SSP5-8.5 RSLR Input Distribution Over Shoreline Types 43
Table 4.6 Geomorphology Class Definitions 43
Table 4.7 Coastal Type 0-80K Geomorphology Group Definition (Emodnet, 2021) 44
Table 4.8 MEDCD Geomorphology Group Definition (Wolff et al., 2018).....45
Table 4.9 EEA Land Use Geomorphology Group Definition (EEA, 2021) 45
Table 4.10 Mao et al. (2022). Geomorphology Group Definition 46
Table 4.11 Number of Locations within Geomorphology Classes 46
Table 4.12 Number of Locations within Beach Slope Classes 49
Table 4.13 Number of Locations within Wave Climate Classes.....50
Table 4.14 Number of Locations within Sediment Budget Classes.....52
Table 4.15 Number of Locations within SSP2-4.5 Extreme Sea Level Classes 53
Table 4.16 Number of Locations within SSP5-8.5 Extreme Sea Level Classes 54
Table 4.17 Number of Locations within Tidal Range Classes.....55
Table 4.18 River Flow Regulation Result Indicator (Nillson et al., 2005) 56

Table 4.19 Number of Locations within River Flow Regulation Classes 58
Table 4.20 Engineering Frontage Indicator Land Usages (EEA, 2021) 60
Table 4.21 Coastal Protection Structures Indicator Land Usages (EEA, 2021) 60
Table 4.22 Number of Locations within Engineering Frontage Classes 61
Table 4.23 Number of Locations within Coastal Protection Structures Classes 62
Table 4.24 Natural Protection Degradation Indicator Land Usages (EEA, 2020).. 64
Table 4.25 Number of Locations within Natural Protection Degradation Classes. 64
Table 5.1 Regional Natural Conservation Zone Erosion Human Impact Scores.... 67
Table 5.2 Regional Natural Conservation Zone Inundation Human Impact Scores68
Table 5.3 Regional Natural Conservation Zone Storm Surge Human Impact Scores 69
Table 5.4 Regional SSP2-4.5 Natural Conservation Zone ErosionPP Scores 70
Table 5.5 Regional SSP2-4.5 Natural Conservation Zone Erosion Scores 71
Table 5.6 SSP2-4.5 Natural Conservation Zone Erosion Jenks & FCVAM Limits73
Table 5.7 Regional SSP2-4.5 Natural Conservation Zone InundationPP Scores ... 74
Table 5.8 Regional SSP2-4.5 Natural Conservation Zone Inundation Scores..... 75
Table 5.9 SSP2-4.5 Natural Conservation Zone Inundation Jenks & FCVAM Limits 77
Table 5.10 Regional SSP2-4.5 Natural Conservation Zone Storm Surge Scores... 79
Table 5.11 Regional SSP2-4.5 Natural Conservation Zone Storm Surge Scores... 80
Table 5.12 SSP2-4.5 Natural Conservation Zone Surge Jenks & FCVAM Limits 81
Table 5.13 SSP2-4.5 Natural Conservation Zone Impact & CVI Scores 83
Table 5.14 SSP2-4.5 Natural Conservation Zone Impact & CVI Scores 83
Table 5.15 SSP2-4.5 Natural Conservation Zone CVI Jenks & FCVAM Limits .. 85
Table 5.16 Regional SSP5-8.5 Natural Conservation Zone ErosionPP Scores 86
Table 5.17 SSP5-8.5 & SSP2-4.5 Natural Conservation Zone ErosionPP Comparison 87
Table 5.18 Regional SSP5-8.5 Natural Conservation Zone Erosion Scores 88
Table 5.19 SSP5-8.5 & SSP2-4.5 Erosion Natural Conservation Zone Comparison 88

Table 5.20 SSP5-8.5 Natural Conservation Zone Erosion Jenks & FCVAM Limits 90
Table 5.21 Regional SSP5-8.5 Natural Conservation Zone InundationPP Scores.. 92
Table 5.22 SSP5-8.5 & SSP2-4.5 Natural Conservation Zone InundationPP Comparison..... 93
Table 5.23 Regional SSP5-8.5 Natural Conservation Zone Inundation Scores 94
Table 5.24 SSP5-8.5 & SSP2-4.5 Natural Conservation Zone Inundation Comparison..... 94
Table 5.25 SSP5-8.5 Natural Conservation Zone Inundation Jenks & FCVAM Limits..... 96
Table 5.26 Regional SSP5-8.5 Natural Conservation Zone Storm SurgePP Scores 98
Table 5.27 SSP5-8.5 & SSP2-4.5 Storm SurgePP Comparison..... 98
Table 5.28 Regional SSP5-8.5 Natural Conservation Zone Storm Surge Scores ... 99
Table 5.29 SSP5-8.5 & SSP2-4.5 Storm Surge Comparison 100
Table 5.30 SSP5-8.5 Natural Conservation Zone Surge Jenks & FCVAM Limits 101
Table 5.31 Regional SSP5-8.5 Natural Conservation Zone CVI Scores 103
Table 5.32 SSP5-8.5 & SSP2-4.5 CVI Comparison 103
Table 5.33 SSP5-8.5 Natural Conservation Zone Impact & CVI Scores..... 104
Table 5.34 SSP5-8.5 & SSP2-4.5 Impact Score Comparison 104
Table 5.35 SSP5-8.5 Natural Conservation Zone CVI Jenks & FCVAM Limits. 105
Table 5.36 Regional Cultural Heritage Site Erosion Human Impact Scores 108
Table 5.37 Regional Cultural Heritage Site Inundation Human Impact Scores.... 109
Table 5.38 Regional Cultural Heritage Site Surge Human Impact Scores..... 110
Table 5.39 Regional SSP2-4.5 Cultural Heritage Site ErosionPP Scores..... 111
Table 5.40 Regional SSP2-4.5 Cultural Heritage Site Erosion Scores 112
Table 5.41 SSP2-4.5 Cultural Heritage Site Erosion Jenks & FCVAM Limits.... 114
Table 5.42 Regional SSP2-4.5 Cultural Heritage Site InundationPP Scores..... 116
Table 5.43 Regional SSP2-4.5 Cultural Heritage Site Inundation Scores 117

Table 5.44 SSP2-4.5 Cultural Heritage Site Inundation Jenks & FCVAM Limits 118
Table 5.45 Regional SSP2-4.5 Cultural Heritage Site Storm Surge Scores 120
Table 5.46 Regional SSP2-4.5 Cultural Heritage Site Storm Surge Scores 121
Table 5.47 SSP2-4.5 Cultural Heritage Site Surge Jenks & FCVAM Limits 122
Table 5.48 Regional SSP2-4.5 Cultural Heritage Site CVI Scores 124
Table 5.49 SSP2-4.5 Cultural Heritage Site Impact & CVI Scores..... 125
Table 5.50 SSP2-4.5 Cultural Heritage Site CVI Jenks & FCVAM Limits..... 126
Table 5.51 Regional SSP5-8.5 Cultural Heritage Site ErosionPP Scores 128
Table 5.52 SSP5-8.5 & SSP2-4.5 Cultural Heritage Site ErosionPP Comparison128
Table 5.53 Regional SSP5-8.5 Cultural Heritage Site Erosion Scores..... 129
Table 5.54 SSP5-8.5 & SSP2-4.5 Cultural Heritage Site Erosion Comparison ... 130
Table 5.55 SSP5-8.5 Cultural Heritage Site Erosion Jenks & FCVAM Limits ... 131
Table 5.56 Regional SSP5-8.5 Cultural Heritage Site InundationPP Scores 133
Table 5.57 SSP5-8.5 & SSP2-4.5 Cultural Heritage Site InundationPP Comparison 133
Table 5.58 Regional SSP5-8.5 Cultural Heritage Site Inundation Scores..... 134
Table 5.59 SSP5-8.5 & SSP2-4.5 Cultural Heritage Site Inundation Comparison 135
Table 5.60 SSP5-8.5 Cultural Heritage Site Inundation Jenks & FCVAM Limits 137
Table 5.61 Regional SSP5-8.5 Cultural Heritage Site Storm SurgePP Scores..... 138
Table 5.62 SSP5-8.5 & SSP2-4.5 Cultural Heritage Site Storm SurgePP Comparison 139
Table 5.63 Regional SSP5-8.5 Cultural Heritage Site Storm Surge Scores 140
Table 5.64 SSP5-8.5 & SSP2-4.5 Cultural Heritage Site Storm Surge Comparison 140
Table 5.65 SSP5-8.5 Cultural Heritage Site Surge Jenks & FCVAM Limits 142
Table 5.66 Regional SSP5-8.5 Cultural Heritage Site CVI Scores 143
Table 5.67 SSP5-8.5 & SSP2-4.5 Cultural Heritage Site CVI Comparison..... 144

Table 5.68 SSP5-8.5 Cultural Heritage Site Impact & CVI Scores 144
Table 5.69 SSP5-8.5 & SSP2-4.5 Cultural Heritage Site Impact Score Comparison 145
Table 5.70 SSP5-8.5 Cultural Heritage Site CVI Jenks & FCVAM Limits 146
Table 5.71 SSP2-4.5 Erosion Impact Score Distributions 149
Table 5.72 SSP5-8.5 Erosion Impact Score Distributions 150
Table 5.73 SSP2-4.5 Inundation Impact Score Distributions 152
Table 5.74 SSP5-8.5 Inundation Impact Score Distributions 153
Table 5.75 SSP2-4.5 Storm Surge Impact Score Distributions 155
Table 5.76 SSP5-8.5 Storm Surge Impact Score Distributions 155
Table 5.77 SSP2-4.5 CVI Score Distributions 157
Table 5.78 SSP5-8.5 CVI Score Distributions 158
Table 5.79 Cultural Heritage Site CVI Results of all Pathways 159
Table 7.1 SSP1-1.9 Natural Conservation Zone Impact & CVI Scores 187
Table 7.2 SSP1-2.6 Natural Conservation Zone Impact & CVI Scores 198
Table 7.3 SSP3-7.0 Natural Conservation Zone Impact & CVI Scores 209
Table 7.4 SSP1-1.9 Cultural Heritage Site Impact & CVI Scores 220
Table 7.5 SSP1-2.6 Cultural Heritage Site Impact & CVI Scores 231
Table 7.6 SSP3-7.0 Cultural Heritage Site Impact & CVI Scores 242

LIST OF FIGURES

FIGURES

Figure 2.1. Sea Surface Level Increase Between 1993 to 2019 (NASA, 2023, n.p.) 8
Figure 2.2. GMSL Scenario Comparisons (NASA, 2023, n.p.) 9
Figure 2.3. Bodrum Peninsula CVI Distribution (Kuleli & Bayazıt, 2023, p. 149) 17
Figure 3.1. RSLR Global Value as 5 Center Points (Ozyurt, 2010, p. 135) 22
Figure 3.2. RSLR Membership Functions 22
Figure 3.3. Example Rule Set 23
Figure 3.4. Example Fuzzy Inference System 23
Figure 3.5. Inundation Human Impact Membership Function 24
Figure 3.6. Inundation Human Impact Distribution Calculation 25
Figure 3.7. First Area Impact Score Comparison with Respect to Weights 28
Figure 3.8. Second Area Impact Score Comparison concerning Weights 29
Figure 3.9. Section of Fis File of Inundation Human Impact System 30
Figure 3.10. Control Surface of Inundation Human Impact 31
Figure 3.11. Shoreline to be Studied Highlighted as Bold Blue Line 33
Figure 3.12. Current Storm Surge Human Impact Score Distribution Calculation 34
Figure 3.13. High-Use Storm Surge Human Impact Score Distribution Calculation 35
Figure 3.14. Results of Current and High Usage Scenario 36
Figure 4.1. SSP1-1.9 RSLR Input Distribution Over Shorelines 41
Figure 4.2. SSP1-2.6 RSLR Input Distribution Over Shorelines 41
Figure 4.3. SSP2-4.5 RSLR Input Distribution Over Shorelines 42
Figure 4.4. SSP3-7.0 RSLR Input Distribution Over Shorelines 42
Figure 4.5. SSP5-8.5 RSLR Input Distribution Over Shorelines 43
Figure 4.6. Geomorphology Class Distribution Map 46
Figure 4.7. DEM with First Methodology 48
Figure 4.8. DEM with Second Methodology 48
Figure 4.9. Beach Slope Class Distribution Map 49

Figure 4.10. Wave Climate Class Distribution Map 50
Figure 4.11. Study Shorelines within Dardanelles 51
Figure 4.12. Sediment Budget Class Distribution Map 52
Figure 4.13. SSP2-4.5 Extreme Sea Level Class Distribution Map 53
Figure 4.14. SSP5-8.5 Extreme Sea Level Class Distribution Map 54
Figure 4.15. Tidal Range Class Distribution Map 55
Figure 4.16. Total River Discharge Data Imported to GIS as 2D Matrix 57
Figure 4.17. River Flow Regulation Class Distribution Map 58
Figure 4.18. Engineering Frontage Class Distribution Map 61
Figure 4.19. Coastal Protection Structures Class Distribution Map 61
Figure 4.20. Groins within Studied Shoreline 62
Figure 4.21. Natural Protection Degradation Class Distribution Map 64
Figure 5.1. Natural Conservation Zone Erosion Human Impact Distribution 66
Figure 5.2. Natural Conservation Zone Erosion Inundation Impact Distribution ... 67
Figure 5.3. Natural Conservation Zone Storm Surge Human Impact Distribution . 68
Figure 5.4. SSP2-4.5 Natural Conservation Zone ErosionPP Distribution 70
Figure 5.5. SSP2-4.5 Natural Conservation Zone Erosion Distribution 71
Figure 5.6. SSP2-4.5 Natural Conservation Zone Erosion (a) Physical Impact Score (b) Human Impact Score 72
Figure 5.7. SSP2-4.5 Natural Conservation Zone Erosion Jenks Distribution 72
Figure 5.8. SSP2-4.5 Natural Conservation Zone Erosion (a) Jenks (b) FCVAM Histograms 73
Figure 5.9. SSP2-4.5 Natural Conservation Zone InundationPP Distribution 74
Figure 5.10. SSP2-4.5 Natural Conservation Zone Inundation Distribution 75
Figure 5.11. SSP2-4.5 Natural Conservation Zone Inundation (a) Physical Impact Score (b) Human Impact Score 76
Figure 5.12. SSP2-4.5 Natural Conservation Zone Inundation Jenks Distribution. 77
Figure 5.13. SSP2-4.5 Natural Conservation Zone Inundation (a) Jenks (b) FCVAM Histograms 78
Figure 5.14. SSP2-4.5 Natural Conservation Zone Storm SurgePP Distribution ... 78

Figure 5.15. SSP2-4.5 Natural Conservation Zone Storm Surge Distribution 79
Figure 5.16. SSP2-4.5 Natural Conservation Zone Storm Surge (a) Physical Impact Score (b) Human Impact Score 80
Figure 5.17. SSP2-4.5 Natural Conservation Zone Storm Surge Jenks Distribution 81
Figure 5.18. SSP2-4.5 Natural Conservation Zone Storm Surge (a) Jenks (b) FCVAM Histograms 82
Figure 5.19. SSP2-4.5 Natural Conservation Zone CVI Distribution 82
Figure 5.20. SSP2-4.5 Natural Conservation Zone CVI Jenks Distribution 84
Figure 5.21. SSP2-4.5 Natural Conservation Zone CVI (a) Jenks (b) FCVAM Histograms 85
Figure 5.22. SSP5-8.5 Natural Conservation Zone ErosionPP Distribution 86
Figure 5.23. SSP5-8.5 Natural Conservation Zone Erosion Distribution 87
Figure 5.24. SSP5-8.5 Natural Conservation Zone Erosion (a) Physical Impact Score (b) Human Impact Score 89
Figure 5.25. SSP5-8.5 Natural Conservation Zone Erosion Jenks Distribution 90
Figure 5.26. SSP5-8.5 Natural Conservation Zone Erosion (a) Jenks (b) FCVAM Histograms 91
Figure 5.27. SSP5-8.5 Natural Conservation Zone InundationPP Distribution 92
Figure 5.28. SSP5-8.5 Natural Conservation Zone Inundation Distribution 93
Figure 5.29. SSP5-8.5 Natural Conservation Zone Inundation Component Histogram 95
Figure 5.30. SSP5-8.5 Natural Conservation Zone Inundation Jenks Distribution 96
Figure 5.31. SSP5-8.5 Natural Conservation Zone Inundation (a) Jenks (b) FCVAM Histograms 97
Figure 5.32. SSP5-8.5 Natural Conservation Zone Storm SurgePP Distribution ... 97
Figure 5.33. SSP5-8.5 Natural Conservation Zone Storm Surge Distribution 99
Figure 5.34. SSP5-8.5 Natural Conservation Zone Surge Component Histogram 100
Figure 5.35. SSP5-8.5 Natural Conservation Zone Storm Surge Jenks Distribution 101

Figure 5.36. SSP5-8.5 Natural Conservation Zone Storm Surge (a) Jenks (b) FCVAM Histograms 102
Figure 5.37. SSP5-8.5 Natural Conservation Zone CVI Distribution 102
Figure 5.38. SSP5-8.5 Natural Conservation Zone CVI Jenks Distribution 105
Figure 5.39. SSP5-8.5 Natural Conservation Zone CVI (a) Jenks (b) FCVAM Histograms 106
Figure 5.40. Cultural Heritage Site Erosion Human Impact Distribution 107
Figure 5.41. Cultural Heritage Site Erosion Inundation Impact Distribution 108
Figure 5.42. Cultural Heritage Site Storm Surge Human Impact Distribution 109
Figure 5.43. SSP2-4.5 Cultural Heritage Site ErosionPP Distribution 111
Figure 5.44. SSP2-4.5 Cultural Heritage Site Erosion Distribution 112
Figure 5.45. SSP2-4.5 Cultural Heritage Site Erosion Component Histogram 113
Figure 5.46. SSP2-4.5 Cultural Heritage Site Erosion Jenks Distribution 113
Figure 5.47. SSP2-4.5 Cultural Heritage Site Erosion (a) Jenks (b) FCVAM Histograms 114
Figure 5.48. SSP2-4.5 Cultural Heritage Site InundationPP Distribution 115
Figure 5.49. SSP2-4.5 Cultural Heritage Site Inundation Distribution 116
Figure 5.50. SSP2-4.5 Cultural Heritage Site Inundation Component Histogram 117
Figure 5.51. SSP2-4.5 Cultural Heritage Site Inundation Jenks Distribution 118
Figure 5.52. SSP2-4.5 Cultural Heritage Site Inundation (a) Jenks (b) FCVAM Histograms 119
Figure 5.53. SSP2-4.5 Cultural Heritage Site Storm SurgePP Distribution 119
Figure 5.54. SSP2-4.5 Cultural Heritage Site Storm Surge Distribution 120
Figure 5.55. SSP2-4.5 Cultural Heritage Site Storm Surge Component Histogram 121
Figure 5.56. SSP2-4.5 Cultural Heritage Site Storm Surge Jenks Distribution 122
Figure 5.57. SSP2-4.5 Cultural Heritage Site Storm Surge (a) Jenks (b) FCVAM Histograms 123
Figure 5.58. SSP2-4.5 Cultural Heritage Site CVI Distribution 123
Figure 5.59. SSP2-4.5 Cultural Heritage Site CVI Jenks Distribution 126

Figure 5.60. SSP2-4.5 Cultural Heritage Site CVI (a) Jenks (b) FCVAM Histograms 126
Figure 5.61. SSP5-8.5 Cultural Heritage Site ErosionPP Distribution 127
Figure 5.62. SSP5-8.5 Cultural Heritage Site Erosion Distribution 129
Figure 5.63. SSP5-8.5 Cultural Heritage Site Erosion Component Histogram 130
Figure 5.64. SSP5-8.5 Cultural Heritage Site Erosion Jenks Distribution 131
Figure 5.65. SSP5-8.5 Cultural Heritage Site Erosion (a) Jenks (b) FCVAM Histograms 132
Figure 5.66. SSP5-8.5 Cultural Heritage Site InundationPP Distribution 132
Figure 5.67. SSP5-8.5 Cultural Heritage Site Inundation Distribution 134
Figure 5.68. SSP5-8.5 Cultural Heritage Site Inundation Component Histogram 135
Figure 5.69. SSP5-8.5 Cultural Heritage Site Inundation Jenks Distribution 136
Figure 5.70. SSP5-8.5 Cultural Heritage Site Inundation (a) Jenks (b) FCVAM Histograms 137
Figure 5.71. SSP5-8.5 Cultural Heritage Site Storm SurgePP Distribution 138
Figure 5.72. SSP5-8.5 Cultural Heritage Site Storm Surge Distribution..... 140
Figure 5.73. SSP5-8.5 Cultural Heritage Site Storm Surge Component Histogram 141
Figure 5.74. SSP5-8.5 Cultural Heritage Site Storm Surge Jenks Distribution.... 141
Figure 5.75. SSP5-8.5 Cultural Heritage Site Storm Surge (a) Jenks (b) FCVAM Histograms 142
Figure 5.76. SSP5-8.5 Cultural Heritage Site CVI Distribution 143
Figure 5.77. SSP5-8.5 Cultural Heritage Site CVI Jenks Distribution 146
Figure 5.78. SSP5-8.5 Cultural Heritage Site CVI (a) Jenks (b) FCVAM Histograms 147
Figure 5.79. SSP2-4.5 & SSP5-8.5 Natural Conservation Zones Erosion Scatter Diagrams (a) SSP2-4.5 (b) SSP-8.5 148
Figure 5.80. SSP2-4.5 & SSP5-8.5 Natural Conservation Zones Inundation Scatter Diagrams (a) SSP2-4.5 (b) SSP-8.5 151

Figure 5.81. SSP2-4.5 & SSP5-8.5 Natural Conservation Zones Storm Surge Scatter Diagrams (a) SSP2-4.5 (b) SSP-8.5 153
Figure 5.82. SSP2-4.5 & SSP5-8.5 Natural Conservation Zones Cumulative Impact Score Scatter Diagrams (a) SSP2-4.5 (b) SSP-8.5 156
Figure 5.83. FCVAM results of Mersin Under Pathway of SSP2-4.5 160
Figure 5.84. Previous Study Results of Mersin (Aykut, 2021, p. 89) 160
Figure 7.1. SSP1-1.9 Natural Conservation Zone ErosionPP Distribution 177
Figure 7.2. SSP1-1.9 Natural Conservation Zone ErosionHI Distribution 177
Figure 7.3. SSP1-1.9 Natural Conservation Zone Erosion Distribution 178
Figure 7.4. SSP1-1.9 Natural Conservation Zone Erosion Jenks Distribution 178
Figure 7.5. SSP1-1.9 Natural Conservation Zone Erosion (a) Physical Impact Score (b) Human Impact Score 179
Figure 7.6. SSP1-1.9 Natural Conservation Zone Erosion (a) Jenks (b) FCVAM Histograms 179
Figure 7.7. SSP1-1.9 Natural Conservation Zone InundationPP Distribution 180
Figure 7.8. SSP1-1.9 Natural Conservation Zone InundationHI Distribution 180
Figure 7.9. SSP1-1.9 Natural Conservation Zone Inundation Distribution 181
Figure 7.10. SSP1-1.9 Natural Conservation Zone Inundation Jenks Distribution 181
Figure 7.11. SSP1-1.9 Natural Conservation Zone Inundation (a) Physical Impact Score (b) Human Impact Score 182
Figure 7.12. SSP1-1.9 Natural Conservation Zone Inundation (a) Jenks (b) FCVAM Histograms 182
Figure 7.13. SSP1-1.9 Natural Conservation Zone Storm SurgePP Distribution . 183
Figure 7.14. SSP1-1.9 Natural Conservation Zone Storm SurgeHI Distribution . 183
Figure 7.15. SSP1-1.9 Natural Conservation Zone Storm Surge Distribution 184
Figure 7.16. SSP1-1.9 Natural Conservation Zone Storm Surge Jenks Distribution 184
Figure 7.17. SSP1-1.9 Natural Conservation Zone Storm Surge (a) Physical Impact Score (b) Human Impact Score 185

Figure 7.18. SSP1-1.9 Natural Conservation Zone Storm Surge (a) Jenks (b) FCVAM Histograms 185
Figure 7.19. SSP1-1.9 Natural Conservation Zone CVI Distribution 186
Figure 7.20. SSP1-1.9 Natural Conservation Zone CVI Jenks Distribution 186
Figure 7.21. SSP1-1.9 Natural Conservation Zone CVI (a) Jenks (b) FCVAM Histograms 187
Figure 7.22. SSP1-2.6 Natural Conservation Zone ErosionPP Distribution 188
Figure 7.23. SSP1-2.6 Natural Conservation Zone ErosionHI Distribution..... 188
Figure 7.24. SSP1-2.6 Natural Conservation Zone Erosion Distribution..... 189
Figure 7.25. SSP1-2.6 Natural Conservation Zone Erosion Jenks Distribution... 189
Figure 7.26. SSP1-2.6 Natural Conservation Zone Erosion (a) Physical Impact Score (b) Human Impact Score 190
Figure 7.27. SSP1-2.6 Natural Conservation Zone Erosion (a) Jenks (b) FCVAM Histograms 190
Figure 7.28. SSP1-2.6 Natural Conservation Zone InundationPP Distribution ... 191
Figure 7.29. SSP1-2.6 Natural Conservation Zone InundationHI Distribution.... 191
Figure 7.30. SSP1-2.6 Natural Conservation Zone Inundation Distribution..... 192
Figure 7.31. SSP1-2.6 Natural Conservation Zone Inundation Jenks Distribution 192
Figure 7.32. SSP1-2.6 Natural Conservation Zone Inundation (a) Physical Impact Score (b) Human Impact Score 193
Figure 7.33. SSP1-2.6 Natural Conservation Zone Inundation (a) Jenks (b) FCVAM Histograms 193
Figure 7.34. SSP1-2.6 Natural Conservation Zone Storm SurgePP Distribution. 194
Figure 7.35. SSP1-2.6 Natural Conservation Zone Storm SurgeHI Distribution. 194
Figure 7.36. SSP1-2.6 Natural Conservation Zone Storm Surge Distribution 195
Figure 7.37. SSP1-2.6 Natural Conservation Zone Storm Surge Jenks Distribution 195
Figure 7.38. SSP1-2.6 Natural Conservation Zone Storm Surge (a) Physical Impact Score (b) Human Impact Score 196

Figure 7.39. SSP1-2.6 Natural Conservation Zone Storm Surge (a) Jenks (b) FCVAM Histograms 196
Figure 7.40. SSP1-2.6 Natural Conservation Zone CVI Distribution 197
Figure 7.41. SSP1-2.6 Natural Conservation Zone CVI Jenks Distribution 197
Figure 7.42. SSP1-2.6 Natural Conservation Zone CVI (a) Jenks (b) FCVAM Histograms 198
Figure 7.43. SSP3-7.0 Natural Conservation Zone ErosionPP Distribution 199
Figure 7.44. SSP3-7.0 Natural Conservation Zone ErosionHI Distribution 199
Figure 7.45. SSP3-7.0 Natural Conservation Zone Erosion Distribution 200
Figure 7.46. SSP3-7.0 Natural Conservation Zone Erosion Jenks Distribution ... 200
Figure 7.47. SSP3-7.0 Natural Conservation Zone Erosion (a) Physical Impact Score (b) Human Impact Score 201
Figure 7.48. SSP3-7.0 Natural Conservation Zone Erosion (a) Jenks (b) FCVAM Histograms 201
Figure 7.49. SSP3-7.0 Natural Conservation Zone InundationPP Distribution 202
Figure 7.50. SSP3-7.0 Natural Conservation Zone InundationHI Distribution 202
Figure 7.51. SSP3-7.0 Natural Conservation Zone Inundation Distribution 203
Figure 7.52. SSP3-7.0 Natural Conservation Zone Inundation Jenks Distribution 203
Figure 7.53. SSP3-7.0 Natural Conservation Zone Inundation (a) Physical Impact Score (b) Human Impact Score 204
Figure 7.54. SSP3-7.0 Natural Conservation Zone Inundation (a) Jenks (b) FCVAM Histograms 204
Figure 7.55. SSP3-7.0 Natural Conservation Zone Storm SurgePP Distribution . 205
Figure 7.56. SSP3-7.0 Natural Conservation Zone Storm SurgeHI Distribution . 205
Figure 7.57. SSP3-7.0 Natural Conservation Zone Storm Surge Distribution 206
Figure 7.58. SSP3-7.0 Natural Conservation Zone Storm Surge Jenks Distribution 206
Figure 7.59. SSP3-7.0 Natural Conservation Zone Storm Surge (a) Physical Impact Score (b) Human Impact Score 207

Figure 7.60. SSP3-7.0 Natural Conservation Zone Storm Surge (a) Jenks (b) FCVAM Histograms 207
Figure 7.61. SSP3-7.0 Natural Conservation Zone CVI Distribution 208
Figure 7.62. SSP3-7.0 Natural Conservation Zone CVI Jenks Distribution 208
Figure 7.63. SSP3-7.0 Natural Conservation Zone CVI (a) Jenks (b) FCVAM Histograms 209
Figure 7.64. SSP1-1.9 Cultural Heritage Site ErosionPP Distribution 210
Figure 7.65. SSP1-1.9 Cultural Heritage Site ErosionHI Distribution 210
Figure 7.66. SSP1-1.9 Cultural Heritage Site Erosion Distribution 211
Figure 7.67. SSP1-1.9 Cultural Heritage Site Erosion Jenks Distribution 211
Figure 7.68. SSP1-1.9 Cultural Heritage Site Erosion (a) Physical Impact Score (b) Human Impact Score 212
Figure 7.69. SSP1-1.9 Cultural Heritage Site Erosion (a) Jenks (b) FCVAM Histograms 212
Figure 7.70. SSP1-1.9 Cultural Heritage Site InundationPP Distribution 213
Figure 7.71. SSP1-1.9 Cultural Heritage Site InundationHI Distribution 213
Figure 7.72. SSP1-1.9 Cultural Heritage Site Inundation Distribution 214
Figure 7.73. SSP1-1.9 Cultural Heritage Site Inundation Jenks Distribution 214
Figure 7.74. SSP1-1.9 Cultural Heritage Site Inundation (a) Physical Impact Score (b) Human Impact Score 215
Figure 7.75. SSP1-1.9 Cultural Heritage Site Inundation (a) Jenks (b) FCVAM Histograms 215
Figure 7.76. SSP1-1.9 Cultural Heritage Site Storm SurgePP Distribution 216
Figure 7.77. SSP1-1.9 Cultural Heritage Site Storm SurgeHI Distribution 216
Figure 7.78. SSP1-1.9 Cultural Heritage Site Storm Surge Distribution 217
Figure 7.79. SSP1-1.9 Cultural Heritage Site Storm Surge Jenks Distribution 217
Figure 7.80. SSP1-1.9 Cultural Heritage Site Storm Surge (a) Physical Impact Score (b) Human Impact Score 218
Figure 7.81. SSP1-1.9 Cultural Heritage Site Storm Surge (a) Jenks (b) FCVAM Histograms 218

Figure 7.82. SSP1-1.9 Cultural Heritage Site CVI Distribution 219
Figure 7.83. SSP1-1.9 Cultural Heritage Site CVI Jenks Distribution 219
Figure 7.84. SSP1-1.9 Cultural Heritage Site CVI (a) Jenks (b) FCVAM Histograms 220
Figure 7.85. SSP1-2.6 Cultural Heritage Site ErosionPP Distribution 221
Figure 7.86. SSP1-2.6 Cultural Heritage Site ErosionHI Distribution 221
Figure 7.87. SSP1-2.6 Cultural Heritage Site Erosion Distribution 222
Figure 7.88. SSP1-2.6 Cultural Heritage Site Erosion Jenks Distribution 222
Figure 7.89. SSP1-2.6 Cultural Heritage Site Erosion (a) Physical Impact Score (b) Human Impact Score 223
Figure 7.90. SSP1-2.6 Cultural Heritage Site Erosion (a) Jenks (b) FCVAM Histograms 223
Figure 7.91. SSP1-2.6 Cultural Heritage Site InundationPP Distribution 224
Figure 7.92. SSP1-2.6 Cultural Heritage Site InundationHI Distribution 224
Figure 7.93. SSP1-2.6 Cultural Heritage Site Inundation Distribution 225
Figure 7.94. SSP1-2.6 Cultural Heritage Site Inundation Jenks Distribution 225
Figure 7.95. SSP1-2.6 Cultural Heritage Site Inundation (a) Physical Impact Score (b) Human Impact Score 226
Figure 7.96. SSP1-2.6 Cultural Heritage Site Inundation (a) Jenks (b) FCVAM Histograms 226
Figure 7.97. SSP1-2.6 Cultural Heritage Site Storm SurgePP Distribution 227
Figure 7.98. SSP1-2.6 Cultural Heritage Site Storm SurgeHI Distribution 227
Figure 7.99. SSP1-2.6 Cultural Heritage Site Storm Surge Distribution 228
Figure 7.100. SSP1-2.6 Cultural Heritage Site Storm Surge Jenks Distribution 228
Figure 7.101. SSP1-2.6 Cultural Heritage Site Storm Surge (a) Physical Impact Score (b) Human Impact Score 229
Figure 7.102. SSP1-2.6 Cultural Heritage Site Storm Surge (a) Jenks (b) FCVAM Histograms 229
Figure 7.103. SSP1-2.6 Cultural Heritage Site CVI Distribution 230
Figure 7.104. SSP1-2.6 Cultural Heritage Site CVI Jenks Distribution 230

Figure 7.105. SSP1-2.6 Cultural Heritage Site CVI (a) Jenks (b) FCVAM Histograms 231
Figure 7.106. SSP3-7.0 Cultural Heritage Site ErosionPP Distribution 232
Figure 7.107. SSP3-7.0 Cultural Heritage Site ErosionHI Distribution 232
Figure 7.108. SSP3-7.0 Cultural Heritage Site Erosion Distribution 233
Figure 7.109. SSP3-7.0 Cultural Heritage Site Erosion Jenks Distribution 233
Figure 7.110. SSP3-7.0 Cultural Heritage Site Erosion (a) Physical Impact Score (b) Human Impact Score 234
Figure 7.111. SSP3-7.0 Cultural Heritage Site Erosion (a) Jenks (b) FCVAM Histograms 234
Figure 7.112. SSP3-7.0 Cultural Heritage Site InundationPP Distribution 235
Figure 7.113. SSP3-7.0 Cultural Heritage Site InundationHI Distribution 235
Figure 7.114. SSP3-7.0 Cultural Heritage Site Inundation Distribution 236
Figure 7.115. SSP3-7.0 Cultural Heritage Site Inundation Jenks Distribution 236
Figure 7.116. SSP3-7.0 Cultural Heritage Site Inundation (a) Physical Impact Score (b) Human Impact Score 237
Figure 7.117. SSP3-7.0 Cultural Heritage Site Inundation (a) Jenks (b) FCVAM Histograms 237
Figure 7.118. SSP3-7.0 Cultural Heritage Site Storm SurgePP Distribution 238
Figure 7.119. SSP3-7.0 Cultural Heritage Site Storm SurgeHI Distribution 238
Figure 7.120. SSP3-7.0 Cultural Heritage Site Storm Surge Distribution..... 239
Figure 7.121. SSP3-7.0 Cultural Heritage Site Storm Surge Jenks Distribution.. 239
Figure 7.122. SSP3-7.0 Cultural Heritage Site Storm Surge (a) Physical Impact Score (b) Human Impact Score 240
Figure 7.123. SSP3-7.0 Cultural Heritage Site Storm Surge (a) Jenks (b) FCVAM Histograms 240
Figure 7.124. SSP3-7.0 Cultural Heritage Site CVI Distribution 241
Figure 7.125. SSP3-7.0 Cultural Heritage Site CVI Jenks Distribution 241
Figure 7.126. SSP3-7.0 Cultural Heritage Site CVI (a) Jenks (b) FCVAM Histograms 242

Figure 7.127. SSP2-4.5 & SSP5-8.5 Cultural Heritage Site Erosion Scatter Diagrams (a) SSP2-4.5 (b) SSP-8.5 243
Figure 7.128. SSP2-4.5 & SSP5-8.5 Cultural Heritage Site Inundation Scatter Diagrams (a) SSP2-4.5 (b) SSP-8.5 243
Figure 7.129. SSP2-4.5 & SSP5-8.5 Cultural Heritage Site Storm Surge Scatter Diagrams (a) SSP2-4.5 (b) SSP-8.5 244
Figure 7.130. SSP2-4.5 & SSP5-8.5 Cultural Heritage Site Cumulative Impact Score Scatter Diagrams (a) SSP2-4.5 (b) SSP-8.5 244

LIST OF ABBREVIATIONS

AR: Assessment Report

ARC: Archeological

CPS: Coastal Protection Structures

CVI: Coastal Vulnerability Index

DEM: Digital Elevation Map

DTM: Digital Terrain Map

EF: Engineering Frontage

E-HI: Erosion Human Impact

E-PP: Erosion Physical Impact

ErosionHI: Erosion Human Impact

ErosionPP: Erosion Physical Impact

ESL: Extreme Sea Level

FCVAM: Fuzzy Coastal Vulnerability Assessment Model

Fis: Fuzzy Inference System

Geo: Geomorphology

GHG: Green House Gases

Hs: Annual Wave Climate

I-HI: Inundation Human Impact

InundationHI: Inundation Human Impact

InundationPP: Inundation Physical Impact

IPCC: Intergovernmental Panel on Climate Change

I-PP: Inundation Physical Impact

MF: Membership Function

NAT: Natural

Natdeg: Natural Protection Degradation

RCP: Representative Concentration Pathways

Rifrag: River Flow Regulation

RSLR: Rate of Sea Level Rise

SedBgt: Sediment Budget

S-HI: Storm Surge Human Impact

S-PP: Storm Surge Physical Impact

SSP: Shared Socioeconomic Pathways

Storm SurgeHI: Storm Surge Human Impact

Storm SurgePP: Storm Surge Physical Impact

Vul: Vulnerability

CHAPTER 1

INTRODUCTION

Throughout history, coastal areas have always been attraction points for humans to settle, and they still are. Around 37 percent of the world's population lives within 100 km of the coast (United Nations, n.d.). In the U.S., this ratio increases to 40% - with 127 million people- living within the 10% of total land stated by NOAA (2019); on the other hand, coastal counties of the U.S. would rank third in the world in gross domestic product behind China and the U.S. itself. This is because various economic activities could be conducted around coastal areas, from tourism to energy production. However, extensive usage for economic activities along with high population density increases the sensitivity of these areas against natural phenomena such as sea level rise, storm surge, erosion, and floods. The main issue for the future is that the occurrence rate and impacts of these are increasing constantly with global climate change.

According to IPCC Annual Report 6 (2023), the global surface temperature was higher, around 1.1°C in 2011–2020 compared to 1850–1900, which is mainly caused by emitted Green Houses Gases (GHG) by human activities after the “Industrial Revolution.” These gases increase the heat-trapping capacity of the atmosphere, and on the ocean surface, increased surface temperatures result in the thermal expansion of water. Thermal expansion of water is one of the main reasons for the rise of the global sea level, along with the loss of glaciers because of the increased surface temperature. In IPCC AR6, five different given corresponded to different GHG emissions, directly affecting Global Mean Sea Level (GMSL) rise. SSP1-1.9, which is the least critical one with a temperature increase of 1.5°C by 2100, results in a GMSL rise to be around 0.23 m, while in the most critical scenario, SSP5-8.5 with a 5°C increase in temperature, this number reaches 0.77 m. Sea level rise not only directly endangers coastal cities but also poses indirect risks by making extreme

events more frequent. According to the report, by 2100 for SSP5-8.5, 82% of 634 tide gauge stations are expected to undergo yearly 1 % historical annual probability extreme sea level (ESL) events. Such an increased ESL occurrence rate and global warming-induced sea level rise threaten countries with coastal cities.

Turkiye, with an 8,333 km shoreline, is among the countries threatened by global warming-induced sea level rise. Many natural protection zones and coastal cultural heritage areas have been located along their shoreline, which are important ecologically and socio-economically. Therefore, assessing and understanding the severity of risk caused by rising sea levels in these areas aligns with Turkiye's sustainable development goals. In other words, conducting vulnerability assessments on these areas against sea level rise will help policymakers develop their strategies more optimally with increased understanding of risks, decreased uncertainties, and knowing how vulnerable the corresponding area is.

1.1 Objective of the Study

In this thesis, the Coastal Vulnerability Index (CVI) assessment against global warming-induced sea level rise was conducted for coastal cultural heritage areas and natural conservation zones of Turkiye, which are located within 10 m elevation from sea level and 1 km inland from shoreline as a part of TUBITAK funded project 122M621 Vulnerability of Coastal Cultural Heritage Areas to Sea Level Rise and Its Impacts. The main purpose of this process was to determine how vulnerable these areas are to sea level rise. Fuzzy Coastal Vulnerability Assessment Model (FCVAM) with three modules was utilized to get the CVI score. 3 three-module version of the model requires 11 different parameters, and input values of these parameters are processed using fuzzy logic rules to get vulnerability scores regarding modules. Then, these scores are evaluated by a set of fuzzy logic rules to calculate the CVI score. By having the module vulnerability impact scores, determining against which factor that the study area is most vulnerable could be detected. Also, having human and natural indexes separately, detecting the natural vulnerability of

the study area and how human usage affects the natural vulnerability could be deduced. This enables policymakers to try alternative scenarios by changing the inputs, detecting the most critical factor, and developing their strategies accordingly, which is crucial. For example, using different sea level rise projections that also result in variations in values of a few of the other model parameters, changes in human usage of the shoreline, or evaluating alternative development goals and scenarios could be applied to the model, and CVI scores would be obtained for each different scenario. In this study, projections of sea level rise based on all the emission scenarios provided by IPCC AR 6 (2023) are used to understand the vulnerability of coastal cultural heritage areas of Turkiye. The main text of the study provides in-depth results on the selected two scenarios, SSP2-4.5 and SSP5-8.5, which represent likely future and worst-case scenarios, respectively. These two scenarios are presented in detail to provide the range of the vulnerability of the assessed sites. The results of the remaining three scenarios are provided in the Appendix to ensure the completeness of the thesis work.

1.2 Outline of the Thesis

This thesis covers six main chapters, including the introduction. The next chapter presents a literature review on the topics of Global Climate Change, Global Mean Sea Level Rise, and Vulnerability Assessment Models. The third chapter, Fuzzy Coastal Vulnerability Assessment Model, Model Changes, MATLAB to Python conversion, is detailed. The fourth chapter explains the input parameters and preprocessing steps of the data. In the fifth chapter, results are presented, and discussions and used databases are provided. Finally, the study is summarized in the conclusion chapter, and remarks with future study recommendations are given. The Appendix provides the results of the three other sea level rise scenarios.

CHAPTER 2

LITERATURE REVIEW

Global climate change is a human-induced phenomenon that poses enormous potential risks and uncertainties, such as experiencing more frequent and profound storms and droughts resulting from heat waves. Because of the broad range of potential risks and uncertainties, the outcomes of this phenomenon also vary abruptly, such as loss of biodiversity or failure of infrastructure systems. Thus, in 2015, with the "Paris Agreement" for the first time in history, all the nations gathered to take ambitious precautions against "Climate Change." This agreement was signed by 195 countries to keep the global temperature increase below 1.5°C. To be more specific, the increase in the worldwide temperature is attempted to be limited to 2°C than the global temperature of pre-industrial periods (United Nations, 2019).

The rise of the global mean sea level (GMSL) is also one of the consequences of global climate change. The main factors of the rise are ocean thermal expansion and the meltdown of mountain glaciers and ice sheets, also resulting from global climate change (Simpson et al., 2024). According to NASA (2019), in the case of melting all glaciers and ice sheets, the GMSL would increase by 60m. On the other hand, AR6 prepared by IPCC (2023) states that in the scenario of a GMSL rise of 0.15m relative to 2020 levels, it would increase the number of people exposed to a 100-year coastal flood by 20% and the number of exposed people would be doubled if the increase was by 0.75m.

The economic effect of global climate change is also nonlinear. In AR6 (IPCC,2023), by 2100, during a 100-year return period of storm and under RCP 4.5 (medium critical scenario) conditions, expected assets within floodplains will be between 7.9 and 12.7 trillion USD dollars. These numbers will be between 8.8 and 14.2 trillion USD dollars under RCP 8.5. Generating the most optimal strategies against the potential losses caused by GMSL rise is crucial. As a result, there has been an

increasing number of studies that have calculated how vulnerable an area is against GMSL rise by using different models. The main advantage of these models is that alternative cases could be tested for various locations by inputting data from other scenarios. This enables policymakers to observe the vulnerability of a location against different parameters under different scenarios and generate their development plans accordingly. This chapter will detail a literature survey about global climate change, coastal vulnerability, vulnerability assessment methods, and examples of applications on Turkish coasts.

2.1 Global Climate Change

After the Industrial Revolution, to generate heat and energy, the consumption of fossil fuels increased dramatically, which also increased the emission of GHG into the atmosphere. According to EPA (2020), in 2020, GHG concentration in the atmosphere was at the highest level in the last 800,000 years. This situation increases global average temperature levels. GHGs, which are carbon dioxide, methane, and nitrous oxide, have the ability to absorb solar radiation, which is normally reflected back into space, especially by glaciers (Filonchyk et al., 2024). As a result of the absorption of solar radiation, GHG molecule energy levels increase and begin to generate thermal radiation, which increases the heat around them. The main problem is that GHG could stay in the atmosphere for centuries and continue to absorb radiation.

The consequences of global climate change have an extensive range. On land, a 1°C increase in temperature might reduce the potato and wheat production rate by 3 – 7 %, or at sea, fishery activities could be jeopardized because of the thermal expansion of the ocean, which would deteriorate ocean dynamics against living organisms (Bandh et al., 2021). Also, an increase in temperatures could be described as a self-sustaining issue. A yearly mean temperature of 22°C is the upper limit without requiring additional cooling applications, but with global climate change, areas with a 22°C annual mean will be decreased, and more energy will be required for cooling

applications, which will increase GHG emissions and contribute to global climate change (Cetin et al., 2023). Therefore, while generating the scenarios, one of the main focuses of IPCC AR6 is potential GHG emissions. Depending on the projected radiative forcing in watts per square meter (W/m^2) in 2100, there are five different scenarios defined, which are SSP1-1.9, SSP1-2.6, SSP2-4, SSP3-7, and SSP5-8.5. Radiate forcing in W/m^2 is given in scenario notation. For instance, SSP1-2.6 is expected to have a radiative forcing of approximately 2.6 W/m^2 in 2100. However, it should not be mistaken that SSP scenarios indicate the possible behavior of society by quantifying socio-economic factors such as population, urbanization, and GDP. These results are then used to predict future GHG emissions and air pollution, and outcomes of which are given in Table 2.1.

Table 2.1 Long-Term Potential Global Average Temperature Increases

Scenario	Long Term, 2081-2100	
	Best Estimate (°C)	Temperature Increase Range (°C)
SSP1-1.9	1.4	1.0 to 1.8
SSP1-2.6	1.8	1.3 to 2.4
SSP2-4.5	2.7	2.1 to 3.5
SSP3-7.0	3.6	2.8 to 4.6
SSP5-8.5	4.4	3.3 to 5.7

IPCC AR6 SSP scenarios could not be directly compared to AR5 RCP scenarios since RCP projections focus more on greenhouse gas emissions than socio-economic behavior. Definitions of SSP scenarios defined in AR6 by IPCC could be given as CO_2 emission declines and becomes zero in 2050 for SSP1-1.9 and in 2070 for SSP1-2.6, a ‘middle-of-the-road’ path (SSP2) in which CO2 level stays the same at the mid of century, ‘regional rivalry’ (SSP3) in which CO2 level doubles in 2100, ‘inequality’ (SSP4), and ‘fossil fuel-intensive’ development (SSP5) in which CO2 level doubles in 2050. Moreover, SSP1-1.9 differs since this scenario directly implements the Paris Agreement. A comparison of the scenarios in terms of surface

temperature increase for a long-term period is given in Table 2.1. As mentioned, in SSP1-1.9, the Paris Agreement goal of keeping the temperature increase below 1.5 °C was satisfied. However, with each scenario, the average surface temperature and the severity of the consequences increase. The rise in the global mean sea level (GMSL) is one outcome of the increase in surface temperature. This phenomenon could be described as an increase in mean sea level for two main reasons: thermal expansion and water intrusion into the ocean by melting glaciers and ice sheets on land. In Figure 2.1, the historical observed sea surface level increase between the years 1993 and 2019 is given.

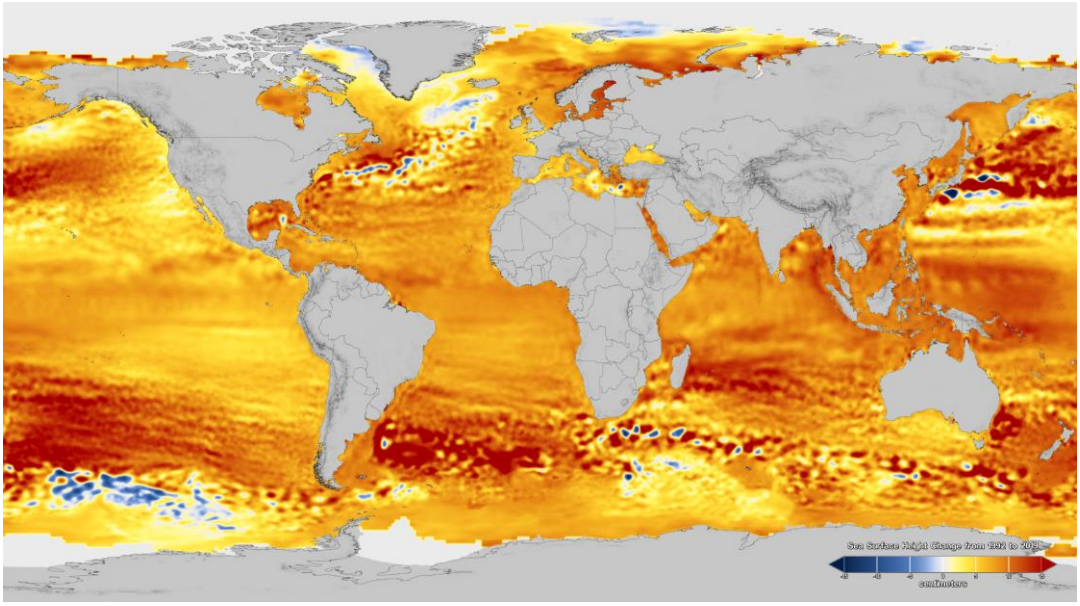


Figure 2.1. Sea Surface Level Increase Between 1993 to 2019 (NASA, 2023, n.p.)

Increased GMSL indicates that extreme events, such as a storm with 50 50-year return period, would be more frequent (Oppenheimer et al., 2019). Observing these events more frequently poses very severe threats since coastal areas have been and still are highly populated despite consisting of a small portion of the total land area. For instance, despite undergoing 71 billion USD in economic losses and 4376 casualties from 1989 to 2014 and accounting for only 2% of the total area, at least 12% of people in China still live in areas with elevations less than 10m (Fang et al., 2021).

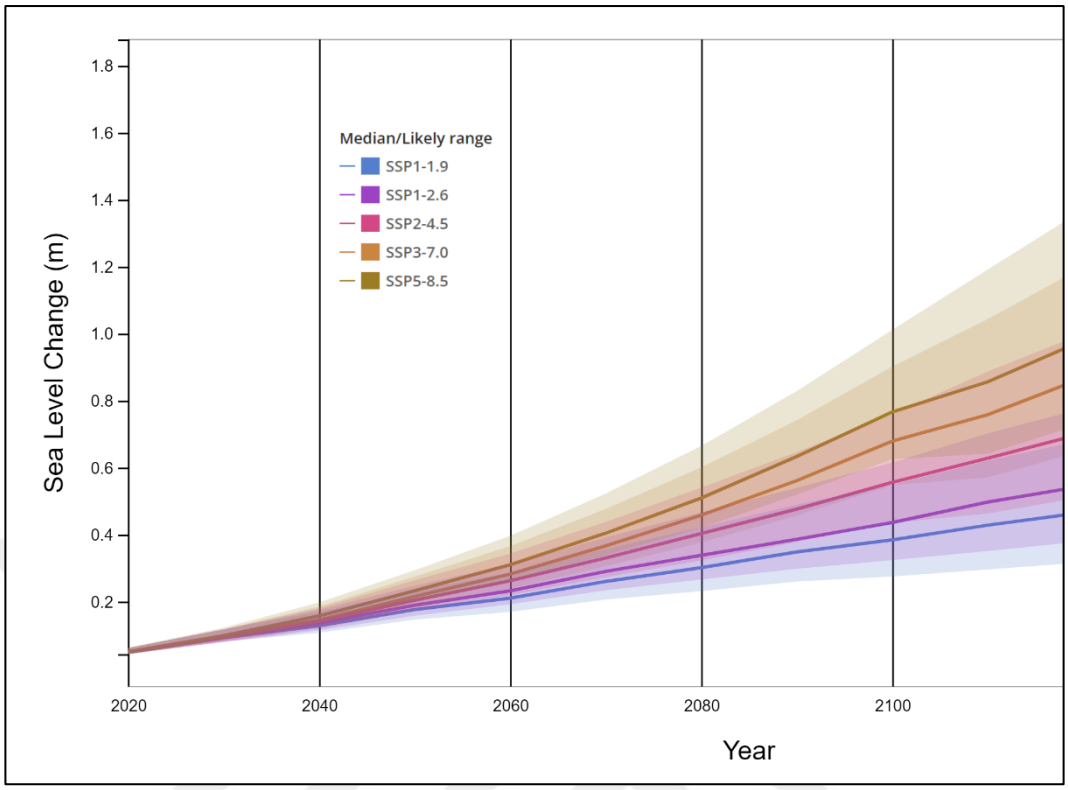


Figure 2.2. GMSL Scenario Comparisons (NASA, 2023, n.p.)

In Figure 2.2, sea level change forecasts concerning scenarios and years are given. Lines indicate the median, and areas are between the 17th – and 83rd percentile. Expected GMSL rise in 2100, depending on the scenarios, are 0.38m for SSP1-1.9, 0.44m for SSP1-2.6, 0.56m for SSP2-4.5, 0.68m for SSP3-7.0 and 0.77m for SSP5-8.5. Considering the proposed GMSL rise, there have been policy adaptations of coastal protection. According to Kato and Tajima (2023), the government of Tokyo has revised the Basic Policy for Coastal Protection from 2020 to 2023. A rise of 0.6 m in sea level (RCP 2.6) and a 100-year return period for typhoons under future conditions were determined as the most critical case for the RCP 2.6 scenario. The revised plan stated in some locations required seawall height range with respect to the low water level of Tokyo must be increased from +4.6 ~ 8.0 m to +5.6 ~ 8.0 m

2.2 Coastal Vulnerability

Although GHGs emitted by human activities have caused GMSL to rise, they are unlikely to have direct control over this phenomenon. However, assessing the potential consequences and preparing adaptation plans accordingly could reduce the rise in GMSL outcomes.

Coastal erosion could be a consequence of any factors that affect sediment transportation behavior. These factors could be exemplified by introducing non-erodible structures or hydrodynamic changes. Hydrodynamic properties might include wave intensity, direction, and sea level (van de Wal et al., 2024). Since sea level rise causes wave energy to increase, shorelines are expected to be exposed to increased wave energy and become more susceptible to erosion (Shadrick et al., 2022). The Basque coast could be an example of how erosion is connected to SLR. By 2100, a shoreline retreat of 14–66 m in the case of RCP 8.5 and 10–45 m for RCP4.5 is expected for 150 km of the Basque coast (van de Wal et al., 2024). From another perspective, according to Athanasiou et al. (2020), the Median shoreline recession increases to 97m for RCP 8.5 or 54m for RCP4.5 by the year 2100 if the entire European shoreline is considered. Regarding coastal land loss, RCP 8.5 results in 2500 km^2, while for RCP 4.5, the expected area to be lost is 1400 km^2.

Increased sea level rise also increases the likelihood of experiencing extreme water levels. However, regions experiencing similar extreme water levels, such as the Tropics, are threatened more since even 5-10 cm SLR will at least double the occurrence rate of extreme water levels by 2030. If low-elevated islands, which are vulnerable to storms even today, are considered, it could be assumed that an increase in the occurrence rate of inundation threatens their existence and sustainability (Vitousek et al., 2017). On the other hand, although rising sea levels do not pose an existential threat to larger land areas, there could still be very detrimental outcomes. For example, in the case of a 1m SLR, the extent of inundation along the California Coast is expected to reach 50-130m further inland (Rahimi et al., 2020). From another point of view, if the population is projected to double by 2100 compared to

today's value, 4.2 million people will be exposed to the threat of inundation in the case of 0.9m SLR. The number of people increases to 13.1 million if the SLR is 1.8 m (Rahimi et al., 2020).

In addition to physical outcomes, SLR also poses chemical risks, such as saltwater intrusion, which is defined as seawater infiltration or brackish water into groundwater or freshwater around coastal areas. The existence of freshwater is especially important for coastal areas since these areas are very densely populated. The study conducted by Zamrsky et al. (2024) over 1200 coastal regions around the world indicated that around 60 million people dwelling 10 km within the shoreline will lose more than 5% of their freshwater resources by 2100 under RCP 8.5 scenario because of SLR while these numbers shift back to 8 million people for RCP 2.6. Groundwater intrusion threatens humans and the coastal wetlands, which are rich in biodiversity. In their study, Mazhar et al. (2022) stated that 15 × 106 ha of coastal wetlands are located within 5m elevation of mean sea level. In the case of a 1m SLR, 64% of the coastal wetland will be destroyed by becoming saline systems. Moreover, depending on the location, some regions will be more detrimentally affected, such as 100% destruction of coastal wetlands expected in the Middle East and North Africa or 74% destruction in Latin America and the Caribbean (Blankespoor et al., 2012).

2.3 Coastal Vulnerability Index and Global Assessments

According to the Third Assessment Report of IPCC (IPCC, 2001), "Vulnerability" refers to the extent to which a system is sensitive to or incapable of enduring the negative impacts of climate change, including climate variability and extremes. Assessing vulnerability is crucial since coastal communities undergoing socio-economic problems such as high populations are significantly more vulnerable to climate change. Therefore, vulnerability assessment is a key factor in developing national and international strategies that consider climate-related risks, ultimately

promoting sustainable development, enhancing adaptive capacity, and reducing vulnerability to other stress factors.

Several methodologies have been developed and utilized to obtain a coastal vulnerability index. Methodologies developed by Gornitz (1990), Thieler and Hammar-Klose (1999), Ozyurt (2010), Gorokhovich et al. (2014), Deb et al. (2024), and Fannassi et al. (2024) could be given as examples of different approaches to obtaining CVI. These assessment methodologies differ depending on the location, aim, parameter assessment approach, and index calculation method.

The study conducted by Gornitz could be considered one of the earliest studies of CVI assessment. The CVI assessment methodology proposed in the study includes seven parameters: relief, rock type, landform, sea level rise rate, shoreline displacement, tidal range, and wave height. Each parameter is assigned a score between 1-5, depending on the parameter value. Then, CVI was calculated by taking the square root of the geometric mean, and a higher score indicates higher vulnerability. The methodology was utilized to determine the vulnerability of the United States' east coast (Gornitz, 1991). In 1999, Thieler and Hammar-Klose generated a modified version of the methodology proposed by Gornitz (1991) to conduct CVI analysis throughout the Atlantic coast of the United States. Geomorphology, shoreline erosion, accretion rates, coastal slope, relative sea level rise rate, mean tidal range and mean wave height were the input parameters. Table 2.2 gives the parameters and CVI ranking relation used during the CVI evaluation of the U.S. Gulf of Mexico by Thieler et al. in 2000. The Table gives more insight into how parameters are assigned a vulnerability score depending on their input values or types. For example, if the studied location has a slope smaller than 2.2%, then the location is considered within the “Very High Vulnerable” class in terms of coastal slope. Thus, for this parameter, location will be scored as “5”.

Table 2.2 Ranking of Coastal Vulnerability Index (Thieler et al.,2000)

	Ranking of Coastal Vulnerability Index				
	Very Low	Low	Moderate	High	Very High
Variable	1	2	3	4	5
Geomorphology	Rocky, Cliffed Coasts Fiords Fiards	Medium Cliffs Indented Coasts	Low Cliffs Glacial Drift Alluvial Plane	Cobble Beaches Estuary Lagoon	Barrier Beaches Sand Beaches Salt Marsh Mud Flats Deltas Mangrove Coral Reefs
Coastal Slope (%)	>0.115	0.115 – 0.055	0.055 – 0.035	0.035 – 0.022	<0.022
Relative Sea Level Change (mm/yr)	<1.8	1.8 – 2.5	2.5 – 3.0	3.0 – 3.4	> 3.4
Shoreline Erosion/ Accretion (m/yr)	>2.0 Accretion	1.0– 2.0 Accretion	-1.0 – +1.0 Stable	-1.1 – -2.0 Erosion	< -2.0 Erosion
Mean Tide Range (m)	> 6.0	4.1 – 6.0	2.0 – 4.0	1.0 – 1.9	<1.0
Mean Wave Height (m)	< 0.55	0.55 – 0.85	0.85 – 1.05	1.05 – 1.25	> 1.25

Many other researchers have used the CVI calculation methodology of Thieler and Hammar-Klose directly or by making further alterations. Gorokhovic et al. (2014) reduced the number of models from 6 to 3 by assuming constant SLR, wave height, and tidal range while studying Kotzebue, Alaska. On the other hand, there are various models which include socio-economic parameters. According to Pramanik et al. (2021), although they conducted CVI analysis for the Krishna-Godavari delta by using five geological (elevation, slope, shoreline change, geomorphology, and coastal bathymetry) and three physical parameters (sea level rise, mean tide level, and significant wave height) after the decision of human-induced factors to affect CVI while assessing CVI of Mumbai, socioeconomic variables (Land use and land cover, population density, tourist density, fisherfolk density) were also included in calculations. To give another example, Deb et al. (2024) considered nine physical parameters (coastal slope, rainfall, storm surge height, rate of sea level rise, wind speed, soil salinity, soil permeability, mean tidal range) as well as six social

parameters (population density, literacy rate, household structure, number of disabled people, number of people either younger than age of 5 years or older than 65, land use land cover) to analyze the southern coastal region of Bangladesh. After assigning scores to each parameter depending on their values, the physical vulnerability index (PVI) and social vulnerability index (SVI) were calculated as the square root of the product mean of physical and social parameters, respectively. CVI was obtained after obtaining PVI and SVI by taking the square root of the product mean of PVI and SVI. A similar multiple type of CVI approach was also adopted by Kantamaneni et. Al (2018), while evaluating several study areas along the UK shoreline. They considered three different vulnerability indexes named the Physical Coastal Vulnerability Index (PCVI), which requires seven physical parameters (beach width, dune width, coastal slope, distance of vegetation behind the back beach, distance of built structures behind the back beach, rocky outcrop, sea defenses), Fiscal Coastal Vulnerability Index (FCVI) with six parameters (Commercial properties, residential properties, economic value of the site, population, coastal erosion, flood impact) and Combined Coastal Vulnerability Index (CCVI). Contrary to previously mentioned approaches, physical parameters are assigned a score between 1-4 depending on their value in this study. However, for the FCVI parameters, scoring bounds are 1-5. Moreover, a direct summation of parameter scores to get PCVI and FCVI was selected as the aggregation method, which indicates PCVI could have a score between 7-28, while for FCVI, the limits are between 6-30. If the area includes multiple cells, PCVI and FCVI were taken as their average of each cell's PCVI and FCVI values. To calculate CCVI, the average of averaged PCVI and FCVI were taken.

New models with more complex structures have been developed with the advancement of new computational techniques and approaches. Examples of these more complex structures are fuzzy logic structures, machine learning, and artificial neural networks. The application of this system could be at the parameter derivation, score calculation, or both stages. While assessing the shores of Vila Belmiro coastal stretches, Sethuraman et al. (2024) used AHP to calculate parameter weights and

used them in their model. However, a random forest algorithm of machine learning was utilized to obtain the LULC parameter value of the studied shoreline. On the other hand, Fanassi et.al (2024) generated their input datasets in GIS environment for the Mediterranean coast of Tangier-Tetouan, but they created new models using machine learning techniques. In their study, 70% of the 10033 points (around 124km) to be assessed were used for training purposes of models generated by utilizing Artificial Neural Network (ANN), Decision Tree (DT), Logistic Regression (LR), Random Forest (RF), and Support Vector Machine (SVM). In comparison, the rest of the 30% of the dataset was used for testing.

CVI scores and distribution results might vary depending on the selected model. Table 2.3 shows the results of a study conducted by Koroglu et al. (2019), which compares the CVI of 4 different models applied to a 160 km-long Barcelona shoreline. CVI values were divided into four equal percentage classes to make a percentage comparison.

Table 2.3 Barcelona Shoreline CVI Distribution (Koroglu et al., 2019)

		Lopez et.al, 2016	Thieler & Hammar-Klose, 2000	Shaw et.al, 1998	Gornitz, 1991
Low	0%-25%	28%	28%	36%	28%
Moderate	25%-50%	30%	37%	30%	22%
High	50%-75%	22%	11%	10%	25%
Very High	75%-100%	20%	24%	24%	25%

Although overall results demonstrate similarity, there have been differences among the cell CVI distributions. According to Koroglu and colleagues (2019), this could be explained by how models consider the parameters. Vulnerability categories of wave climate and shoreline change demonstrate minimal deviations contrary to coastal slope and elevation, relative sea level rise, and tidal range.

According to the authors, different approaches, such as describing vulnerability against SLR by coastal elevation, which models of Gornitz and Shaw adopted, were not very valid approaches for Barcelona. Therefore, the model and study area should be investigated extensively before deciding on the CVI assessment model.

2.4 CVI Applications Along Turkish Coasts

With an 8333 km long shoreline adjacent to four seas with different properties, Turkiye is also threatened by GMSL. Therefore, a few studies have been conducted to determine CVI in the resolution of a specific study area or entire cities. In 2015, Simav et al. published their study on how vulnerable the coastal cities of Turkiye are by considering the parameters of the coastal area, population, vegetation, exposure to natural hazards, topography, and human development. The study's findings indicated that Adana, Aydın, Çanakkale, Balıkesir, and Samsun are the most vulnerable cities against sea level rise. Although obtaining CVI for each coastal city is important to get a general opinion, CVI values of the entire shorelines of cities (between 27.1 km – 1255.6 km in length) are not localized enough to be considered representative. To be more specific, to generate development plans, CVI analysis should be conducted for areas with a smaller scale as done by Ozyurt and Ergin in 2009 for Amasra, Göcek and Göksu Delta, Kuleli and Beyazıt in 2023 for Bodrum peninsula, Ozsahin et al. in 2023 for Thrace Peninsula, Aykut and Tezcan in 2024 for Mersin and Iskenderun Bays. To obtain CVI values of Amasra, Göcek, and Göksu Delta, Ozyurt and Ergin used a model developed by Ozyurt (2007). The model takes 12 physical and seven human parameters as inputs under coastal erosion, flooding due to storm surge, flooding, saltwater intrusion into groundwater resources, and saltwater intrusion into rivers/estuaries. Then, a coastal vulnerability matrix is created using regional data and vulnerability ranks to obtain sub-indices, which would be used to get CVI. Results of the study demonstrated that Amasra was classified as Low vulnerable, and Gocek was Moderate. At the same time, the Göksu Delta was highly vulnerable, although the rise in sea level was the same for Gocek

and Göksu. In the study of Kuleli and Bayazıt (2023), marine-type maritime transportation infrastructure (MTI) locations around the Bodrum peninsula were focused on for CVI calculations. 30m x 30m cells were created from shoreline to 250 m inland, and CVI assessment of this system was conducted using Gornitz 1990 and 1991. Results showed that 3 of 8 MTI locations are very high, 2 of 8 are high, and three are moderately vulnerable.

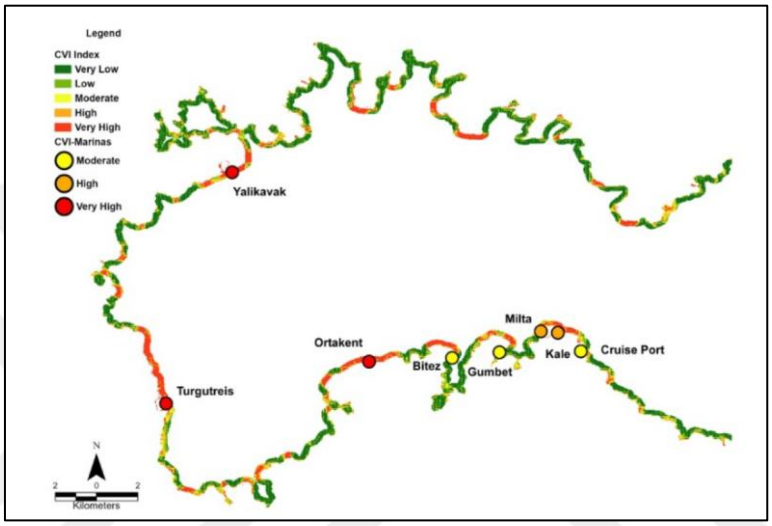


Figure 2.3. Bodrum Peninsula CVI Distribution (Kuleli & Bayazıt, 2023, p. 149)

In 2023, Ozsahin et al. evaluated the vulnerability of the Thrace peninsula against sea level rise. DEM with 5m resolution was used as an input to evaluate the shoreline with a 922 km length. AR6 scenarios for the near-, mid-, and long-term periods and the Thiler-Klose 1999 model were used. According to the authors, the peninsula is susceptible to natural and socio-economic outcomes of SLR. Aykut and Tezcan, in 2024, evaluated Mersin and Iskenderun bays by using the methodology proposed by McLaughlin and Cooper (2010). This methodology uses three sub-indices of Coastal Characteristics (Slope, Geomorphology, Distance to 20m water depth, shoreline change), Coastal Forcing (Significant wave height, tidal range, sea level change projection), and Socioeconomic Factors (Population density, land use, road to coast distance, and protected area). The cell system was constructed as 100m x 100m and from the shoreline to 500 m inland throughout the study area, which has a length of

520 km. Results indicated that 24.7% (128 km) of the studied strip was very highly vulnerable, 27.4% (142 km) highly vulnerable, 23.7% (123 km) moderately vulnerable, and 24.3% (126 km) low vulnerable. The main properties of high and very highly vulnerable areas are erodible geomorphology, gentle slopes, and significant socioeconomic values.

When available databases that would be used for CVI analysis of Turkiye shorelines were investigated, most were denoted as not complete enough (more information is given in Chapter 4). Moreover, since more than one database was expected to be utilized for the majority of parameters, uncertainty related to various incomplete, incompatible databases would be increased.

2.5 Assessment Approaches and Socioeconomic Data Limitations

Many different coastal vulnerability assessment methodologies have been developed using various indices and aggregation systems. According to Hinkel (2011), the reason for this is that since vulnerability is not an observable phenomenon, a standardized methodology to obtain vulnerability has not been agreed upon. Until Cutter's definition of the social vulnerability index in 2003, assessment models maintained a geophysical approach. They did not include socio-economic indices, resulting in higher consistencies among the models compared to those using the social vulnerability index approach. However, different types of available data, depending on the study areas, resulted in the use of various approaches and variables. As a result, the models have less consistency (Roukounis & Tsihrintzis, 2022). Moreover, despite using the variable in the case of tidal range, while some researchers argue that low values of 'tidal range' signify higher vulnerability, others contend the opposite (Roukounis & Tsihrintzis, 2022). Considered indices, calculation approaches, and scale of analyses mainly depend on the aim of the study and where the study is being conducted. For example, according to Nguyen et al. (2016), an index indicating household vulnerability against natural hazards in Mozambique might be inapplicable to Germany. However, the application of the

models for the same country also does not imply consistency between them, as observed in Australia, where although several assessment methodologies were specially developed for the country, the methodologies were not coherent. In order to address the differences between the methodologies, in their study, Bukvic et al. (2020), 65 studies published between 2009 and 2016 were examined, and quantification with respect to parameters such as scale, considered systems, or several considered coastal hazards was conducted. Among the studies, only 22 considered socioeconomic parameters, while 42 of the 65 studies considered natural systems. On the other hand, 39 studies utilized data from a single point in time, while this number dropped to 10 for future projected scenarios. Two main issues related to socioeconomic data are that their availability is significantly affected by developing and developed countries. Even though future scenarios are studied, static socioeconomic data, which only contains information about current status, is often utilized, while physical data, mainly projected data, is considered (Bukvic et al., 2020) (Anfuso et al., 2021). Time dependency of socioeconomic data was also emphasized in older articles, such as the study conducted by McLaughlin et al. in 2002. According to this study, socio-economic parameters such as roads or railways are more straightforward to incorporate into models since these generally occupy defined areas. In contrast, considering land use, especially monetary value, was much more complex since the required data was unavailable. As a result, the authors had to use subjective economic assessment of land use types depending on humans' perceived value. However, this approach raises two issues: land-use alterations and human perception. To sum up, using socioeconomic variables resulted in less harmony among the models due to a few factors. Firstly, researchers have to use different variables since the same data is unavailable throughout all countries, especially in developing countries. However, not having solid rules makes vulnerability analysis models have different kinds of approaches to the issue. Therefore, the same variable could be handled differently among the models.

In other words, despite geophysical variables being mostly agreed on, socioeconomic variables are still subjective. Also, the study's scale, location, and aim must be well-defined to overcome potential data incompatibilities. Secondly, although human usage within the area is a dynamic process, the limited availability of forecasts in human usage datasets has the consequence of using the current situation of the study area with forecasted physical data while assessing future vulnerability.

CHAPTER 3

METHODOLOGY

3.1 Fuzzy Coastal Vulnerability Assessment Model

FCVAM was developed by Dr. Gülizar Özyurt Tarakcıoğlu in 2010 (Ozyurt, 2010). The original version of this model has five modules and 18 input parameters, 11 of which are classified as “Physical Parameters,” and the rest could be denoted as “Human Parameters.” The original five modules were “Coastal Erosion,” “Storm Surge,” “Inundation,” “Salinity Intrusion to Rivers,” and “Salinity Intrusion to Groundwater.” However, the thesis scope did not include “Salinity Intrusion to Rivers” and “Salinity Intrusion to Groundwater” for this study. Therefore, only three modules of the FCVAM model are utilized, which reduced the number of assessment parameters to “7” and “5” for “Physical Parameters” and “Human Parameters,” respectively.

Within the FCVAM, each impact module consists of Physical and Human Inference Systems that build on parameters that describe the physical characteristics of the shoreline and the human activities that impact the shoreline's changes, respectively. Each inference system has its own “IF-THEN” based fuzzy logic rule set along with parameter weights, “Membership Functions” limits of which were defined by K-means clustering methods, and “Aggregation Function” which is ”Probabilistic Or (Probor)” in the case of inference systems. Module vulnerability score is calculated after obtaining results from both physical and impact inference systems. In the case of Module vulnerability score calculations, “Max / Min” aggregation functions are used. CVI is obtained by taking the center of gravity of aggregated module distributions. Detailed information about the theoretical background and calculation steps of FCVAM was given in Ozyurt (2010). In the PhD thesis of Dr. Gülizar Özyurt Tarakcıoğlu, in order to define the membership function limits, the FCM

algorithm provided in the Fuzzy Logic Toolbox of MATLAB was executed over parameter datasets to determine the locations of 5 center points. In Figure 3.1, resultant distributions of the FCM algorithm are provided for RSLR. Using the distributions of the Figure, the membership function of RSLR was generated and provided in Figure 3.2. For further information, please refer to section 6.6.1.2 of PhD thesis of Dr. Gülizar Özyurt Tarakcıoğlu.

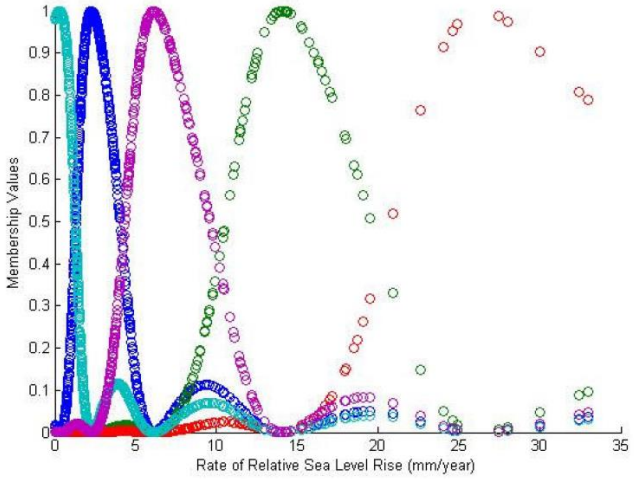


Figure 3.1. RSLR Global Value as 5 Center Points (Ozyurt, 2010, p. 135)

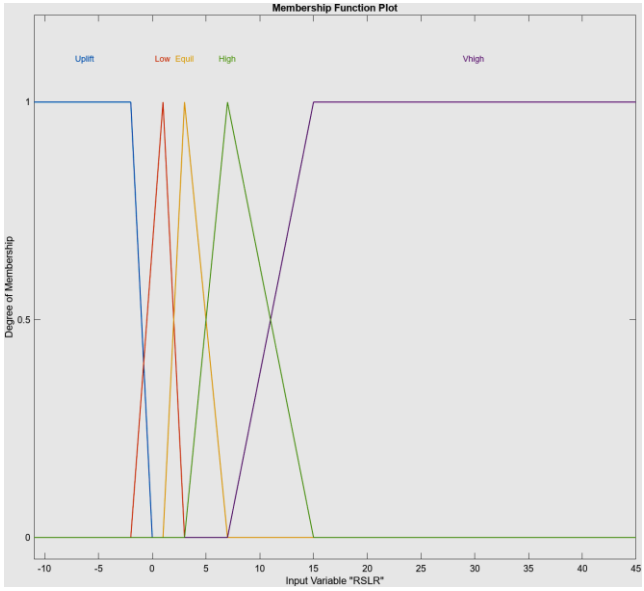


Figure 3.2. RSLR Membership Functions

Depending on the data and approach used while generating membership functions, function limits and function types (trapezoidal, triangular, and crisp) differ for each parameter. After defining each membership function of parameters, the IF-THEN-based linguistic ruleset was constructed for each impact score. Physical, human, and module impact scores are calculated for each module. Figure 3.3 presents the IF-THEN rule of inundation human impact score and the corresponding fuzzy inference system in Figure 3.4.

	Rule	Weight	Name
1	If natdeg is excellent then HIVulInd is vlow	0.63	rule1
2	If natdeg is good then HIVulInd is low	0.63	rule2
3	If natdeg is underpressure then HIVulInd is moderate	0.63	rule3
4	If natdeg is degradation then HIVulInd is high	0.63	rule4
5	If natdeg is majordegradation then HIVulInd is vhigh	0.63	rule5
6	If CPS is none then HIVulInd is vhigh	0.37	rule6
7	If CPS is few then HIVulInd is high	0.37	rule7
8	If CPS is some then HIVulInd is moderate	0.37	rule8
9	If CPS is protected then HIVulInd is low	0.37	rule9
10	If CPS is fully_protected then HIVulInd is vlow	0.37	rule10

Figure 3.3. Example Rule Set

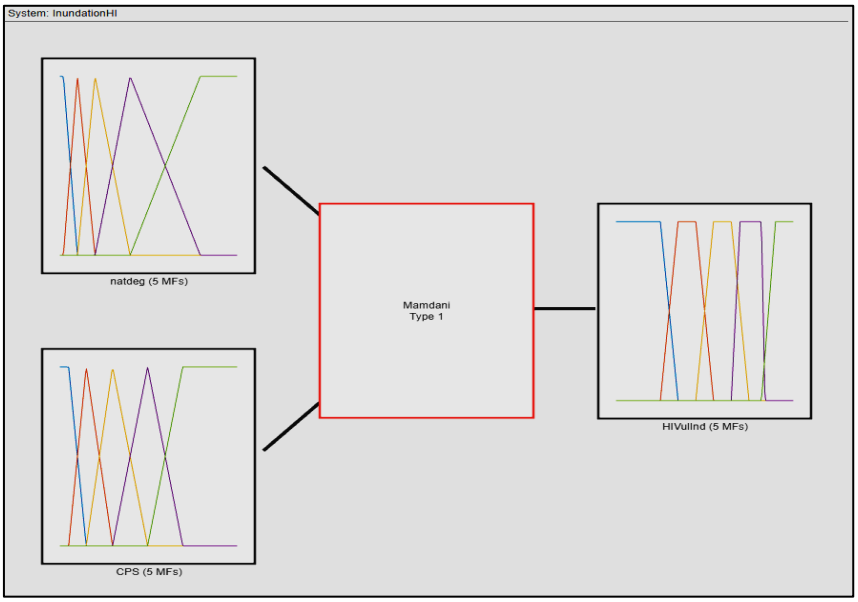


Figure 3.4. Example Fuzzy Inference System

The ruleset algorithm could be explained as, firstly, input values are read by the system. Following this, for each parameter, every rule is checked to see whether the input is within the limits provided by that ruleset or not. Moreover, these rules assign all related parameters to a weight that determines their relative contribution. For example, suppose the natural degradation is within the limits of “good." In that case, the system considers the “good” membership function of natdeg and the “low” membership function of inundation human impact, as given in Figure 3.5. Then, the intersection of the input value with “good” MF is multiplied by the weight of 0.63, and a line is drawn to “low” MF from the weighted value. Intersected area below the line, and the corresponding MF is taken. It should be noted that one input value could be intersected with multiple MFs. Figure 3.6 gives an example of the inundation human impact score calculation process. After controlling each of the rules, determined areas are aggregated, and the impact score is calculated by taking the first moment of the aggregated area.

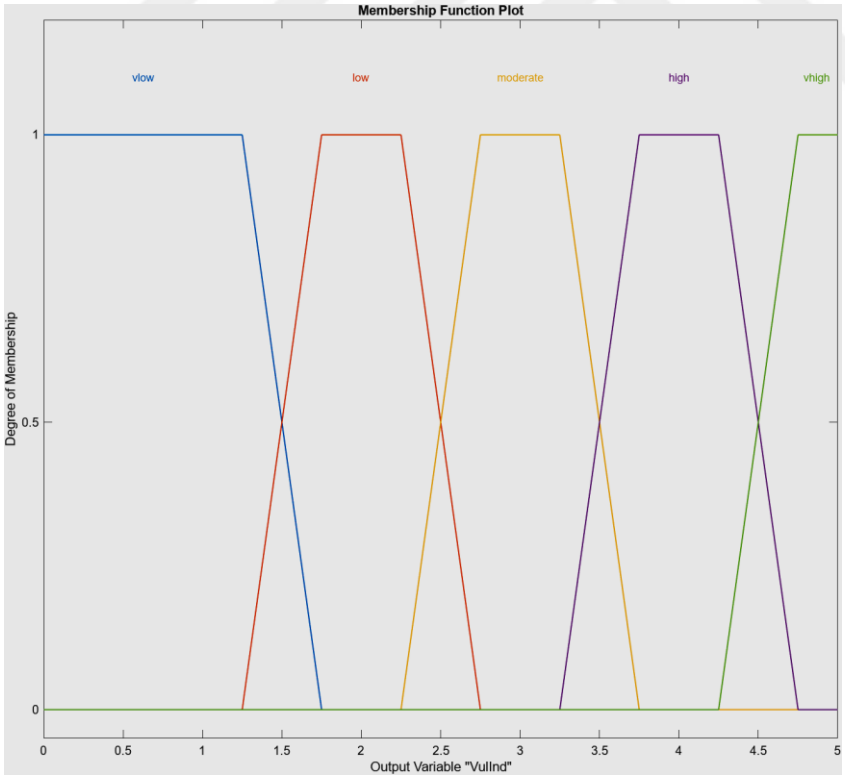


Figure 3.5. Inundation Human Impact Membership Function

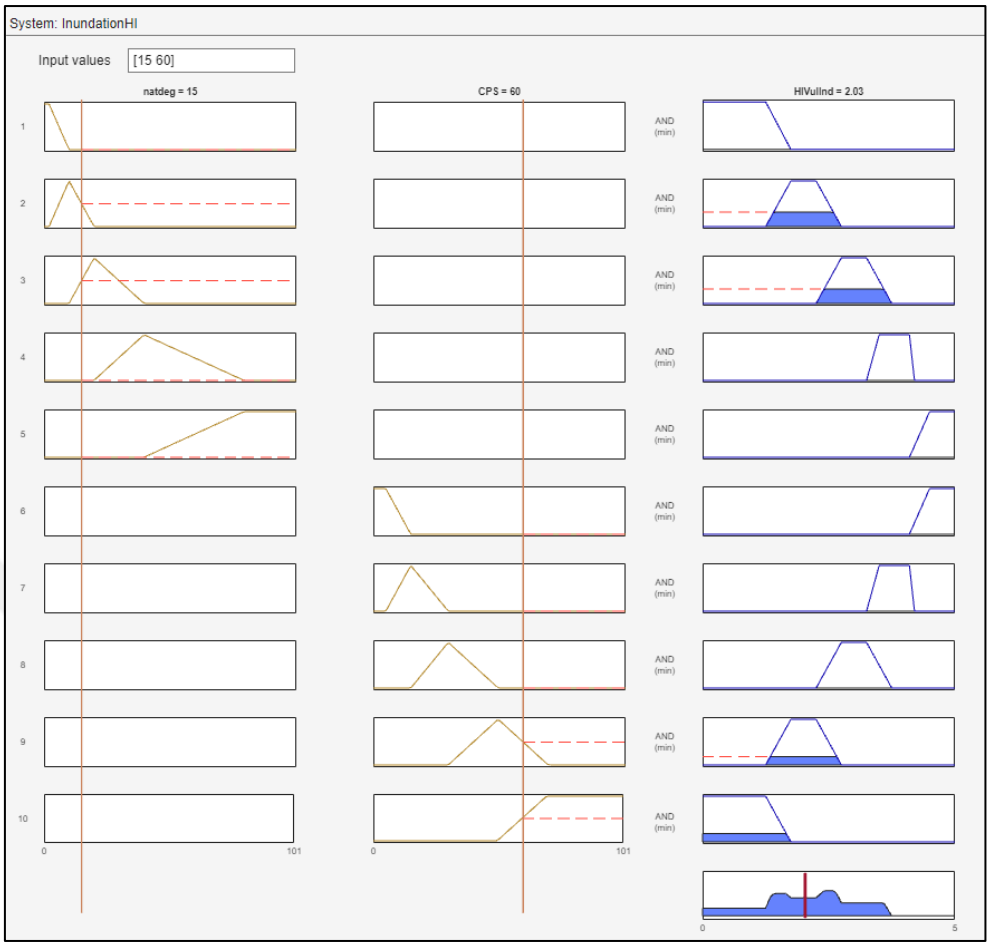


Figure 3.6. Inundation Human Impact Distribution Calculation

After the calculation of physical and human impact scores, the process of obtaining module impact scores also follows the explained steps, but the only difference is that physical and human impact scores have the same weight of 0.5. All of the module distributions are aggregated to calculate CVI, and the first moment of the aggregated area is taken to calculate the center of gravity, which gives CVI. In Table 3.1, model parameters and related module lists are given. Despite being given in the Table, "Reduction of Sediment Supply" was also removed from the FCVAM while applying the model to "Coastal Cultural Heritage Areas" and "Natural Conservation Zones" along Turkish coasts. Reasoning and model changes of this decision were given in Section 3.1.1. Thus, CVI calculations were conducted with 7 "Physical" and 4 "Human" parameters. CVI class definitions are given in Table 3.2.

Table 3.1 Input Parameters and Affected Vulnerabilities of Compact FCVAM

	Parameter Name	**Affected Model Vulnerabilities**
Physical Parameters	Rate of Sea Level Rise (RSLR)	• Inundation • Erosion • Surge
	Geomorphology	• Erosion
	Beach Slope	• Inundation • Erosion • Surge
	Annual mean wave height	• Erosion
	Sediment Budget	• Erosion
	Tidal Amplitude	• Inundation • Erosion • Surge
	Extreme Water Level	• Surge
Human Parameters	Reduction of Sediment Supply	• Erosion
	River Flow Regulation	• Erosion
	Engineered Frontage	• Surge • Erosion
	Natural Protection Degradation	• Inundation • Erosion • Surge
	Coastal Protection Structures	• Inundation • Erosion • Surge

Table 3.2 CVI Classes and Class Limits

CVI Class	**Class Limits**
Very Low Vulnerability	CVI < 1.5
Low Vulnerability	1.5 < CVI < 2.5
Moderate Vulnerability	2.5 < CVI < 3.5
High Vulnerability	3.5 < CVI < 4.5
Very High Vulnerability	CVI > 4.25

3.1.1 Parameter Changes

In the original version of the model, “Reduction of Sediment Supply” was considered as a different parameter for the model. This parameter only affects the natural Module and considers the additional human activities that could change the sediment supply of the region, such as dredging. The impact of rivers and control structures along the rivers are assessed in another parameter, River Flow Regulation. Therefore, the reduction of sediment supply is a significant parameter for locations where urbanization and coastal activities are allowed. However, in the conservation zones of Turkiye, activities such as sand dredging are not allowed. Coupled with the fact that there is no nationwide dataset to observe how sediment supply is affected by human activities, the significance and accuracy of the Reduction of Sediment Supply parameter was considered to be negligible. Additionally, it is assumed that any reduction in sediment supply where the other activities are considered negligible could be addressed only by River Flow Regulation. As a result, “Reduction of Sediment Supply” was removed from the model, and weights of the remaining parameters used in the Erosion – Human Impact module were arranged accordingly by redistributing the original weights. Changes in the parameter weights are given in Table 3.3.

Table 3.3 Parameter Weight Comparison

Parameter	Original Weight	New Weight
Reduction of Sediment Supply	0.4	-
River Flow Regulation	0.13	0.45
Engineered Frontage	0.20	0.23
Natural Protection Degradation	0.12	0.14
Coastal Protection Structures	0.15	0.18

The most significant change was applied to the weight of River Flow Regulation. This is mainly due to the integration of “Reduction of Sediment Supply” into “River

Flow Regulation." In order to compare the model results of the "Original" and "New" weighted models and show that such integration does not impact the model integrity significantly, two different locations were analyzed by taking the AR6 SSP2 4.5 scenario as a basis. The first study area does not contain any river within, and the "Impact Scores" are given in Figure 3.7.

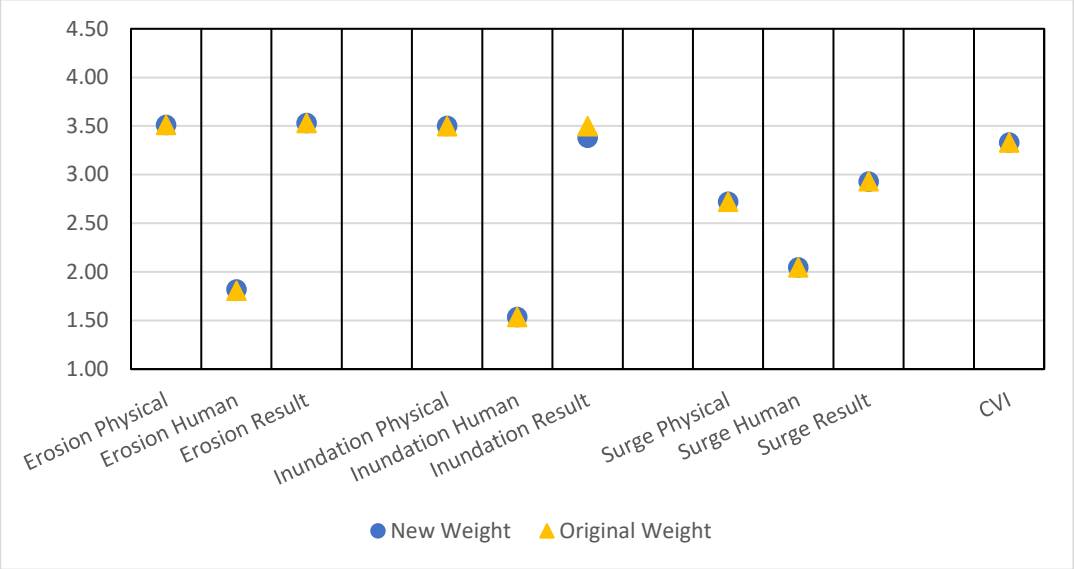


Figure 3.7. First Area Impact Score Comparison with Respect to Weights

The erosion-Human module is the only module affected by both "River Flow Regulation" and "Reduction of Sediment Supply." Thus, this module was expected to be affected by the weight changes in the parameters. For the case of Side, these two parameters were assigned the lowest input value because there was no river within the area. Weight changes in the other parameters increased the Erosion-Human Impact score from 1.81 to 1.82. This increase did not result in any significant increase in Erosion Score and CVI, which stayed at 3.53 and 3.33, respectively.

In the second area, in contrast to the first one, a river affects the shoreline to be studied. To get "River Flow Regulation" for this river, the methodology expressed by Nilsson et al. (2005) was applied, and the score indicated that river flow was affected moderately by human activities. Moreover, "Reduction of Sediment Supply" was also decided as moderately affected because the pre-assumption of

"River Flow Regulation" is the only factor that plays an important role in "Reduction of Sediment Supply" for conservation zones. Impact Scores of the second area are given in Figure 3.8

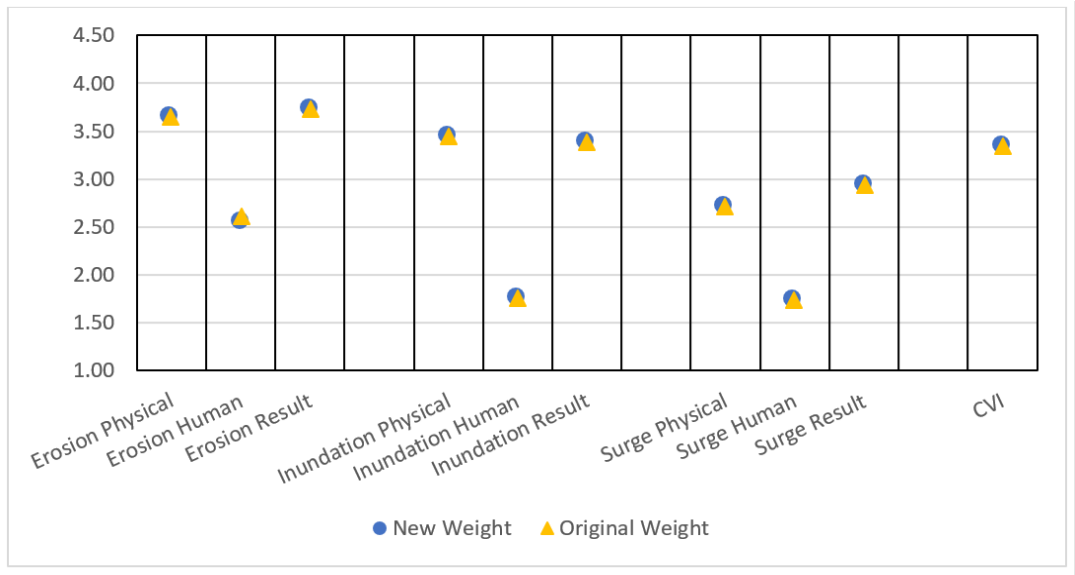


Figure 3.8. Second Area Impact Score Comparison concerning Weights

When the CVI and Impact Scores of the New and Original Weights were compared, the CVI and Erosion vulnerability scores showed no significant change and stayed at 3.73 and 3.35, respectively. Modifications related to reducing sediment supply and river flow regulation resulted in a slight decrease in the Erosion-Human impact score from 2.63 to 2.55. However, it is still considered to be in the same vulnerability range. Other impact scores were not affected significantly.

3.1.2 MATLAB to Python Conversion

The original version of the model was written using the Fuzzy Logic Toolbox of MATLAB, which uses an a Fis file to read fuzzy logic rule sets, membership function properties, parameter weights, and aggregation functions. Figure 3.9 gives a sample view. Depending on the model, built-in functions such as min, max, and Probor could be used.

```
[Input2]
Name='CPS'
Range=[0 100]
NumMFs=5
MF1='none':'trapmf',[0 0 5 15]
MF2='few':'trimf',[5 15 30]
MF3='some':'trimf',[15 30 50]
MF4='protected':'trimf',[30 50 70]
MF5='fully_protected':'trapmf',[50 70 100 100]

[Output1]
Name='HIVulInd'
Range=[0 5]
NumMFs=5
MF1='vlow':'trapmf',[-2.144 -0.2242 1.25 1.75]
MF2='low':'trapmf',[1.25 1.75 2.25 2.75]
MF3='moderate':'trapmf',[2.25 2.75 3.25 3.75]
MF4='high':'trapmf',[3.25 3.75 4.25 4.75]
MF5='vhigh':'trapmf',[4.25 4.75 5 5]

[Rules]
1 0, 1 (0.63) : 1
2 0, 2 (0.63) : 1
3 0, 3 (0.63) : 1
4 0, 4 (0.63) : 1
5 0, 5 (0.63) : 1
0 1, 5 (0.37) : 1
0 2, 4 (0.37) : 1
0 3, 3 (0.37) : 1
0 4, 2 (0.37) : 1
0 5, 1 (0.37) : 1
```

Figure 3.9. Section of Fis File of Inundation Human Impact System

There are a few strong points of this toolbox. Firstly, the toolbox has a built-in "Probabilistic Or (Probor)," which is essential for FCVAM since this function is used as an aggregation function to calculate module impact scores. Second, and the most important one, the Fuzzy Logic Designer package is available on MATLAB, which could be used while creating, examining, and editing fuzzy inference systems since this package includes a rule editor and a control surface creator.

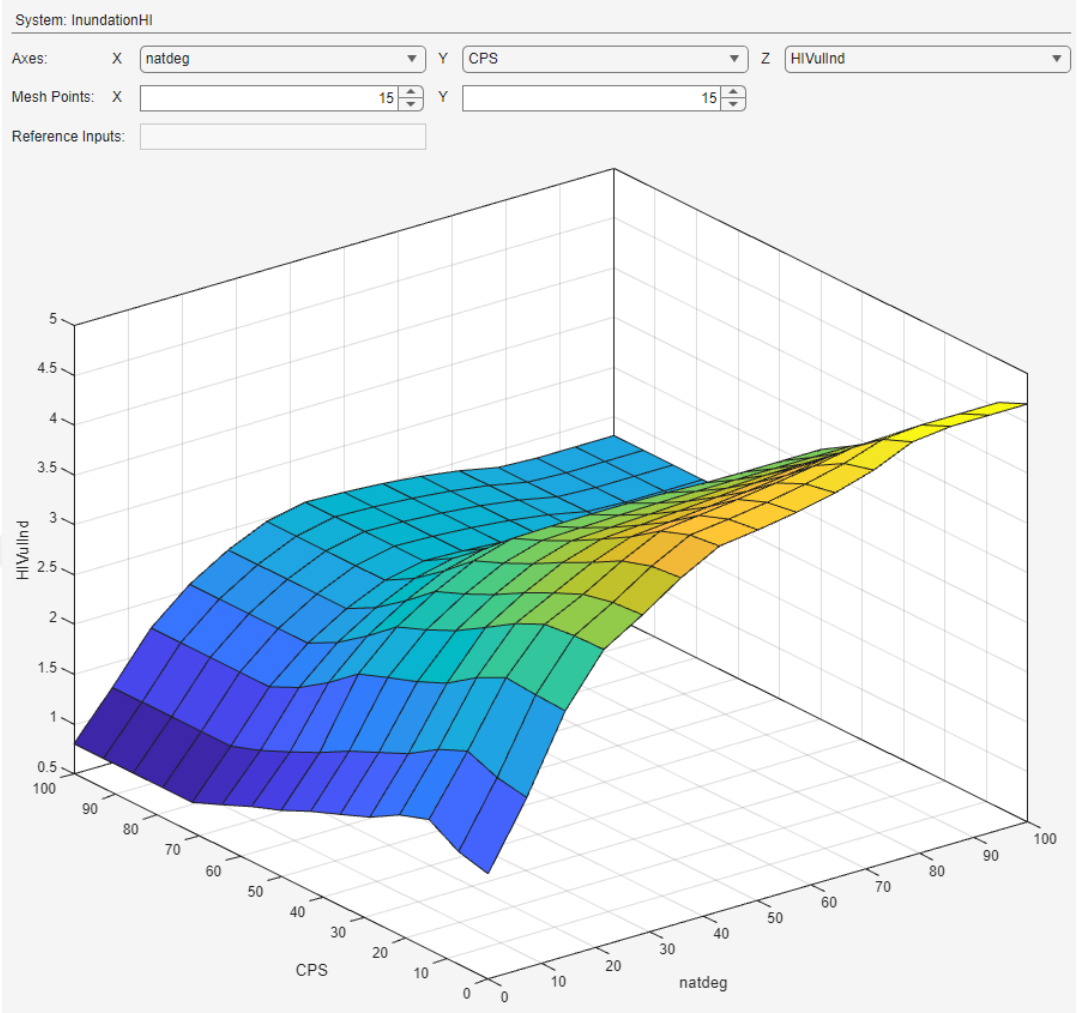


Figure 3.10. Control Surface of Inundation Human Impact

Despite the strong points of the Fuzzy Logic Toolbox, there is a significant drawback: MATLAB is not an open-source language. In other words, MATLAB has a license requirement. In addition, the Fuzzy Logic Toolbox requires an additional license if the user intends to use this toolbox. Therefore, it was decided to rewrite FCVAM using an open-source language. Python was selected since this open-source programming language and a few fuzzy logic libraries were available. Different libraries were evaluated after this decision, and "Simpful (Spolaor et al., 2020)" was chosen. Having all the required MF and a similar structure of fuzzy inference system to MATLAB contributed significantly to this decision.

Although Simpful was chosen as the library to be used, the library did not have all the required features so that FCVAM could be rewritten entirely in Python. The base version of the library lacked a few very crucial capabilities. Firstly, the feature of parameter weights in rule sets was not added to the library. When the source code was checked, it was realized that the library could read the parameter weights; however, it could not utilize them. By making changes, this option became fully operational. Secondly, the library did not have a built-in Probor function. Thus, a Probor function was added to the library's source code. Thirdly, the library was designed to give the result directly instead of iteration points along with the aggregated distributions. Fortunately, the library must create the aggregated distribution to calculate the result. Thus, the source code was modified to write an iteration point with the corresponding value for the executed fuzzy inference system to an external file. Then, the code reads the corresponding external file to calculate the module vulnerability. Finally, aggregated module vulnerability distributions were aggregated again to obtain the distribution of CVI, and the first-degree moment of the distribution was calculated to obtain CVI. All of the modifications were shared with the library publishers.

3.2 Example Study Case

In this section, the model application of an example area is demonstrated. An unnamed “Qualified Natural Conservation Zone,” given in Figure 3.11, located in Dikili, İzmir, was selected to demonstrate how human usage has an impact on vulnerability results by comparing two scenarios of the current situation and higher human usage. Although the Turkish coast has more important and socio-economically valuable natural conservation zones and cultural heritage sites, this area is the only one that has a different river flow regulation score that enables it to show a change in future and natural protection structures that could be degraded but did not. Thus, the alternative scenario could also include river flow regulation and natural protection degradation.



Figure 3.11. Shoreline to be Studied Highlighted as Bold Blue Line

In Table 3.4, current and alternative human usage scenario inputs are given for SSP5-8.5, denoted as "N" and "H," respectively. In scenario "H," only CPS input was kept as it is. To be more specific, river flow regulation was set to the most critical score, and EF was considered to be 85% of the total area. For natural protection degradation, around 5% of the area considered was formed by this type of morphology. Therefore, in the high-usage scenario, all these morphological features were assumed to be destroyed completely.

Table 3.4 FCVAM Inputs of Current and High Usage Scenario

	RSLR	Geo	Slope	Hs	SedBgt	ESL	Tide	Rifrag	EF	NATDEG	CPS
N	11	5	3.21	0.33	-54.55	1.74	0.08	2	11.14	0	1.13
H	11	5	3.21	0.33	-54.55	1.74	0.08	3	85.00	5	1.13

To demonstrate how human input parameters affect the merged area, Figure 3.12 and Figure 3.13 show that human impact membership functions of storm surge are given for both cases. In the current situation, the 1st row of the inference system (MF1 of Natdeg & MF1 of impact score), 6th row (MF1 of CPS and MF5 of impact score),11th row (MF1 of EF & MF1 of impact score), and 12th row (MF2 of EF and

MF2 of impact score) were utilized. After merging and taking the center of gravity of the mentioned human impact MFs, the inundation human impact score was calculated as 1.46.

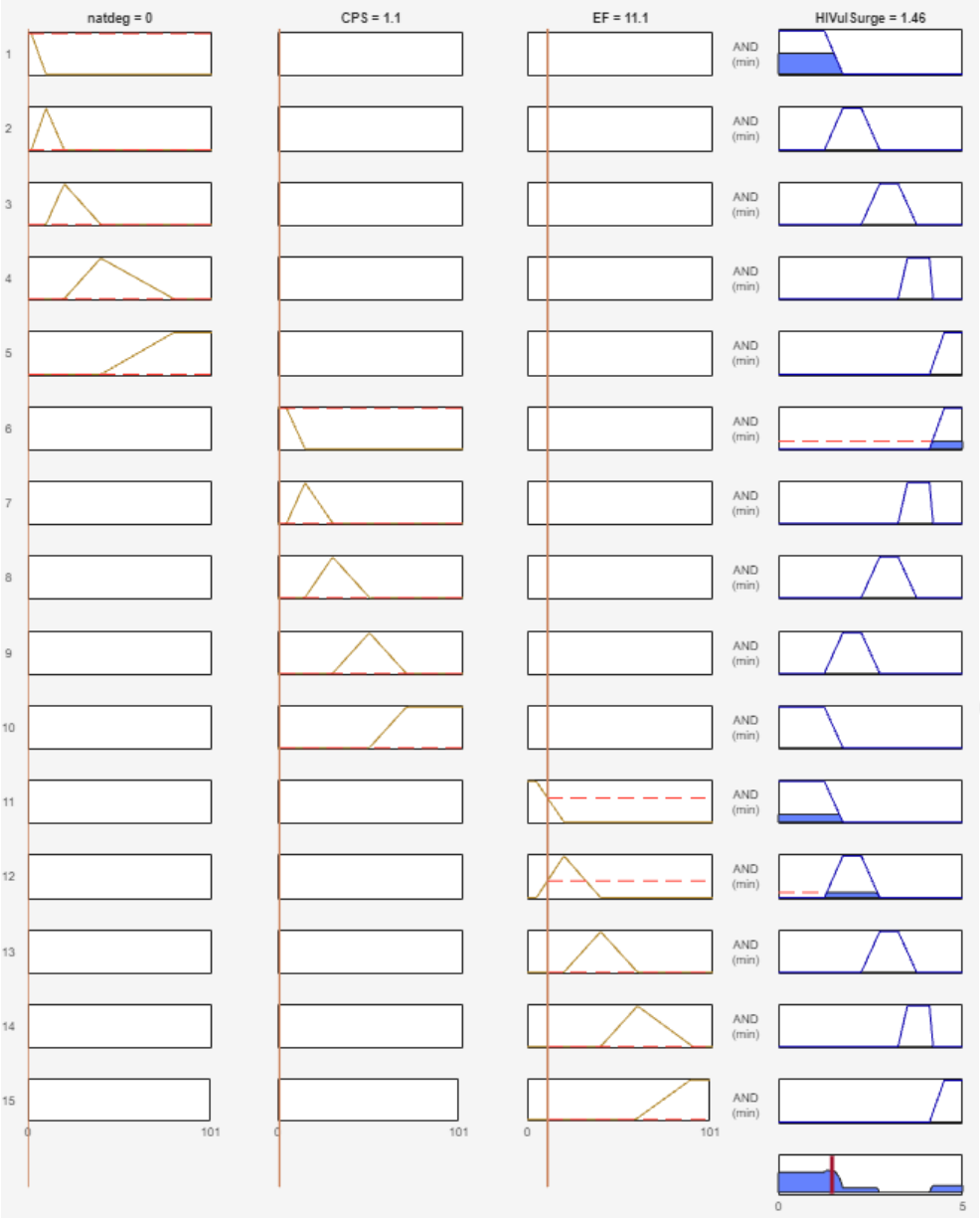


Figure 3.12. Current Storm Surge Human Impact Score Distribution Calculation

In the alternative scenario, Natdeg input had an intersection with Natdeg MF 1 & 2, which were related to MF1 & MF2 of human impact score respectively (in the

original case, MF1 of Natdeg & MF1 of impact score), given in inference system row 1 & row 2. For CPS, since CPS input was not changed, the same ruleset was applied. In the case of EF, MF5 of EF & MF5 of impact score was used, given in the 15th row (originally MF1 of EF & MF1 of impact score and MF2 of EF and MF2 of impact score). Due to these changes, the storm surge impact score was raised from 1.46 to 2.36.

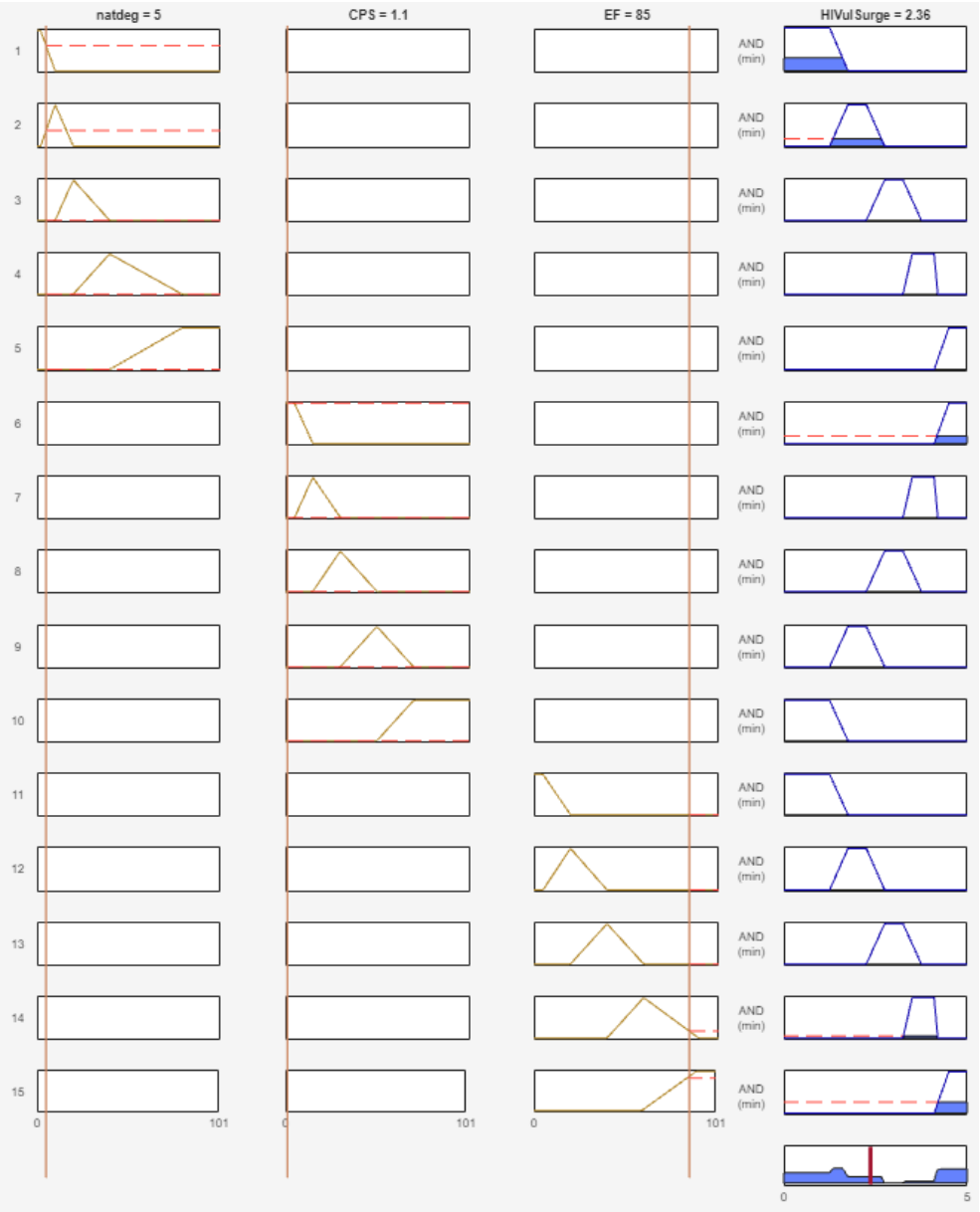


Figure 3.13. High-Use Storm Surge Human Impact Score Distribution Calculation

In Table 3.5, corresponding alternative scenario results are provided. According to the table, the most significant increase was observed in the erosion of human impact since the class changed from low to high vulnerability. Moreover, the erosion impact vulnerability class was also changed from moderate to high vulnerable due to increased human impact scores. In the case of other modules, although inundation and storm surge human impact scores increased, inundation and storm surge impact scores stayed the same. However, an increase in the erosion impact score also increased the CVI score. As a result, the CVI class became highly vulnerable, which was initially moderately vulnerable. In Figure 14, score changes are presented.

Table 3.5 Results of Current and High Usage Scenario

	E-PP	E-HI	E-Sc	I-PP	I-HI	I-Sc	S-PP	S-HI	S-Sc	CVI
N	3.16	2.34	3.00	4.00	1.69	4.00	2.86	1.46	3.00	3.37
H	3.16	3.56	3.62	4.00	2.04	4.00	2.86	2.36	3.00	3.57

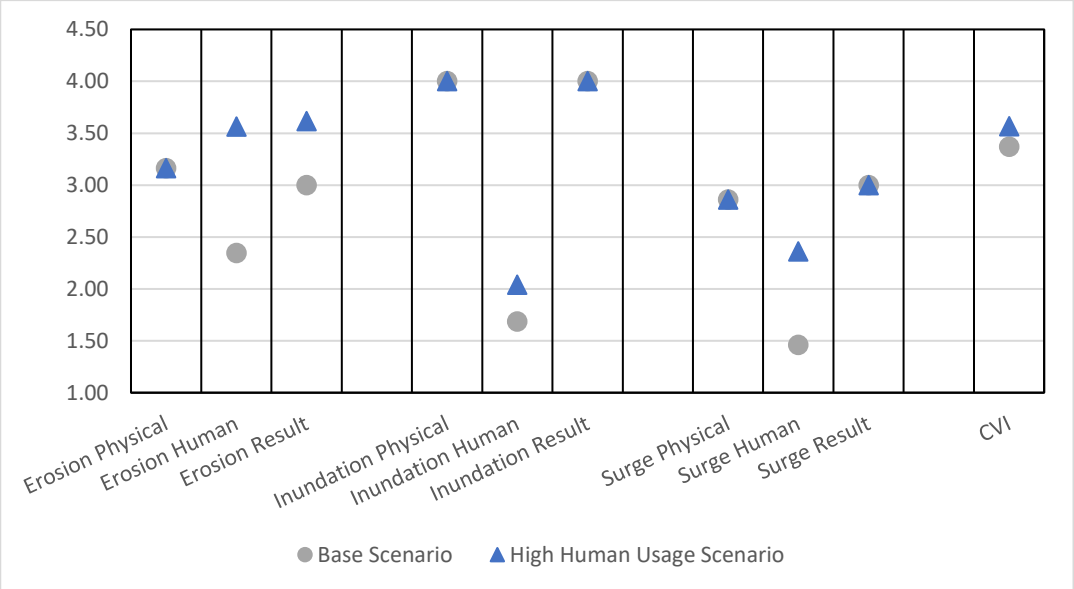


Figure 3.14. Results of Current and High Usage Scenario

3.3 Jenks Natural Breaks

In order to determine how the obtained corresponding results of Türkiye could be arranged into different classes based on the range of site specific data rather than the global classification of FCVAM model, Jenks Natural Breaks, proposed by George Frederick Jenks in 1967, was applied using five classes via ArcGIS. The method's primary goal is to ensure minimal variance within the class while maximizing the variance between the classes. In other words, the class breaks group data with similar values together. To achieve this, Jenks Natural Breaks follows an iterative algorithm. Firstly, the algorithm is taken in the data and the number of classes. Secondly, input class numbers minus one initial class boundary are generated, whether uniform or random. Thirdly, the mean of the initial class boundaries is calculated, and the sum of squared deviations between the mean and individual data points is computed to obtain the total sum of squared deviations. Lastly, the total sum of squared deviations is also computed by considering the mean value of adjacent classes to check whether the value could be reduced. The procedure is repeated until the total sum of squared deviations becomes smaller than the threshold level (Smith et al., 2018). After obtaining the Jenks Natural Breaks, the class distribution pattern considering these breaks and the classes defined in FCVAM were compared. This comparison provides insight into how the data's inherent limits deviate from the class limits defined by considering global results.

CHAPTER 4

DATASETS & PRE-PROCESSING

4.1 Studied Shorelines

While selecting coastal areas for study, the first step was to identify Cultural Heritage sites and Natural Protection areas that were located within 1 km of the coastline and had an elevation of no more than 10 meters. During these calculations, each area's geographical center and average elevation values were evaluated, and areas meeting the criteria were recorded. Two groups examined these areas: Cultural Heritage sites and Natural Protection Zones. A 1 km buffer zone was applied to each area. After this, the resulting regions intersected with the coastline. The working areas obtained from the intersections were reviewed individually, and modifications were made where necessary.

The first issue encountered was that intersections occurred on both sides of the peninsula, on opposite coastlines, especially in narrow peninsulas. To resolve this, each area was first examined to determine which side of the peninsula the coastline was on, and the intersections on the opposite side were removed. The second issue appeared in narrow coves or bays. When a buffer zone was applied to the areas within narrow coves or bays, intersections were observed on the opposite coastlines. Since the Coastal Vulnerability Index (CVI) analysis on the opposite coastlines could not accurately represent the CVI score of the working area, necessary corrections were made on those coastlines as well. Thirdly, the study area needed to be located along the mainland coastline. In other words, islands' intersections were not considered part of the study area and were removed from the layer. After filtering, 1171 Natural Protection Zones and 1176 Cultural Heritage Sites were studied in this thesis.

4.2 Model Input Parameters

3 module version of the FCVAM model (Erosion, Inundation, and Surge) requires seven physical and four human input parameters. However, databases that use the input parameters that would be obtained could not be used in raw format. In other words, data that would be used to derive input parameters require some preprocessing step. In the following section, both the data for input parameters and the preprocessing steps are explained in detail.

4.2.1 Rate of Sea Level Rise

In order to obtain the sea level rise data, the IPCC AR6 databank with 1° resolution was selected. In AR6, there are five different SLR scenarios, which are SSP1-1.9 "Very Low," SSP1-2.6 "Low," SSP2-4.5 "Medium," SSP3-7.0 "High" and SSP5-8.5 "Very High." In this study, all of the scenarios were used with respect to data assigned to 2100. Moreover, extreme sea level data was also adjusted to the RSLR scenario being used.

Available RSLR data requires preprocesses before use. In more detail, the database was downloaded for each available geographical latitude–longitude pair next to Turkish Coasts. Then, available data were grouped with respect to latitude-longitude coordinates instead of the RSLR scenario. After that, a Python script was prepared, which reads all the downloaded data, filters the medium confidence interval, and groups the data with respect to scenarios and corresponding years. The output file has a CSV extension; thus, it was added to the GIS environment as an XYZ file. After the dataset preparation process was completed, data were assigned to the corresponding study area by spatial join function. Figures 4.1-4.5 and Tables 4.1-4.5 present the input data distribution used in the study areas.

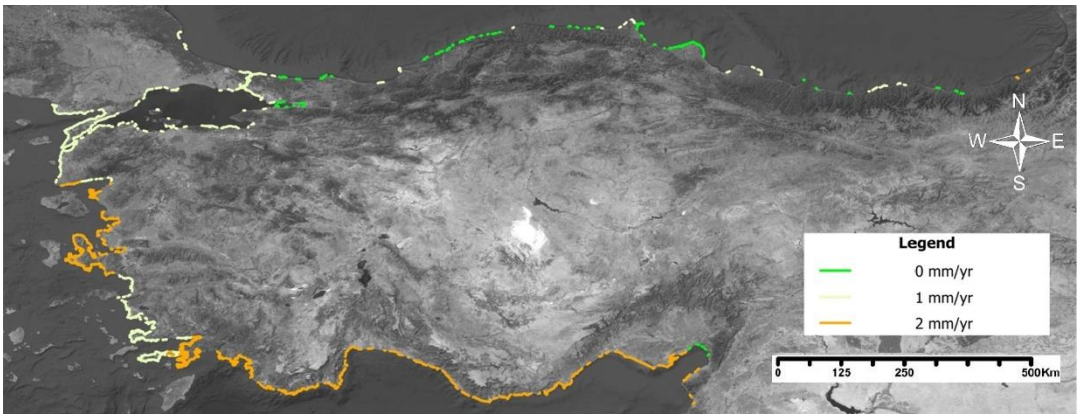


Figure 4.1. SSP1-1.9 RSLR Input Distribution Over Shorelines

Table 4.1 SSP1-1.9 RSLR Input Distribution Over Shoreline Types

RSLR SSP1 1.9	**0 mm/yr**	**1 mm/yr**	**2 mm/yr**
Cultural Heritage	128	524	524
Natural Conservation	74	566	531

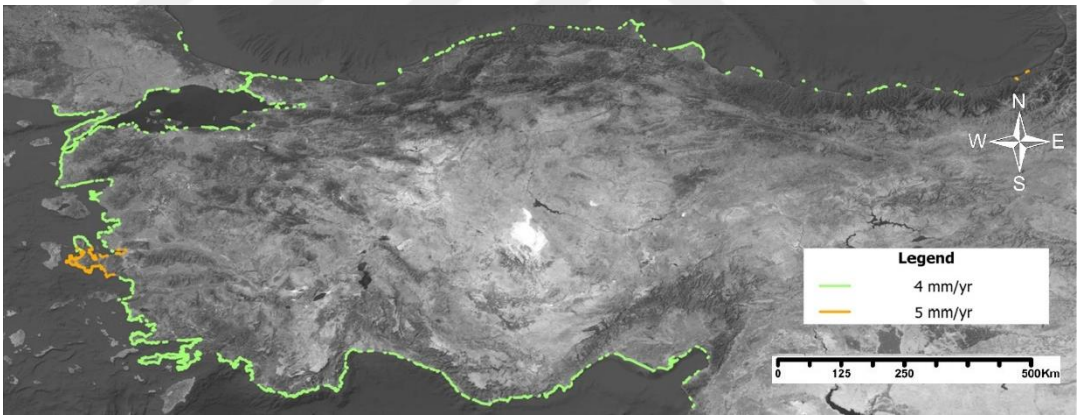


Figure 4.2. SSP1-2.6 RSLR Input Distribution Over Shorelines

Table 4.2 SSP1-2.6 RSLR Input Distribution Over Shoreline Types

RSLR SSP1 26	**4 mm/yr**	**5 mm/yr**
Cultural Heritage	1105	71
Natural Conservation	1046	125

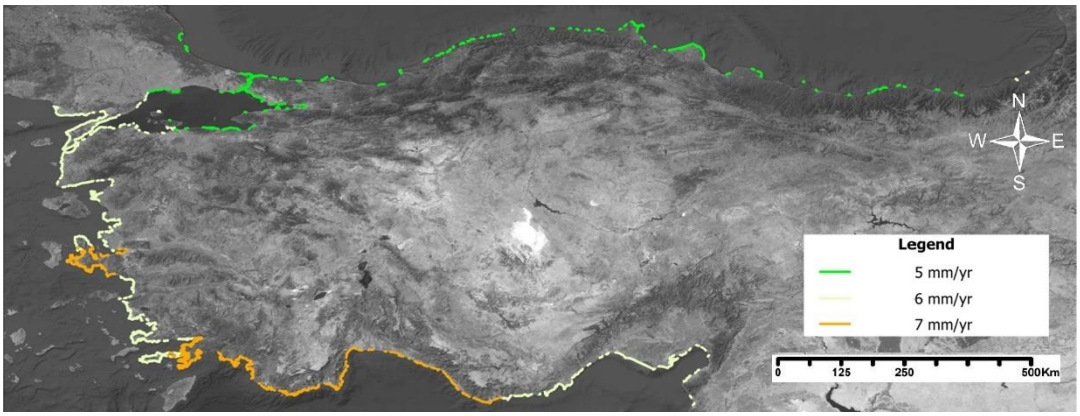


Figure 4.3. SSP2-4.5 RSLR Input Distribution Over Shorelines

Table 4.3 SSP2-4.5 RSLR Input Distribution Over Shoreline Types

RSLR SSP2 45	**5 mm/yr**	**6 mm/yr**	**7 mm/yr**
Cultural Heritage	214	617	345
Natural Conservation	346	473	352

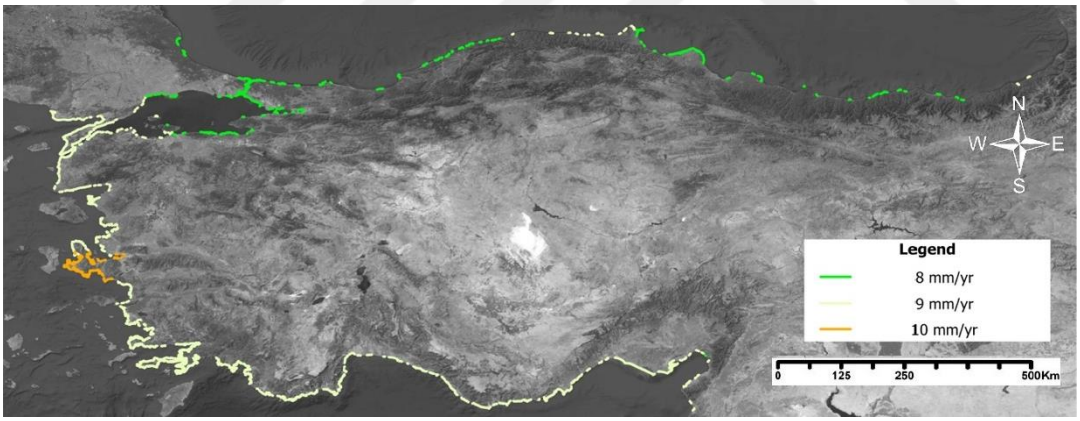


Figure 4.4. SSP3-7.0 RSLR Input Distribution Over Shorelines

Table 4.4 SSP3-7.0 RSLR Input Distribution Over Shoreline Types

RSLR SSP3 70	**8 mm/yr**	**9 mm/yr**	**10 mm/yr**
Cultural Heritage	201	904	71
Natural Conservation	333	715	123

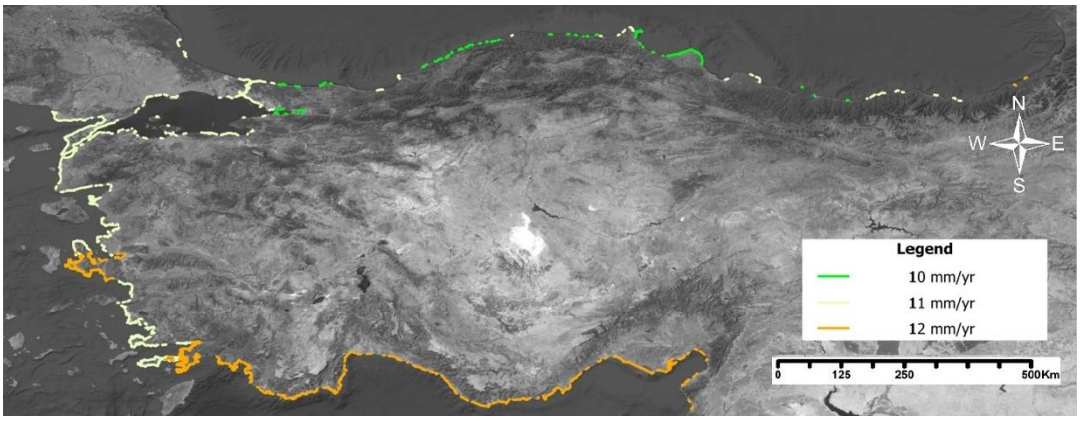


Figure 4.5. SSP5-8.5 RSLR Input Distribution Over Shorelines

Table 4.5 SSP5-8.5 RSLR Input Distribution Over Shoreline Types

RSLR SSP5 85	**10 mm/yr**	**11 mm/yr**	**12 mm/yr**
Cultural Heritage	122	603	501
Natural Conservation	68	701	402

4.2.2 Geomorphology

While investigating the geomorphology of the studied shoreline, both lithology and surface structure were considered. Since no geomorphology dataset completely encompasses Turkish coasts, a set of databases was combined with an algorithm to obtain which group these shorelines belong to by the definitions used in FCVAM, given in Table 4.6.

Table 4.6 Geomorphology Class Definitions

Class	**Geomorphology Type**
Group 1	Rocky cliff coasts, fiords
Group 2	Medium cliffs, indented coasts
Group 3	Low cliffs, glacial drift, alluvial plains
Group 4	Cobble Beaches, estuary, lagoon
Group 5	Sand – Barrier beach, salt marsh, mudflats, deltas, mangrove, coral reefs

The first step is using classification or scoring, conducted manually if available. This process was utilized mainly for the Black Sea Region since this region is where the databases lack the most. After the determination of shorelines to be studied, one by one, they were assigned to a geomorphology type. However, this method was avoided whenever possible since it is subjective and time-consuming. Secondly, if the studied shoreline was classified as "Group 5" according to Coastal Zones Land Cover/Land Use 2018 (EEA, 2021), a geomorphology score of 5 was assigned. This dataset uses a 5-digit code to provide information about land cover; thus, codes related to geomorphology were initially identified and categorized to match the groups to be used as inputs. Although this dataset includes geomorphological features of different classes, it was observed that Coastal Zones Land Cover/Land Use 2018 successfully detected Group 5 features of sandy beaches, dunes, inland marshes, and salines. Thirdly, the Coastal Type 0-80K dataset (Emodnet, 2021) was checked to determine whether the studied shoreline was assigned a geomorphology value from this dataset. For Turkish coasts, the geomorphology data could be grouped into Group 4 and Group 5, as only the geomorphological features of these two groups are available for Turkish shores in this dataset. Scoring classifications are given in Table 4.7.

Table 4.7 Coastal Type 0-80K Geomorphology Group Definition (Emodnet, 2021)

Geomorphology	**Score**
Artificial beach	5
Beach that is part of extensive non-cohesive sedimentary systems (barrier, spit, tombolo)	4
Beach with beach rock	4
Estuary	4
Sand beach fronting upland (> 1 Km long)	5
Vegetated beach	4

Fourthly, the Mediterranean Coastal Database—MEDCD (Wolff et al., 2018) classes and scores were considered. The data classification of this dataset is given in Table 4.8. However, the main drawback of this database is that no data is available around

the Black Sea. Also, available data is not continuous. In other words, this database contains information only at specific locations.

Table 4.8 MEDCD Geomorphology Group Definition (Wolff et al., 2018)

Geomorphology	**Score**
Sand	5
Unerodable	2
Mud	5
Rock with Pocket Beaches	3

Fifthly, the Coastal Zones Land Cover/Land Use 2018 (EEA, 2021) classification from Group 1 to Group 4 was checked. In Table 4.9, group details are given. As in the second step, if they contain geomorphological information, 5-digit codes were allocated to a specific geomorphology class and score.

Table 4.9 EEA Land Use Geomorphology Group Definition (EEA, 2021)

Geomorphology	**Score**
Shingle beaches	4
Bare rocks and outcrops	2
Coastal cliffs	2
Glaciers and perpetual snow	3
Lagoons	4
Estuaries	4
Marine inlets and fjords	1

The last step is using the database given in the study of Mao et al. (2022) named "Evaluating Coastal Vulnerability on the global scale." This database was generated by image processing methods and contains three types of geomorphologies grouped into two classes given in Table 4.10.

Table 4.10 Mao et al. (2022). Geomorphology Group Definition

Geomorphology	**Score**
Beach	5
Bedrock	2
Wetland	5

Figure 4.6 shows the geomorphology input distribution for natural conservation zones and coastal cultural heritage site projections over shorelines nationally.

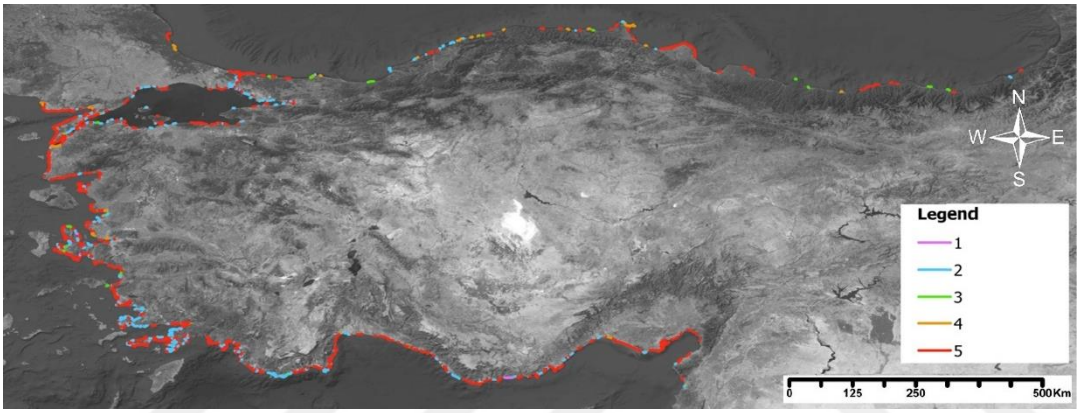


Figure 4.6. Geomorphology Class Distribution Map

The Figure shows that the majority of shorelines to be studied were assigned to class 5. In other words, regarding geomorphology, corresponding shorelines demonstrate very high vulnerability. Table 4.11 presents class distributions with respect to two types of projected shorelines, which also supports the claim.

Table 4.11 Number of Locations within Geomorphology Classes

Geomorphology	**Class 1**	**Class 2**	**Class 3**	**Class 4**	**Class 5**
Cultural Heritage	5	493	33	58	587
Natural Conservation	37	369	32	28	705

The main limitation of generating this parameter is that there is no complete geomorphology dataset for Turkish coasts. Different datasets were used with an

algorithm mentioned in this chapter to overcome this issue. However, especially for unerodable features, the sets do not consider parameters such as how high the cliff is. Cliff height is a determinant factor for unerodable features, and for cliffs, depending on the height, the input score might change between 1 and 3. Also, features such as indented coasts were not considered in datasets. On the other hand, while assigning a score to a shore, if there are intersections of multiple different features, the most critical of them was considered. However, even though it was attempted to be minimized, there have been some encounters in which geomorphology was assigned wrong. For example, on rare occasions, the dataset proposed by Mao et al. (2022) confuses bedrock with the beach. Such discrepancies were tried to be corrected as much as possible.

4.2.3 Beach Slope

This parameter indicates how elevation change occurs within the area to be studied. Since no database solely focused on the slope around the Turkish Coasts was found, the slope was derived using bathymetry and Digital Elevation Maps (DEM). The first database investigated was EU-DEM v.1.1 2016 (EEA, 2016). However, during the parameter-deriving process, the dataset was archived. Thus, alternative ones were sought for DEM. Copernicus GLO-30 (ESA, 2024) with 30 m resolution was selected as the DEM database. EMODnet Digital Bathymetry DTM 2022 (EMODnet Bathymetry Consortium, 2022) Tiles 7 and 8 were preferred for bathymetry. However, zero slope bands were observed near the shoreline after the slope map was generated using only a combination of these two datasets. When the elevation values of the combined dataset were checked, the reason for this issue was noticed, which was 0 m depth values near the shoreline, although, in real life, those areas are covered with sea. To overcome this issue, available SHOD maps in contour form were used. These maps were in dwg format, which requires the deletion of unnecessary lines, such as map frames, since GIS software misinterprets them as topographical features. Then, a contour map of EMODnet Digital Bathymetry DTM 2022 with 10 m

intervals was created, and data between 0 – 50m depth was replaced by SHOD contours data of 0 to 50m depth. Moreover, the 2018 EEA shoreline contour was integrated into the generated contour map. The new contour map was converted to a raster format and merged with the Copernicus GLO-30 dataset. While there are minor differences due to replacing the 0-contour line with the EEA 2018 shoreline, the overall pattern of the maps is acceptable, as shown by the comparison of elevation data distribution in Figures 4.7 and 4.8. This is particularly relevant for creating a slope map. After generating the slope map, the average slope within 30 meters of each study shoreline was calculated and used as input.

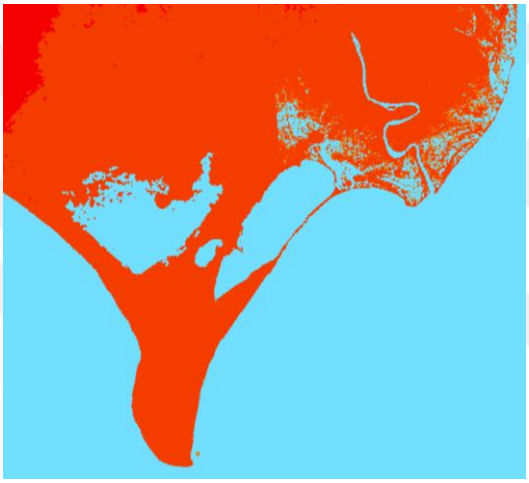


Figure 4.7. DEM with First Methodology

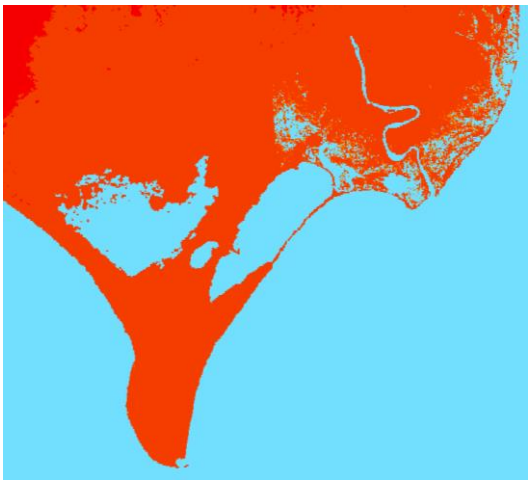


Figure 4.8. DEM with Second Methodology

Figure 4.9 presents the slope characteristics of the analyzed shorelines. As anticipated, steeper slopes are predominantly observed in the Mediterranean region, attributed to cliff formations.

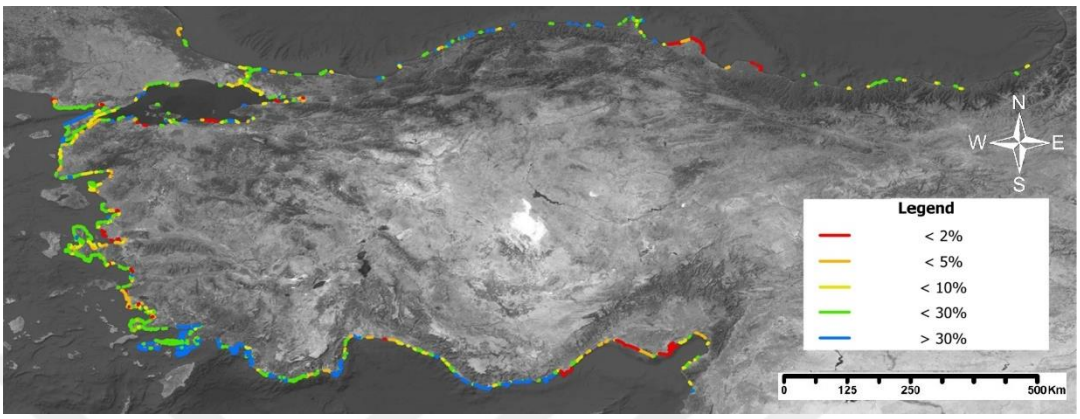


Figure 4.9. Beach Slope Class Distribution Map

Table 4.12 Number of Locations within Beach Slope Classes

Beach Slope	**< 2%**	**< 5%**	**< 10%**	**< 30%**	**> 30%**
Cultural Heritage	47	162	262	540	165
Natural Conservation	49	112	186	637	187

Table 4.12 provides a detailed breakdown of slope distribution across various categories. According to the data, slopes ranging from 10% to 30% represent the most frequent category, likely due to the shoreline locations along the Aegean Sea, where slopes typically fall within this range.

4.2.4 Annual Mean Wave Height

Annual mean wave height is one of the physical parameters used as an input to FCVAM that reflects the wave energy to drive possible shoreline change. In order to obtain a representative Annual mean wave height value for a study area, the ERA5 Re-analysis dataset generated by Copernicus Climate Change Service was used. In this dataset, in addition to the historical wave time series calculated using the re-

analysis of ERA5 wind data, future time series projections are derived from climate projections. For Turkiye, projections have a resolution of 30 km. From the dataset, the hourly time series between the years 1976-2017 was extracted as a NetCDF file. In the MATLAB environment, extracted hourly time series were cropped for Turkish coasts, and Annual mean wave height values were obtained for each year and location. Finally, the average of every year's data was taken, and the parameter was obtained. The class distribution map and number of locations within groups are given in Figure 4.10 and Table 4.13, respectively.

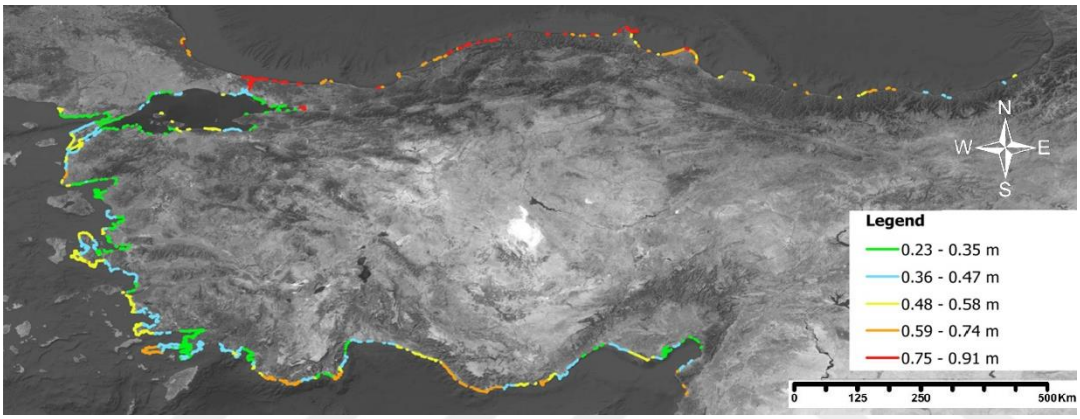


Figure 4.10. Wave Climate Class Distribution Map

Table 4.13 Number of Locations within Wave Climate Classes

Annual Mean Wave Height	**0.35m - 0.23m**	**0.47m - 0.36m**	**0.58m - 0.48m**	**0.74m - 0.59m**	**0.91m - 0.75m**
Cultural Heritage	255	421	270	153	77
Natural Conservation	251	396	225	94	205

The annual mean wave height parameter determines the wave climate of the corresponding study area. Therefore, the data should be located within a certain distance of the study area. In the case of more complex morphology, it is not preferable for land features to be located between the nearest data point and the study area. In Figure 4.11, the area emphasized with a yellow-lined rectangle is named Dardanelles.

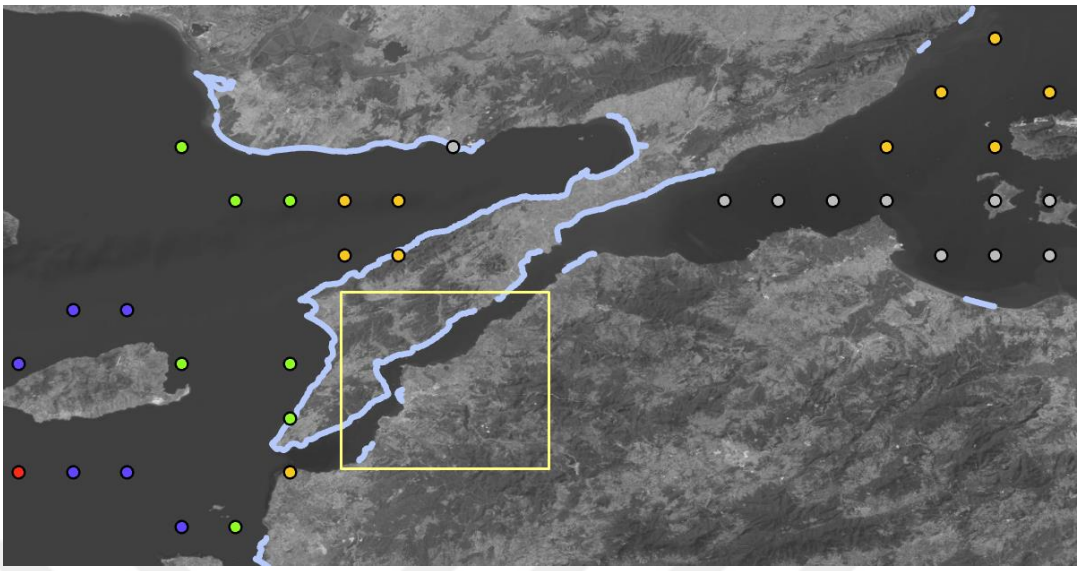


Figure 4.11. Study Shorelines within Dardanelles

Bold magenta lines indicate study areas, while dots are Annual mean wave height data points. The issue is that the database does not contain any data inside the strait. Thus, some of the study areas located inside the strait assigned Annual mean wave height data located on the other side of the Gallipoli Peninsula.

4.2.5 Sediment Budget

The sediment budget was examined using the Coastal Migration Via Satellite Data of the EMODNET database (EMODNET, 2023). This dataset identifies coastal line changes observed between 2007 and 2017 through satellite imagery, providing annual rates of change at 500-meter intervals. In the coordinate point data obtained from the EMODNET database, coastal line recession is represented by erosion rates smaller than -2 m/year, while a neutral coastal line is indicated by rates between -2 m/year and 2 m/year. Accretion is represented by values greater than 2 m/year. To determine the FCVAM input value, the intersection of EMODNET data nodes with assessed shorelines was analyzed to understand the trend of the shoreline (accretion, stable, or erosion) through a percentage of the behavior along the shoreline and the dominant behavior identified from these intersections was used.

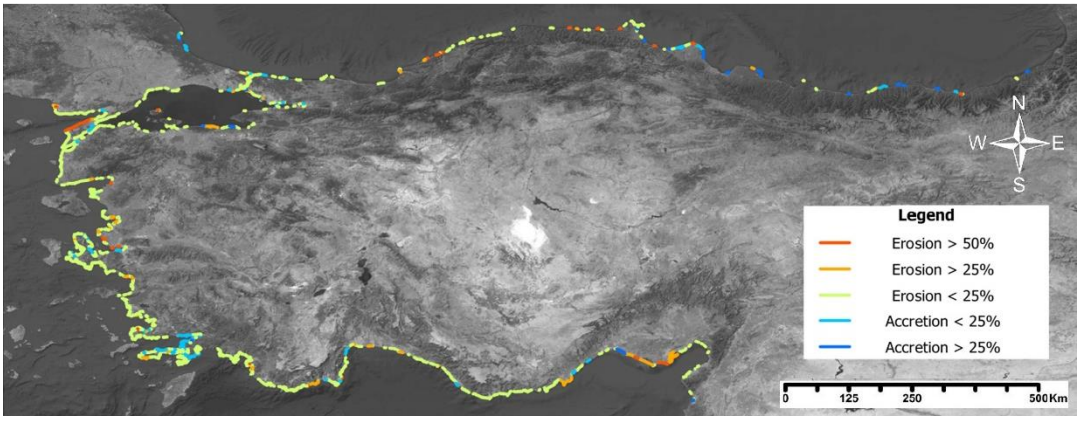


Figure 4.12. Sediment Budget Class Distribution Map

Figure 4.12 and Table 4.14 present shoreline behavior breakdowns. Shoreline projections of coastal cultural heritage areas demonstrate accretion. For natural conservation zones, shorelines mainly accumulate between erosion < 25% and Accretion < 25%. The main drawback of the used dataset is that at specific locations, the node contains unrealistic information (-99.99 m/year erosion as an example). Moreover, especially at bays, no data is available. Thus, data was manually matched with the shoreline.

Table 4.14 Number of Locations within Sediment Budget Classes

Sediment Budget	**Erosion > 50%**	**Erosion > 25%**	**Erosion < 25%**	**Accretion < 25%**	**Accretion > 25%**
Cultural Heritage	36	28	3	1096	13
Natural Conservation	23	104	376	580	88

4.2.6 Extreme Sea Level

Extreme sea level data is one of the physical parameters that is used as an input to FCVAM that covers the accumulated value of tide, storm surge, and sea level rise at the selected area. The scenario selected for this parameter was selected by considering the scenario used in the RSLR parameter. The database used in this thesis was generated within the LISCOAST project (Vousdoukas, 2018) for

European coasts. The database presents the components of ESL, such as Tide, Sea Level Rise, and Storm Surge data. For the calculations, 2100 forecasted values were considered for RCP 4.5 and RCP 8.5 scenarios. After the filtering process, data were cropped for Turkish coasts. In Figures 4.13 and 4.14, extreme sea level distributions over the shoreline to be studied were demonstrated for Lisflood data generated by using AR5 RCP 4.5 and RCP 8.5. While calculating CVI for SSP2 – 4.5, Lisflood data generated by AR5 RCP 4.5 was used, and for SSP5 – 8.5, Lisflood data by AR5 RCP 8.5 was considered. Detailed data distribution with respect to the studied shoreline is given in Tables 4.15 and 4.16.

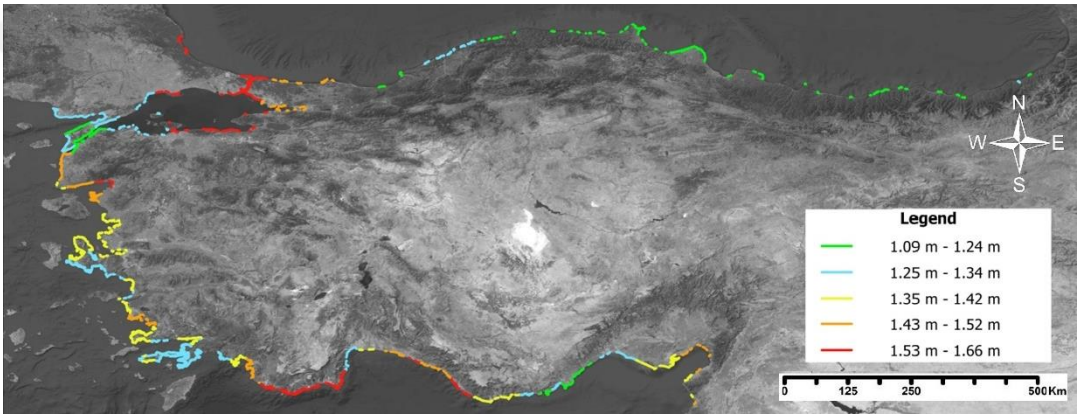


Figure 4.13. SSP2-4.5 Extreme Sea Level Class Distribution Map

Table 4.15 Number of Locations within SSP2-4.5 Extreme Sea Level Classes

ESL SSP2 45	**1.24 m - 1.09 m**	**1.34 m - 1.25 m**	**1.42 m - 1.35 m**	**1.52 m - 1.43 m**	**1.66 m - 1.53 m**
Cultural Heritage	163	292	338	224	159
Natural Conservation	88	310	367	134	272

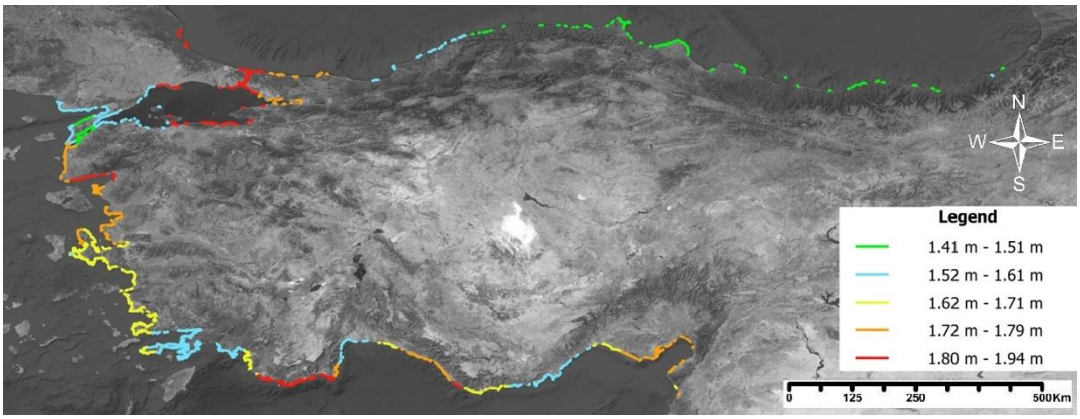


Figure 4.14. SSP5-8.5 Extreme Sea Level Class Distribution Map

Table 4.16 Number of Locations within SSP5-8.5 Extreme Sea Level Classes

ESL SSP5 85	**1.51 m - 1.41 m**	**1.61 m - 1.52 m**	**1.71 m - 1.62 m**	**1.79 m - 1.72 m**	**1.94 m - 1.80 m**
Cultural Heritage	52	352	400	231	141
Natural Conservation	50	285	378	166	292

4.2.7 Tidal Range

The tidal parameter affects indicators of permanent inundation, coastal erosion, and periodic flooding within the vulnerability model that accounts for sea level rise impacts. In this project, tidal data was obtained from the FES2014 dataset provided by AVISO Altimetry. This global dataset has a resolution of 1/16° and includes all tidal components individually. The FES2014 data was acquired in NetCDF format, processed in MATLAB to focus on Turkey's coastline, and converted to a comma-separated values (CSV) file. Turkey is located in a micro-tidal region; therefore, only the main semi-diurnal tidal components were used. In cases where the semi-diurnal components were in phase, the two components were directly summed to determine high tide magnitude. Conversely, when the components were in opposite phases, the difference between the two components was taken, resulting in low tide height.

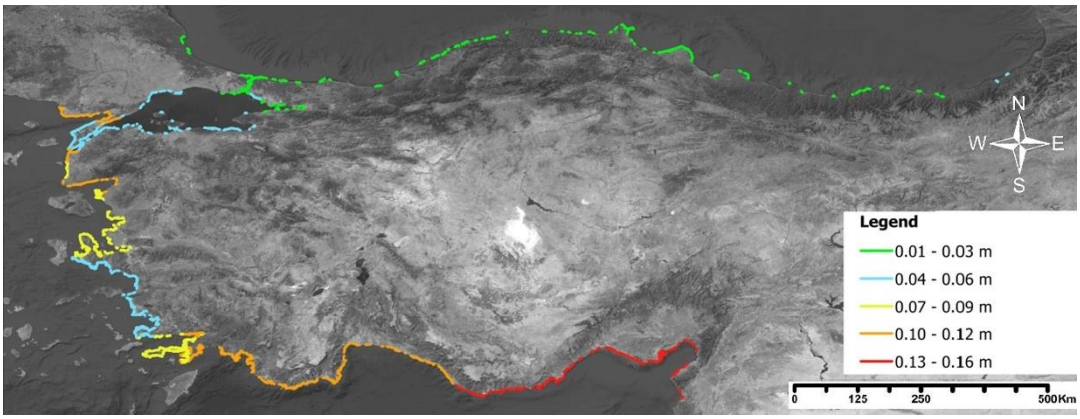


Figure 4.15. Tidal Range Class Distribution Map

Figure 4.15 presents tide values across the studied shorelines and Table 4.17 contains class breakdowns. It should be noted that limits given in the Table were derived with respect to the available data. Since Türkiye experiences micro tides, observed tidal ranges fall into very low tide class of FCVAM which indicates very high vulnerability.

Table 4.17 Number of Locations within Tidal Range Classes

Tide	**0.03m - 0.01m**	**0.06m - 0.04m**	**0.09m - 0.07m**	**0.12m - 0.10m**	**0.16m - 0.13m**
Cultural Heritage	146	411	276	179	164
Natural Conservation	141	450	390	134	56

4.2.8 River Flow Regulation

The river flow regulation parameter indicates how human activities, such as the existence of dams and other water storage structures, control and manage river systems. Dams and other types of water storage structures also trap sediment carried by river flow, which reduces the amount of sediment that nourishes the corresponding shoreline where the river meets the sea. Since the reduction of sediment supply was not considered in this study, as explained in Chapter 3, this

parameter becomes more significant. To calculate how severely the flow is regulated, the methodology proposed by Nillson et al. in 2005 was utilized.

Table 4.18 River Flow Regulation Result Indicator (Nillson et al., 2005)

Fragmentation (Main channel + tributaries)	Flow regulation (%)		
	Not affected	Moderately affected	Strongly affected
0+0	0		
0+1	≤ 2	>2	
0+2	≤ 1	>1	
1+0		≤ 30	> 30
1 + 1		≤ 25	> 25
1+2, 2+0		≤ 20	> 20
2+1		≤ 15	> 15
2 + 2, 3 + 0		≤ 10	> 10
3 + 1		≤ 5	> 5
3 +2, 4 + 0, 1, 2			≥ 0

The methodology follows a certain algorithm. Firstly, the storage capacities of all dams on a river system are calculated. Secondly, the total discharge of the river system is determined. Thirdly, the percent ratio of storage capacities and total discharges is taken. Fourthly, the ratio of the longest main channel segment without a dam to the entire channel length is calculated. The score is to get the main channel value in Table 4.18. for the main channel is done by considering 0 = 100%; 1 = 75-99%; 2 = 50- 74%; 3 = 25-49%; and 4 = 0-24%. Fifthly, tributary scoring used in Table 4.18 considers classifications of 0 = no dams; 1 = dams only in the catchment of minor tributaries; 2 = dams also in the catchment of the largest tributary. Finally, the percent ratio calculated in the third step is combined with inputs determined in the fourth and fifth steps as inputs for Table 4.18 to get how the system is affected. In CVI calculations, not affected means FCVAM input is equal to 1. For moderately affected, the value is two, and for strongly affected, it is equal to 3. Calculations of inputs that are used in the explained methodology require some preprocesses. Initially, if the studied shoreline does not have any intersection with a river system,

then it is automatically assigned a score of “1”. Otherwise, the river system is identified by using the EU-Hydro River Network Database 2006-2012 (EEA, 2019). This database contains information about the geographical extent of the system. Moreover, additional information is also provided by nodes placed on river systems. For instance, if there is a possibility of the existence of a water storage system, then this is indicated by a node located in that system. However, the mentioned node does not give information about the discharge or storage capacity. Thus, additional datasets were sought to fill the information gaps. Total discharge values of river systems were obtained from River discharge and related historical data from the European Flood Awareness System – v 5.0 (Mazzetti et al., 2023) database. From this database, discharge values with 6-hour intervals were taken for 2023 in NETCDF format. To get a yearly total discharge in a format that could be recognizable by the GIS environment, data manipulation was required. To accomplish this, MATLAB was used. However, containing discharge information over latitude, longitude and time results in a three-dimensional matrix. Thus, by initially summing the data at 6-hour intervals and adjusting the data units, the three-dimensional matrix was reduced to two dimensions. After importing newly generated data into the GIS environment, discharge values were matched with corresponding shoreline projections of study areas manually.

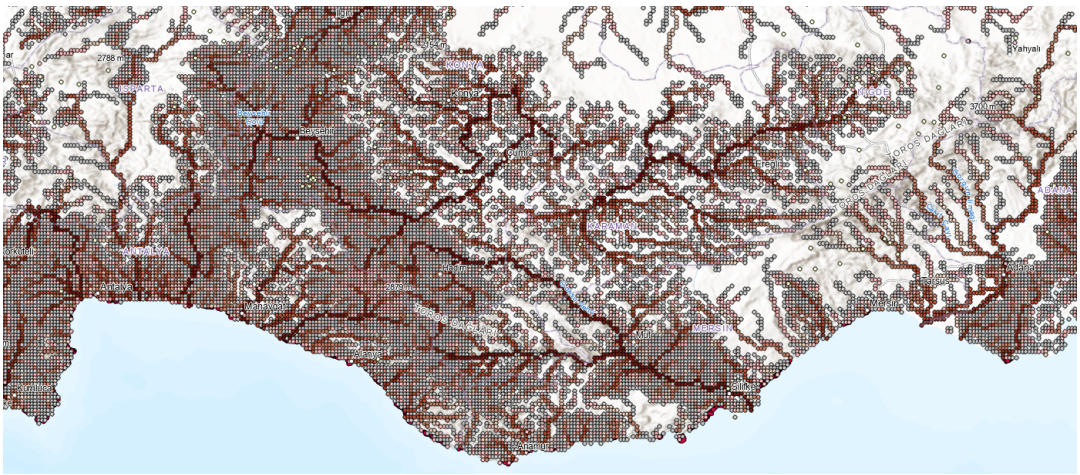


Figure 4.16. Total River Discharge Data Imported to GIS as 2D Matrix

Storage capacity calculations of water storage structures along the river system are the other essential step in determining river flow regulation. To obtain dam reservoir capacities, firstly, the server of State Hydraulic Agency – Dam Capacities (in WMS) was checked manually and identified storage structure nodes were added to the information given in this dataset. However, since nodes given in the EU-Hydro River Network Database 2006-2012 are not complete for Turkish dams, missing nodes were added manually. On the other hand, the State Hydraulic Agency server also had missing information. Therefore, information given in Global Dam Tracker (Zhang, Gu, 2023) was utilized to overcome this issue. After the completion of dam capacity data, river systems that pass-through study areas were identified, and all the cumulative capacities of dams on the river system were taken, as well as the river discharge value. Finally, the percent ratio of these two values was calculated and inputted into Table 4.18. River flow regulation input values of study shorelines and distribution over classes are given in Figure 4.17 and Table 4.19, respectively. According to these, more than 90% of studied shorelines are not affected by this parameter.

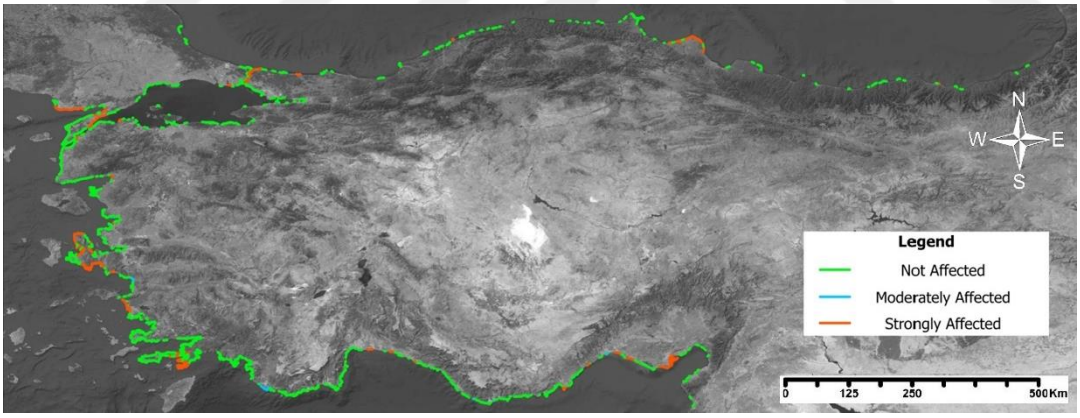


Figure 4.17. River Flow Regulation Class Distribution Map

Table 4.19 Number of Locations within River Flow Regulation Classes

River Flow Regulation	Not Affected	Moderately Affected	Strongly Affected
Cultural Heritage	1145	7	23
Natural Conservation	1081	12	78

The main issue related to the mentioned databases is that these are not complete for Türkiye and need to be updated. For river discharge, discharge values must be obtained by field measurements instead of using meteorological models. This approach results in a deviation of discharge values regarding both obtained discharge and node location. For storage capacities, there are inconsistencies between the State Hydraulic Agency server, EU-Hydro River Network Database 2006-2012 dam nodes, and satellite images. To be more specific, in some cases, although there was a water storage structure visible on satellite images, it was not listed in either of these datasets. Also, in a few occurrences, although it was listed in both the server and dataset, discharge values in the server were missing. Such discrepancies were tried to be corrected as much as possible during this thesis.

4.2.9 Engineered Frontage and Coastal Protection Structure

Since the same methodology and dataset were applied for both engineered frontage and coastal protection structures parameters, these two parameters are explained together in this section. Coastal Zones Land Cover/Land Use 2018 (EEA, 2021) was used to obtain these two parameter input values. As preprocesses, firstly, a single side buffer of 50m inland was generated for shorelines. 50 m wide buffer was selected by considering Zone A definition defined in Coastal Law, in which no engineered structure other than coastal protection and coastal structures are allowed to ensure that the use of the structures in the database could be considered located at the shore and could be related to coastal processes. In the second step, land cover types given in Table 4.20 were assigned as “1,” and the rest were “0”. The intersection of the dataset and the buffered shoreline was taken in the third step, and the total percentage distribution of land cover assigned to “1” over the buffered shore was taken. Finally, the percentage distribution of the engineering features was taken as input values.

Table 4.20 Engineering Frontage Indicator Land Usages (EEA, 2021)

Code and Usage	Code and Usage
11110 Continuous urban fabric (IMD ≥80%)	12340 Naval port
11120 Dense urban fabric (IMD ≥30-80%)	12350 Marinas
11130 Low-density fabric (IMD <30%)	12360 Local multi-functional harbors
11210 Industrial, commercial, public, and military units (other)	12370 Shipyards
11220 Nuclear energy plants and associated land	12400 Airports and associated land
12100 Road networks and associated land	13110 Mineral extraction sites
12200 Railways and associated land	13120 Dump sites
12310 Cargo port	13130 Construction sites
12320 Passenger port	13200 Land without current use
12330 Fishing port	14000 Green urban, sports, and leisure facilities

The only difference between EF and CPS is that engineered frontage includes all types of human-made structures, while CPS only considers structures that have the main aim of protecting the shoreline given in Table 4.21.

Table 4.21 Coastal Protection Structures Indicator Land Usages (EEA, 2021)

Code and Usage	Code and Usage
11210 Industrial, commercial, public, and military units (other)	12340 Naval port
12310 Cargo port	12350 Marinas
12320 Passenger port	12360 Local multi-functional harbors
12330 Fishing port	12370 Shipyards

According to Figure 4.18, more than half of all the shorelines studied demonstrate less than 20% engineered land cover, which is also supported by the input distribution given in Table 4.22. From a regional perspective, the Marmara Region indicates more engineered frontage than other regions.

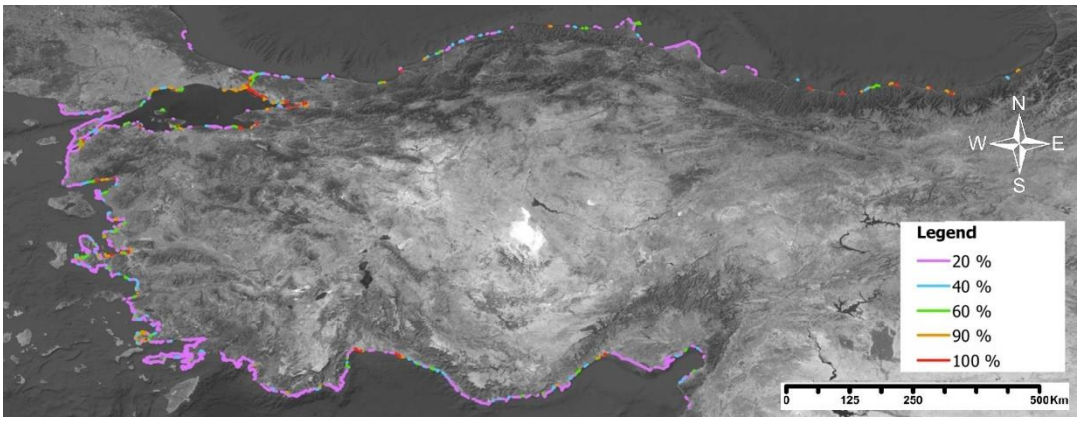


Figure 4.18. Engineering Frontage Class Distribution Map

Table 4.22 Number of Locations within Engineering Frontage Classes

EF	**< 20%**	**< 40%**	**< 60%**	**< 90%**	**< 100%**
Cultural Heritage	594	173	157	171	81
Natural Conservation	659	166	86	135	125

On the other hand, Figure 4.19 and Table 4.23 show coastal protection structure coverage. According to them, in more than 80% of shorelines studied, coastal protection structures cover less than 15% of buffered areas.

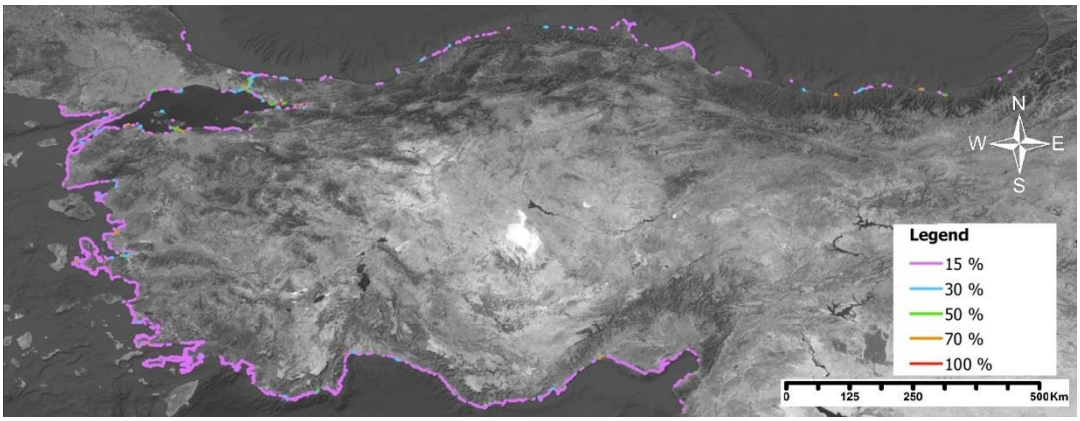


Figure 4.19. Coastal Protection Structures Class Distribution Map

Table 4.23 Number of Locations within Coastal Protection Structures Classes

CPS	**< 15%**	**< 30%**	**< 50%**	**< 70%**	**< 100%**
Cultural Heritage	1024	102	30	16	4
Natural Conservation	949	125	59	21	17

The main drawback of the Coastal Zones Land Cover/Land Use 2018 dataset (EEA, 2021) is that its land cover data reflects only the year 2018. In other words, any structures constructed after that year are not included. Figure 4.20 illustrates this issue.



Figure 4.20. Groins within Studied Shoreline

Although a set of groins has since been built, the dataset still indicates the area as a sandy beach and provides no information about the presence of these groins. This situation also indicates that the dataset does not contain any land cover prediction.

4.2.10 Natural Protection Degradation

Natural protection degradation could be defined as how much of the natural conservation structures that reduce the area's vulnerability have been degraded. Dunes, wetlands, and mangroves could be given for this kind of structure. The Coastal Zones Land Cover/Land Use Change 2012-2018 (EEA, 2020) dataset was used to obtain how much of the natural protection structures recessed. This dataset gives the land use for both the years 2012 and 2018. Thus, alterations between these two years could be determined.

In order to calculate the value of this parameter for sturdy shorelines, firstly, a 100 m buffer inland was defined for the corresponding shoreline, which represents Zone A, the first 50 m buffer, and Zone B, the second 50 m, given in Coastal Law of Turkiye. In Zone A, other than coastal structures such as harbors, no construction is allowed, while in Zone B, recreational facilities are allowed. Following this, usage code changes were investigated. To point out the existence of natural protection degradation, natural protection structures have to be available in 2012, and these structures should be destroyed fully or partially in 2018. Thus, 2012 land cover data was initially checked for features in Table 4.24. If the existence of these was detected within a 100m buffered area, its percentage distribution was calculated. Then, in 2018, land cover was checked to obtain differences in land usage. The same procedure was applied to obtain the percent distribution in 2018. If the accumulation of percent distribution decreases in 6 years of interval, then the difference is calculated for the input value. On the other hand, if originally any natural protection structure did not exist, then this area is given a score of 0%.

In more than 90% of studied shorelines, natural protection degradation was calculated as less than 10%, as could be observed in Table 4.25. Also, in Figure 4.21, natural protection degradation scores of shorelines are given. The calculations were conducted between 2012 and 2018, which is the main drawback since, after 2018, there is no up-to-date data available. As a result, the calculated degradation percentage might not represent today's conditions.

Table 4.24 Natural Protection Degradation Indicator Land Usages (EEA, 2020)

Code and Usage	**Code and Usage**
31100 Natural & semi-natural broadleaved forest	62112 Shingle beaches
31200 Highly artificial broadleaved plantations	62120 Dunes
32100 Natural & semi-natural coniferous forest	71100 Inland marshes
32200 Highly artificial coniferous plantations	71210 Exploited peat bogs
33100 Natural & semi-natural mixed forest	71220 Unexploited peat bogs
33200 Highly artificial mixed plantations	72100 Salt marshes
61100 Sparse vegetation on sands	72200 Salines
62111 Sandy beaches	72300 Intertidal flats

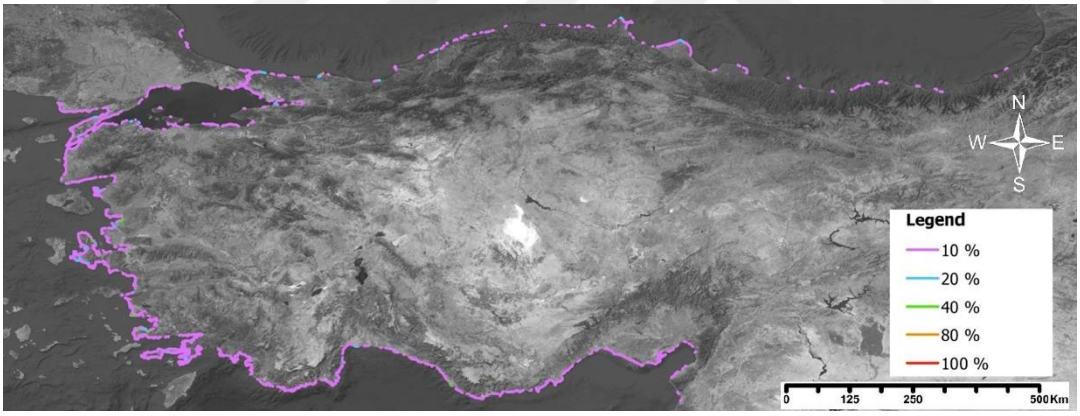


Figure 4.21. Natural Protection Degradation Class Distribution Map

Table 4.25 Number of Locations within Natural Protection Degradation Classes

NATDEG	**< 10%**	**< 20%**	**< 40%**	**< 80%**	**< 100%**
Cultural Heritage	1106	52	13	5	0
Natural Conservation	1104	54	13	0	0

CHAPTER 5

RESULTS & DISCUSSIONS

5.1 FCVAM Application Results

After preparation of input values to FCVAM, the model was applied for 1171 Natural Conservation Zones along with 1176 Coastal Cultural Heritage Areas.5 different IPCC AR6 Sea level rise scenario was considered during the application. Moreover, the extreme sea level scenario was also changed depending on the considered scenario. For instance, corresponding LISFLOOD data, which considers the AR5 RCP 4.5 scenario to make predictions of ESL, were chosen while using AR6 SSP 4.5. The same logic applies to vice versa. LISFLOOD data considers AR5 RCP 8.5 for ESL projections, which were utilized when results corresponding to AR6 SSP5-8.5 were investigated. In this section, the results of AR6 SSP 4.5 and AR6 SSP5-8.5 were given. For physical and human impacts, given results cover model classes, while for module and CVI results, both model classes and five interval Jenks were demonstrated. Also, corresponding results of other scenarios were given in the appendices section.

5.2 Natural Conservation Zones

5.2.1 Human Impact Scores

In this study, the primary assumption was that there would be no changes related to human behavior around study areas to focus on how AR6 SSP scenarios of sea level rise and corresponding expected changes on the extreme sea levels alter the vulnerability. Although SSP scenarios indicate expected changes or motivation of human activities, there is no data on such projections for Turkish coastlines. Therefore, the effects of changes in human activity in the future are not included. This means SSP2-4.5 and SSP5-8.5 are expected to give the same human impact scores for the same study area. Thus, in this section, human impact scores given for natural conservation zones are independent of scenarios.

5.2.1.1 Erosion

Figure 5.1 shows the distribution of erosion human impact scores throughout natural conservation zones regarding classes defined in FCVAM. According to the figure, Turkish coasts are mainly very low and vulnerable to erosion due to human impact.

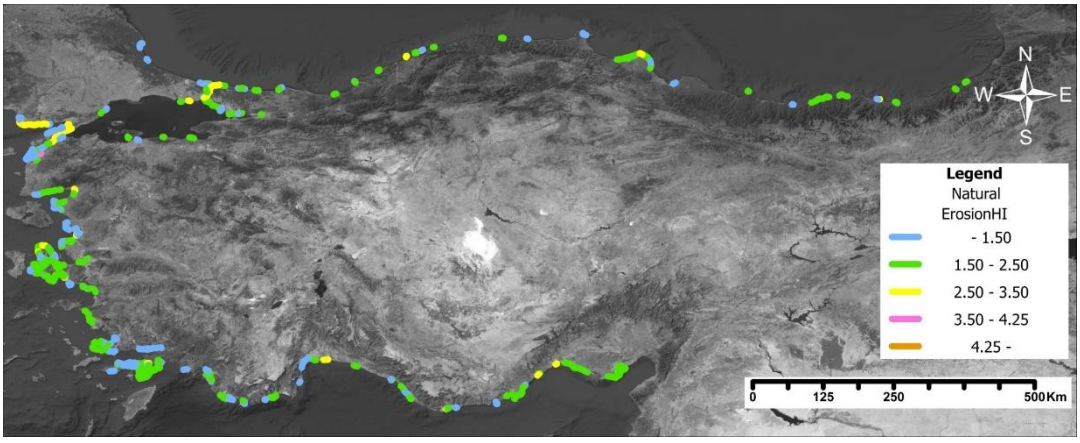


Figure 5.1. Natural Conservation Zone Erosion Human Impact Distribution

In the regional aspect, the most vulnerable areas are located in the Aegean Region. This statement is also supported by Table 5.1, in which only the Aegean Region has shorelines that could be classified as high vulnerable. On the other hand, the least vulnerable region could be deduced to the Mediterranean Region. Although this region has more moderate vulnerable shorelines than the Marmara Region, the percentage of very low vulnerable areas is higher in the Mediterranean Region.

Table 5.1 Regional Natural Conservation Zone Erosion Human Impact Scores

Erosion HI	Mediterranean	Aegean	Marmara	Black Sea
< 1.5 Very Low	103 (8.8%)	356 (30.4%)	34 (2.9%)	93 (7.9%)
1.5 – 2.5 Low	41 (3.5%)	280 (23.9%)	116 (9.9%)	94 (8.0%)
2.5 – 3.5 Moderate	10 (0.9%)	22 (1.9%)	3 (0.3%)	17 (1.5%)
3.5 – 4.25 High	0	2 (0.2%)	0	0
4.25 > Very High	0	0	0	0

5.2.1.2 Inundation

In Figure 5.2, the distribution of inundation human impact score throughout natural conservation zones in terms of classes defined in FCVAM is given.

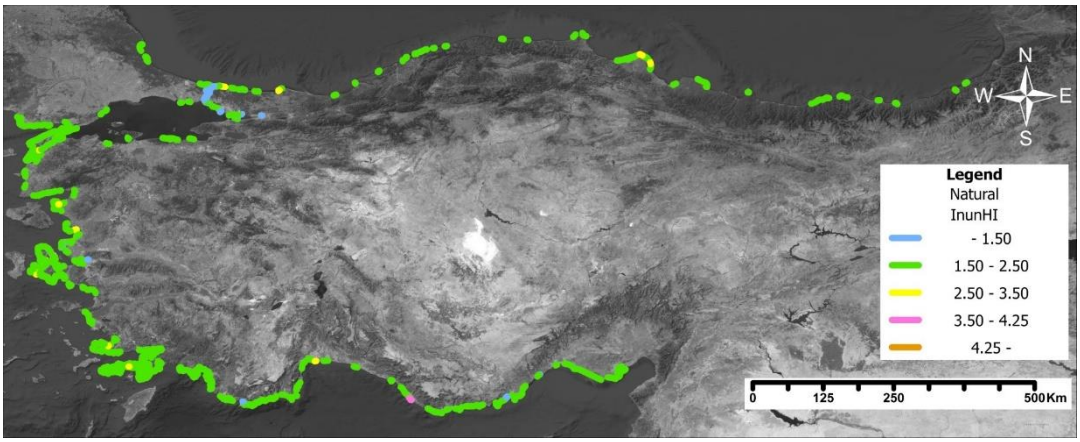


Figure 5.2. Natural Conservation Zone Erosion Inundation Impact Distribution

According to the Figure, the Turkish shorelines of natural conservation zones demonstrate Low vulnerability to inundation, considering the human impact parameters. For regional aspects, the Aegean and Mediterranean Regions are the only regions with shorelines classified as High Vulnerable in terms of Inundation Human impact score. However, when the regional outputs given in Table 5.2 are investigated, the Aegean Region shorelines could be denoted as the most vulnerable to Inundation Human impact, contrary to the Marmara Region, where the least vulnerable shorelines are located.

Table 5.2 Regional Natural Conservation Zone Inundation Human Impact Scores

Inundation HI	**Mediterranean**	**Aegean**	**Marmara**	**Black Sea**
< 1.5 Very Low	11 (0.9%)	14 (1.2%)	59 (5.0%)	30 (2.6%)
1.5 – 2.5 Low	135 (11.5%)	591 (50.4%)	94 (8.0%)	163 (13.9%)
2.5 – 3.5 Moderate	6 (0.5%)	48 (4.1%)	0	11 (0.9%)
3.5 – 4.25 High	2 (0.2%)	7 (0.6%)	0	0
4.25 > Very High	0	0	0	0

5.2.1.3 Storm Surge

Figure 5.3 shows the storm surge human impact score distribution throughout natural conservation zones regarding classes defined in FCVAM.

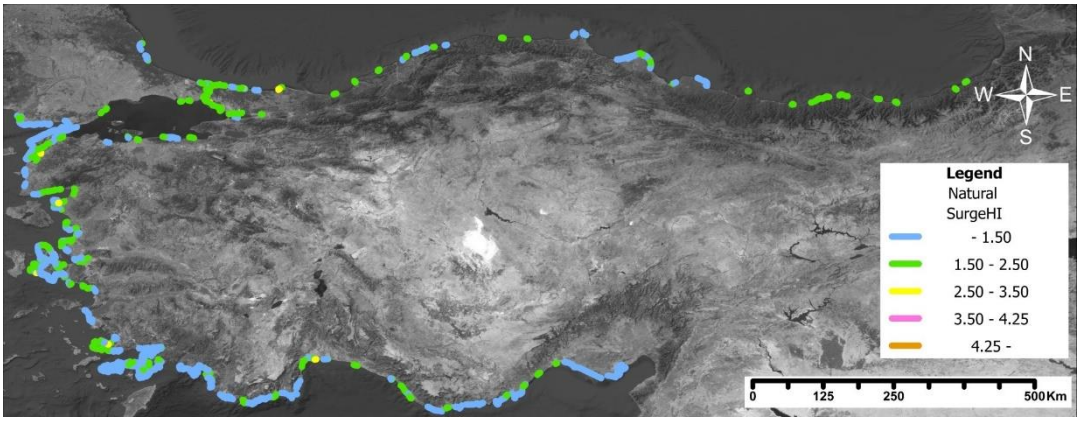


Figure 5.3. Natural Conservation Zone Storm Surge Human Impact Distribution

Turkish shoreline projections of natural conservation zones are determined as very low and low vulnerable against storm surge for human impact parameters. From a regional perspective, the Aegean Region is the only region with shorelines classified as high vulnerable. In contrast, the majority of studied shorelines in the Mediterranean region demonstrate very low vulnerability, as seen in Table 5.3.

Table 5.3 Regional Natural Conservation Zone Storm Surge Human Impact Scores

Surge HI	Mediterranean	Aegean	Marmara	Black Sea
< 1.5 Very Low	106 (9.1%)	317 (27.1%)	12 (1.0%)	74 (6.3%)
1.5 – 2.5 Low	45 (3.8%)	307 (26.2%)	140 (12.0%)	121 (10.3%)
2.5 – 3.5 Moderate	3 (0.3%)	31 (2.6%)	1 (0.09%)	9 (0.8%)
3.5 – 4.25 High	0	5 (0.4%)	0	0
4.25 > Very High	0	0	0	0

5.2.2 AR6 SSP2 – 4.5 Physical Impact Scores

This section presents the natural conservation zone's physical impact and CVI results, calculated using predicted RSLR and ESL values based on the IPCC AR6 SSP2–4.5 scenarios.

5.2.2.1 Erosion

5.2.2.1.1 ErosionPP

In Figure 5.4, erosion physical impact score distribution throughout natural conservation zones for the SSP2 - 4.5 pathway in terms of classes defined in FCVAM is given. On a national scale, low and moderate vulnerabilities against the physical impact of erosion are dominant. This claim is also supported by regional results in Table 5.4, according to which most moderate vulnerable areas are located in the Aegean Region.

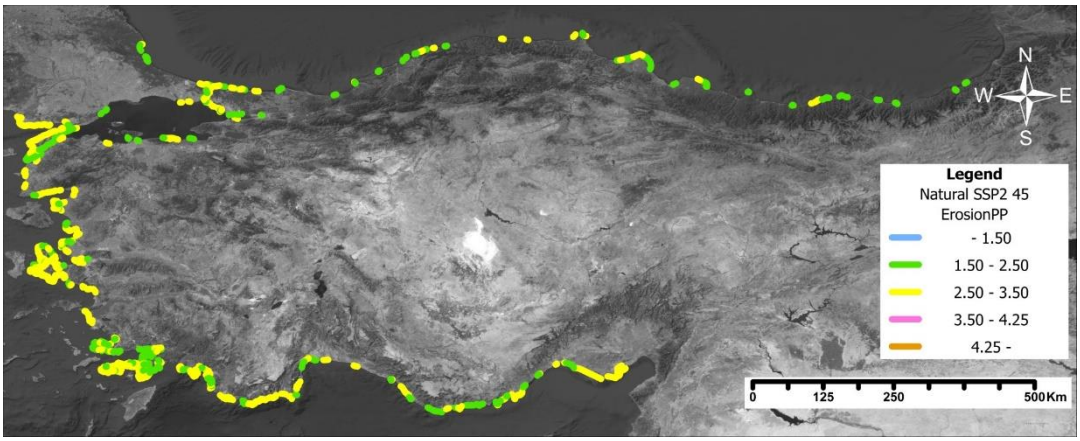


Figure 5.4. SSP2-4.5 Natural Conservation Zone ErosionPP Distribution

On the other hand, shoreline vulnerability class distributions indicate that since there are no very low-vulnerable areas in the Mediterranean and Black Sea Regions and the distribution patterns of these two regions tend toward higher vulnerability classes compared to areas in the Marmara Regions, the Marmara Regions could be claimed as the least vulnerable region considering erosion physical impact parameters.

Table 5.4 Regional SSP2-4.5 Natural Conservation Zone ErosionPP Scores

Erosion PP	Mediterranean	Aegean	Marmara	Black Sea
< 1.5 Very Low	0	10 (0.9%)	4 (0.3%)	0
1.5 – 2.5 Low	70 (6.0%)	382 (32.6%)	115 (9.8%)	117 (10.0%)
2.5 – 3.5 Moderate	84 (7.2%)	268 (22.9%)	34 (2.9%)	87 (7.4%)
3.5 – 4.25 High	0	0	0	0
4.25 > Very High	0	0	0	0

5.2.2.1.2 Erosion Impact Score

Erosion physical and human impact scores were aggregated to obtain erosion vulnerability scores, demonstrated in Figure 5.5 under the pathway of AR6 SSP2-4.5. According to the class distribution in the Figure, low-vulnerable shorelines against erosion are the most common vulnerability class along Turkish shorelines.

Moreover, no studied shorelines are classified as high or very high vulnerable in terms of erosion vulnerability.

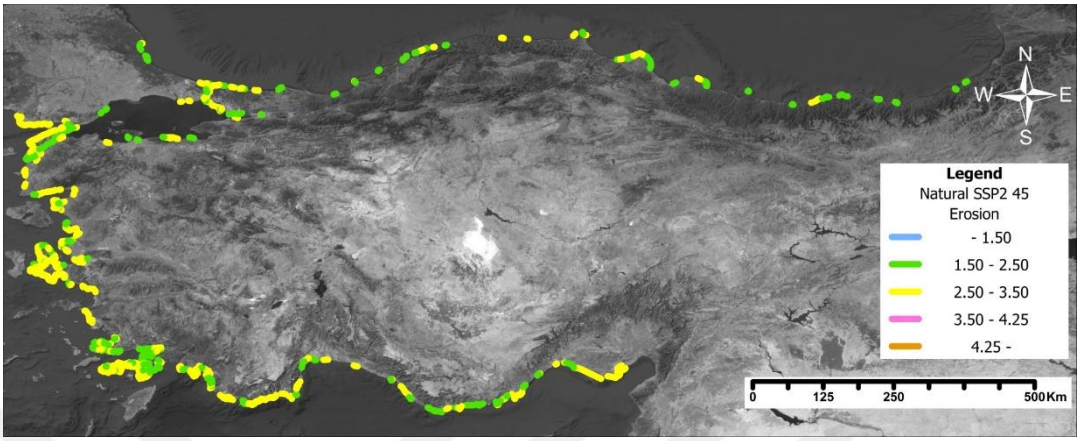


Figure 5.5. SSP2-4.5 Natural Conservation Zone Erosion Distribution

More detailed results are given in Table 5.5. at a regional scale. According to that Table, most moderate vulnerable shorelines are located in the Aegean Region. On the other hand, the distribution of vulnerability classes for regions demonstrates a similar pattern to erosion physical impact scores (section 5.2.2.1.1, Table 5.4).

Table 5.5 Regional SSP2-4.5 Natural Conservation Zone Erosion Scores

Erosion	Mediterranean	Aegean	Marmara	Black Sea
< 1.5 Very Low	0	10 (0.9%)	0	0
1.5 – 2.5 Low	70 (6.0%)	379 (32.3%)	115 (10.2%)	117 (10.0%)
2.5 – 3.5 Moderate	84 (7.2%)	271 (23.1%)	34 (2.9%)	87 (7.4%)
3.5 – 4.25 High	0	0	0	0
4.25 > Very High	0	0	0	0

A comparison of erosion vulnerability score distribution with physical and human impact scores indicated that erosion vulnerabilities were mainly dictated by physical impact scores. Figure 5.6 shows a histogram comparison of physical and human impact scores. The figure demonstrates that physical impact is more critical in the case of erosion than human impact scores.

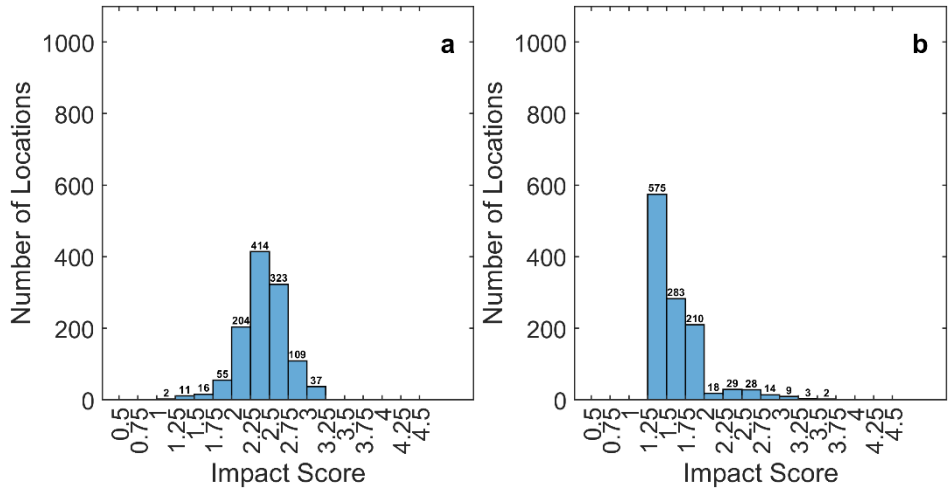


Figure 5.6. SSP2-4.5 Natural Conservation Zone Erosion (a) Physical Impact Score (b) Human Impact Score

Figure 5.7 gives score classifications in Jenks Natural Breaks instead of FCVAM class definitions. When ordinary FCVAM class limits are utilized, erosion vulnerability classes are narrowed down into three categories: very low, low, and moderate since no study area has been classified as high or very high vulnerable. With Jenks classification, we could group the natural heritage areas into five groups with relative vulnerabilities determined by their CVI scores. Therefore, we could determine the most vulnerable locations for the Turkish natural heritage sites.

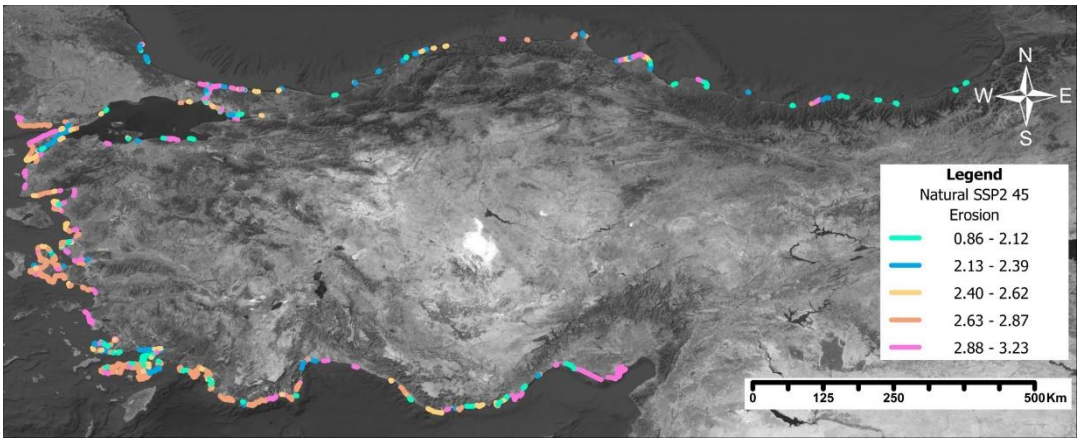


Figure 5.7. SSP2-4.5 Natural Conservation Zone Erosion Jenks Distribution

Table 5.6 demonstrates a more detailed comparison of Jenks and FCVAM classes. Moreover, Figure 5.8 shows a histogram with Jenks limit and 0.25 increment impact scores. According to it, erosion impact scores of Turkish natural conservation zone projections over shoreline are mainly between 2 and 3, with 16.7% of them in the moderate to high vulnerability range, indicating that these locations are most vulnerable to coastal erosion.

Table 5.6 SSP2-4.5 Natural Conservation Zone Erosion Jenks & FCVAM Limits

Jenks Natural Breaks	**Results**	**FCVAM Class**	**Results**
< 2.12	325 (27.8%)	< 1.5 Very Low	10 (0.9%)
2.13 – 2.39	208 (17.8%)	1.5 – 2.5 Low	685 (58.5%)
2.40 – 2.62	222 (19.0%)	2.5 – 3.5 Moderate	476 (40.6%)
2.63 – 2.87	220 (18.8%)	3.5 – 4.25 High	0
2.88 <	196 (16.7%)	4.25 < Very High	0

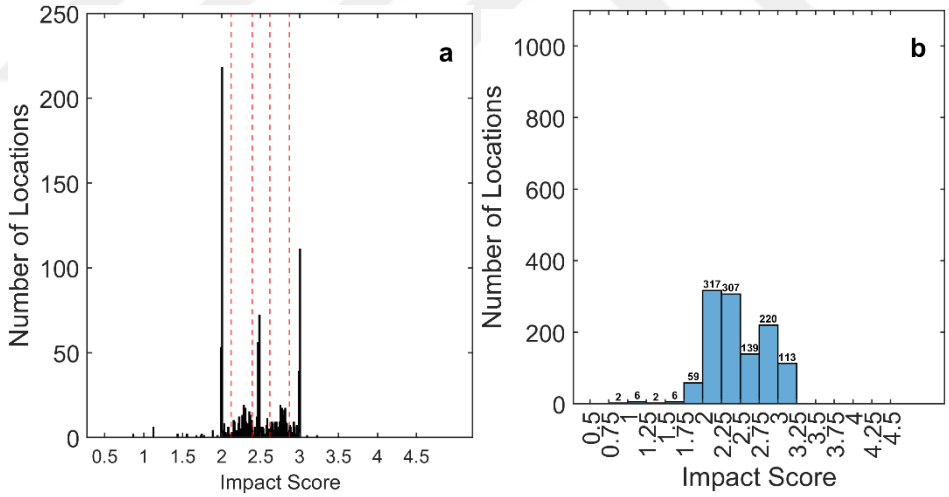


Figure 5.8. SSP2-4.5 Natural Conservation Zone Erosion (a) Jenks (b) FCVAM Histograms

5.2.2.2 Inundation

5.2.2.2.1 InundationPP

Figure 5.9 shows the inundation physical impact score distribution throughout natural conservation zones for the SSP2 - 4.5 pathway regarding classes defined in FCVAM. On a national scale, no shoreline projections demonstrate very low vulnerability. Therefore, the dominant behavior of shores is low vulnerability in terms of inundation physical impact scores.

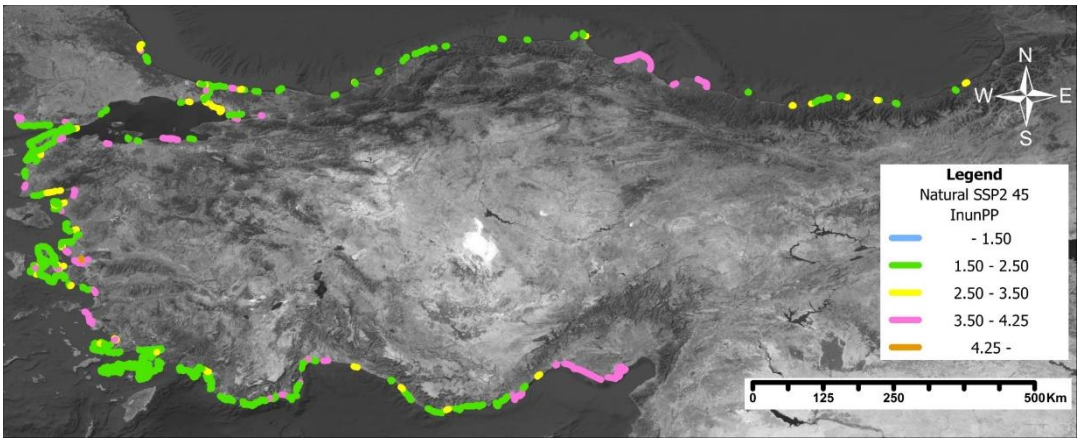


Figure 5.9. SSP2-4.5 Natural Conservation Zone InundationPP Distribution

On the other hand, every region has at least one high vulnerable shoreline, as well as in the Aegean Region, there is a very high vulnerable shoreline to be studied Results are presented in Table 5.7.

Table 5.7 Regional SSP2-4.5 Natural Conservation Zone InundationPP Scores

Inundation PP	Mediterranean	Aegean	Marmara	Black Sea
< 1.5 Very Low	0	0	0	0
1.5 – 2.5 Low	101 (8.6%)	535 (45.7%)	103 (8.8%)	156 (13.3%)
2.5 – 3.5 Moderate	17 (1.5%)	64 (5.5%)	34 (2.9%)	25 (2.1%)
3.5 – 4.25 High	36 (3.1%)	60 (5.1%)	16 (1.4%)	23 (2.0%)
4.25 > Very High	0	1 (0.09%)	0	0

5.2.2.2.2 Inundation Impact Score

Inundation physical and human impact scores were aggregated to obtain inundation vulnerability scores, which are given in Figure 5.10 for AR6 SSP2-4.5. According to the class distribution in the Figure, low vulnerable shorelines against inundation are the most common vulnerability class along Turkish shorelines.

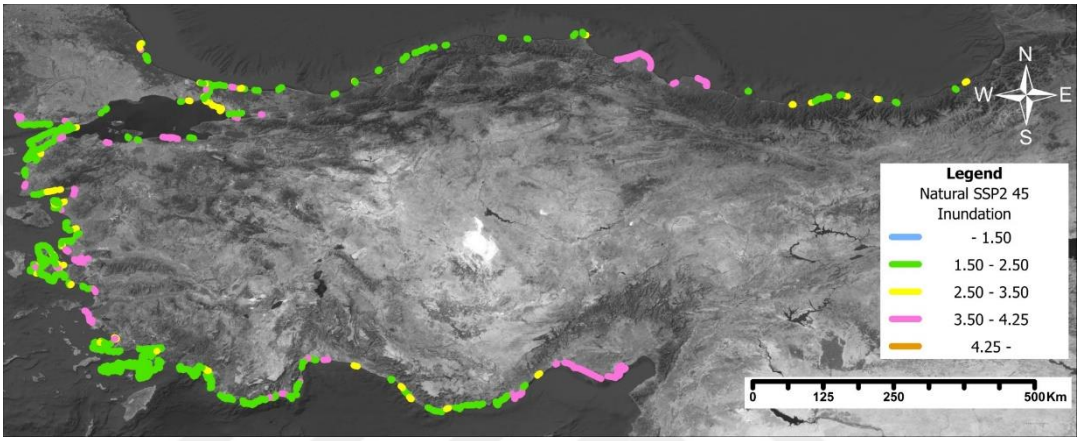


Figure 5.10. SSP2-4.5 Natural Conservation Zone Inundation Distribution

On a national scale, no areas are very low or very high vulnerable regarding inundation impact score, which is also supported by results in Table 5.8. at a regional scale. According to that Table, most of the high vulnerable shorelines are located in the Aegean Region.

Table 5.8 Regional SSP2-4.5 Natural Conservation Zone Inundation Scores

Inundation	Mediterranean	Aegean	Marmara	Black Sea
< 1.5 Very Low	0	0	0	0
1.5 – 2.5 Low	99 (8.5%)	526 (44.9%)	103 (8.8%)	156 (13.3%)
2.5 – 3.5 Moderate	19 (1.6%)	73 (6.2%)	34 (2.9%)	25 (2.1%)
3.5 – 4.25 High	36 (3.1%)	61 (5.2%)	16 (1.4%)	23 (2.0%)
4.25 > Very High	0	0	0	0

Figure 5.11 presents histograms of inundation physical and human impact scores. From the histograms, it could be deduced that physical impact scores become more dominant as impact scores increase compared to human impact scores. Since inundation vulnerability is calculated by aggregating these two scores, the vulnerability is more dictated by the physical impact score. The outcome could be observed if the physical and human impact score distribution over regions is compared with the results in the regional inundation table. Patterns given in the physical impact score resemble the inundation vulnerability pattern more.

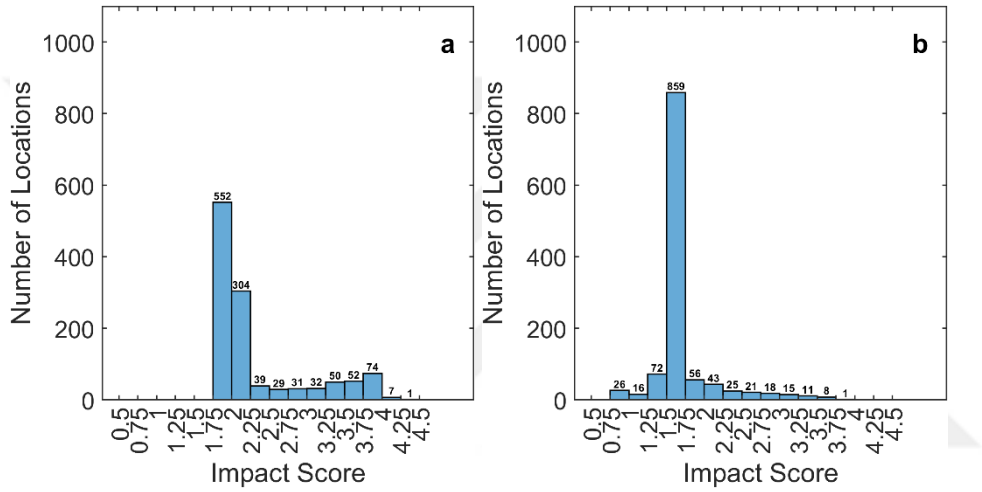


Figure 5.11. SSP2-4.5 Natural Conservation Zone Inundation (a) Physical Impact Score (b) Human Impact Score

In Figure 5.12, inundation score classifications are given in Jenks Natural Breaks instead of FCVAM class definitions. When ordinary FCVAM class limits are utilized, inundation vulnerability classes are narrowed down into three categories concerning global classification: low, moderate, and high vulnerable. With Jenks classification, we determine the most vulnerable natural heritage sites for the Turkish coastline among all the natural heritage sites of Turkiye.

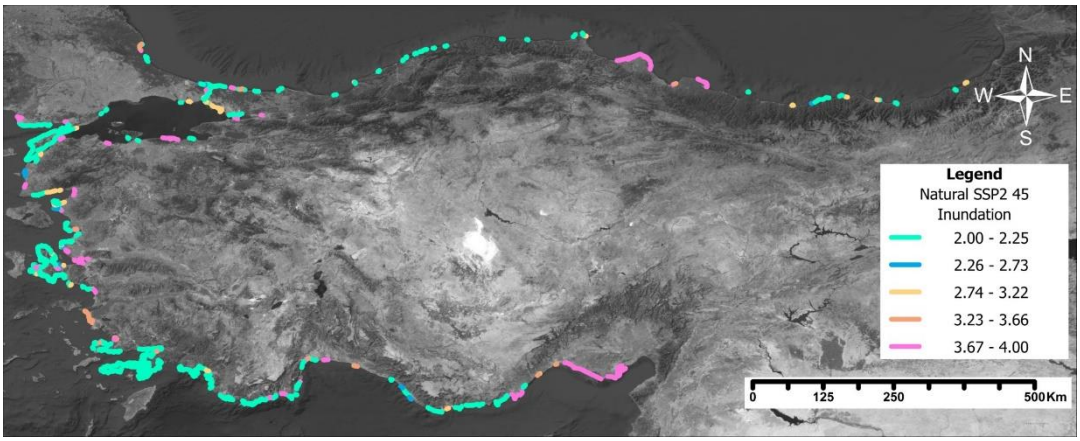


Figure 5.12. SSP2-4.5 Natural Conservation Zone Inundation Jenks Distribution

In Table 5.9, a more detailed comparison of Jenks and FCVAM classes is demonstrated. Making classification concerning natural Jenks breaks indicated that about 10.3% of the studied shorelines, which are high vulnerable according to the original class limits, belong to the most critical class against inundation. Also, in Figure 5.13, a histogram with Jenks limit and 0.25 increment impact scores are given for further distribution detail. According to it, although there is an accumulation around inundation impact scores of "3" and "4", the majority of shorelines are given the vulnerability score of "2".

Table 5.9 SSP2-4.5 Natural Conservation Zone Inundation Jenks & FCVAM Limits

Jenks Natural Breaks	**Results**	**FCVAM Class**	**Results**
< 2.25	860 (73.4%)	< 1.5 Very Low	0
2.26 – 2.73	46 (3.9%)	1.5 – 2.5 Low	884 (75.5%)
2.74 – 3.22	95 (8.1%)	2.5 – 3.5 Moderate	151 (12.9%)
3.23 – 3.66	49 (4.2%)	3.5 – 4.25 High	136 (11.6%)
> 3.67	121 (10.3%)	4.25 < Very High	0

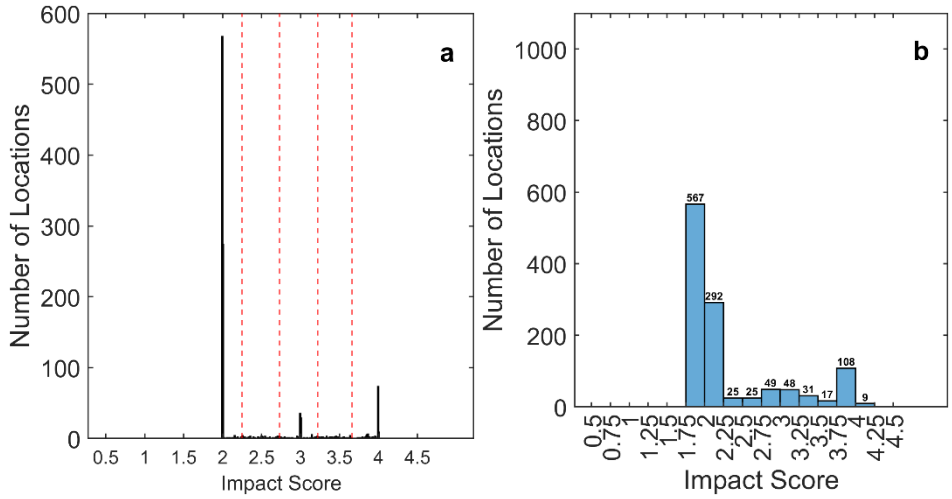


Figure 5.13. SSP2-4.5 Natural Conservation Zone Inundation (a) Jenks (b) FCVAM Histograms

5.2.2.3 Storm Surge

5.2.2.3.1 SurgePP

Figure 5.14 shows the storm surge physical impact score distribution throughout natural conservation zones for the SSP2 - 4.5 pathway in terms of classes defined in FCVAM.

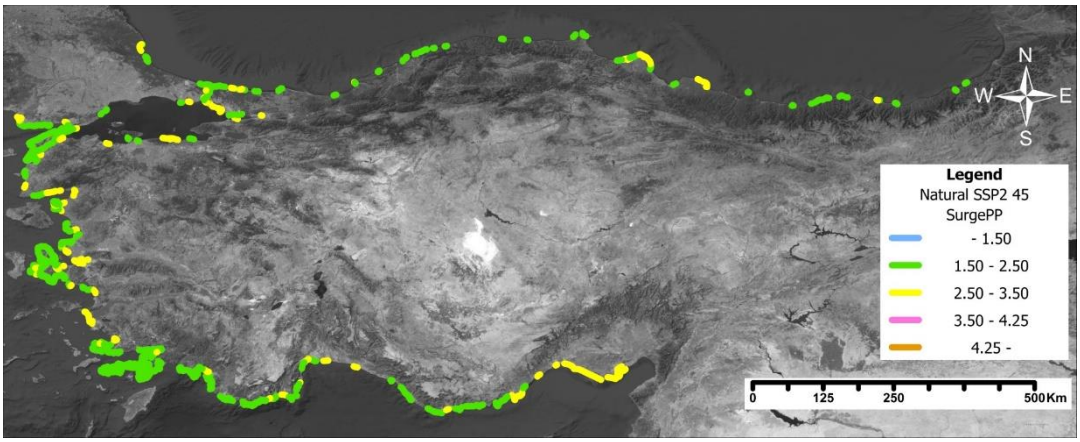


Figure 5.14. SSP2-4.5 Natural Conservation Zone Storm SurgePP Distribution

The national-wide vulnerability of the Turkish natural conservation zone assessment indicates that in terms of storm surge impact scores, only low and moderate vulnerable areas are located around Turkish coasts, which is also supported by Table 5.10. According to regional results presented in the Table, more than 75% of studied shorelines were classified as Low vulnerable.

Table 5.10 Regional SSP2-4.5 Natural Conservation Zone Storm Surge Scores

SurgePP	Mediterranean	Aegean	Marmara	Black Sea
< 1.5 Very Low	0	0	0	0
1.5 – 2.5 Low	105 (9.0%)	547 (46.7%)	104 (8.9%)	174 (14.9%)
2.5 – 3.5 Moderate	49 (4.2%)	113 (9.6%)	49 (4.2%)	30 (2.6%)
3.5 – 4.25 High	0	0	0	0
4.25 > Very High	0	0	0	0

5.2.2.3.2 Storm Surge Impact Score

Storm surge physical and human impact scores were aggregated to obtain storm surge vulnerability scores, demonstrated in Figure 5.15 for AR6 SSP2-4.5. According to the Figure, in terms of storm surge impact score, studied shorelines along Turkish coasts could be narrowed down into 2 classes of low and moderate vulnerability.

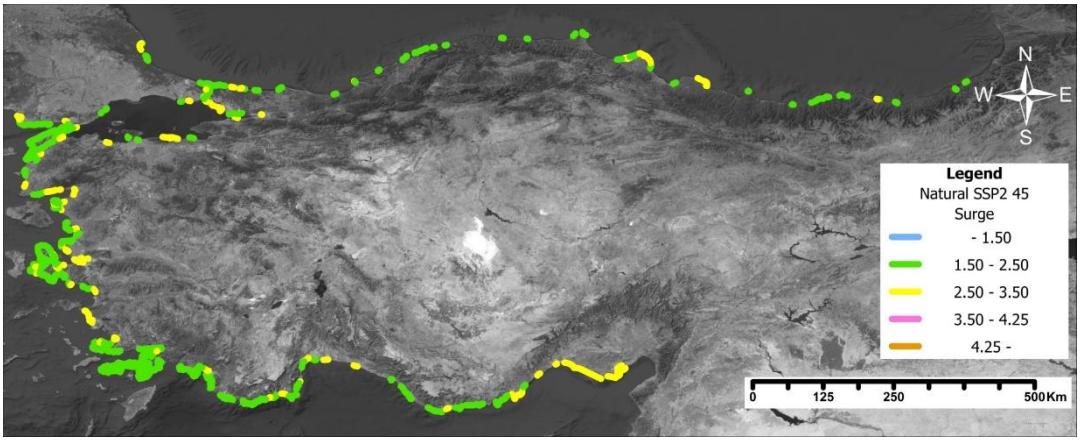


Figure 5.15. SSP2-4.5 Natural Conservation Zone Storm Surge Distribution

Regional results in Table 5.11 also confirm this statement, according to which, similar to storm surge physical impact scores, more than 75% of studied shorelines are classified as low vulnerable.

Table 5.11 Regional SSP2-4.5 Natural Conservation Zone Storm Surge Scores

Surge	Mediterranean	Aegean	Marmara	Black Sea
< 1.5 Very Low	0	0	0	0
1.5 – 2.5 Low	105 (9.0%)	540 (46.1%)	104 (8.9%)	174 (14.9%)
2.5 – 3.5 Moderate	49 (4.2%)	120 (10.2%)	49 (4.2%)	30 (2.6%)
3.5 – 4.25 High	0	0	0	0
4.25 > Very High	0	0	0	0

Figure 5.16 shows the distribution of physical and human impact scores. According to the histograms, physical impact scores are clustered in a narrow area between 1.75 and 3, compared to human impact scores, distributed over a wider area between 1.25 and 3.75.

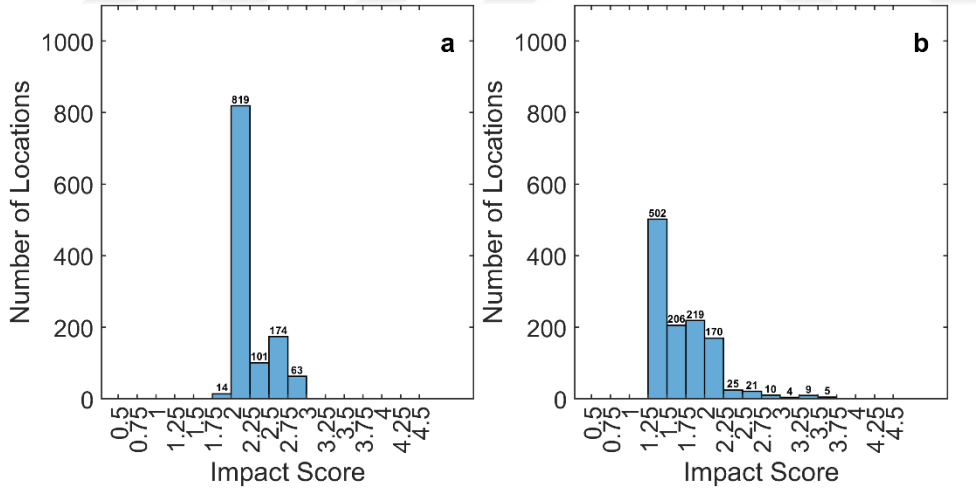


Figure 5.16. SSP2-4.5 Natural Conservation Zone Storm Surge (a) Physical Impact Score (b) Human Impact Score

Figure 5.17 gives score classifications in Jenks Natural Breaks instead of FCVAM class definitions. When ordinary FCVAM class limits are utilized, storm surge

vulnerability classes are narrowed down into low and moderate vulnerability categories. Table 5.12 also presents a more detailed comparison of Jenks and FCVAM classes. With relative grouping of vulnerability, it is determined that around 10% of the natural heritage sites are moderate to high vulnerable and belong to the most vulnerable group among Turkish coastlines for storm surge flooding.

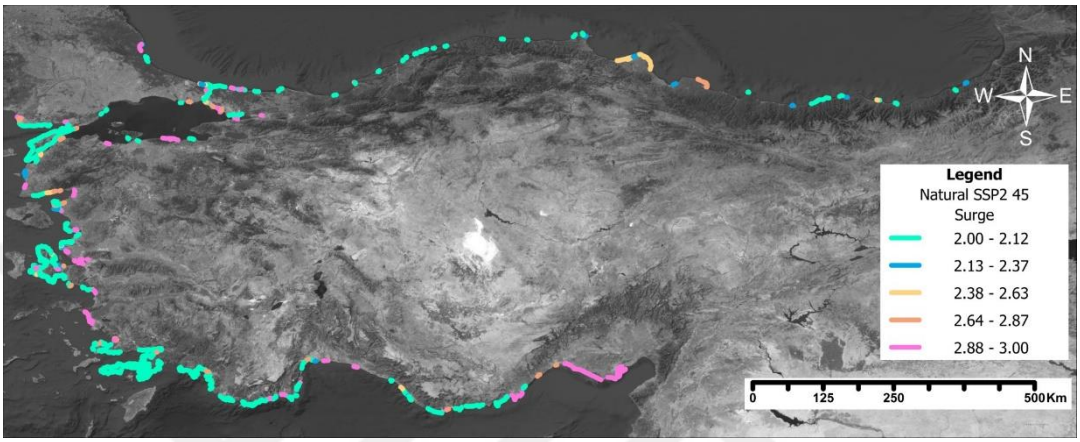


Figure 5.17. SSP2-4.5 Natural Conservation Zone Storm Surge Jenks Distribution

Moreover, in Figure 5.18, a histogram with Jenks limit and 0.25 increment impact scores are given. According to the histograms, although there is accumulation around storm surge impact score of "3", most shorelines are given the vulnerability score of "2".

Table 5.12 SSP2-4.5 Natural Conservation Zone Surge Jenks & FCVAM Limits

Jenks Natural Breaks	**Results**	**FCVAM Class**	**Results**
< 2.12	852 (72.8%)	< 1.5 Very Low	0
2.13 – 2.37	52 (4.4%)	1.5 – 2.5 Low	923 (78.8%)
2.38 – 2.63	48 (4.1%)	2.5 – 3.5 Moderate	248 (21.2%)
2.64 – 2.87	94 (8.0%)	3.5 – 4.25 High	0
> 2.88	125 (10.7%)	4.25 > Very High	0

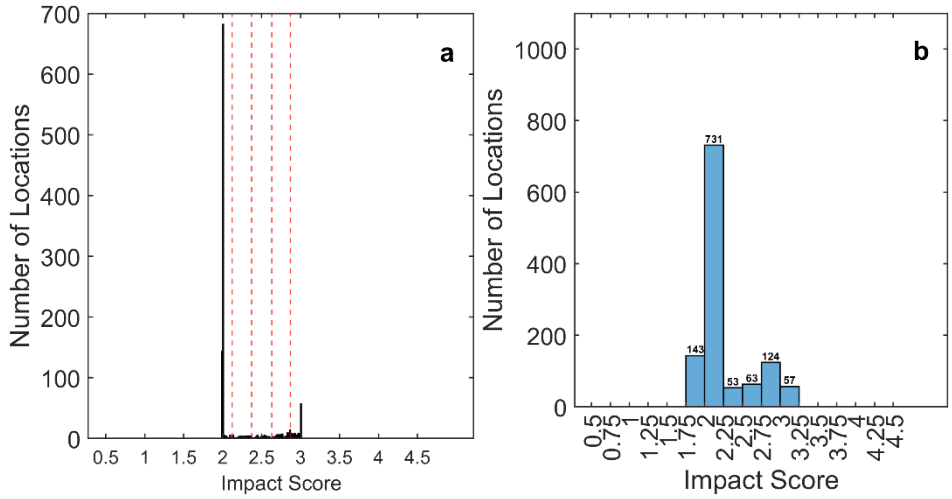


Figure 5.18. SSP2-4.5 Natural Conservation Zone Storm Surge (a) Jenks (b) FCVAM Histograms

5.2.2.4 Coastal Vulnerability Index

All three erosion, inundation, and storm surge vulnerability scores were aggregated to obtain CVI, the distribution of which is demonstrated in Figure 5.19 for AR6 SSP2-4.5. According to the class distribution given in the Figure, although a few very low-vulnerable shorelines are located in the Aegean Region, most are classified as low-vulnerable.

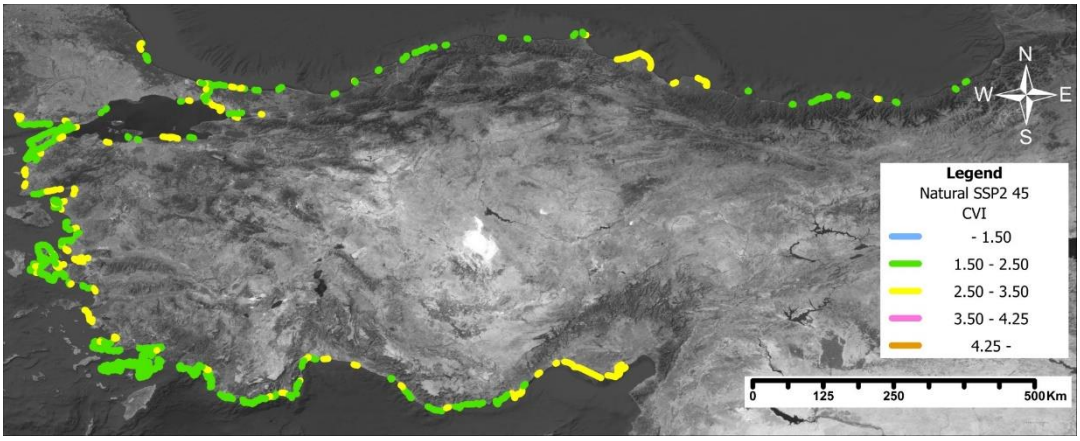


Figure 5.19. SSP2-4.5 Natural Conservation Zone CVI Distribution

According to regional results in Table 5.13, since most areas are located in the Aegean Region, this region has the most studied shorelines for each of the three narrowed-down vulnerability classes of very low, low, and moderate vulnerability. On the other hand, if the percent distribution within regions is studied, the Black Sea Region could be denoted as the least vulnerable region.

Table 5.13 SSP2-4.5 Natural Conservation Zone Impact & CVI Scores

CVI	**Mediterranean**	**Aegean**	**Marmara**	**Black Sea**
< 1.5 Very Low	0	2 (0.2%)	0	0
1.5 – 2.5 Low	100 (8.5%)	528 (45.1%)	105 (9.0%)	158 (13.5%)
2.5 – 3.5 Moderate	54 (4.6%)	130 (11.1%)	48 (4.1%)	46 (3.9%)
3.5 – 4.25 High	0	0	0	0
4.25 > Very High	0	0	0	0

In Table 5.14, score distributions concerning module and vulnerability class were given.

Table 5.14 SSP2-4.5 Natural Conservation Zone Impact & CVI Scores

NAT SSP2-45	Erosion			Inundation			Storm Surge			CVI
	PP	HI	Vul	PP	HI	Vul	PP	HI	Vul	
< 1.5 Very Low	14	586	10	0	114	0	0	509	0	2
1.5 – 2.5 Low	684	531	685	895	983	884	930	613	923	891
2.5 – 3.5 Moderate	473	52	476	140	65	151	241	44	248	278
3.5 – 4.25 High	0	2	0	135	9	136	0	5	0	0
4.25 > Very High	0	0	0	1	0	0	0	0	0	0

When modules are investigated, it becomes more apparent that inundation physical and impact scores and vulnerability are more critical compared to other module scores. Inundation physical impact is the only group with a shoreline classified as very highly vulnerable. Moreover, since the inundation physical impact group is the only physical impact group that has high vulnerable shores, in terms of module vulnerabilities, inundation is the module that has high vulnerable shores. On the other hand, although a few shorelines in terms of erosion and storm surge human impact scores are classified as high vulnerable, most high vulnerable shorelines regarding human impacts are also due to inundation human impact scores.

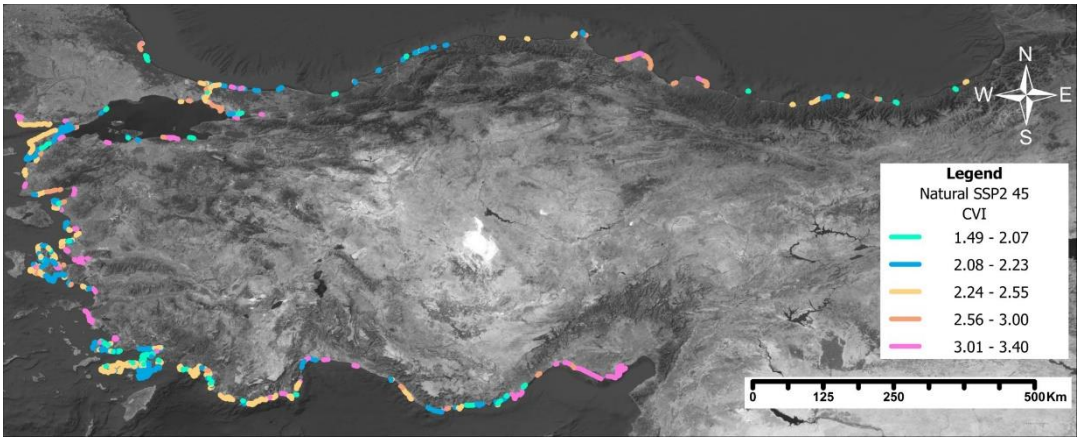


Figure 5.20. SSP2-4.5 Natural Conservation Zone CVI Jenks Distribution

In Figure 5.20, CVI classifications are given in Jenks Natural Breaks instead of FCVAM class definitions. When ordinary FCVAM class limits are utilized, CVI classes are narrowed down into three categories: very low, low, and moderate vulnerable. In Table 5.15, a more detailed comparison of Jenks and FCVAM classes is demonstrated. The Jenks grouping shows that 11.6% of the natural heritage sites are relatively among the most vulnerable sites and have a CVI score towards the high vulnerable range. Moreover, in Figure 5.21, a histogram with Jenks limit and 0.25 increment impact scores are given.

Table 5.15 SSP2-4.5 Natural Conservation Zone CVI Jenks & FCVAM Limits

Jenks Natural Breaks	Results	FCVAM Class	Results
< 2.12	304 (26.0%)	< 1.5 Very Low	2 (0.2%)
2.13 – 2.37	342 (29.2%)	1.5 – 2.5 Low	891 (76.1%)
2.38 – 2.63	255 (21.8%)	2.5 – 3.5 Moderate	278 (23.7%)
2.64 – 2.87	134 (11.4%)	3.5 – 4.25 High	0
> 2.88	136 (11.6%)	4.25 > Very High	0

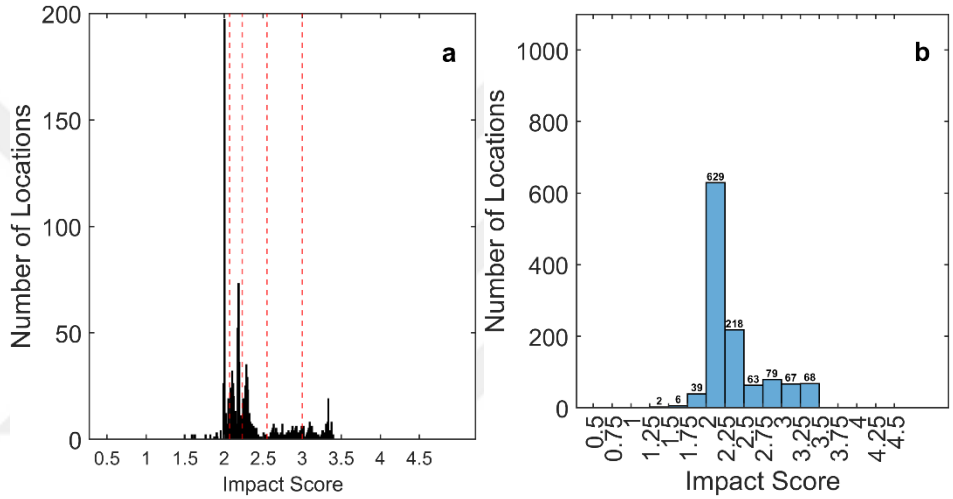


Figure 5.21. SSP2-4.5 Natural Conservation Zone CVI (a) Jenks (b) FCVAM Histograms

FCVAM class limits were determined using a global dataset and the implementation of the model for multiple countries. On the other hand, Jenks Natural Break limits defined in this study were generated by utilizing local results. This situation also explains why Turkish coasts are less likely to be classified as very high vulnerable. A few input parameters, such as wave climate and ESL, associated with Turkish coasts, are generally very insignificant compared to other parts of the world.

5.2.3 AR6 SSP5 – 8.5 Physical Impact Scores

5.2.3.1 Erosion

5.2.3.1.1 ErosionPP

In Figure 5.22, the distribution of erosion physical impact score distribution throughout natural conservation zones for the SSP5 - 8.5 pathway in terms of classes defined in FCVAM is given. On a national scale, like the SSP2 - 4.5, vulnerabilities against the physical impact of erosion are mainly classified as low and moderate. This claim is also supported by regional results in Table 5.16, according to which most moderate vulnerable areas are located in the Aegean Region.

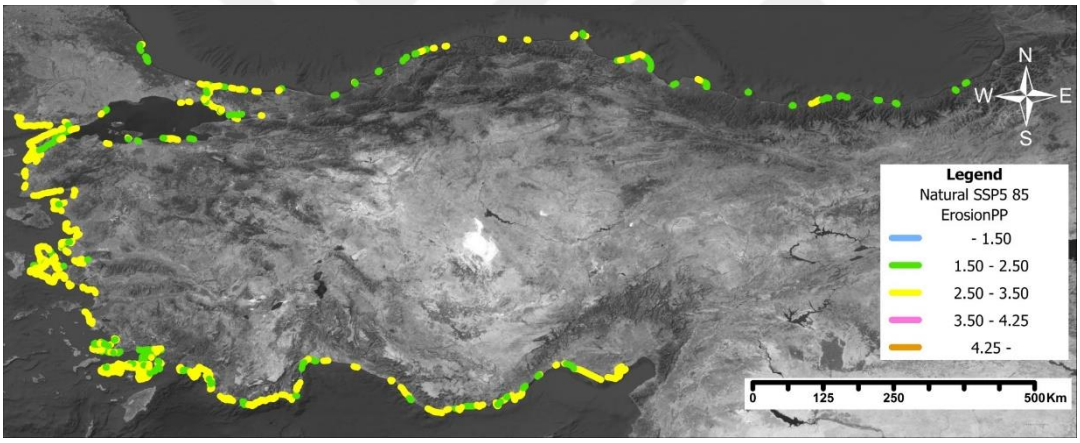


Figure 5.22. SSP5-8.5 Natural Conservation Zone ErosionPP Distribution

Table 5.16 Regional SSP5-8.5 Natural Conservation Zone ErosionPP Scores

ErosionPP	Mediterranean	Aegean	Marmara	Black Sea
< 1.5 Very Low	0	10 (0.9%)	3 (0.3%)	0
1.5 – 2.5 Low	53 (4.5%)	279 (23.8%)	103 (8.8%)	104 (8.9%)
2.5 – 3.5 Moderate	101 (8.6%)	371 (31.7%)	47 (4.0%)	100 (8.5%)
3.5 – 4.25 High	0	0	0	0
4.25 > Very High	0	0	0	0

Table 5.17 compares the SSP2-4.5 and SSP5-8.5 scenarios at the regional scale. As anticipated, the physical impact of erosion increases. However, as seen under the SSP2-4.5 scenario, the most severe vulnerability class of the studied shorelines remains moderate.

Table 5.17 SSP5-8.5 & SSP2-4.5 Natural Conservation Zone ErosionPP Comparison

ErosionPP Comparison	**Mediterranean**	**Aegean**	**Marmara**	**Black Sea**
< 1.5 Very Low	0	0	-1	0
1.5 – 2.5 Low	-17	-103	-12	-13
2.5 – 3.5 Moderate	17	103	13	13
3.5 – 4.25 High	0	0	0	0
4.25 > Very High	0	0	0	0

5.2.3.1.2 Erosion Impact Score

In Figure 5.23, the erosion impact score distribution over studied shorelines are given at a national scale for the AR6 SSP5-8.5 pathway.

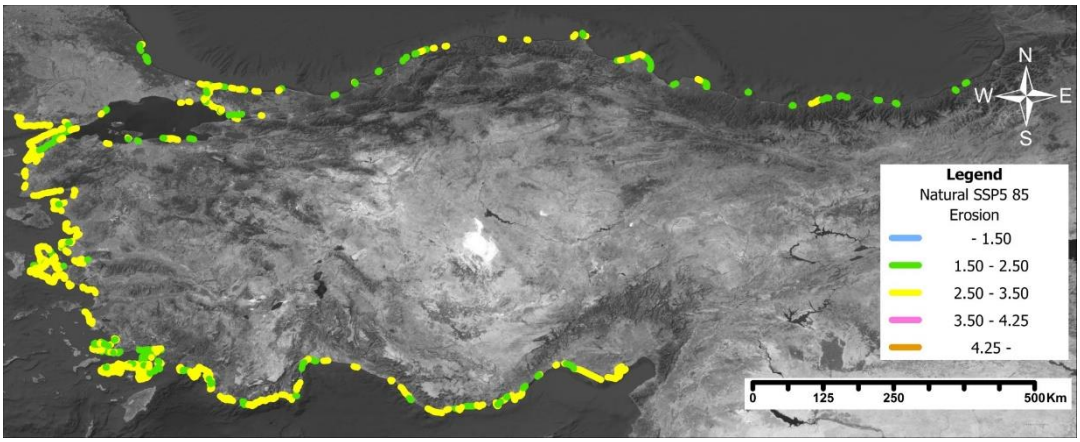


Figure 5.23. SSP5-8.5 Natural Conservation Zone Erosion Distribution

According to the Figure, most observed classes are low and moderate vulnerable, as could also be observed in Table 5.18. The only region with very low vulnerable shores is the Aegean Region. On the other hand, the Aegean Region also contains most of the moderate vulnerable shorelines, which is the most critical vulnerability class observed for erosion impact score.

Table 5.18 Regional SSP5-8.5 Natural Conservation Zone Erosion Scores

Erosion	Mediterranean	Aegean	Marmara	Black Sea
< 1.5 Very Low	0	10 (0.9%)	0	0
1.5 – 2.5 Low	53 (4.5%)	279 (23.8%)	106 (9.1%)	104 (8.9%)
2.5 – 3.5 Moderate	101 (8.6%)	371 (31.7%)	47 (4.0%)	100 (8.5%)
3.5 – 4.25 High	0	0	0	0
4.25 > Very High	0	0	0	0

To illustrate the effect of the applied AR6 SSP pathway on impact score class distributions, Table 5.19 shows shoreline classification changes when adopting the AR6 SSP5-8.5 scenario instead of SSP2-4.5. According to the Table, 143 shorelines originally classified as low vulnerability shifted to a moderate vulnerability class.

Table 5.19 SSP5-8.5 & SSP2-4.5 Erosion Natural Conservation Zone Comparison

Erosion Comparison	Mediterranean	Aegean	Marmara	Black Sea
< 1.5 Very Low	0	0	0	0
1.5 – 2.5 Low	-17	-100	-13	-13
2.5 – 3.5 Moderate	17	100	13	13
3.5 – 4.25 High	0	0	0	0
4.25 > Very High	0	0	0	0

Similar to SSP2-4.5, a comparison of erosion vulnerability score distribution with physical and human impact scores indicated that physical impact scores mainly

dictated erosion vulnerabilities. However, since the severity of erosion physical impact scores increased under SSP5-8.5 and human score distributions stayed as in SSP2-4.5, erosion physical scores became more dominant. Figure 5.24 gives a histogram comparison of physical and human impact scores. The figure demonstrates that, as in the case of SSP2-4.5, physical impact is more critical compared to human impact scores.

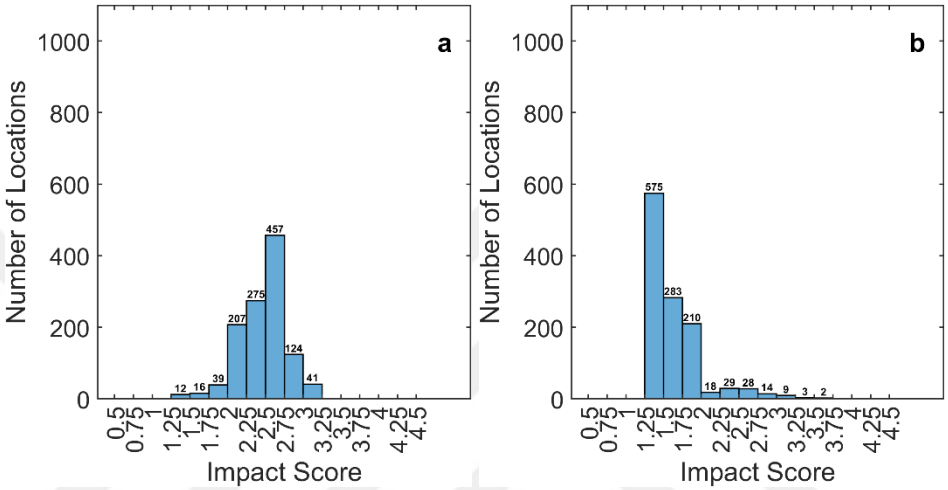


Figure 5.24. SSP5-8.5 Natural Conservation Zone Erosion (a) Physical Impact Score (b) Human Impact Score

Figure 5.25 presents score classifications using Jenks Natural Breaks rather than FCVAM class definitions. When the standard FCVAM class limits are applied, erosion vulnerability is narrowed down into three categories—very low, low, and moderate—since no study areas are classified as high or very high vulnerable. By applying Jenks classification, natural heritage sites are grouped into five categories based on relative vulnerabilities determined by their CVI scores. This approach enables the most vulnerable shoreline projections of natural heritage sites to be identified accordingly.

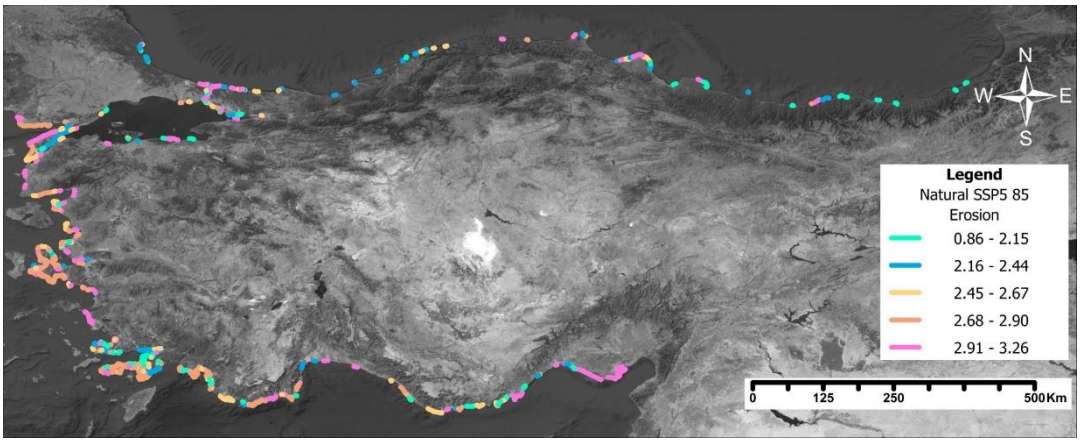


Figure 5.25. SSP5-8.5 Natural Conservation Zone Erosion Jenks Distribution

In Table 5.20, a more detailed comparison of Jenks and FCVAM classes is demonstrated. Moreover, in Figure 5.26, a histogram with Jenks limit and 0.25 increment impact scores are given. According to the findings, the erosion impact scores for projections of Turkish natural conservation zones along the shoreline primarily range between 2 and 3, similar to SSP2-4.5 results. However, under the SSP5-8.5 scenario, with adjusted Jenks natural breaks, it was indicated that 18.4% of the shorelines studied—those within the moderate to high vulnerability range according to standard FCVAM limits—are most susceptible to coastal erosion, representing a 1.7% increase compared to SSP2-4.5.

Table 5.20 SSP5-8.5 Natural Conservation Zone Erosion Jenks & FCVAM Limits

Jenks Natural Breaks	**Results**	**FCVAM Class**	**Results**
< 2.15	321 (27.4%)	< 1.5 Very Low	10 (0.9%)
2.16 – 2.44	207 (17.7%)	1.5 – 2.5 Low	542 (46.3%)
2.45 – 2.67	229 (19.6%)	2.5 – 3.5 Moderate	619 (52.9%)
2.68 – 2.90	198 (16.9%)	3.5 – 4.25 High	0
> 2.91	216 (18.4%)	4.25 < Very High	0

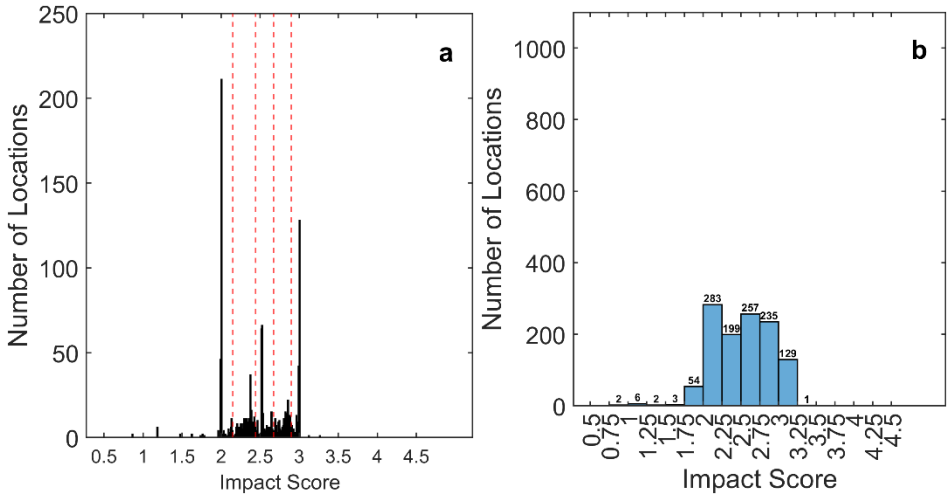


Figure 5.26. SSP5-8.5 Natural Conservation Zone Erosion (a) Jenks (b) FCVAM Histograms

5.2.3.2 Inundation

5.2.3.2.1 InundationPP

In Figure 5.27, the distribution of the inundation physical impact score throughout natural conservation zones for the SSP5 - 8.5 pathway in terms of classes defined in FCVAM is given. On a national scale, similar to SSP2-4.5 findings, no shoreline projections demonstrate very low vulnerability. Therefore, the dominant behavior of shores is low vulnerability in terms of inundation physical impact scores. However, compared to SSP2-4.5, impact scores tend to shift toward higher vulnerability classes, as illustrated in the Figure. Under the SSP5-8.5 scenario, new areas of very high vulnerability class have emerged along the Mediterranean and Black Sea coasts, as well as an increase in the number of very high vulnerable shorelines in the Aegean region.

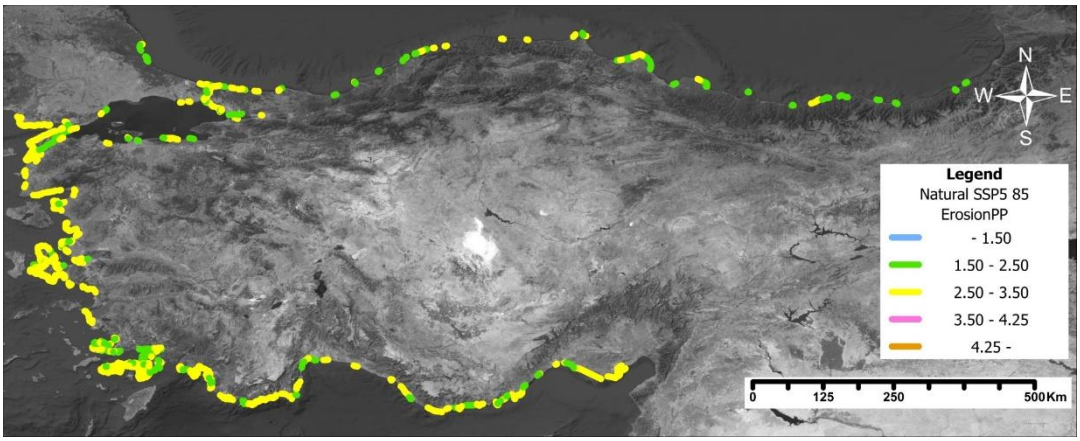


Figure 5.27. SSP5-8.5 Natural Conservation Zone InundationPP Distribution

Table 5.21 presents inundation physical impact scores at a regional scale. As mentioned, other than the Marmara Region, all regions have shorelines that are classified as very high vulnerable. Moreover, regarding high and very high vulnerable areas, the Aegean Region is the most susceptible region against inundation physical impacts as observed in SSP2-4.5. Despite the most vulnerable region staying the same when SSP5-8.5 was applied instead of SSP2-4.5, according to the comparison of vulnerability distributions given in Table 5.22, the number of very high vulnerable shores increased in the Black Sea region the most. Some locations have changed two vulnerability classes from one scenario to the other; therefore, these locations become the most vulnerable in the long term.

Table 5.21 Regional SSP5-8.5 Natural Conservation Zone InundationPP Scores

InundationPP	**Mediterranean**	**Aegean**	**Marmara**	**Black Sea**
< 1.5 Very Low	0	0	0	0
1.5 – 2.5 Low	101 (8.6%)	525 (44.8%)	102 (8.7%)	154 (13.2%)
2.5 – 3.5 Moderate	8 (0.7%)	58 (5.0%)	28 (2.4%)	16 (1.4%)
3.5 – 4.25 High	42 (3.6%)	73 (6.2%)	23 (2.0%)	30 (2.6%)
4.25 > Very High	3 (0.3%)	4 (0.3%)	0	4 (0.3%)

Table 5.22 SSP5-8.5 & SSP2-4.5 Natural Conservation Zone InundationPP Comparison

InundationPP Comparison	Mediterranean	Aegean	Marmara	Black Sea
< 1.5 Very Low	0	0	0	0
1.5 – 2.5 Low	0	-10	-1	-2
2.5 – 3.5 Moderate	-9	-6	-6	-9
3.5 – 4.25 High	6	13	7	7
4.25 > Very High	3	3	0	4

5.2.3.2.2 Inundation Impact Score

Inundation physical and human impact scores were aggregated to obtain inundation vulnerability scores in Figure 5.28 for AR6 SSP5-8.5. According to the class distribution given in the Figure, low vulnerable shorelines against inundation are the most common vulnerability class along Turkish shorelines, as observed in SSP2-4.5.

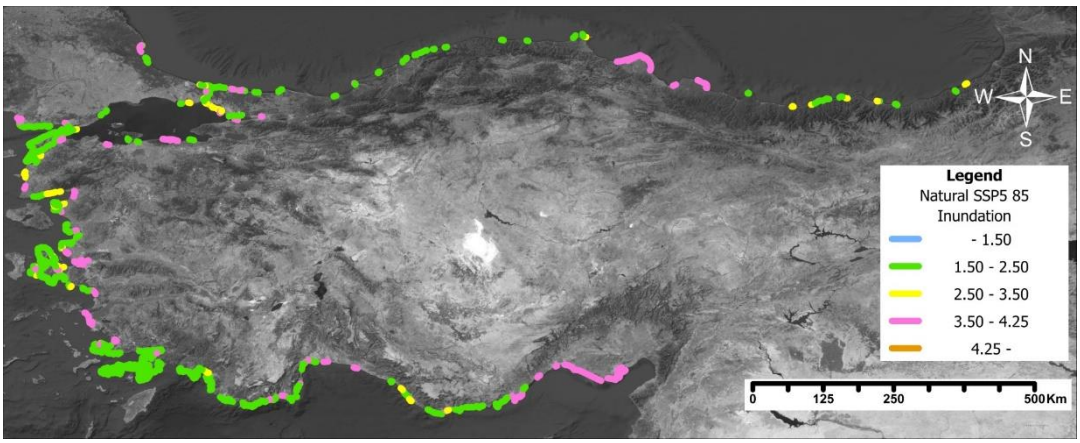


Figure 5.28. SSP5-8.5 Natural Conservation Zone Inundation Distribution

On a national scale, although there are nine shorelines that became very high vulnerable in terms of inundation impact score when the SSP5-8.5 pathway was considered, there are no shores that are very high vulnerable in terms of inundation impact score, which is also supported by results given in Table 5.23. at a regional

scale. According to the table, most of the high vulnerable shorelines are located in the Aegean Region, and no very high vulnerable areas exist in any of the regions.

Table 5.23 Regional SSP5-8.5 Natural Conservation Zone Inundation Scores

Inundation	Mediterranean	Aegean	Marmara	Black Sea
< 1.5 Very Low	0	0	0	0
1.5 – 2.5 Low	99 (8.5%)	516 (44.1%)	102 (8.7%)	154 (13.2%)
2.5 – 3.5 Moderate	10 (0.9%)	67 (5.7%)	28 (2.4%)	16 (1.4%)
3.5 – 4.25 High	45 (3.8%)	77 (6.6%)	23 (2.0%)	34 (2.9%)
4.25 > Very High	0	0	0	0

In Table 5.24, two pathway findings are compared. According to that Table, a change in the considered scenario resulted in 43 new study shorelines being classified as high vulnerable. The results show that human parameters for many of these locations tend to increase the region's resilience, considering the higher physical impact vulnerability compared to aggregated values.

Table 5.24 SSP5-8.5 & SSP2-4.5 Natural Conservation Zone Inundation Comparison

Inundation Comparison	Mediterranean	Aegean	Marmara	Black Sea
< 1.5 Very Low	0	0	0	0
1.5 – 2.5 Low	0	-10	-1	-2
2.5 – 3.5 Moderate	-9	-6	-6	-9
3.5 – 4.25 High	9	16	7	11
4.25 > Very High	0	0	0	0

Figure 5.29 presents histograms of inundation physical and human impact scores. From the histograms, it could be deduced that physical impact scores become more dominant as impact scores increase compared to human impact scores. Since

inundation vulnerability is calculated by aggregating these two scores, the vulnerability is more dictated by the physical impact score. Moreover, since SSP5-8.5 vulnerability distributions are more critical compared to SSP2-4.5, the effect of this domination is expected to be increased. The outcome could be observed if the distribution of physical and human impact scores over regions is compared with regional inundation results. Patterns given in the physical impact score resemble inundation vulnerability, which results in behavior more.

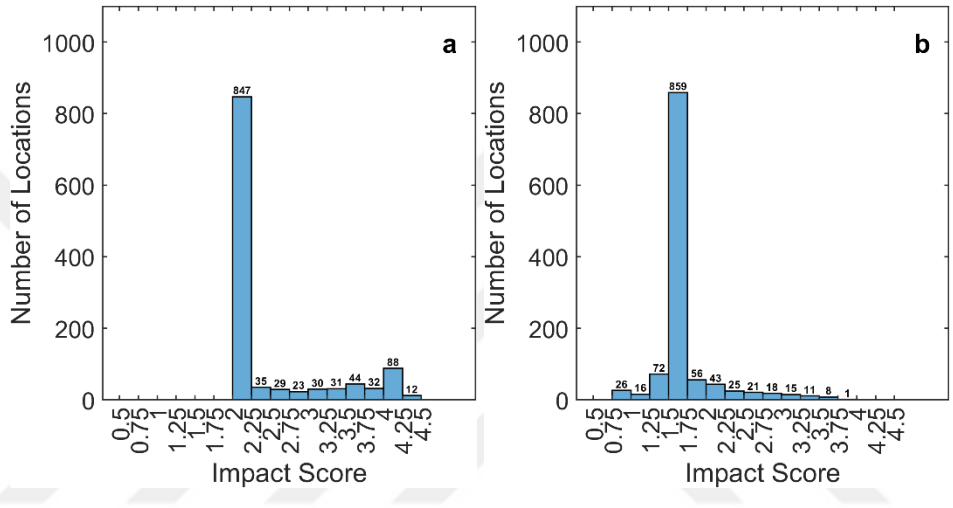


Figure 5.29. SSP5-8.5 Natural Conservation Zone Inundation Component Histogram

In Figure 5.30, inundation score classifications are given in Jenks Natural Breaks instead of FCVAM class limits. When ordinary FCVAM class limits are utilized, inundation vulnerability classes are narrowed down into three categories of low, moderate, and high vulnerability concerning global classification, as observed in SSP2-4.5. With Jenks classification, the most vulnerable natural heritage sites for the Turkish coastline among all the natural heritage sites of Turkiye are determined.

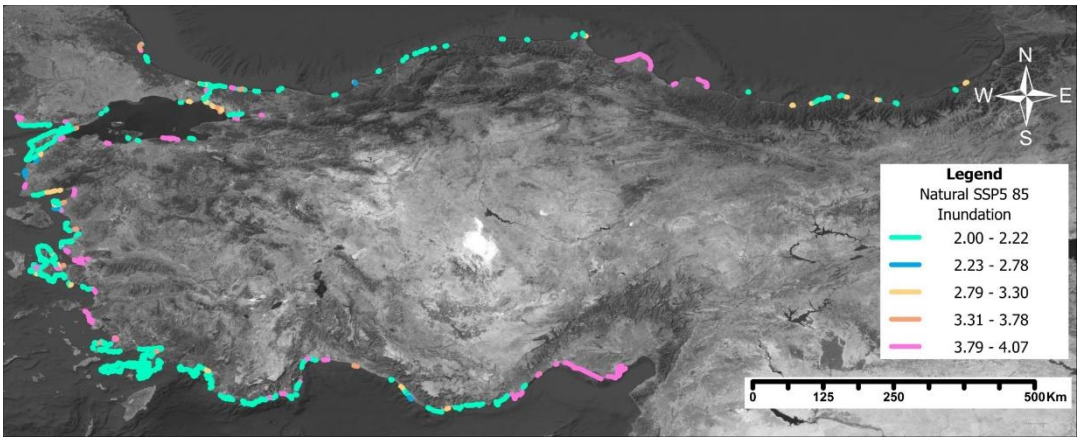


Figure 5.30. SSP5-8.5 Natural Conservation Zone Inundation Jenks Distribution

In Table 5.25, a more detailed comparison of Jenks and FCVAM classes is demonstrated. Making classification concerning natural Jenks breaks indicated that about 12.1% of the studied shorelines, which are high vulnerable according to the original class limits, belong to the most critical class against inundation. Compared with SSP2-4.5, the most critical area ratio, there was about a 1.8% increase in SSP5-8.5. In Figure 5.31, a histogram with Jenks limit and 0.25 increment impact scores are also given for further distribution detail. According to them, although there is accumulation around inundation impact scores of "3" and "4", the majority of shorelines are given the vulnerability score of "2". However, although SSP2-4.5 has nine shores scored between 4 - 4.25, this number increased to 19 locations in SSP5-8.5.

Table 5.25 SSP5-8.5 Natural Conservation Zone Inundation Jenks & FCVAM Limits

Jenks Natural Breaks	**Results**	**FCVAM Class**	**Results**
< 2.22	847 (72.3%)	< 1.5 Very Low	0
2.23 – 2.78	50 (4.3%)	1.5 – 2.5 Low	871 (74.4%)
2.79 – 3.30	88 (7.5%)	2.5 – 3.5 Moderate	121 (10.3%)
3.31 – 3.78	44 (3.8%)	3.5 – 4.25 High	179 (15.3%)
> 3.79	142 (12.1%)	4.25 < Very High	0

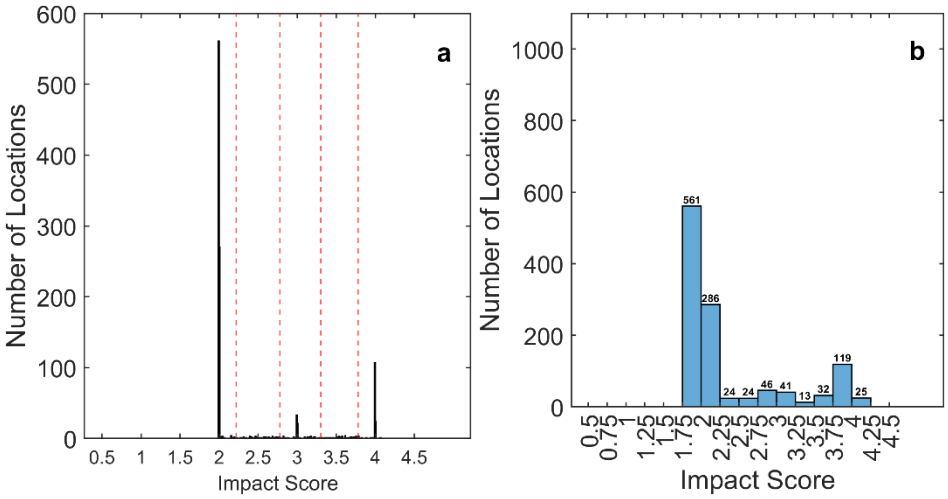


Figure 5.31. SSP5-8.5 Natural Conservation Zone Inundation (a) Jenks (b) FCVAM Histograms

5.2.3.3 Storm Surge

5.2.3.3.1 Storm SurgePP

Figure 5.32 shows the storm surge physical impact score distribution throughout natural conservation zones for the SSP5 - 8.5 pathway in terms of classes defined in FCVAM.

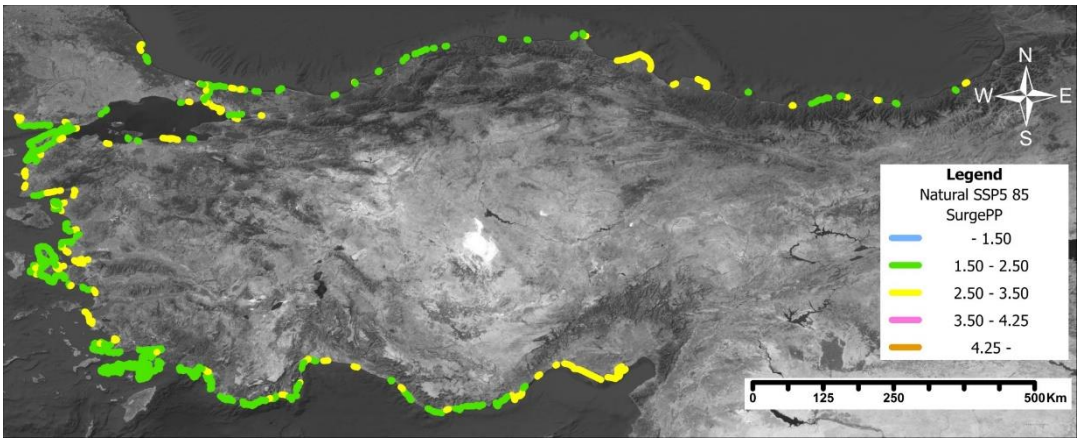


Figure 5.32. SSP5-8.5 Natural Conservation Zone Storm SurgePP Distribution

The national-wide vulnerability of the Turkish natural conservation zone assessment indicates that in terms of storm surge impact scores, only low and moderate vulnerable areas are located around Turkish coasts for SSP5-8.5, as observed in SSP2-4.5, supported by Table 5.26. However, the number of moderate vulnerable locations increases with the application of SSP5-8.5; changes are presented in Table 5.27. Despite having fewer studied shorelines, with 19 locations, the Black Sea Region demonstrated an increase in the most significant number of class increases.

Table 5.26 Regional SSP5-8.5 Natural Conservation Zone Storm SurgePP Scores

SurgePP	Mediterranean	Aegean	Marmara	Black Sea
< 1.5 Very Low	0	0	0	0
1.5 – 2.5 Low	100 (8.5%)	530 (45.3%)	101 (8.6%)	155 (13.2%)
2.5 – 3.5 Moderate	54 (4.6%)	130 (11.1%)	52 (4.4%)	49 (4.2%)
3.5 – 4.25 High	0	0	0	0
4.25 > Very High	0	0	0	0

Table 5.27 SSP5-8.5 & SSP2-4.5 Storm SurgePP Comparison

SurgePP Comparison	Mediterranean	Aegean	Marmara	Black Sea
< 1.5 Very Low	0	0	0	0
1.5 – 2.5 Low	-5	-17	-3	-19
2.5 – 3.5 Moderate	5	17	3	19
3.5 – 4.25 High	0	0	0	0
4.25 > Very High	0	0	0	0

5.2.3.3.2 Storm Surge Impact Score

Storm surge physical and human impact scores were aggregated to obtain storm surge vulnerability scores, demonstrated in Figure 5.33 for AR6 SSP5-8.5. According to the Figure, in terms of storm surge impact score, studied shorelines

along Turkish coasts could be narrowed down into 2 classes of low and moderate vulnerability, as observed in SSP2-4.5.

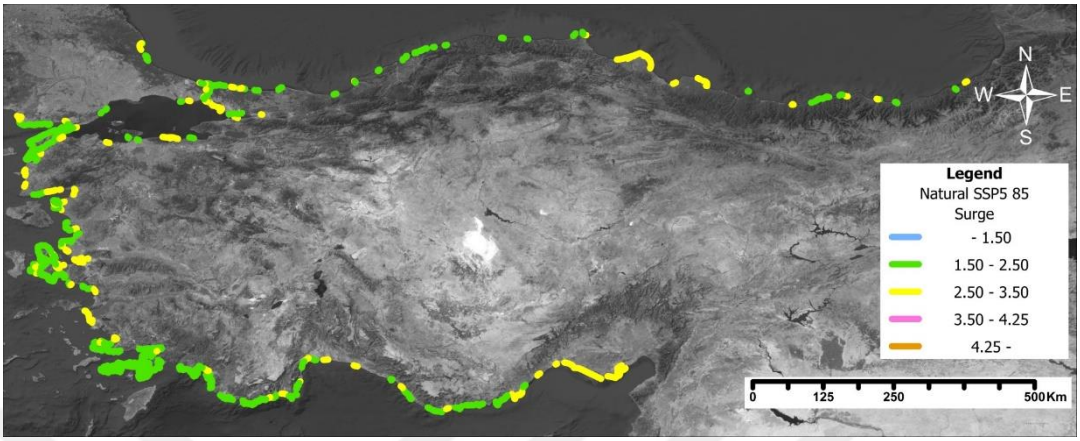


Figure 5.33. SSP5-8.5 Natural Conservation Zone Storm Surge Distribution

Regional results given in Table 5.28 also confirm the statement. Although there are some class changes according to Table 5.29, these changes occurred between low and moderate vulnerability classes. Effects of physical impact score class changes could also be reflected in storm surge scores. As in the storm surge physical impact scores, despite having fewer locations within the Aegean Region, the Black Sea Region demonstrated the highest number of changes. The sites that increased in vulnerability across all regions correspond to around 3% of all the cultural heritage sites.

Table 5.28 Regional SSP5-8.5 Natural Conservation Zone Storm Surge Scores

Surge	Mediterranean	Aegean	Marmara	Black Sea
< 1.5 Very Low	0	0	0	0
1.5 – 2.5 Low	100 (8.5%)	523 (44.7%)	101 (8.6%)	155 (13.2%)
2.5 – 3.5 Moderate	54 (4.6%)	137 (11.7%)	52 (4.4%)	49 (4.2%)
3.5 – 4.25 High	0	0	0	0
4.25 > Very High	0	0	0	0

Table 5.29 SSP5-8.5 & SSP2-4.5 Storm Surge Comparison

Surge Comparison	Mediterranean	Aegean	Marmara	Black Sea
< 1.5 Very Low	0	0	0	0
1.5 – 2.5 Low	-5	-17	-3	-19
2.5 – 3.5 Moderate	5	17	3	19
3.5 – 4.25 High	0	0	0	0
4.25 > Very High	0	0	0	0

The score distribution histogram of physical and human impact scores is given in Figure 5.34.

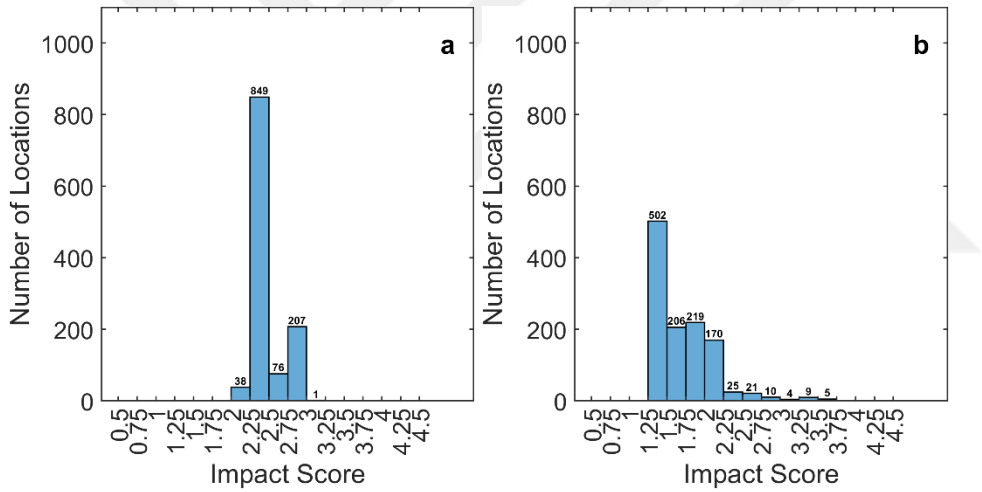


Figure 5.34. SSP5-8.5 Natural Conservation Zone Surge Component Histogram

According to the Figure, physical impact scores are clustered at a narrower area of between 2 to 3.25 in SSP5-8.5 -limits were 1.75 to 3 in SSP2-4.5, compared to human impact scores, which are distributed over a wider between 1.25 to 3.75. This comparison indicates that cultural heritage sites have similar characteristics considering the parameters assessed, whereas a broader range of human activities occurs around them. Although the influence of human activities is much lower, which is also expected as most of these sites are protected by laws, limiting some of

the activities assessed by the FCVAM model and increasing the resilience as the shorelines tend to be more natural. Figure 5.35 gives score classifications in Jenks Natural Breaks instead of FCVAM class definitions.

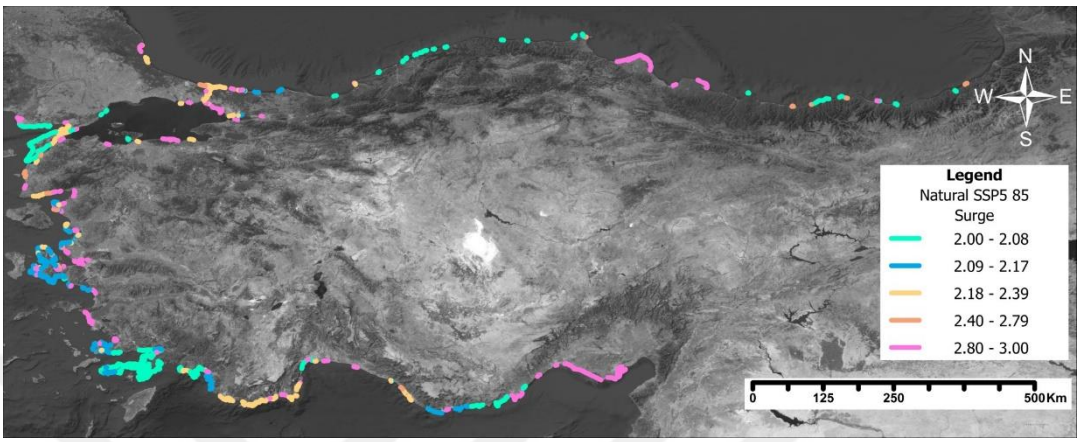


Figure 5.35. SSP5-8.5 Natural Conservation Zone Storm Surge Jenks Distribution

When ordinary FCVAM class limits are utilized, storm surge vulnerability classes are narrowed down into low and moderate vulnerable categories. Table 5.30 also presents a more detailed comparison of Jenks and FCVAM classes. Grouping vulnerability with renewed Natural Jenks breaks for SSP5-8.5, it is determined that around 20.7% of the natural heritage sites are moderate to high vulnerable and belong to the most vulnerable group among Turkish coastlines for storm surge flooding with an increase of about 10% comparing to SSP2-4.5.

Table 5.30 SSP5-8.5 Natural Conservation Zone Surge Jenks & FCVAM Limits

Jenks Natural Breaks	**Results**	**FCVAM Class**	**Results**
< 2.08	315 (26.9%)	< 1.5 Very Low	0
2.09 – 2.17	273 (23.3%)	1.5 – 2.5 Low	879 (75.1%)
2.18 – 2.39	273 (23.3%)	2.5 – 3.5 Moderate	292 (24.9%)
2.40 – 2.79	68 (5.8%)	3.5 – 4.25 High	0
> 2.80	242 (20.7%)	4.25 < Very High	0

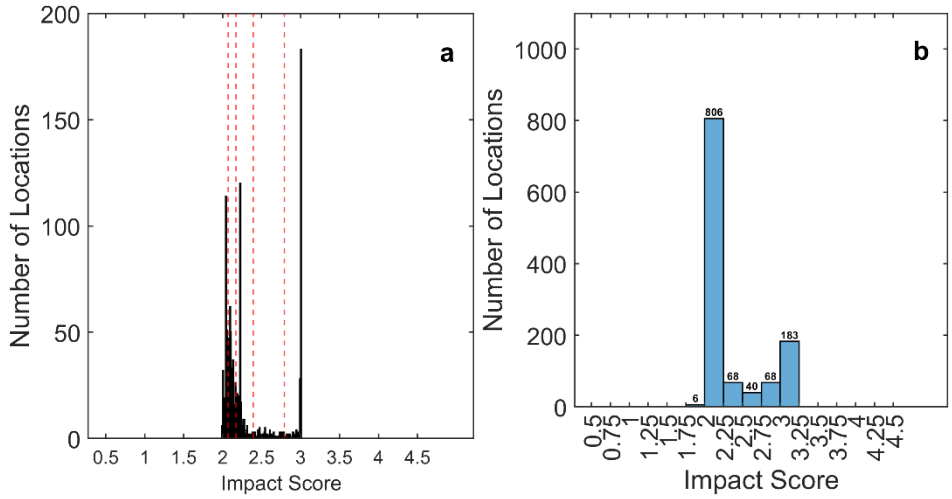


Figure 5.36. SSP5-8.5 Natural Conservation Zone Storm Surge (a) Jenks (b) FCVAM Histograms

5.2.3.4 Coastal Vulnerability Index

All three erosion, inundation, and storm surge vulnerability scores were aggregated to obtain CVI, the distribution of which is demonstrated in Figure 5.37 for AR6 SSP5-8.5. According to the class distribution in the Figure, contrary to SSP2-4.5, there are no very low vulnerable locations. However, like SSP2-4.5, most observed vulnerability classes are still moderate.

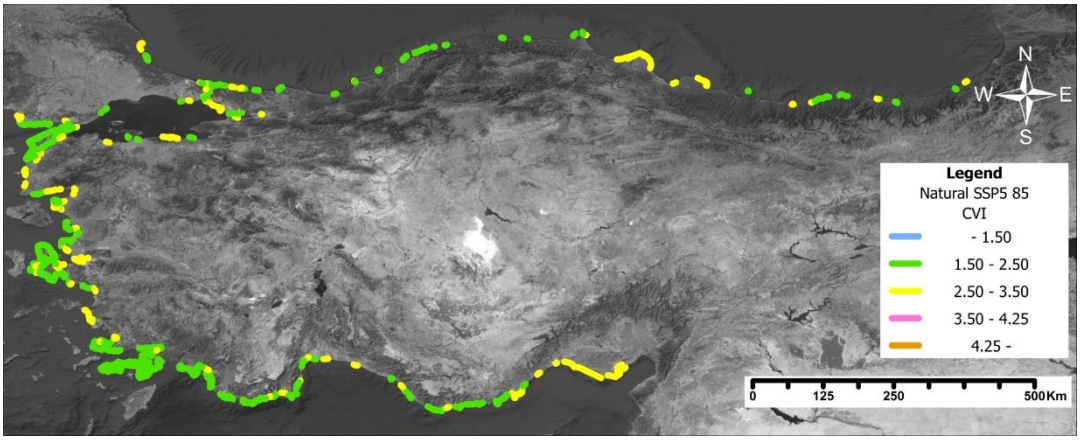


Figure 5.37. SSP5-8.5 Natural Conservation Zone CVI Distribution

According to regional results in Table 5.31, if several vulnerable areas are considered, it could be deduced that the Aegean Region contains most of the low vulnerable areas. At the same time, the Mediterranean Region has the least number. On the other hand, percentage distribution considering the locations within the region indicates the Black Sea Region as the least vulnerable region, the same as SSP2-4.5. In Table 5.32, regional scale changes are presented. In SSP2-4.5, there were only 2 locations classified as very low vulnerable throughout the Turkish shoreline in the Aegean Region. However, with SSP5-8.5, their vulnerability classes were changed.

Table 5.31 Regional SSP5-8.5 Natural Conservation Zone CVI Scores

CVI	**Mediterranean**	**Aegean**	**Marmara**	**Black Sea**
< 1.5 Very Low	0	0	0	0
1.5 – 2.5 Low	100 (8.5%)	515 (44.0%)	103 (8.8%)	154 (13.2%)
2.5 – 3.5 Moderate	54 (4.6%)	145 (12.4%)	50 (4.3%)	50 (4.3%)
3.5 – 4.25 High	0	0	0	0
4.25 > Very High	0	0	0	0

Table 5.32 SSP5-8.5 & SSP2-4.5 CVI Comparison

CVI Comparison	**Mediterranean**	**Aegean**	**Marmara**	**Black Sea**
< 1.5 Very Low	0	-2	0	0
1.5 – 2.5 Low	0	-13	-2	-4
2.5 – 3.5 Moderate	0	15	2	4
3.5 – 4.25 High	0	0	0	0
4.25 > Very High	0	0	0	0

As a summary of results for SSP5-8.5 Table 5.33, score distributions concerning module and vulnerability class were given. From the Table, it could be deduced that module vulnerability scores demonstrate similar behaviors with physical impact scores. In terms of modules, Turkish shores are most sensitive to inundation,

especially because of physical factors. Moreover, inundation is the only module against which a portion of studied shores demonstrated high vulnerability.

Table 5.33 SSP5-8.5 Natural Conservation Zone Impact & CVI Scores

NAT SSP5-85	Erosion			Inundation			Storm Surge			CVI
	PP	HI	Vul	PP	HI	Vul	PP	HI	Vul	
< 1.5 Very Low	13	586	10	0	114	0	0	509	0	0
1.5 – 2.5 Low	539	531	542	882	983	871	886	613	879	872
2.5 – 3.5 Moderate	619	52	619	110	65	121	285	44	292	299
3.5 – 4.25 High	0	2	0	168	9	179	0	5	0	0
4.25 > Very High	0	0	0	11	0	0	0	0	0	0

Table 5.34 SSP5-8.5 & SSP2-4.5 Impact Score Comparison

SSP2-45 SSP5-85	Erosion			Inundation			Storm Surge			CVI
	PP	HI	Vul	PP	HI	Vul	PP	HI	Vul	
< 1.5 Very Low	-1	0	0	0	0	0	0	0	0	-2
1.5 – 2.5 Low	-145	0	-143	-13	0	-13	-44	0	-44	-19
2.5 – 3.5 Moderate	146	0	143	-30	0	-30	44	0	44	21
3.5 – 4.25 High	0	0	0	33	0	43	0	0	0	0
4.25 > Very High	0	0	0	10	0	0	0	0	0	0

Table 5.34 presents scenario vulnerability class distribution changes of modules and impact scores. According to that table, the highest number of class shifts occurred in erosion physical impact. In contrast, in terms of vulnerability class severity, inundation physical impact scores demonstrated the most drastic increases.

In Figure 5.38, CVI classifications are given in Jenks Natural Breaks instead of FCVAM class definitions for SSP5-8.5. Moreover, Table 5.35 demonstrates a more detailed comparison of Jenks and FCVAM classes.

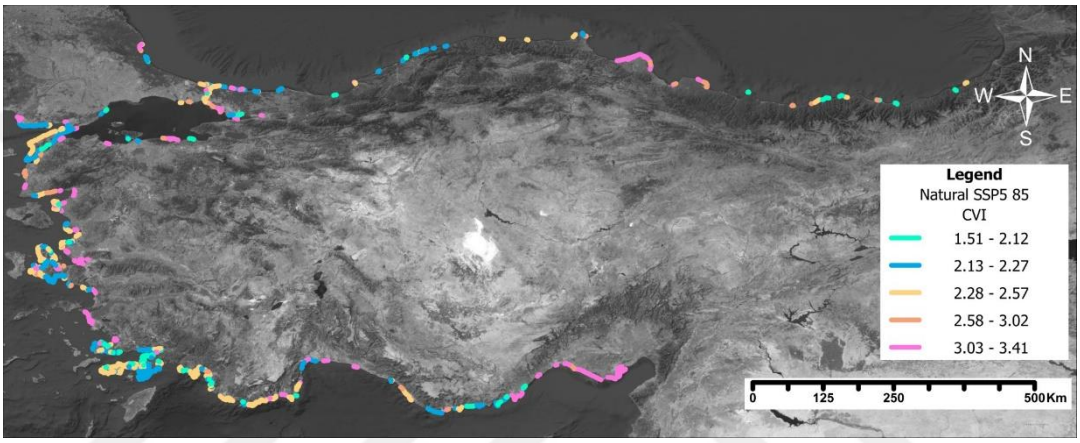


Figure 5.38. SSP5-8.5 Natural Conservation Zone CVI Jenks Distribution

The Jenks grouping shows that with renewed natural breaks compared to SSP2-4.5, the percentage distribution of natural heritage sites among the most vulnerable sites relatively increased from 11.6% to 15.6%. Moreover, in Figure 5.39, a histogram with Jenks limit and 0.25 increment impact scores are given.

Table 5.35 SSP5-8.5 Natural Conservation Zone CVI Jenks & FCVAM Limits

Jenks Natural Breaks	**Results**	**FCVAM Class**	**Results**
< 2.12	281 (24%)	< 1.5 Very Low	0
2.13 – 2.27	333 (28.4%)	1.5 – 2.5 Low	872 (74.5%)
2.28 – 2.57	271 (23.1%)	2.5 – 3.5 Moderate	299 (25.5%)
2.58 – 3.02	103 (8.8%)	3.5 – 4.25 High	0
> 3.03	183 (15.6%)	4.25 < Very High	0

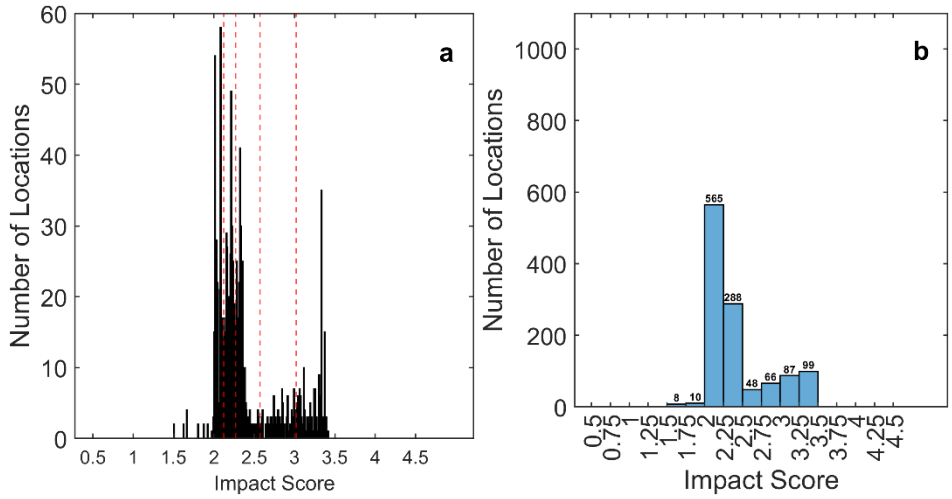


Figure 5.39. SSP5-8.5 Natural Conservation Zone CVI (a) Jenks (b) FCVAM Histograms

Even though CVI scores became more critical with the change of adopted pathway, there are still no high or very high vulnerable shoreline projections of natural conservation zones. This is because FCVAM class limits were determined using a global dataset along with the implementation of the model for multiple countries, the effect of which could be observed when FCVAM limits are compared with natural Jenks breaks. Few input parameters, such as wave climate and ESL associated with Turkish coasts, are generally very insignificant compared to other parts of the world.

5.3 Coastal Cultural Heritage Sites

5.3.1 Human Impact Scores

As explained in section 5.2.1, While SSP scenarios suggest anticipated changes or motivations behind human activities, no such projections are available specifically for Turkish coastlines. Consequently, the potential effects of future changes in human activity have not been included. This implies that SSP2-4.5 and SSP5-8.5 scenarios are expected to yield identical human impact scores for the same study area. Therefore, this section presents human impact scores for cultural heritage areas as scenario-independent.

5.3.1.1 Erosion

In Figure 5.40, erosion human impact score distribution throughout cultural heritage areas in terms of classes defined in FCVAM is given. According to the Figure, Turkish coasts of archeological heritage sites are mainly very low and low vulnerable to erosion in terms of human impact.

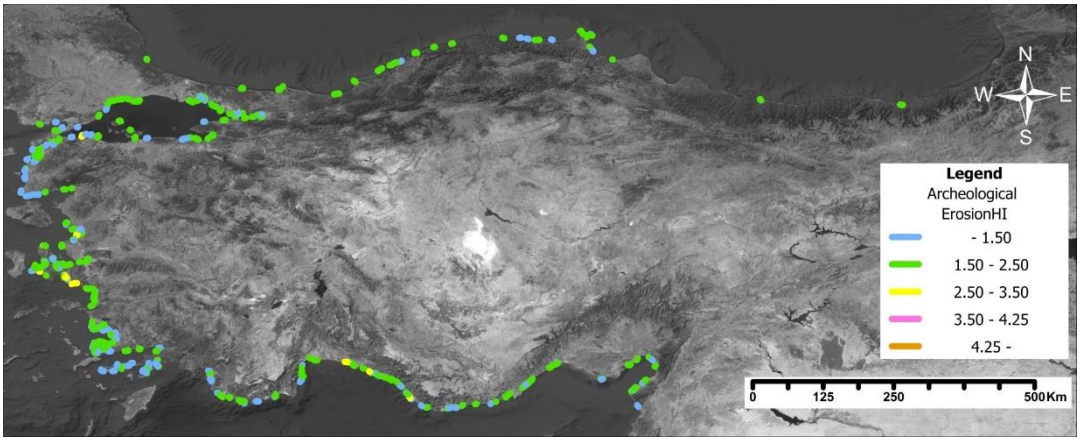


Figure 5.40. Cultural Heritage Site Erosion Human Impact Distribution

In the regional aspect, the most vulnerable areas are located in the Aegean Region. This statement is also supported by Table 5.36, in which only the Aegean Region

has a shoreline that could be classified as high vulnerable. On the other hand, the highest number of very low vulnerable shores are also located in the Aegean Region, followed by the Mediterranean Region.

Table 5.36 Regional Cultural Heritage Site Erosion Human Impact Scores

Erosion HI	Mediterranean	Aegean	Marmara	Black Sea
< 1.5 Very Low	169 (14.4%)	300 (25.5%)	41 (3.5%)	38 (3.2%)
1.5 – 2.5 Low	146 (12.4%)	287 (24.4%)	100 (8.5%)	74 (6.3%)
2.5 – 3.5 Moderate	5 (0.4%)	13 (1.1%)	2 (0.2%)	0
3.5 – 4.25 High	0	1 (0.1%)	0	0
4.25 > Very High	0	0	0	0

5.3.1.2 Inundation

In Figure 5.41, the distribution of inundation human impact scores throughout cultural heritage areas in terms of classes defined in FCVAM is given. The Turkish shorelines of cultural heritage areas demonstrate low vulnerability to inundation, considering the human impact parameters.

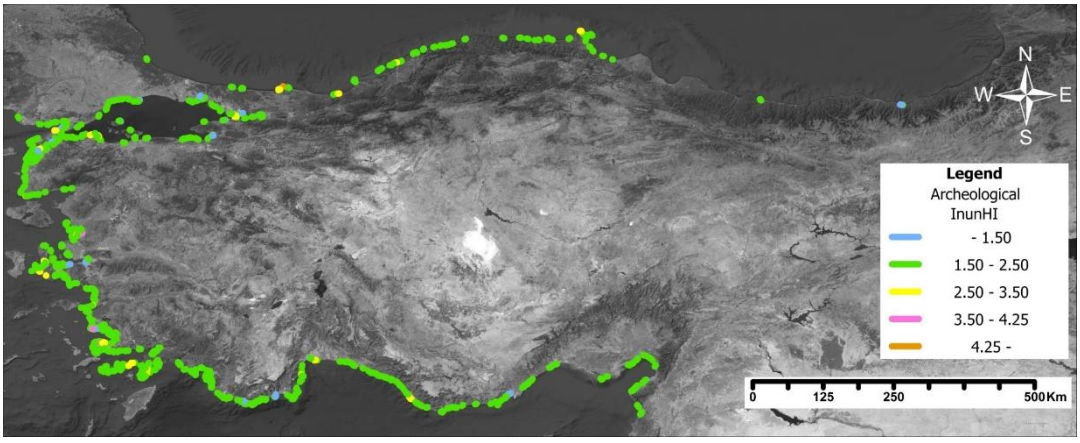


Figure 5.41. Cultural Heritage Site Erosion Inundation Impact Distribution

In Table 5.37, cultural heritage area inundation vulnerability results are given at a regional scale. For this aspect, the Aegean and Black Sea Regions are the only

regions with shorelines classified as high vulnerable regarding the Inundation Human impact score. Although the number of high-vulnerable shores is higher in the Aegean Region, the Black Sea Region is the only region with a shoreline classified as very high vulnerable. Contrary to the Black Sea, the Marmara Region contains the most shores classified as very low-vulnerable.

Table 5.37 Regional Cultural Heritage Site Inundation Human Impact Scores

Inundation HI	Mediterranean	Aegean	Marmara	Black Sea
< 1.5 Very Low	19 (1.6%)	20 (1.7%)	33 (2.8%)	14 (1.2%)
1.5 – 2.5 Low	295 (25.1%)	519 (44.1%)	106 (9%)	90 (7.7%)
2.5 – 3.5 Moderate	6 (0.5%)	49 (4.2%)	4 (0.3%)	6 (0.5%)
3.5 – 4.25 High	0	13 (1.1%)	0	1 (0.1%)
4.25 > Very High	0	0	0	1 (0.1%)

5.3.1.3 Storm Surge

Figure 5.42 shows the distribution of storm surge human impact score distribution throughout cultural heritage areas regarding classes defined in FCVAM. Projections of cultural heritage areas over the Turkish shoreline indicated very low and low vulnerability against storm surge for human impact parameters.

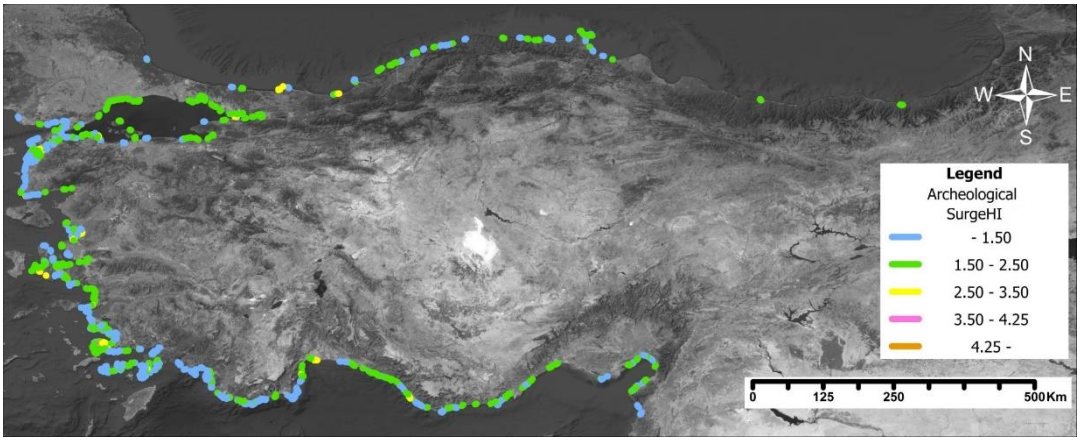


Figure 5.42. Cultural Heritage Site Storm Surge Human Impact Distribution

In Table 5.38, regional scale vulnerability distributions are presented. From a regional perspective, only the Aegean and Black Sea Region contain high vulnerable shorelines. Contrary to this, the highest number of very low vulnerable shorelines are also located in the Aegean Region.

Table 5.38 Regional Cultural Heritage Site Surge Human Impact Scores

Surge HI	Mediterranean	Aegean	Marmara	Black Sea
< 1.5 Very Low	139 (11.8%)	254 (21.6%)	22 (1.9%)	35 (3%)
1.5 – 2.5 Low	174 (14.8%)	305 (25.9%)	117 (9.9%)	71 (6%)
2.5 – 3.5 Moderate	7 (0.6%)	35 (3%)	4 (0.3%)	5 (0.4%)
3.5 – 4.25 High	0	7 (0.6%)	0	1 (0.1%)
4.25 > Very High	0	0	0	0

5.3.2 AR6 SSP2-4.5 Physical Impact Scores

This section presents the physical impact, aggregated impact, and CVI results of cultural heritage areas, calculated using predicted RSLR and ESL values based on the IPCC AR6 SSP2–4.5 scenario.

5.3.2.1 Erosion

5.3.2.1.1 ErosionPP

In Figure 5.43, erosion physical impact score distribution throughout cultural heritage areas for the SSP2 - 4.5 pathway in terms of classes defined in FCVAM is given. On a national scale, low vulnerability against the physical impact of erosion is dominant. This claim is also supported by regional results given in Table 5.39, according to which the majority of low-vulnerable areas are located in the Aegean Region, followed by the Mediterranean Region. On the other hand, the Aegean and

Mediterranean Regions also have the highest number of moderate vulnerable shores, the most critical class observed for erosion physical impact scores.

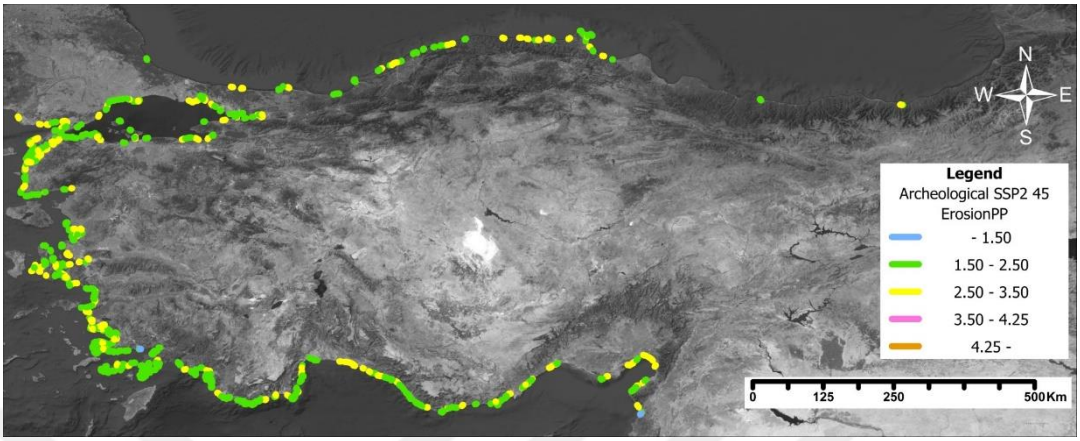


Figure 5.43. SSP2-4.5 Cultural Heritage Site ErosionPP Distribution

Table 5.39 Regional SSP2-4.5 Cultural Heritage Site ErosionPP Scores

Erosion PP	Mediterranean	Aegean	Marmara	Black Sea
< 1.5 Very Low	1 (0.1%)	2 (0.2%)	0	0
1.5 – 2.5 Low	223 (19%)	420 (35.7%)	92 (7.8%)	82 (7%)
2.5 – 3.5 Moderate	96 (8.2%)	179 (15.2%)	51 (4.3%)	30 (2.6%)
3.5 – 4.25 High	0	0	0	0
4.25 > Very High	0	0	0	0

5.3.2.1.2 Erosion Impact Score

Erosion physical and human impact scores were aggregated to obtain erosion vulnerability scores, demonstrated in Figure 5.44 under the pathway of AR6 SSP2-4.5 for cultural heritage sites. According to the class distribution in the Figure, low vulnerable shorelines against erosion are the most common vulnerability class along Turkish shorelines. Moreover, no shorelines have been studied as high or very high in erosion vulnerability.

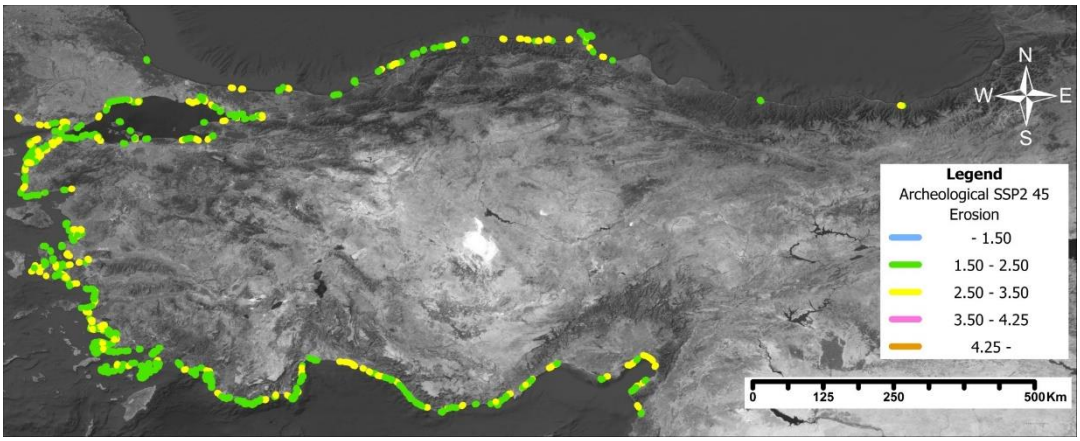


Figure 5.44. SSP2-4.5 Cultural Heritage Site Erosion Distribution

More detailed results are given in Table 5.40 at a regional scale. According to that table, the most vulnerable shorelines are in the Aegean region. The general distribution of the Erosion impact score demonstrates similarities with the erosion physical impact score given in Table 5.39.

Table 5.40 Regional SSP2-4.5 Cultural Heritage Site Erosion Scores

Erosion	Mediterranean	Aegean	Marmara	Black Sea
< 1.5 Very Low	2 (0.2%)	2 (0.2%)	0	0
1.5 – 2.5 Low	222 (18.9%)	420 (35.7%)	92 (7.8%)	82 (7%)
2.5 – 3.5 Moderate	96 (8.2%)	179 (15.2%)	51 (4.3%)	30 (2.6%)
3.5 – 4.25 High	0	0	0	0
4.25 > Very High	0	0	0	0

The distribution of erosion vulnerability scores with physical and human impact scores indicated that physical impact scores mainly dictated erosion vulnerabilities. Figure 5.45 shows a histogram comparison of physical and human impact scores. Histograms demonstrate that physical impact is more critical than human impact scores in the case of erosion.

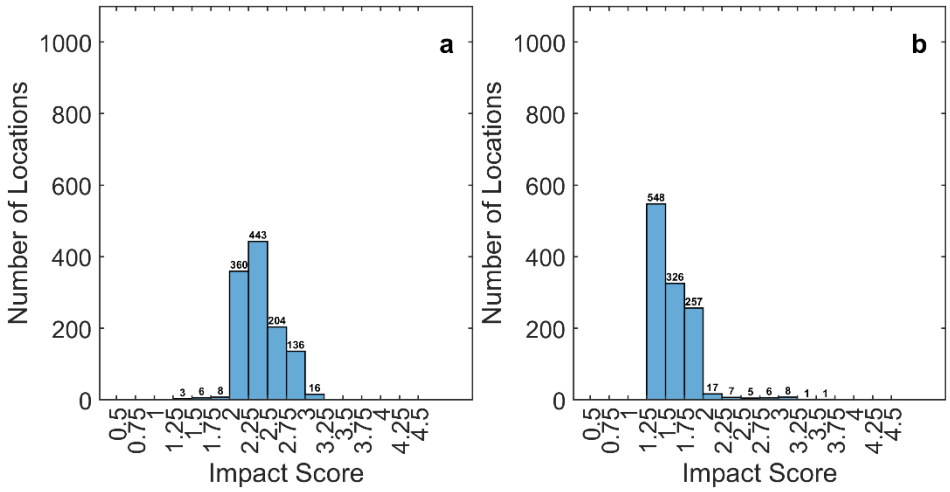


Figure 5.45. SSP2-4.5 Cultural Heritage Site Erosion Component Histogram

Figure 5.46 presents score classifications using Jenks Natural Breaks rather than the standard FCVAM class definitions. When standard FCVAM class limits are applied, erosion vulnerability is limited to three categories—very low, low, and moderate—since no study areas were classified as high or very high vulnerable. Using Jenks classification, natural heritage areas could be divided into five groups based on relative vulnerability levels determined by their CVI scores. This approach allows for identifying the most vulnerable locations among Turkish natural heritage sites.

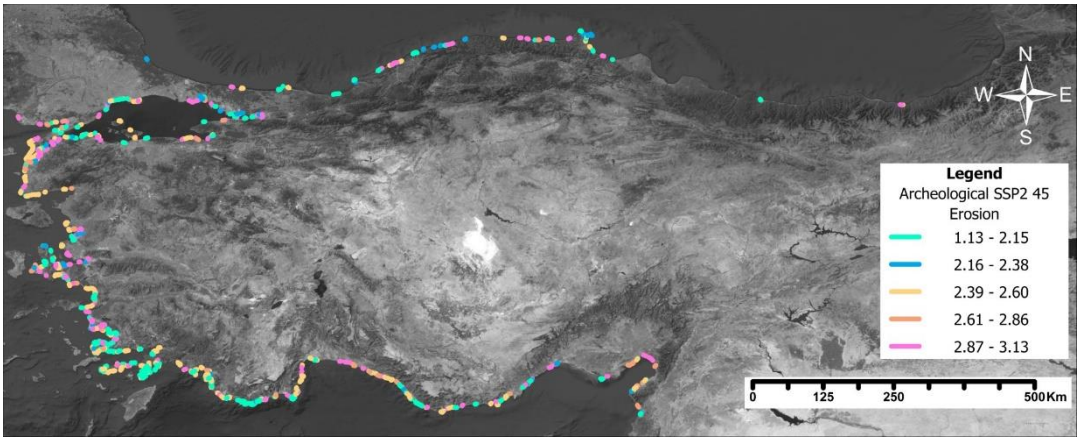


Figure 5.46. SSP2-4.5 Cultural Heritage Site Erosion Jenks Distribution

In Table 5.41, a more detailed comparison of Jenks and FCVAM classes is demonstrated. Moreover, in Figure 5.47, a histogram with Jenks limit and 0.25

increment impact scores are given. According to them, the erosion impact scores of Turkish cultural heritage area projections over the shoreline are between 1.75 and 3.25. Also, 19.2% of the studied shorelines, within moderate vulnerable according to FCVAM, are in the most susceptible evaluated shores of Turkish coasts against erosion.

Table 5.41 SSP2-4.5 Cultural Heritage Site Erosion Jenks & FCVAM Limits

Jenks Natural Breaks	**Results**	**FCVAM Class**	**Results**
< 2.15	413 (35.1%)	< 1.5 Very Low	4 (0.3%)
2.16 – 2.38	123 (10.5%)	1.5 – 2.5 Low	816 (69.4%)
2.39 – 2.60	312 (26.5%)	2.5 – 3.5 Moderate	356 (30.3%)
2.61 – 2.86	102 (8.7%)	3.5 – 4.25 High	0
> 2.87	226 (19.2%)	4.25 < Very High	0

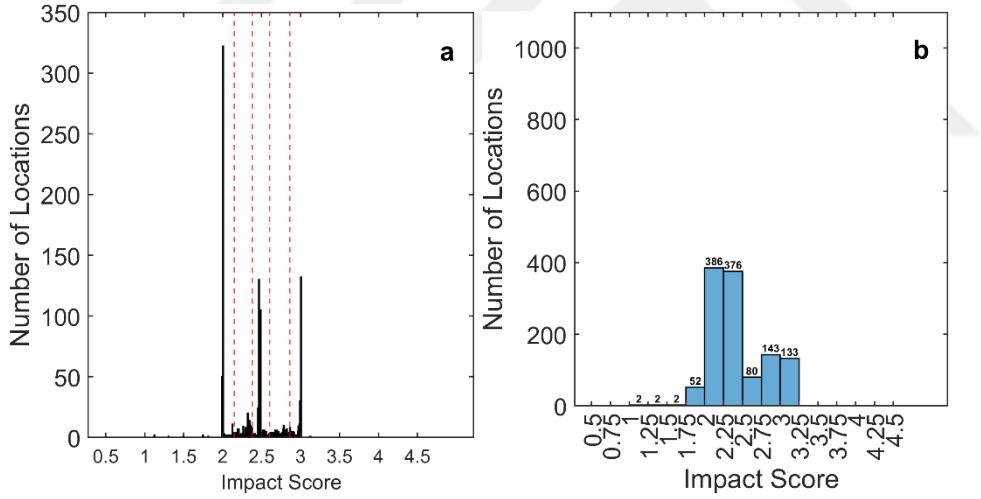


Figure 5.47. SSP2-4.5 Cultural Heritage Site Erosion (a) Jenks (b) FCVAM Histograms

5.3.2.2 Inundation

5.3.2.2.1 InundationPP

In Figure 5.48, the distribution of the inundation physical impact score throughout cultural heritage sites for the SSP2 - 4.5 pathway in terms of classes defined in FCVAM is given. On a national scale, no shoreline projections demonstrate very low vulnerability. Therefore, the dominant behavior of shores is low vulnerability in terms of inundation physical impact scores. In contrast, many locations in the Aegean Region are classified as high vulnerable.

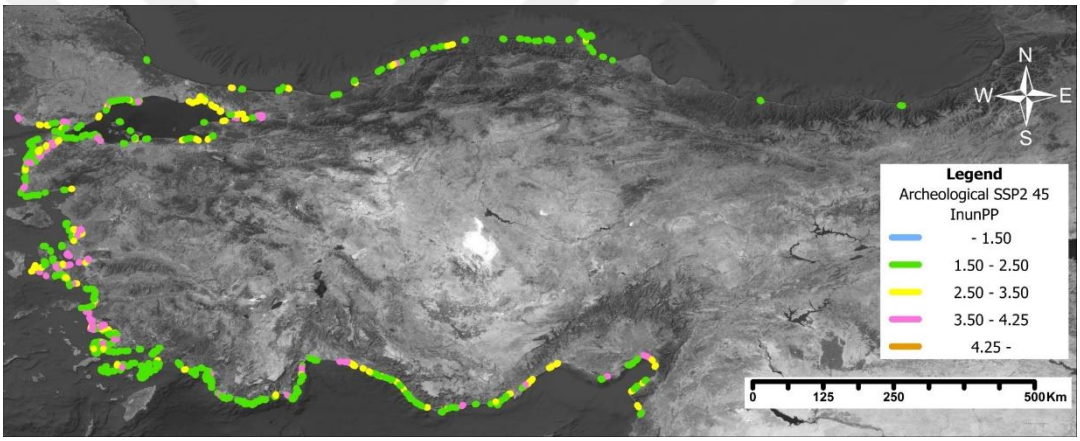


Figure 5.48. SSP2-4.5 Cultural Heritage Site InundationPP Distribution

In Table 5.42, regional scores are also presented for vulnerability classes. As mentioned, the Aegean Region has the highest number of high vulnerable locations, ahead of the Marmara Region. In the case of low vulnerable shores, the Aegean Region contains the majority of low vulnerable shores, followed by the Mediterranean Region.

Table 5.42 Regional SSP2-4.5 Cultural Heritage Site InundationPP Scores

Inundation PP	Mediterranean	Aegean	Marmara	Black Sea
< 1.5 Very Low	0	0	0	0
1.5 – 2.5 Low	238 (20.2%)	381 (32.4%)	69 (5.9%)	96 (8.2%)
2.5 – 3.5 Moderate	57 (4.8%)	106 (9%)	46 (3.9%)	13 (1.1%)
3.5 – 4.25 High	25 (2.1%)	114 (9.7%)	28 (2.4%)	3 (0.3%)
4.25 > Very High	0	0	0	0

5.3.2.2.2 Inundation Impact Score

Inundation physical and human impact scores were aggregated to obtain inundation vulnerability scores, which are given in Figure 5.49 for AR6 SSP2-4.5. According to the class distribution in the Figure, low vulnerable shorelines against inundation are the most common vulnerability class along Turkish shorelines.

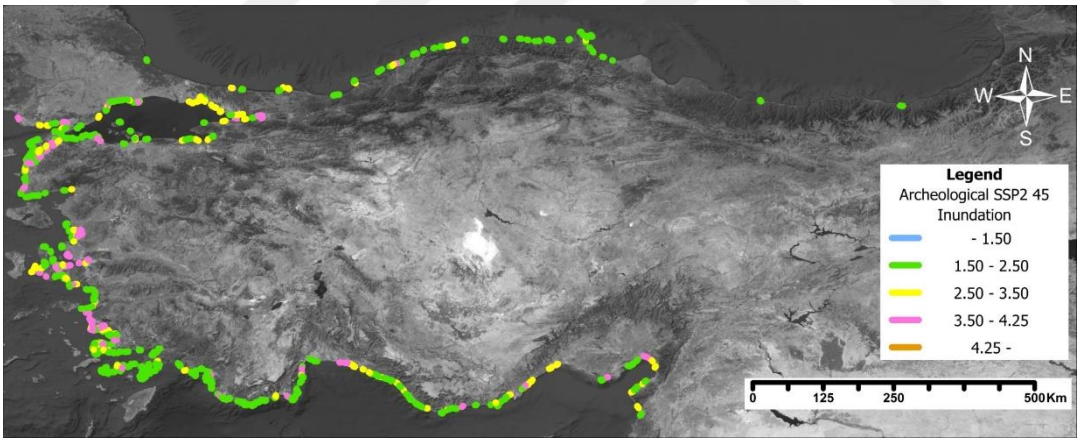


Figure 5.49. SSP2-4.5 Cultural Heritage Site Inundation Distribution

On a national scale, no areas are classified as very low or very high in terms of inundation impact scores, as corroborated by the results presented in Table 5.43 at the regional level. According to this Table, most high vulnerable shorelines and low vulnerability areas are concentrated in the Aegean region.

Table 5.43 Regional SSP2-4.5 Cultural Heritage Site Inundation Scores

Inundation	Mediterranean	Aegean	Marmara	Black Sea
< 1.5 Very Low	0	0	0	0
1.5 – 2.5 Low	238 (20.2%)	374 (31.8%)	69 (5.9%)	95 (8.1%)
2.5 – 3.5 Moderate	57 (4.8%)	109 (9.3%)	46 (3.9%)	14 (1.2%)
3.5 – 4.25 High	25 (2.1%)	118 (10%)	28 (2.4%)	3 (0.3%)
4.25 > Very High	0	0	0	0

In Figure 5.50, histograms display the inundation of physical and human impact scores. These histograms show that physical impact scores become increasingly dominant as impact scores rise, compared to human impact scores. Since inundation vulnerability is calculated by aggregating these two scores, the resulting vulnerability is primarily influenced by the physical impact score.

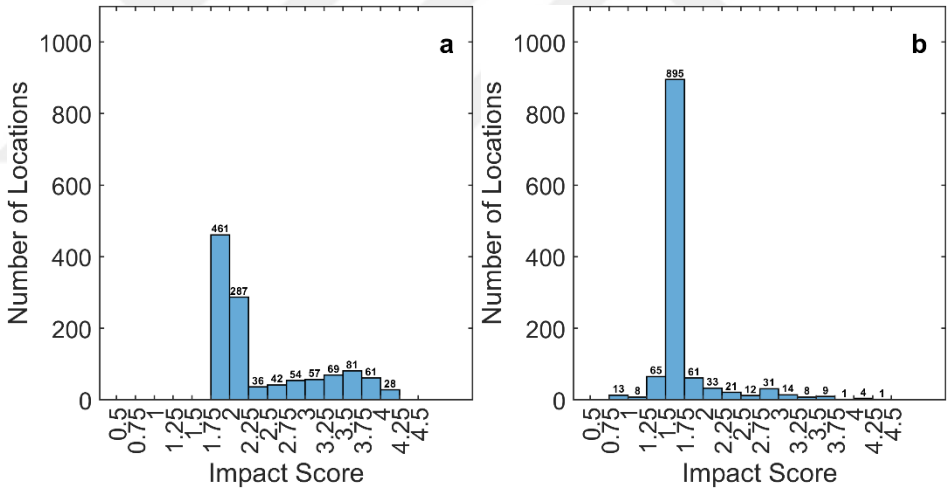


Figure 5.50. SSP2-4.5 Cultural Heritage Site Inundation Component Histogram

Figure 5.51 presents inundation score classifications using Jenks Natural Breaks rather than the standard FCVAM class definitions. When the conventional FCVAM class limits are applied, inundation vulnerability is condensed into three categories—low, moderate, and high vulnerability—relative to the global classification. Using Jenks classification, the most vulnerable natural heritage sites along the Turkish coastline could be identified among Türkiye's natural heritage sites.

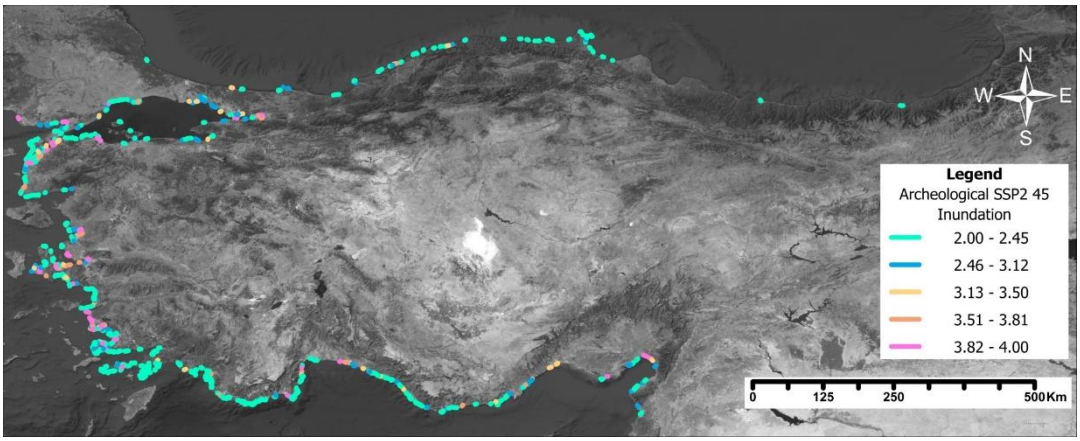


Figure 5.51. SSP2-4.5 Cultural Heritage Site Inundation Jenks Distribution

Table 5.44 presents a more detailed comparison of Jenks and FCVAM classifications. Classification using Jenks natural breaks reveals that approximately 9.6% of the shorelines classified as high vulnerable under the original class limits fall into the most critical category for inundation vulnerability along Turkish coasts. Additionally, in Figure 5.52, histograms with Jenks limits and 0.25 increment impact scores provide further details on score distribution. These histograms indicate that, while there is a concentration of scores around inundation impact levels of "3" and "4," the majority of shorelines have a vulnerability score of "2."

Table 5.44 SSP2-4.5 Cultural Heritage Site Inundation Jenks & FCVAM Limits

Jenks Natural Breaks	**Results**	**FCVAM Class**	**Results**
< 2.45	772 (65.6%)	< 1.5 Very Low	0
2.46 – 3.12	169 (14.4%)	1.5 – 2.5 Low	776 (66%)
3.13 – 3.50	61 (5.2%)	2.5 – 3.5 Moderate	226 (19.2%)
3.51 – 3.81	61 (5.2%)	3.5 – 4.25 High	174 (14.8%)
> 3.82	113 (9.6%)	4.25 < Very High	0

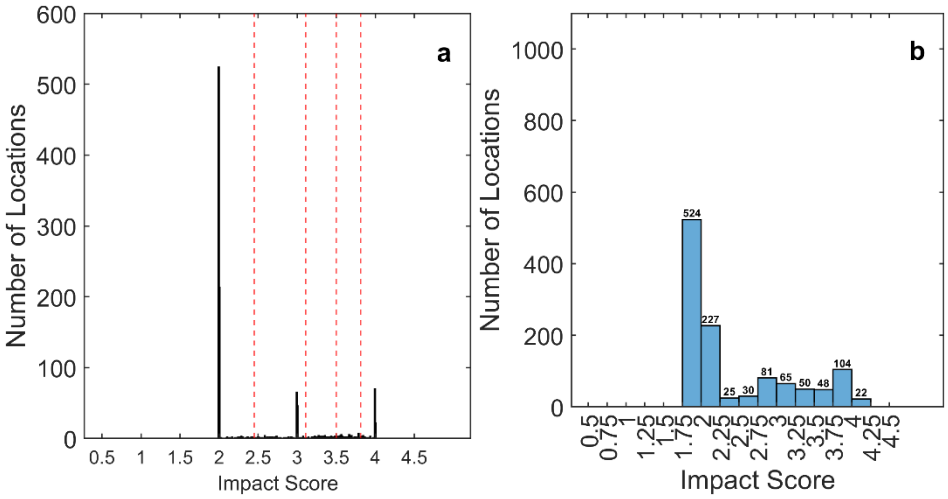


Figure 5.52. SSP2-4.5 Cultural Heritage Site Inundation (a) Jenks (b) FCVAM Histograms

5.3.2.3 Storm Surge

5.3.2.3.1 Storm SurgePP

Figure 5.53 shows the storm surge physical impact score distribution throughout cultural heritage sites for the SSP2 - 4.5 pathway in terms of classes defined in FCVAM.

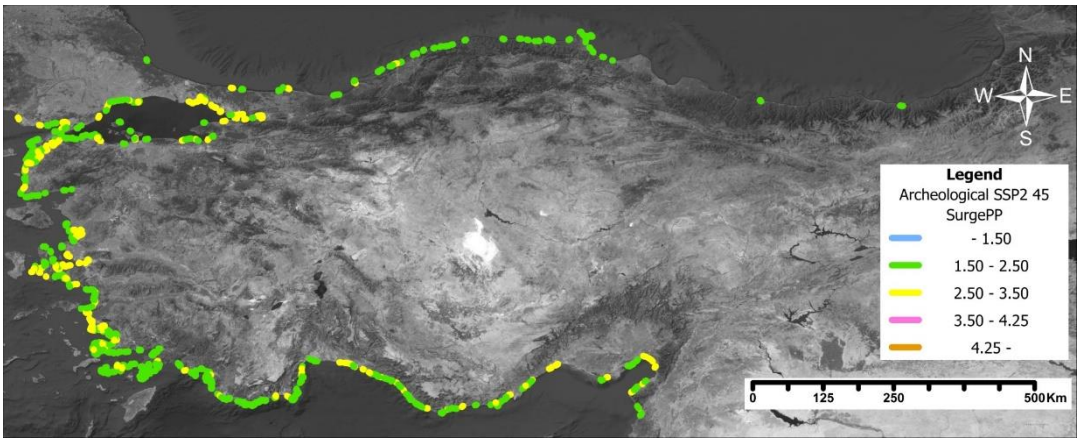


Figure 5.53. SSP2-4.5 Cultural Heritage Site Storm SurgePP Distribution

National wide vulnerability of Turkish cultural heritage site assessment indicates that in terms of storm surge impact scores, only low and moderate vulnerable areas are located around Turkish coasts, which is also supported by Table 5.45. According to regional results presented in the Table, more than 60% of studied shorelines were classified as Low vulnerable.

Table 5.45 Regional SSP2-4.5 Cultural Heritage Site Storm Surge Scores

Surge PP	Mediterranean	Aegean	Marmara	Black Sea
< 1.5 Very Low	0	0	0	0
1.5 – 2.5 Low	256 (21.8%)	403 (34.3%)	71 (6%)	101 (8.6%)
2.5 – 3.5 Moderate	64 (5.4%)	198 (16.8%)	72 (6.1%)	11 (0.9%)
3.5 – 4.25 High	0	0	0	0
4.25 > Very High	0	0	0	0

5.3.2.3.2 Storm Surge Impact Score

Storm surge physical and human impact scores were aggregated to obtain storm surge vulnerability scores demonstrated in Figure 5.54 for AR6 SSP2-4.5.

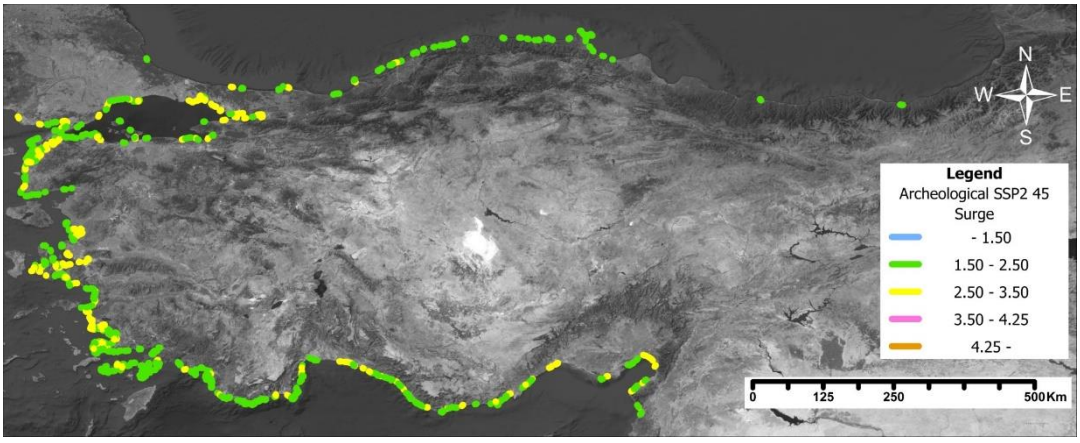


Figure 5.54. SSP2-4.5 Cultural Heritage Site Storm Surge Distribution

According to the Figure, in terms of storm surge impact score, although the dominant class against storm surge is low vulnerability, the Aegean and Black Sea Regions

contain high vulnerable locations, which are also presented in regional scale results given in Table 5.46.

Table 5.46 Regional SSP2-4.5 Cultural Heritage Site Storm Surge Scores

Surge	Mediterranean	Aegean	Marmara	Black Sea
< 1.5 Very Low	0	0	0	0
1.5 – 2.5 Low	256 (21.8%)	397 (33.8%)	71 (6%)	101 (8.6%)
2.5 – 3.5 Moderate	64 (5.4%)	202 (17.2%)	72 (6.1%)	10 (0.9%)
3.5 – 4.25 High	0	2 (0.2%)	0	1 (0.1%)
4.25 > Very High	0	0	0	0

To address the cause of high vulnerable locations, the distribution of physical and human impact scores presented in Figure 5.55 is evaluated. According to them, physical impact scores are clustered at a narrower area between 1.75 and 3, compared to human impact scores, which are distributed over a wider area between 1.25 and 4. Thus, at least for high vulnerable locations, it could be deduced that the storm surge human impact score determined the classes.

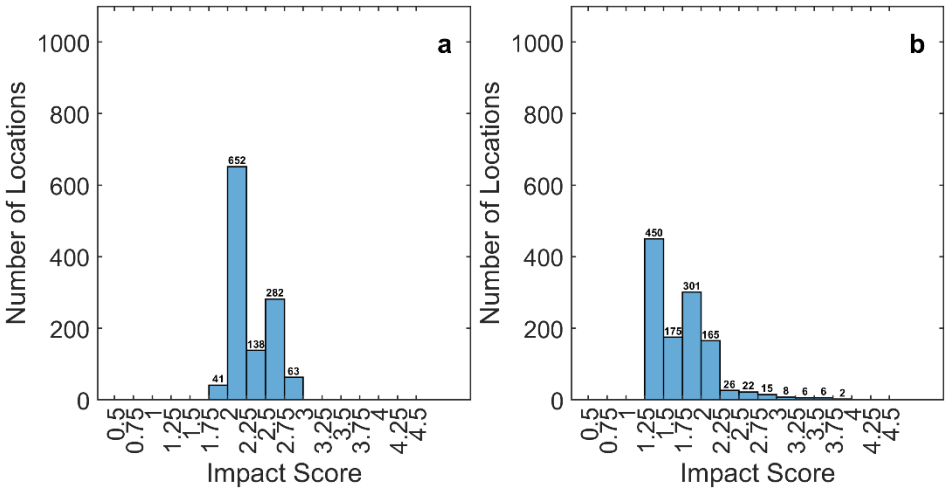


Figure 5.55. SSP2-4.5 Cultural Heritage Site Storm Surge Component Histogram

Figure 5.56 presents score classifications using Jenks Natural Breaks rather than the standard FCVAM class definitions. When standard FCVAM class limits are applied,

storm surge vulnerability is condensed into three categories—low, moderate, and high vulnerability—as shown in Table 5.47, providing a more detailed comparison between Jenks and FCVAM classifications. Through relative grouping of vulnerability, it was found that approximately 11.3% of the cultural heritage sites form the most susceptible area group along the Turkish coastlines for storm surge flooding. These areas were classified as moderate to high vulnerable concerning FCVAM limits.

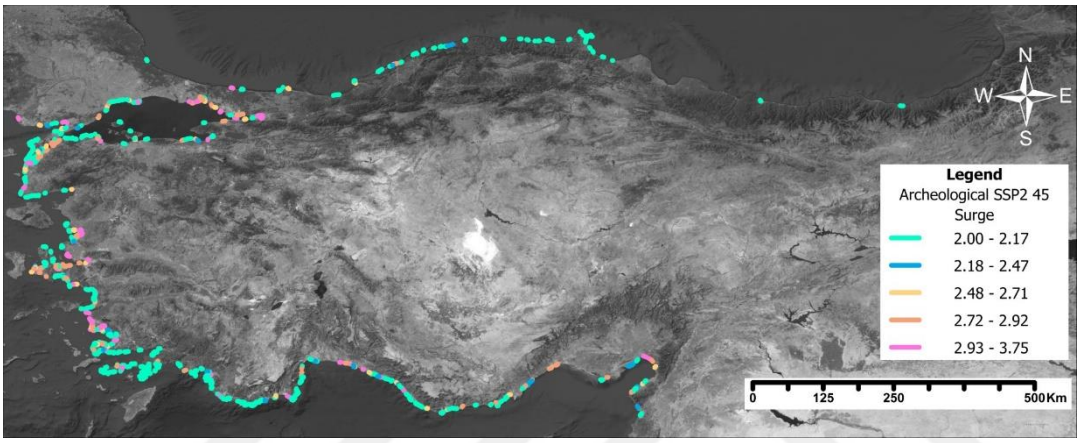


Figure 5.56. SSP2-4.5 Cultural Heritage Site Storm Surge Jenks Distribution

Table 5.47 SSP2-4.5 Cultural Heritage Site Surge Jenks & FCVAM Limits

Jenks Natural Breaks	Results	FCVAM Class	Results
< 2.17	757 (64.4%)	< 1.5 Very Low	0
2.18 – 2.47	62 (5.3%)	1.5 – 2.5 Low	825 (70.2%)
2.48 – 2.71	82 (7%)	2.5 – 3.5 Moderate	348 (29.6%)
2.72 – 2.92	142 (12.1%)	3.5 – 4.25 High	3 (0.3%)
> 2.93	133 (11.3%)	4.25 < Very High	0

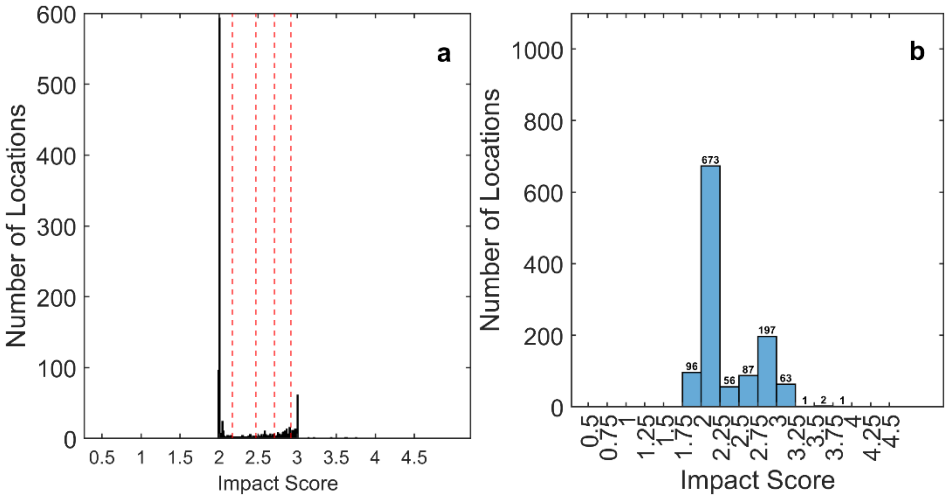


Figure 5.57. SSP2-4.5 Cultural Heritage Site Storm Surge (a) Jenks (b) FCVAM Histograms

5.3.2.4 Coastal Vulnerability Index

All three erosion, inundation, and storm surge vulnerability scores were aggregated to obtain CVI, the distribution of which is demonstrated in Figure 5.58 for AR6 SSP2-4.5.

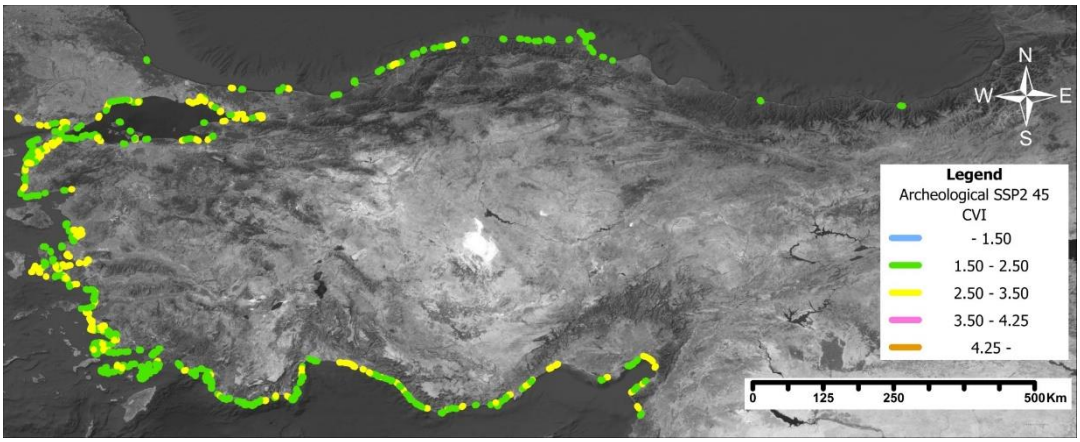


Figure 5.58. SSP2-4.5 Cultural Heritage Site CVI Distribution

According to the class distribution in the Figure, the dominant vulnerabilities of studied shorelines could be low. Moreover, other than 1 location in the Black Sea

Region, all of the CVI results belong to low and moderate vulnerability classes. Moreover, regional results given in Table 5.48 indicate that most of the low vulnerable shores are located in the Aegean Region, which the Mediterranean Region follows. Despite having the least number of studied cases, the only high vulnerable location is within the borders of the Black Sea Region. Marmara Region demonstrates a balanced distribution between low and moderate CVI scores.

Table 5.48 Regional SSP2-4.5 Cultural Heritage Site CVI Scores

CVI	Mediterranean	Aegean	Marmara	Black Sea
< 1.5 Very Low	0	0	0	0
1.5 – 2.5 Low	243 (20.7%)	383 (32.6%)	70 (6%)	98 (8.3%)
2.5 – 3.5 Moderate	77 (6.5%)	218 (18.5%)	73 (6.2%)	13 (1.1%)
3.5 – 4.25 High	0	0	0	1 (0.1%)
4.25 > Very High	0	0	0	0

In Table 5.49, score distributions concerning module and vulnerability class were given. Besides storm surge, module vulnerabilities demonstrate a similar pattern to corresponding physical impact score distributions. Inundation is the most critical case for the Turkish coasts because they have much more high vulnerable areas than others. Moreover, very high vulnerability is only observed for inundation human impact score. The table also shows that for coastal archeological sites, the human impact parameters show a wider range, which influences the overall vulnerability ranking. This is also expected since many cultural heritage sites are very close to urban areas where human activities change the shoreline.

Table 5.49 SSP2-4.5 Cultural Heritage Site Impact & CVI Scores

ARC SSP2-45	Erosion			Inundation			Storm Surge			CVI
	PP	HI	Vul	PP	HI	Vul	PP	HI	Vul	
< 1.5 Very Low	3	548	4	0	86	0	0	450	0	0
1.5 – 2.5 Low	817	607	816	784	1010	776	831	667	825	794
2.5 – 3.5 Moderate	356	20	356	222	65	226	345	51	348	381
3.5 – 4.25 High	0	1	0	170	14	174	0	8	3	1
4.25 > Very High	0	0	0	0	1	0	0	0	0	0

In Figure 5.59, CVI classifications are displayed using Jenks Natural Breaks rather than the standard FCVAM class definitions. When the standard FCVAM class limits are applied, CVI classifications are condensed into very low, low, and moderate vulnerability. Table 5.50 provides a more detailed comparison of Jenks and FCVAM classifications, indicating that 16.1% of the natural heritage sites are among the most vulnerable, with CVI scores within the medium vulnerability range. This situation is caused by global applications determining FCVAM limits while natural Jenks breaks consider the input data. Thus, even though 189 locations belong to the most critical group considering Turkish shores, there is only one shore denoted as high vulnerable and no shore as high vulnerable with respect to FCAM limits. Additionally, in Figure 5.60, histograms with Jenks limits and 0.25 increment impact scores are presented. CVI scores are accumulated between 1.5 and 3.75.

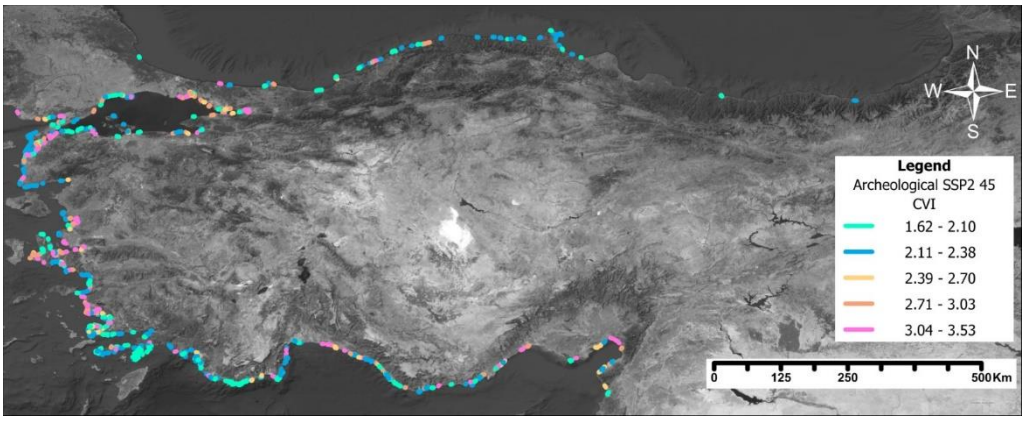


Figure 5.59. SSP2-4.5 Cultural Heritage Site CVI Jenks Distribution

Table 5.50 SSP2-4.5 Cultural Heritage Site CVI Jenks & FCVAM Limits

Jenks Natural Breaks	Results	FCVAM Class	Results
< 2.10	405 (34.4%)	< 1.5 Very Low	0
2.11 – 2.38	364 (31%)	1.5 – 2.5 Low	794 (67.5%)
2.39 – 2.70	79 (6.7%)	2.5 – 3.5 Moderate	381 (32.4%)
2.71 – 3.03	139 (11.8%)	3.5 – 4.25 High	1 (0.1%)
> 3.04	189 (16.1%)	4.25 < Very High	0

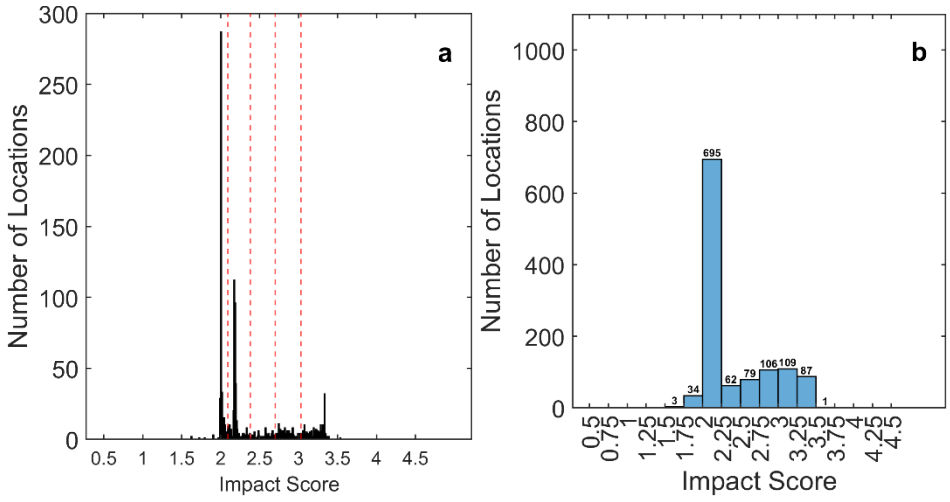


Figure 5.60. SSP2-4.5 Cultural Heritage Site CVI (a) Jenks (b) FCVAM Histograms

5.3.3 AR6 SSP5-8.5 Physical Impact Scores

This section presents the physical impact and CVI results of cultural heritage areas, calculated using predicted RSLR and ESL values based on the IPCC AR6 SSP5–8.5 scenario.

5.3.3.1 Erosion

5.3.3.1.1 ErosionPP

In Figure 5.61, erosion physical impact score distribution throughout cultural heritage areas for the SSP5 - 8.5 pathway in terms of classes defined in FCVAM is given. Contrary to SSP2-4.5, moderate vulnerability against the physical impact of erosion is dominant on a national scale. This claim is also supported by regional results given in Table 5.51, according to which the highest number of moderate vulnerable areas are located in the Aegean Region, followed by the Mediterranean Region. On the other hand, the Aegean and Mediterranean Regions are the only regions with very low vulnerable locations, the same as the findings of SSP2-4.5 indicated.

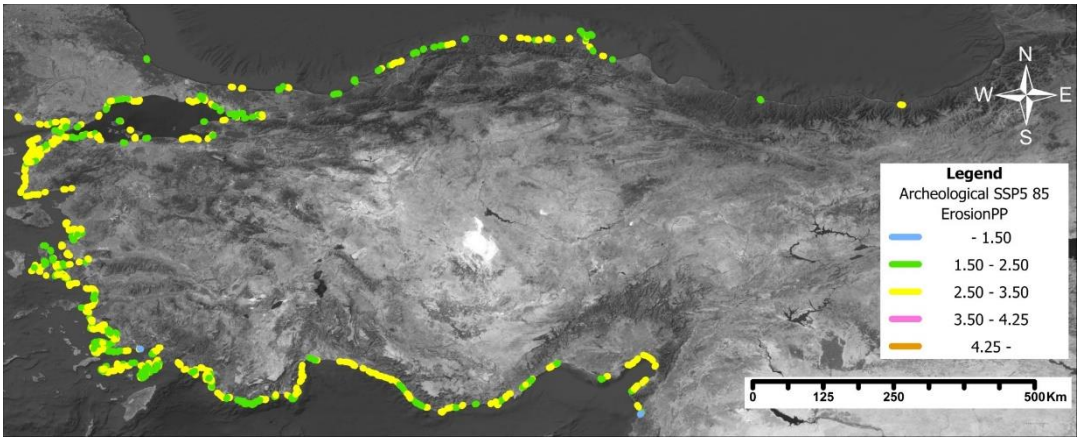


Figure 5.61. SSP5-8.5 Cultural Heritage Site ErosionPP Distribution

Table 5.51 Regional SSP5-8.5 Cultural Heritage Site ErosionPP Scores

ErosionPP	Mediterranean	Aegean	Marmara	Black Sea
< 1.5 Very Low	1 (0.1%)	2 (0.2%)	0	0
1.5 – 2.5 Low	140 (11.9%)	269 (22.9%)	67 (5.7%)	76 (6.5%)
2.5 – 3.5 Moderate	179 (15.2%)	330 (28.1%)	76 (6.5%)	36 (3.1%)
3.5 – 4.25 High	0	0	0	0
4.25 > Very High	0	0	0	0

In Table 5.52, the comparison of SSP5-8.5 and SSP2-4.5 concerning erosion physical impact vulnerability class distribution is given. According to this Table, the highest number of class changes occurred in the Aegean Region, in contrast to the Black Sea Region, in which the least number of changes were observed.

Table 5.52 SSP5-8.5 & SSP2-4.5 Cultural Heritage Site ErosionPP Comparison

ErosionPP Comparison	Mediterranean	Aegean	Marmara	Black Sea
< 1.5 Very Low	0	0	0	0
1.5 – 2.5 Low	-83	-151	-25	-6
2.5 – 3.5 Moderate	83	151	25	6
3.5 – 4.25 High	0	0	0	0
4.25 > Very High	0	0	0	0

5.3.3.1.2 Erosion Impact Score

Erosion physical and human impact scores were combined to produce erosion vulnerability scores, as shown in Figure 5.62 for cultural heritage sites under the AR6 SSP5-8.5 pathway. According to the class distribution in the Figure, low vulnerability to erosion remains the most common classification along Turkish shorelines under SSP5-8.5, consistent with SSP2-4.5 results. Furthermore, no studied shorelines are classified as high vulnerable to erosion vulnerability.

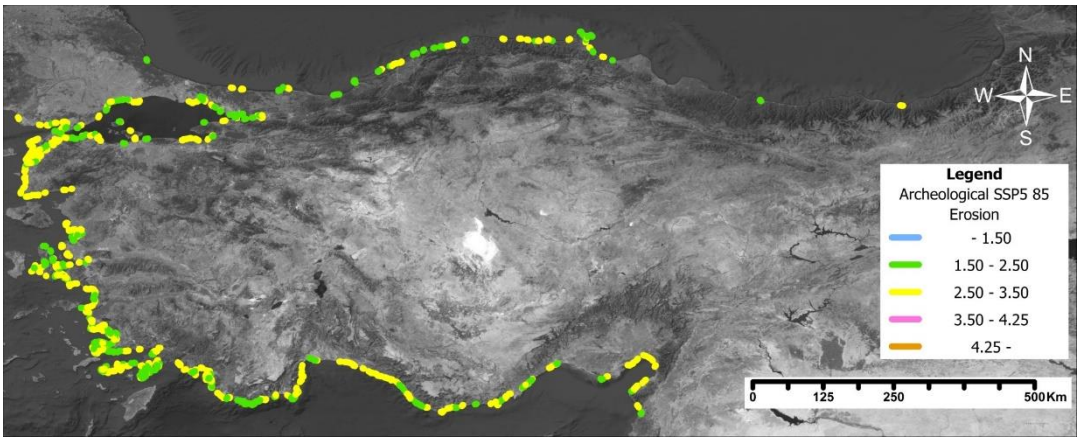


Figure 5.62. SSP5-8.5 Cultural Heritage Site Erosion Distribution

Table 5.53 provides more detailed results at the regional scale. According to this Table, the majority of low-vulnerability shorelines are located in the Aegean region. Furthermore, a few locations classified as very low-vulnerable are located in the Mediterranean and Aegean Regions. It should be noted that similar findings were inferred in the case of SSP2-4.5.

Table 5.53 Regional SSP5-8.5 Cultural Heritage Site Erosion Scores

Erosion	Mediterranean	Aegean	Marmara	Black Sea
< 1.5 Very Low	2 (0.2%)	2 (0.2%)	0	0
1.5 – 2.5 Low	222 (18.9%)	420 (35.7%)	92 (7.8%)	82 (7%)
2.5 – 3.5 Moderate	96 (8.2%)	179 (15.2%)	51 (4.3%)	30 (2.6%)
3.5 – 4.25 High	0	0	0	0
4.25 > Very High	0	0	0	0

Table 5.54 compares erosion impact scores. This Table indicates that although impact scores shifted compared to SSP2-4.5 results, this was not enough to observe high or very high vulnerable areas in the case of SSP5-8.5. On the other hand, the number of very low vulnerable shores decreased in the Mediterranean Region.

Table 5.54 SSP5-8.5 & SSP2-4.5 Cultural Heritage Site Erosion Comparison

Erosion Comparison	Mediterranean	Aegean	Marmara	Black Sea
< 1.5 Very Low	-1	0	0	0
1.5 – 2.5 Low	-82	-151	-25	-6
2.5 – 3.5 Moderate	83	151	25	6
3.5 – 4.25 High	0	0	0	0
4.25 > Very High	0	0	0	0

Figure 5.63 gives a histogram comparison of physical and human impact scores. A comparison of erosion vulnerability score distribution with physical and human impact scores indicated that physical impact scores mainly dictated erosion vulnerabilities. More than 90% of erosion human impact scores are between 1.25 and 2, while for physical impact scores, the boundaries are 2 to 3.

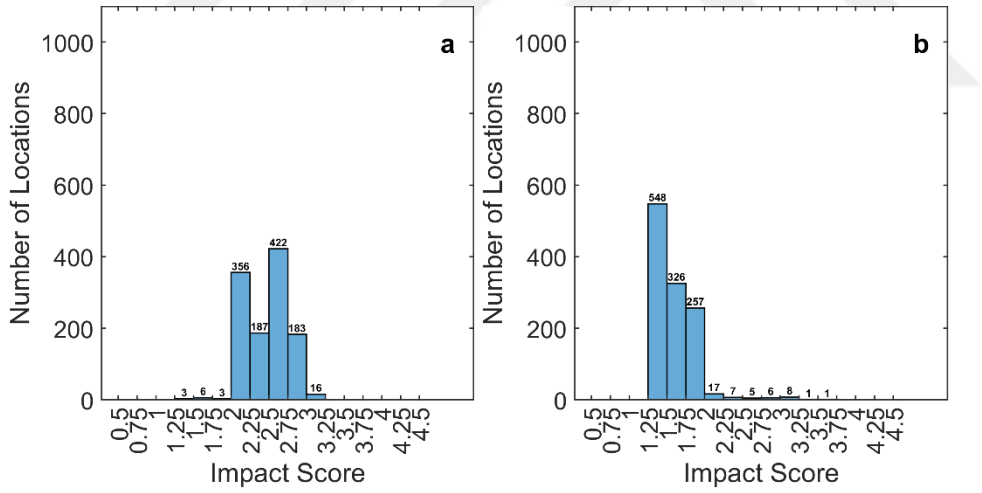


Figure 5.63. SSP5-8.5 Cultural Heritage Site Erosion Component Histogram

Figure 5.64 presents score classifications using Jenks Natural Breaks rather than the standard FCVAM class definitions. When standard FCVAM class limits are applied to SSP5-8.5 erosion impact scores, erosion vulnerability is narrowed down to three categories—very low, low, and moderate—since no study areas were classified as

high or very high vulnerable as in the case of SSP2-4.5. Using Jenks classification, cultural heritage areas could be divided into five groups based on relative vulnerability levels determined by their CVI scores. This allows for identifying the most vulnerable locations among Turkish cultural heritage sites.

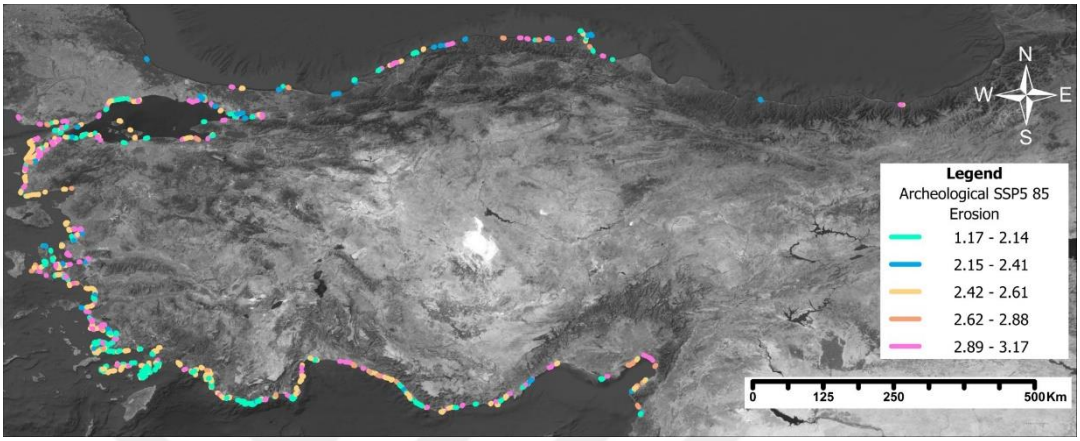


Figure 5.64. SSP5-8.5 Cultural Heritage Site Erosion Jenks Distribution

In Table 5.55, a more detailed comparison of Jenks and FCVAM classes is presented. Moreover, in Figure 5.65, a histogram with Jenks limit and 0.25 increment impact scores are given. According to them, the erosion impact scores of Turkish cultural heritage area projections over the shoreline are between 1.75 and 3.25. Also, for SSP5-8.5, by considering new natural Jenks breaks, with an increase of 1.5% compared to SSP2-4.5, 20.7% of the studied shorelines are in the group of most susceptible evaluated shores of Turkish coasts against erosion, which are moderate vulnerable according to FCVAM limits.

Table 5.55 SSP5-8.5 Cultural Heritage Site Erosion Jenks & FCVAM Limits

Jenks Natural Breaks	**Results**	**FCVAM Class**	**Results**
< 2.14	389 (33.1%)	< 1.5 Very Low	3 (0.3%)
2.15 – 2.41	111 (9.4%)	1.5 – 2.5 Low	552 (46.9%)
2.42 – 2.61	342 (29.1%)	2.5 – 3.5 Moderate	621 (52.8%)
2.62 – 2.88	91 (7.7%)	3.5 – 4.25 High	0
> 2.89	243 (20.7%)	4.25 < Very High	0

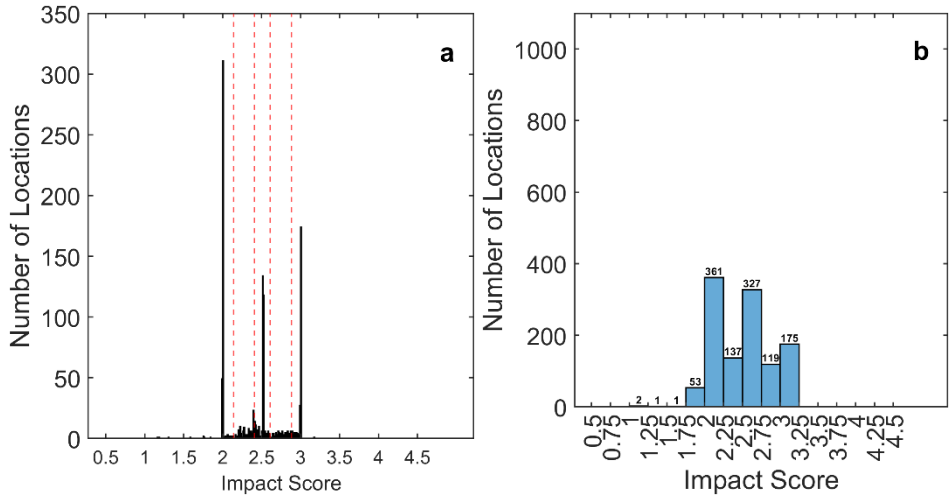


Figure 5.65. SSP5-8.5 Cultural Heritage Site Erosion (a) Jenks (b) FCVAM Histograms

5.3.3.2 Inundation

5.3.3.2.1 InundationPP

Figure 5.66 shows the inundation of physical impact scores distribution throughout cultural heritage sites for the SSP5 - 8.5 pathway regarding classes defined in FCVAM.

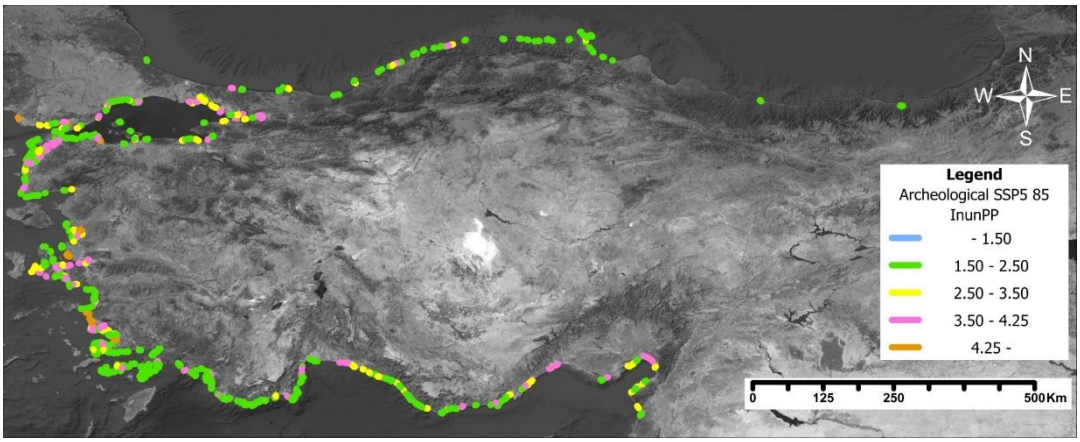


Figure 5.66. SSP5-8.5 Cultural Heritage Site InundationPP Distribution

On a national scale, in contrast to SSP2-4.5, there are very vulnerable locations in terms of inundation physical impact scores in the Aegean and Marmara Regions. On the other hand, an increase in inundation of physical impact scores compared to SSP2-4.5 was not enough to change the most frequently observed class, which is low vulnerability. In Table 5.56, regional scores are given for SSP5-8.5; in Table 5.57, SSP5-8.5 findings are compared with SSP2-4.5. In SSP5-8.5, although the most observed vulnerability class is "low" in the case of SSP5-8.5, same as SSP2-4.5, in the Aegean and Marmara Regions, there is a total of 26 new locations classified as very high vulnerable.

Table 5.56 Regional SSP5-8.5 Cultural Heritage Site InundationPP Scores

InundationPP	**Mediterranean**	**Aegean**	**Marmara**	**Black Sea**
< 1.5 Very Low	0	0	0	0
1.5 – 2.5 Low	226 (19.2%)	375 (31.9%)	68 (5.8%)	96 (8.2%)
2.5 – 3.5 Moderate	56 (4.8%)	85 (7.2%)	36 (3.1%)	9 (0.8%)
3.5 – 4.25 High	38 (3.2%)	118 (10%)	36 (3.1%)	7 (0.6%)
4.25 > Very High	0	23 (2%)	3 (0.3%)	0

Table 5.57 SSP5-8.5 & SSP2-4.5 Cultural Heritage Site InundationPP Comparison

InundationPP Comparison	**Mediterranean**	**Aegean**	**Marmara**	**Black Sea**
< 1.5 Very Low	0	0	0	0
1.5 – 2.5 Low	-12	-6	-1	0
2.5 – 3.5 Moderate	-1	-21	-10	-4
3.5 – 4.25 High	13	4	8	4
4.25 > Very High	0	23	3	0

5.3.3.2.2 Inundation Impact Score

Inundation physical and human impact scores were combined to produce inundation vulnerability scores, as shown in Figure 5.67 for AR6 SSP5-8.5. According to the class distribution in the Figure, low vulnerability to inundation remains the most prevalent category along Turkish shorelines, as in the SSP2-4.5 scenario.

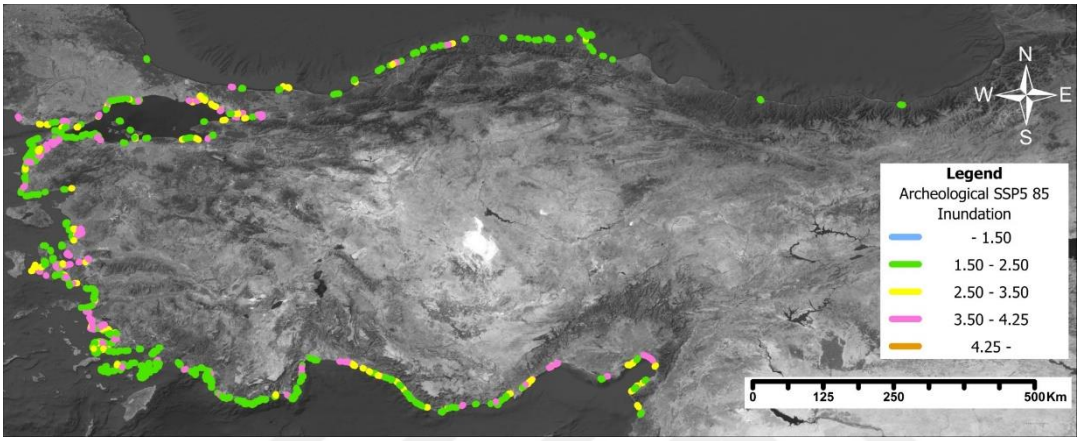


Figure 5.67. SSP5-8.5 Cultural Heritage Site Inundation Distribution

On a national scale, same as SSP2-4.5, there are no areas classified as either very low or very high in terms of inundation impact scores despite the increase in physical impact scores when SSP5-8.5 considered, as corroborated by the results presented in Table 5.58 at the regional level.

Table 5.58 Regional SSP5-8.5 Cultural Heritage Site Inundation Scores

Inundation	Mediterranean	Aegean	Marmara	Black Sea
< 1.5 Very Low	0	0	0	0
1.5 – 2.5 Low	226 (19.2%)	370 (31.5%)	68 (5.8%)	95 (8.1%)
2.5 – 3.5 Moderate	56 (4.8%)	87 (7.4%)	36 (3.1%)	10 (0.9%)
3.5 – 4.25 High	38 (3.2%)	144 (12.2%)	39 (3.3%)	7 (0.6%)
4.25 > Very High	0	0	0	0

According to this Table, most high vulnerable shorelines and low vulnerability areas are concentrated in the Aegean region. Moreover, in Table 5.59., SSP5-8.5 inundation vulnerability results are compared with SSP2-4.5. This Table indicates that, in the Aegean Region, the highest number of class changes was observed, contrary to the Black Sea Region. Additionally, it is seen that some low-vulnerable areas shifted to two vulnerable classes, especially in the Mediterranean, indicating that these cultural heritage sites would experience a higher level of change based on pathway than the rest of the sites assessed in the study.

Table 5.59 SSP5-8.5 & SSP2-4.5 Cultural Heritage Site Inundation Comparison

Inundation Comparison	**Mediterranean**	**Aegean**	**Marmara**	**Black Sea**
< 1.5 Very Low	0	0	0	0
1.5 – 2.5 Low	-12	-4	-1	0
2.5 – 3.5 Moderate	-1	-22	-10	-4
3.5 – 4.25 High	13	26	11	4
4.25 > Very High	0	0	0	0

In Figure 5.68, histograms give information on the inundation physical and human impact score distribution over a 0.25 increment.

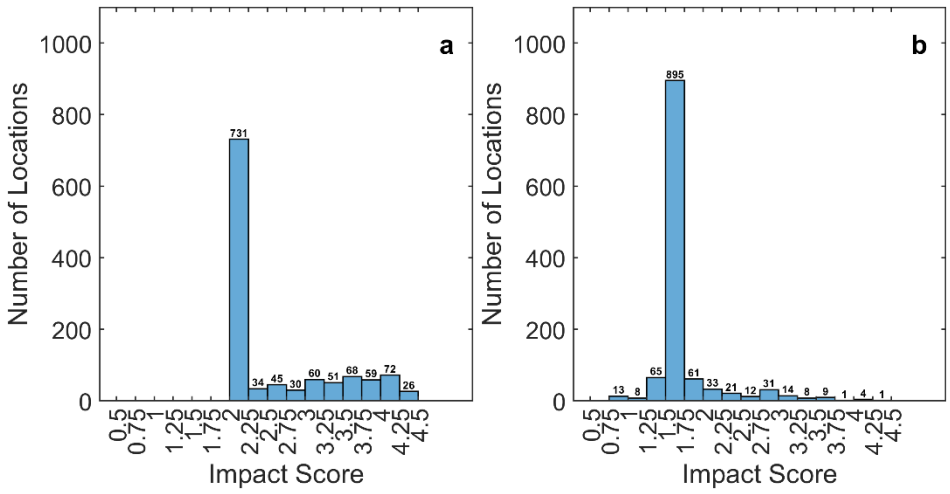


Figure 5.68. SSP5-8.5 Cultural Heritage Site Inundation Component Histogram

From these histograms, it could be inferred that physical impact scores are much more critical than human impact scores. Since inundation vulnerability is calculated by aggregating these two scores, the obtained vulnerability classes were primarily influenced by the physical impact score. In Figure 5.69, inundation score classifications are presented using Jenks Natural Breaks rather than the standard FCVAM class definitions to highlight the most vulnerable locations of Turkish coasts compared to others.

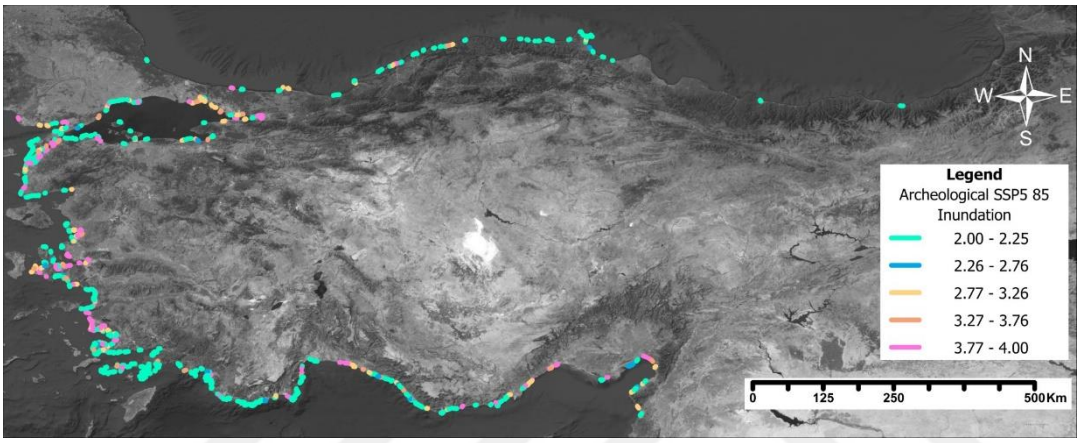


Figure 5.69. SSP5-8.5 Cultural Heritage Site Inundation Jenks Distribution

When the conventional FCVAM class limits are applied to SSP5-8.5 inundation impact scores, inundation vulnerability is condensed into three categories—low, moderate, and high—relative to the global classification, as in SSP2-4.5. Table 5.60 presents a more detailed comparison of Jenks and FCVAM classifications. Classification of SSP5-8.5 using renewed natural Jenks breaks reveals that approximately 15.4% of the studied shorelines belong to a most critical group for Turkish coasts, 9.6% for SSP2-4.5. Additionally, in Figure 5.70, histograms with Jenks limits and 0.25 increment impact scores provide further details on score distribution. These histograms indicate that the main concentration of scores occurs around “2,” followed by “4”.

Table 5.60 SSP5-8.5 Cultural Heritage Site Inundation Jenks & FCVAM Limits

Jenks Natural Breaks	Results	FCVAM Class	Results
< 2.25	742 (63.1%)	< 1.5 Very Low	0
2.26 – 2.76	40 (3.4%)	1.5 – 2.5 Low	759 (64.5%)
2.77 – 3.26	141 (12%)	2.5 – 3.5 Moderate	189 (16.1%)
3.27 – 3.76	72 (6.1%)	3.5 – 4.25 High	228 (19.4%)
> 3.77	181 (15.4%)	4.25 < Very High	0

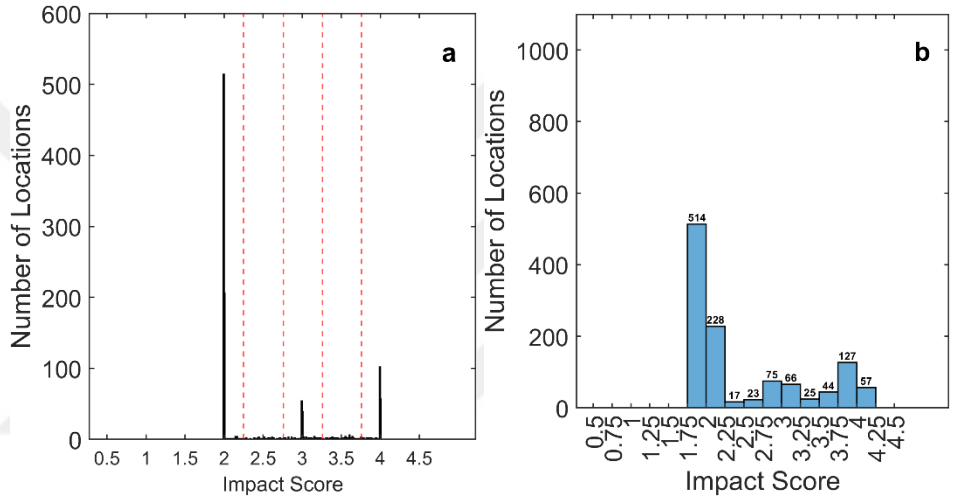


Figure 5.70. SSP5-8.5 Cultural Heritage Site Inundation (a) Jenks (b) FCVAM Histograms

5.3.3.3 Storm Surge

5.3.3.3.1 Storm SurgePP

Figure 5.71 shows the storm surge physical impact score distribution throughout cultural heritage sites for the SSP5 - 8.5 pathway regarding classes defined in FCVAM.

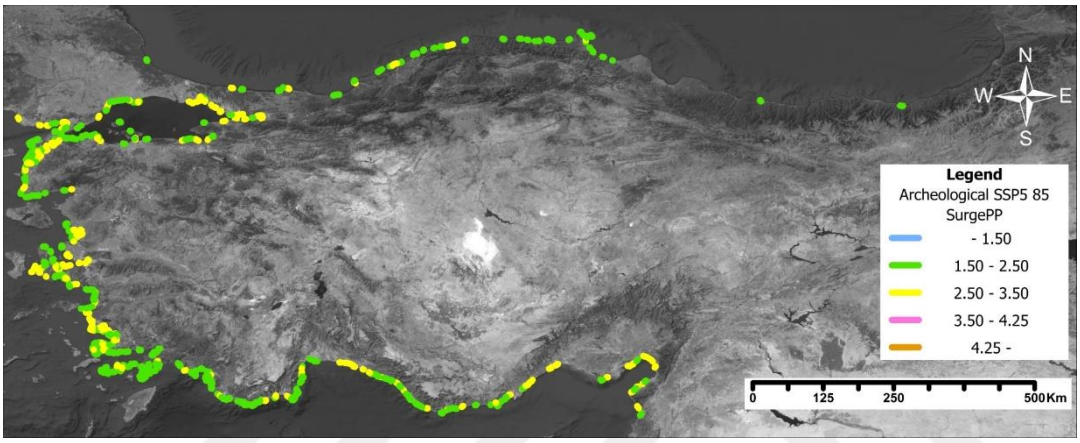


Figure 5.71. SSP5-8.5 Cultural Heritage Site Storm SurgePP Distribution

National-wide vulnerability of Turkish cultural heritage site assessment indicates that in terms of SSP5-8.5 storm surge impact scores, only low and moderate vulnerable areas are located around Turkish coasts, as observed in SSP2-4.5, supported by Table 5.61.

Table 5.61 Regional SSP5-8.5 Cultural Heritage Site Storm SurgePP Scores

SurgePP	Mediterranean	Aegean	Marmara	Black Sea
< 1.5 Very Low	0	0	0	0
1.5 – 2.5 Low	233 (19.8%)	381 (32.4%)	69 (5.9%)	96 (8.2%)
2.5 – 3.5 Moderate	87 (7.4%)	220 (18.7%)	74 (6.3%)	16 (1.4%)
3.5 – 4.25 High	0	0	0	0
4.25 > Very High	0	0	0	0

According to regional results presented in the Table, more than 60% of studied shorelines were classified as Low vulnerable. To indicate the changes with the applied pathway, in Table 5.62, SSP5-8.5 score distributions are compared with SSP2-4.5. Despite having fewer study areas, the Mediterranean Region demonstrated the highest number of changes, followed by the Aegean Region. However, storm surge physical impact score increases were insufficient to reach vulnerable locations.

Table 5.62 SSP5-8.5 & SSP2-4.5 Cultural Heritage Site Storm SurgePP Comparison

SurgePP Comparison	Mediterranean	Aegean	Marmara	Black Sea
< 1.5 Very Low	0	0	0	0
1.5 – 2.5 Low	-23	-22	-2	-5
2.5 – 3.5 Moderate	23	22	2	5
3.5 – 4.25 High	0	0	0	0
4.25 > Very High	0	0	0	0

5.3.3.3.2 Storm Surge Impact Score

Storm surge physical and human impact scores were aggregated to obtain storm surge vulnerability scores, demonstrated in Figure 5.72 for AR6 SSP5-8.5. As observed in SSP2-4.5, dominant behavior of Turkish coasts for SSP5-8.5 is low vulnerability while having high vulnerable locations in Aegean and Black Sea Regions. Regional results are given in Table 5.63, which supports the claim. Moreover, in Table 5.64, the results of SSP5-8.5 are compared with SSP2-4.5. According to this Table, despite having fewer locations, the highest number of class shifting was observed in the Mediterranean Region.

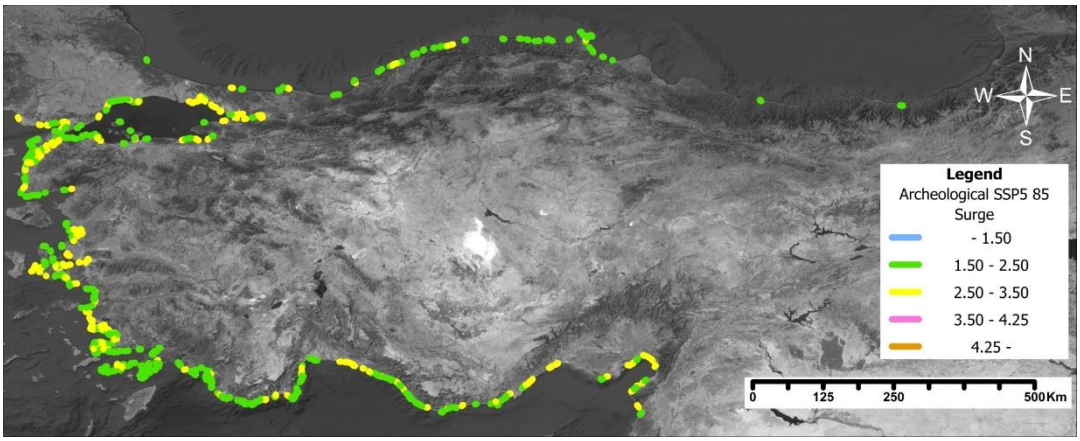


Figure 5.72. SSP5-8.5 Cultural Heritage Site Storm Surge Distribution

Table 5.63 Regional SSP5-8.5 Cultural Heritage Site Storm Surge Scores

Surge	Mediterranean	Aegean	Marmara	Black Sea
< 1.5 Very Low	0	0	0	0
1.5 – 2.5 Low	233 (19.8%)	376 (32%)	69 (5.9%)	96 (8.2%)
2.5 – 3.5 Moderate	87 (7.4%)	222 (18.9%)	74 (6.3%)	15 (1.3%)
3.5 – 4.25 High	0	3 (0.3%)	0	1 (0.1%)
4.25 > Very High	0	0	0	0

Table 5.64 SSP5-8.5 & SSP2-4.5 Cultural Heritage Site Storm Surge Comparison

Surge Comparison	Mediterranean	Aegean	Marmara	Black Sea
< 1.5 Very Low	0	0	0	0
1.5 – 2.5 Low	-23	-21	-2	-5
2.5 – 3.5 Moderate	23	20	2	5
3.5 – 4.25 High	0	1	0	0
4.25 > Very High	0	0	0	0

The distribution of physical and human impact scores is presented in Figure 5.73.

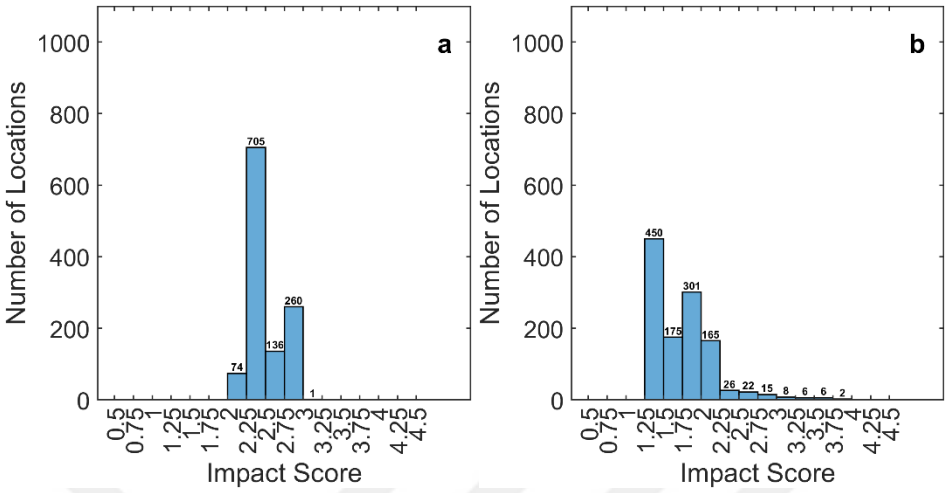


Figure 5.73. SSP5-8.5 Cultural Heritage Site Storm Surge Component Histogram

When the physical impact score distribution is checked, it could be observed that for SSP5-8.5, scores are accumulated within 2 to 3.25, while for SSP2-4.5, these limits were 1.75 to 3. Since human impact scores are distributed over a wider range of 1.25 to 4, they were more dominant during the classification of locations, especially after they were larger than 3. Figure 5.74 presents score classifications using renewed natural Jenks breaks for SSP5-8.5 rather than the standard FCVAM class definitions.

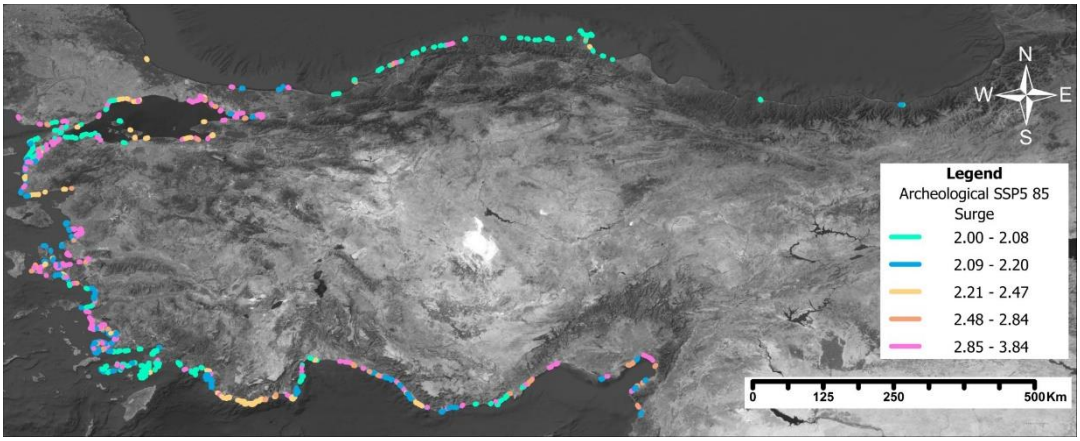


Figure 5.74. SSP5-8.5 Cultural Heritage Site Storm Surge Jenks Distribution

When standard FCVAM class limits are applied, storm surge vulnerability is condensed into three categories—low, moderate, and high vulnerability, as also

observed in SSP2-4.5—as shown in Table 5.65, which also provides a more detailed comparison between Jenks and FCVAM classifications. Through relative grouping of vulnerability, it was found that -with a 14.2% increase compared to SSP2-4.5- approximately 26.5% of the cultural heritage sites form the most susceptible area group along the Turkish coastlines for storm surge flooding. These areas were classified as moderate to high vulnerable concerning FCVAM limits.

Table 5.65 SSP5-8.5 Cultural Heritage Site Surge Jenks & FCVAM Limits

Jenks Natural Breaks	**Results**	**FCVAM Class**	**Results**
< 2.08	326 (27.7%)	< 1.5 Very Low	0
2.09 – 2.20	298 (25.3%)	1.5 – 2.5 Low	774 (65.8%)
2.21 – 2.47	143 (12.2%)	2.5 – 3.5 Moderate	398 (33.8%)
2.48 – 2.84	97 (8.2%)	3.5 – 4.25 High	4 (0.3%)
> 2.85	312 (26.5%)	4.25 < Very High	0

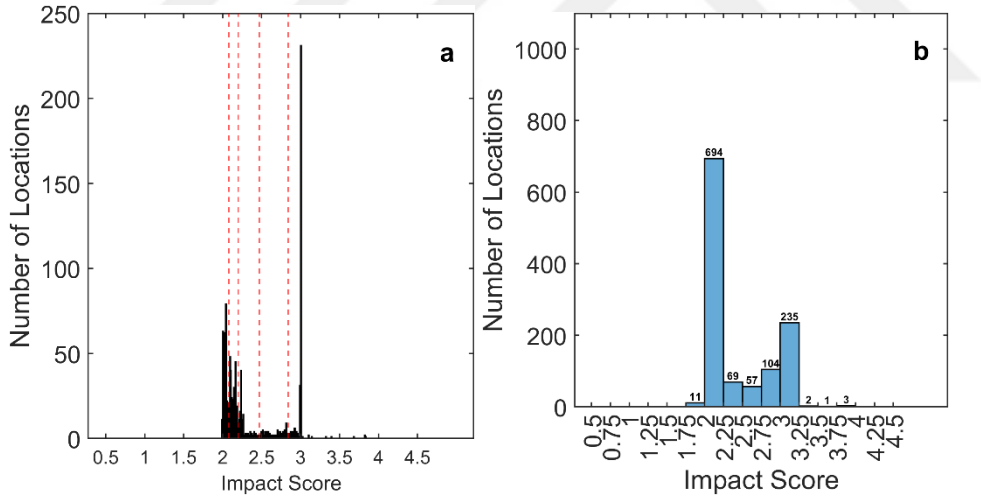


Figure 5.75. SSP5-8.5 Cultural Heritage Site Storm Surge (a) Jenks (b) FCVAM Histograms

5.3.3.4 Coastal Vulnerability Index

All three erosion, inundation, and storm surge vulnerability scores were aggregated to obtain CVI, the distribution of which is demonstrated in Figure 5.76 for AR6 SSP5-8.5. In the Figure, SSP5-8.5 demonstrated the same vulnerability classes as SSP2-4.5 distributions. Thus, low-vulnerable shores are still the highest fraction.

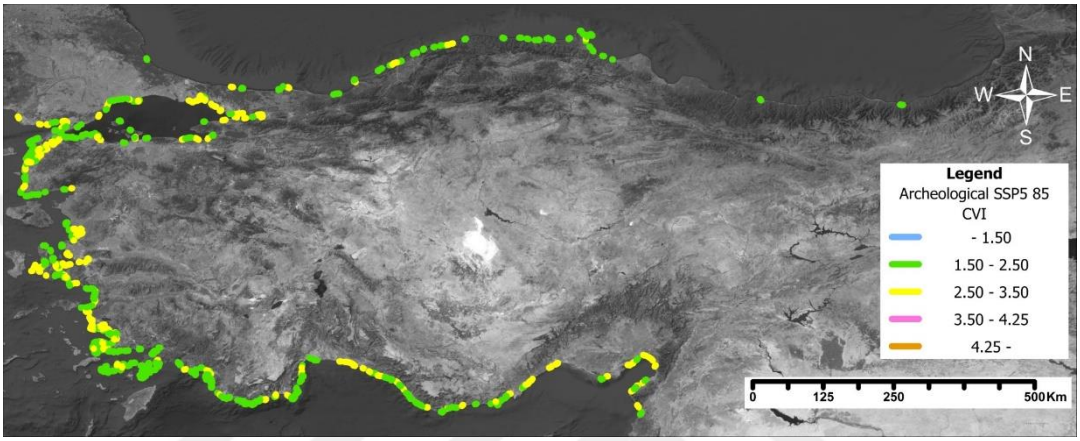


Figure 5.76. SSP5-8.5 Cultural Heritage Site CVI Distribution

Regional scale results and pathway-based comparison are given in Table 5.66 and Table 5.67, respectively.

Table 5.66 Regional SSP5-8.5 Cultural Heritage Site CVI Scores

CVI	Mediterranean	Aegean	Marmara	Black Sea
< 1.5 Very Low	0	0	0	0
1.5 – 2.5 Low	225 (19.1%)	374 (31.8%)	69 (5.9%)	96 (8.2%)
2.5 – 3.5 Moderate	95 (8.1%)	227 (19.3%)	74 (6.3%)	15 (1.3%)
3.5 – 4.25 High	0	0	0	1 (0.1%)
4.25 > Very High	0	0	0	0

Table 5.67 SSP5-8.5 & SSP2-4.5 Cultural Heritage Site CVI Comparison

CVI Comparison	**Mediterranean**	**Aegean**	**Marmara**	**Black Sea**
< 1.5 Very Low	0	0	0	0
1.5 – 2.5 Low	-18	-9	-1	-2
2.5 – 3.5 Moderate	18	9	1	2
3.5 – 4.25 High	0	0	0	0
4.25 > Very High	0	0	0	0

When changes between pathway results are evaluated, despite almost having half as many study locations within, the Mediterranean Region demonstrated the highest susceptibility to considered pathways by having the highest number of vulnerability class increases. On the other hand, the Aegean Region still contains the highest number of moderate vulnerable shores, while the Black Sea Region has the only high-vulnerable location. Table 5.68 gives score distributions concerning module and vulnerability class for SSP5-8.5.

Table 5.68 SSP5-8.5 Cultural Heritage Site Impact & CVI Scores

ARC SSP5-85	Erosion			Inundation			Storm Surge			CVI
	PP	HI	Vul	PP	HI	Vul	PP	HI	Vul	
< 1.5 Very Low	3	548	3	0	86	0	0	450	0	0
1.5 – 2.5 Low	552	607	552	765	1010	759	779	667	774	764
2.5 – 3.5 Moderate	621	20	621	186	65	189	397	51	398	411
3.5 – 4.25 High	0	1	0	199	14	228	0	8	4	1
4.25 > Very High	0	0	0	26	1	0	0	0	0	0

As observed in SSP2-4.5, other than storm surge module vulnerabilities, demonstrate a similar pattern to corresponding physical impact score distributions. Inundation is the most critical case for the Turkish coasts because they have much more high vulnerable areas than others. Inundation is the only module that has resulted in very high vulnerability in terms of both physical and human impact scores. To review how the considered pathway affected the scores in detail, Table 5.69. contains result comparison of scenarios. In terms of several locations, erosion physical impact score and, as a result, erosion vulnerability were affected the most. On the other hand, in terms of increased class vulnerability, inundation physical impact scores went up to very high vulnerability, and the number of high vulnerable locations in terms of inundation impact score was increased. The shifts in some locations happened across two vulnerability classes, highlighting these regions as more sensitive to the pathway change.

Table 5.69 SSP5-8.5 & SSP2-4.5 Cultural Heritage Site Impact Score Comparison

SSP2-45 SSP5-85	Erosion			Inundation			Storm Surge			CVI
	PP	HI	Vul	PP	HI	Vul	PP	HI	Vul	
< 1.5 Very Low	0	0	-1	0	0	0	0	0	0	0
1.5 – 2.5 Low	-265	0	-264	-19	0	-17	-52	0	-51	-30
2.5 – 3.5 Moderate	265	0	265	-36	0	-37	52	0	50	30
3.5 – 4.25 High	0	0	0	29	0	54	0	0	1	0
4.25 > Very High	0	0	0	26	0	0	0	0	0	0

Figure 5.77 illustrates CVI classifications using renewed Jenks Natural Breaks rather than the standard FCVAM class definitions for SSP5-8.5.

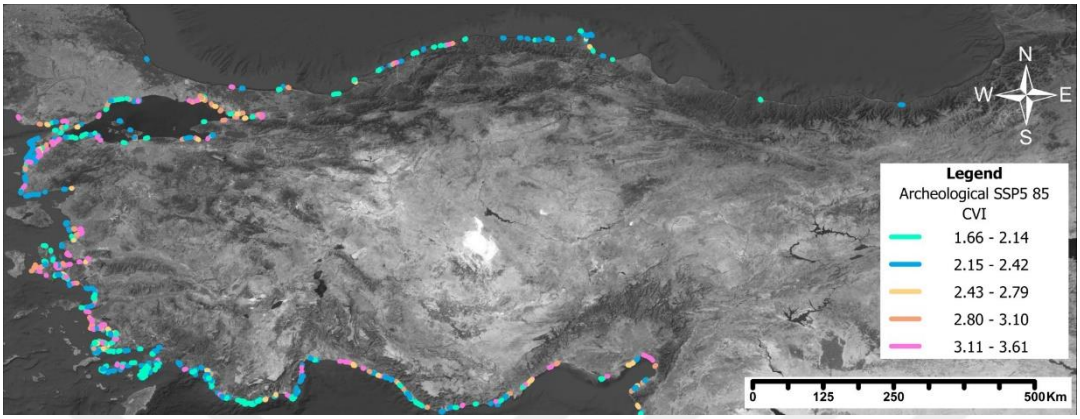


Figure 5.77. SSP5-8.5 Cultural Heritage Site CVI Jenks Distribution

When the standard FCVAM class limits were applied, CVI classifications were narrowed down into three categories: very low, low, and moderate vulnerability, as in SSP2-4.5. Table 5.70 provides a more detailed comparison of Jenks and FCVAM classifications, indicating that 17.3% of the cultural heritage sites -1.2% increase compared to SSP2-4.5- form the group of most vulnerable sites of Turkish shores, while having CVI scores in between medium and high vulnerability classes. This situation is caused by global applications determining FCVAM limits while natural Jenks breaks consider the input data.

Table 5.70 SSP5-8.5 Cultural Heritage Site CVI Jenks & FCVAM Limits

Jenks Natural Breaks	**Results**	**FCVAM Class**	**Results**
< 2.14	393 (33.4%)	< 1.5 Very Low	0
2.15 – 2.42	364 (31%)	1.5 – 2.5 Low	764 (65%)
2.43 – 2.79	75 (6.4%)	2.5 – 3.5 Moderate	411 (34.9%)
2.80 – 3.10	141 (12%)	3.5 – 4.25 High	1 (0.1%)
> 3.11	203 (17.3%)	4.25 < Very High	0

Even though 203 locations belong to the most critical group considering Turkish coasts under SSP5-8.5 conditions, only one shore is denoted as high vulnerable, and no shore is as high vulnerable with respect to FCAM limits as observed in SSP2-4.5. Additionally, in Figure 5.78, histograms with Jenks limits and 0.25 increment impact scores are presented for SSP5-8.5. As in the case of SSP2-4.5, CVI scores are accumulated between 1.5 and 3.75.

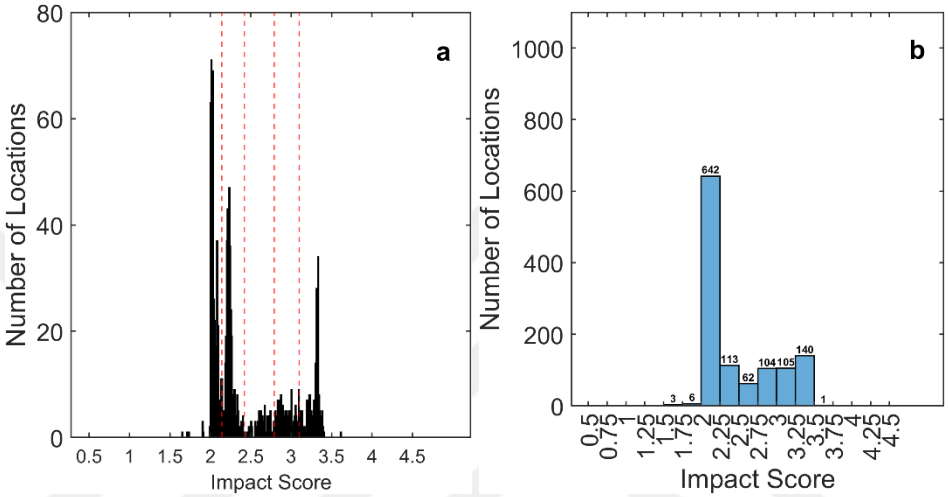


Figure 5.78. SSP5-8.5 Cultural Heritage Site CVI (a) Jenks (b) FCVAM Histograms

5.4 Discussions

5.4.1 Impact Score Distribution Behavior

In this section, physical and human impact score distributions over cumulative and cumulative impact scores over CVI for natural conservation zones are given for all three modules, and SSP2-4.5 and SSP5-8.5 pathways. The scatter diagrams of cultural heritage sites and other SSPs are presented in the appendix section since the general observed scatter behavior of cultural heritage sites is very similar to that of natural conservation zones.

5.4.1.1 Erosion Impact Scores

Figure 5.79 compares the natural conservation zone erosion physical and human impact score distribution with erosion impact scores for both SSP2-4.5 and SSP5-8.5.

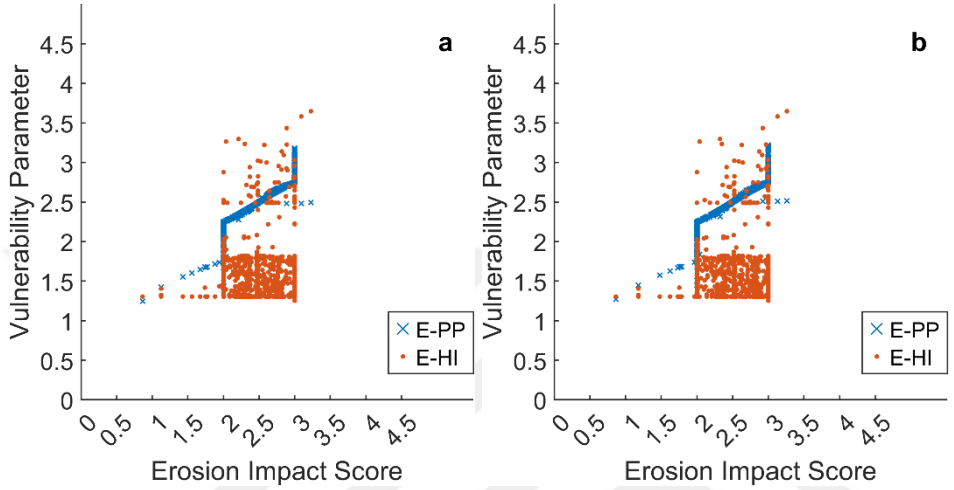


Figure 5.79. SSP2-4.5 & SSP5-8.5 Natural Conservation Zones Erosion Scatter Diagrams (a) SSP2-4.5 (b) SSP-8.5

According to the distribution of physical and human impact scores of erosion concerning the cumulative erosion scores, as long as the human impact scores are lower than the physical impact scores, the cumulative erosion score follows the physical impact score trends almost linearly. In other words, physical impact scores govern the cumulative erosion vulnerability when human activities have limited influence on coastal erosion. However, especially when human activities become significantly higher than physical impact scores, as seen on the higher end of the erosion impact score, the cumulative vulnerability also increases, although the shoreline might be physically more resilient in its natural state. This outcome is mainly a reflection of the fuzzy logic rule system in which it is assumed that the natural state of the shoreline would govern the vulnerability unless significant patterns of change are observed due to human activities. Lack of human activities could not change the inherent vulnerability of a shoreline based on its physical

characteristics. For coastal erosion, human activities would require a significant change in the sediment budget of the region as well as coastal protection measures against coastal erosion. On the other hand, cumulative erosion scores of 2 and 3 act as focus points where these sites have physical and human impact parameters, all within a similar range of 1.7-2.2 and 2.7-3.2, either of the groups higher or lower than the other. Therefore, combining these individual scores provides the same cumulative erosion vulnerability score, either 2 or 3. These results indicate that although different shorelines might have precisely the same cumulative erosion vulnerability score, the composition of the vulnerability could be different, albeit the ranges of individual components are close to each other; therefore, not one of these components (physical or human) governs the vulnerability as it is. For the scenario cases, the increase in physical impact scores follows a consistent pattern across the different scenarios. The only difference observed is the minimum and maximum physical impact scores. However, the maximum observed physical impact score does not change the cumulative score. Therefore, it could be concluded that the coastal erosion vulnerability of natural heritage sites of Turkey is not very sensitive to the scenario pathways regarding SLR and ESL but is governed more by other parameters related to the coastal erosion process. In Tables 5.71 and 5.72, cumulative erosion impact score distributions of natural conservation zones and cultural heritage sites are compared for the pathways of SSP2-4.5 and SSP5-8.5, respectively.

Table 5.71 SSP2-4.5 Erosion Impact Score Distributions

FCVAM Class (SSP2-4.5)	**Natural Conservation**	**Cultural Heritage**
< 1.5 Very Low	10 (0.9%)	4 (0.3%)
1.5 – 2.5 Low	685 (58.5%)	816 (69.4%)
2.5 – 3.5 Moderate	476 (40.6%)	356 (30.3%)
3.5 – 4.25 High	0	0
4.25 < Very High	0	0

Since several natural conservation zones (1171) and cultural heritage sites (1176) are almost equal, percentage distributions were directly compared. In SSP2-4.5, natural conservation zones are more vulnerable to erosion than cultural heritage sites, with 120 more moderate vulnerable shores. However, when SSP5-8.5 is considered, it could be observed that the distribution of natural conservation zones and cultural heritage sites demonstrates minimal differences. This situation resulted from the sensitivity of cultural heritage sites to considered scenarios, with a 22.5% increase of moderate vulnerable areas across the scenarios, while this number drops to 12.3%. Thus, if less severe scenarios are considered, it could be deduced that natural conservation zones are more vulnerable while cultural heritage demonstrates higher sensitivity to SLR and ESL increase.

Table 5.72 SSP5-8.5 Erosion Impact Score Distributions

FCVAM Class (SSP5-8.5)	**Natural Conservation**	**Cultural Heritage**
< 1.5 Very Low	10 (0.9%)	3 (0.3%)
1.5 – 2.5 Low	542 (46.3%)	552 (46.9%)
2.5 – 3.5 Moderate	619 (52.9%)	621 (52.8%)
3.5 – 4.25 High	0	0
4.25 < Very High	0	0

5.4.1.2 Inundation Impact Scores

In Figure 5.80, the distribution of physical and human impact scores for inundation in natural conservation zones is compared with overall inundation impact scores for SSP2-4.5 and SSP5-8.5 scenarios.

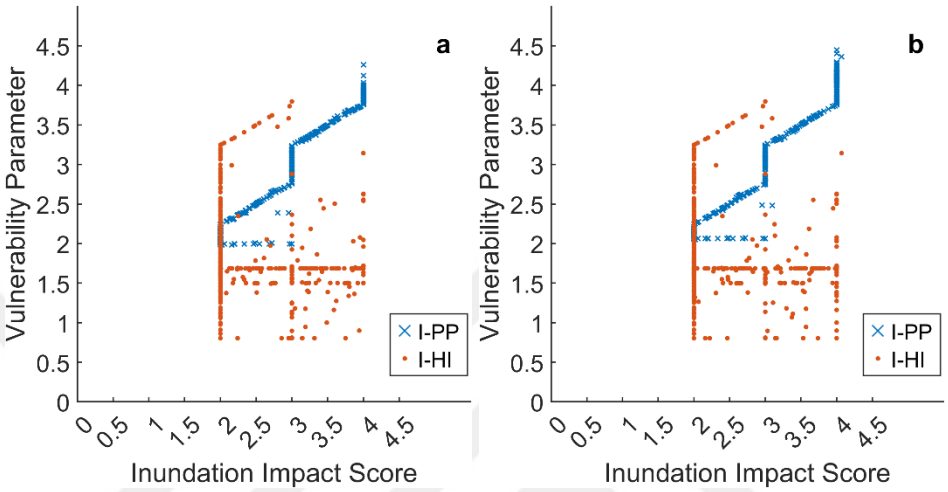


Figure 5.80. SSP2-4.5 & SSP5-8.5 Natural Conservation Zones Inundation Scatter Diagrams (a) SSP2-4.5 (b) SSP-8.5

The distribution patterns of physical and human impact scores for inundation, about cumulative inundation scores, show that when physical impact scores are higher than human impact scores, the cumulative inundation score follows a nearly linear increase similar to that of the physical impact scores. However, at cumulative inundation scores of 2 and 3, concentration points are observed where the physical impact parameters are within the ranges of 1.7–2.2 and 2.7–3.2, respectively, near the concentration points. When human impact scores exceed physical inundation impact scores, they do not affect the cumulative inundation score if they remain below 3.2, as the cumulative impact score stays at two up to this threshold. Considering the concentration point at a cumulative impact score of 2, it could be inferred that cumulative impact scores are more sensitive to changes in physical impact scores than human impact scores. This is due to the fuzzy logic rule structure, which prioritizes the influence of natural elements over human usage. The inundation

human impact score accounts for natural protection degradation and coastal protection structures. In most cases, the human impact score is primarily influenced by coastal protection structures, as over 90% of the studied shorelines have a natural protection degradation value of less than 10%. Therefore, changes in human impact scores are primarily related to coastal protection structures. On the other hand, inundation physical impact scores, based on SSP scenarios, were compared to observe how changes in physical parameters affect the distribution of physical and cumulative inundation scores. The results show that physical impact scores follow a consistent pattern across the different scenarios, except for a few locations where the maximum observed cumulative inundation impact score increased. However, this increase is insignificant, as the overall pattern did not change substantially. Therefore, sea-level rise (SLR) and extreme sea levels (ESL) are not the primary governing parameters for inundation. In Tables 5.73 and 5.74, cumulative inundation score distributions of natural conservation zones and cultural heritage sites are compared for the pathways of SSP2-4.5 and SSP5-8.5, respectively.

Table 5.73 SSP2-4.5 Inundation Impact Score Distributions

FCVAM Class (SSP2-4.5)	**Natural Conservation**	**Cultural Heritage**
< 1.5 Very Low	0	0
1.5 – 2.5 Low	884 (75.5%)	776 (66%)
2.5 – 3.5 Moderate	151 (12.9%)	226 (19.2%)
3.5 – 4.25 High	136 (11.6%)	174 (14.8%)
4.25 < Very High	0	0

Since several natural conservation zones (1171) and cultural heritage sites (1176) are almost equal, percentage distributions were directly compared. The percent distributions of cultural heritage sites over medium and high-vulnerable classes in both pathways are more significant than natural conservation zones. Moreover, for the high vulnerable class, natural conservation zones demonstrated a 3.7% increase from SSP2-4.5 to SSP5-8.5, while this number increased by 4.6% for cultural

heritage sites. Therefore, cultural heritage sites could be denoted as more vulnerable to SLR and ESL increase.

Table 5.74 SSP5-8.5 Inundation Impact Score Distributions

FCVAM Class (SSP5-8.5)	Natural Conservation	Cultural Heritage
< 1.5 Very Low	0	0
1.5 – 2.5 Low	871 (74.4%)	759 (64.5%)
2.5 – 3.5 Moderate	121 (10.3%)	189 (16.1%)
3.5 – 4.25 High	179 (15.3%)	228 (19.4%)
4.25 < Very High	0	0

5.4.1.3 Storm Surge Impact Scores

In Figure 5.81, the distribution of physical and human impact scores for storm surge in natural conservation zones is compared with overall storm surge impact scores for both SSP2-4.5 and SSP5-8.5 scenarios.

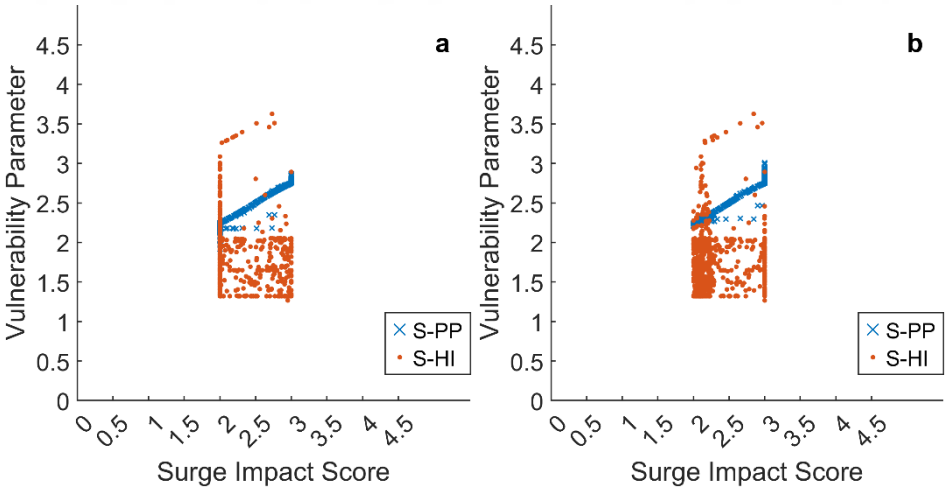


Figure 5.81. SSP2-4.5 & SSP5-8.5 Natural Conservation Zones Storm Surge Scatter Diagrams (a) SSP2-4.5 (b) SSP-8.5

The distribution of physical and human impact scores for coastal storm surge cumulative storm surge scores shows that as long as human impact scores remain

lower than physical impact scores, the cumulative storm surge score follows the trends of the physical impact scores almost linearly, which means that physical impact scores predominantly determine cumulative storm surge vulnerability when human activities not effective on coastal storm surge. However, when human activities significantly surpass physical impact scores, the cumulative vulnerability increases, even if natural vulnerability is low. The critical point for the human impact score is around 3.2; until then, the storm surge vulnerability score stays at 2 for SSP2-4.5. However, this behavior changes in the case of SSP5-8.5 since homogeneous accumulation around cumulative impact score of 2 shifts to upper cumulative impact scores. However, the critical point of 3.2 is scenario-independent. Thus, a linear increase is observed after this level. In the case of natural resilience, the cumulative scores of 2 and 3 act as concentration points, independent of the scenario considered around which the upper and lower limits of natural impact scores are 2.2 and 2.7, respectively. However, the upper limit of the natural impact score around the focal point of 3 is vague. The natural impact score has a lower critical level than the human score on the focal cumulative impact score of 2 because the outcome primarily reflects the fuzzy logic rule system, which assumes that a shoreline's natural state governs its vulnerability unless significant changes occur due to human activities. Storm surge considers three parameters: NATDEG, CPS, and EF. The inundation section states that the NATDEG parameter is generally less effective than other parameters. Thus, locations without protection structures, including engineered frontage, are under threat. These findings suggest that, although different shorelines may have the same cumulative storm surge vulnerability score, the composition of the vulnerability could differ, with the individual components' ranges being close to one another. In this case, neither physical nor human impacts exclusively govern the vulnerability. Regarding scenario cases, the increase in physical impact scores follows a consistent pattern across different scenarios, with the only variations being in the minimum and maximum physical impact scores. However, the maximum observed physical impact score does not result in a change in the cumulative score. Therefore, it could be concluded that the coastal storm surge vulnerability of

Turkey's natural heritage sites is not high sensitive to scenario pathways related to sea-level rise (SLR) and extreme sea levels (ESL). Instead, it is more influenced by other parameters related to the coastal storm surge process.

In Tables 5.75 and 5.76, cumulative storm surge score distributions of natural conservation zones and cultural heritage sites are compared for the pathways of SSP2-4.5 and SSP5-8.5, respectively.

Table 5.75 SSP2-4.5 Storm Surge Impact Score Distributions

FCVAM Class (SSP2-4.5)	**Natural Conservation**	**Cultural Heritage**
< 1.5 Very Low	0	0
1.5 – 2.5 Low	923 (78.8%)	825 (70.2%)
2.5 – 3.5 Moderate	248 (21.2%)	348 (29.6%)
3.5 – 4.25 High	0	3 (0.3%)
4.25 < Very High	0	0

Table 5.76 SSP5-8.5 Storm Surge Impact Score Distributions

FCVAM Class (SSP5-8.5)	**Natural Conservation**	**Cultural Heritage**
< 1.5 Very Low	0	0
1.5 – 2.5 Low	879 (75.1%)	774 (65.8%)
2.5 – 3.5 Moderate	292 (24.9%)	398 (33.8%)
3.5 – 4.25 High	0	4 (0.3%)
4.25 < Very High	0	0

Since several natural conservation zones (1171) and cultural heritage sites (1176) are almost equal to each other, percentage distributions were directly compared to each other. In both pathways, the percent distributions of cultural heritage sites over medium and high-vulnerable classes are greater than natural conservation zones. Although the number of high vulnerable areas increased by 1 for cultural heritage

sites, for the moderate vulnerable class, these zones demonstrated a 4.2% increase from SSP2-4.5 to SSP5-8.5. In comparison, this number is 3.7% for natural conservation zones. Therefore, cultural heritage sites could be denoted as more vulnerable to SLR and ESL increase.

5.4.1.4 CVI and Cumulative Impact Scores

In Figure 5.82, erosion, inundation, and storm surge impact score versus CVI distribution are presented for SSP2-4.5 and SSP5-8.5.

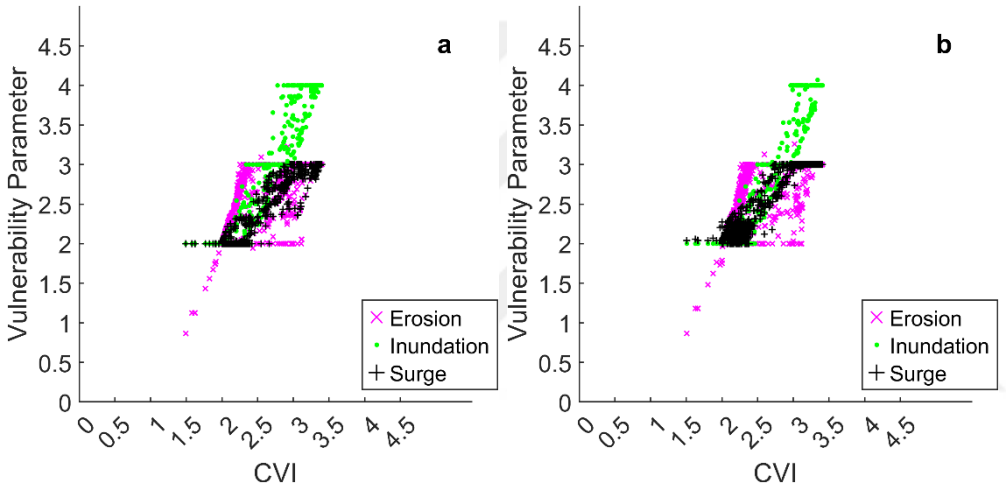


Figure 5.82. SSP2-4.5 & SSP5-8.5 Natural Conservation Zones Cumulative Impact Score Scatter Diagrams (a) SSP2-4.5 (b) SSP-8.5

The initial comparison between scenario behaviors indicates that the maximum observed CVI value does not vary significantly; the SSP5-8.5 pathway results in higher CVI values across all three module impact scores. This implies that the distributions of module scores are generally shifted toward higher CVI values in SSP5-8.5. When examining the distribution of the three modules in both scenarios, storm surge correlates more strongly with CVI increases than the other modules. Furthermore, while some locations with erosion scores around 2 could reach CVI scores greater than 3, this is not the case for inundation, where higher parameter vulnerability scores are needed to achieve comparably high CVI values. In the case

of storm surge, the highest overall CVI levels are observed when the storm surge score is 3. Regarding module impact scores versus CVI distributions, if the pattern of accumulated data is considered, storm surge demonstrates a higher correlation with CVI since between parameter impact scores of 2 and 3, storm surge data have an almost linear pattern with a milder slope compared to others. In the case of inundation impact sores, although the accumulated data behavior is again almost linear, the observed inclination angle is greater than the angle of storm surge. Finally, for erosion, accumulated data have the highest inclination angle. Moreover, the data is mainly distributed over an area instead of accumulated over a trendline. Thus, the effect of erosion over CVI is the least. In Tables 5.77 and 5.78, cumulative CVI score distributions of natural conservation zones and cultural heritage sites are compared for the pathways of SSP2-4.5 and SSP5-8.5, respectively.

Table 5.77 SSP2-4.5 CVI Score Distributions

FCVAM Class (SSP2-4.5)	**Natural Conservation**	**Cultural Heritage**
< 1.5 Very Low	2 (0.2%)	0
1.5 – 2.5 Low	891 (76.1%)	794 (67.5%)
2.5 – 3.5 Moderate	278 (23.7%)	381 (32.4%)
3.5 – 4.25 High	0	1 (0.1%)
4.25 < Very High	0	0

Since the number of natural conservation zones (1171) and cultural heritage sites (1176) are nearly identical, their percentage distributions were directly compared. In both pathways, the CVI percentage distributions of cultural heritage sites in the medium vulnerable classes are greater than those of natural conservation zones. In addition to this, the only high vulnerable shoreline belongs to the cultural heritage site group.

Table 5.78 SSP5-8.5 CVI Score Distributions

FCVAM Class (SSP5-8.5)	Natural Conservation	Cultural Heritage
< 1.5 Very Low	0	0
1.5 – 2.5 Low	872 (74.5%)	764 (65%)
2.5 – 3.5 Moderate	299 (25.5%)	411 (34.9%)
3.5 – 4.25 High	0	1 (0.1%)
4.25 < Very High	0	0

Although the number of high vulnerable areas did not increase for cultural heritage sites, the moderate vulnerable class increased by 2.5%. In comparison, this number is 1.8% for natural conservation zones when considering the pathway change from SSP2-4.5 to SSP5-8.5. Therefore, cultural heritage sites could be considered more vulnerable to increased sea-level rise (SLR) and extreme sea levels (ESL).

5.4.2 Vulnerability Distribution of SSP1-1.9, SSP1-2.6, SSP3-7.0

Impact scores and vulnerabilities regarding SSP2-4.5 and SSP5-8.5 pathways were explained in Chapter 4. These two pathways were selected to be presented in detail since SSP2-4.5 indicates moderate criticality while SSP5-8.5 is the worst case. However, as explained in Chapter 2, the other three pathways were defined in IPCC AR6. SSP1-1.9 implies a global average temperature increase would be 1.4°C; in SSP1-2.6, this number increases to 1.8°C, and for SSP3-7.0, the corresponding increase is 3.6°C. As observed between SSP2-4.5 and SSP5-8.5, overall vulnerability becomes more critical with each pathway corresponding to higher GHG emissions. Table 5.79 presents cultural heritage site CVI results of every IPCC AR6 pathway.

Table 5.79 Cultural Heritage Site CVI Results of all Pathways

ARC CVI	IPCC AR6 SSP				
	SSP1-1.9	SSP1-2.6	SSP2-4.5	SSP3-7.0	SSP5-8.5
< 1.5	1	0	0	0	0
1.5 – 2.5	856	801	794	769	764
2.5 – 3.5	319	374	381	406	411
3.5 – 4.25	0	1	1	1	1
4.25 >	0	0	0	0	0

The comparison of CVI class distribution, as shown in Table 5.79, further supports this claim. For instance, the shoreline classified as "very low vulnerable" (CVI < 1.5) was identified under the SSP1-1.9 pathway, and it shifts to "low vulnerable" under the SSP1-2.6 scenario. Additionally, under SSP1-2.6, a shoreline classified as "high vulnerable" (CVI between 3.5 and 4.25) was identified. In summary, as the severity of the scenario increases, the vulnerability pattern shifts toward higher vulnerability classes. Detailed results for all three pathways, including both natural conservation zones and cultural heritage sites, are provided in the Appendices section.

5.4.3 Result Comparison of FCVAM with Other Assessment

As mentioned in Chapter 3, there are various CVI methods, and selecting which one to use might result in different CVI results. Although differences in parameters selected and classes defined in each model limit a direct comparison of the results, similar trends in vulnerability from several models would ensure higher certainty in a region's vulnerability. Thus, in this section, the results of this study are compared with CVI maps published in Aykut's master's thesis (2021) for the Mersin province. In Figure 5.83 and Figure 5.84, CVI distribution maps created by FCVAM results of SSP2-4.5 and Aykut (2021) are presented, respectively, for Mersin.

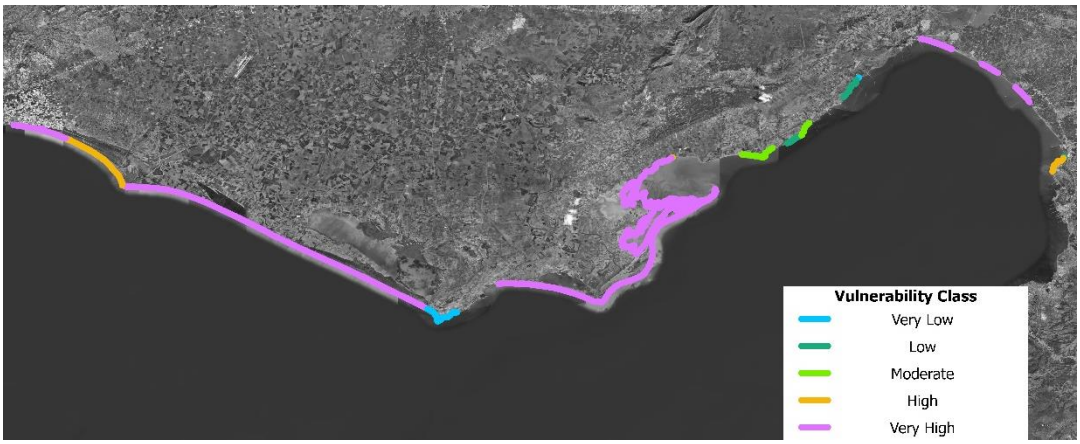


Figure 5.83. FCVAM results of Mersin Under Pathway of SSP2-4.5

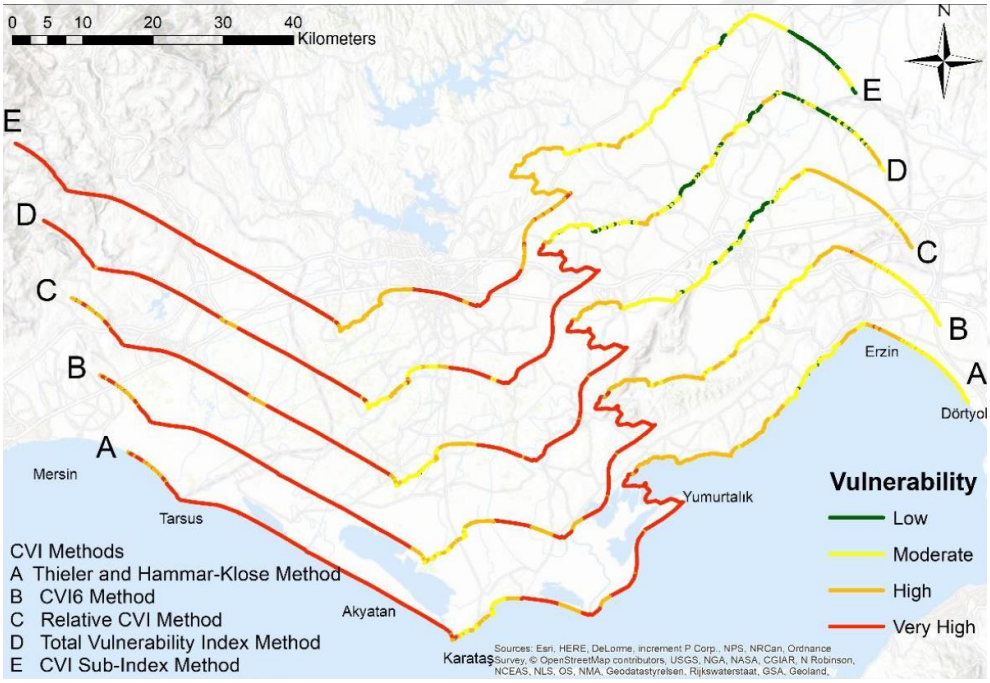


Figure 5.84. Previous Study Results of Mersin (Aykut, 2021, p. 89)

The general pattern of the FCVAM findings demonstrates similar patterns with the other methods presented in Aykut (2021). However, at some specific locations, FCVAM results differ from the other methods, for example, at the northern-east part of the shoreline of Mersin. For this location, there are also inconsistencies among the other methods. However, none of them classified these shores as very high vulnerable entirely although Thieler & Hammar -Klose and CVI6 models also

indicate that a few very high vulnerable cells exist along this part of these shores. On the other hand, at the southern part of the shoreline of Mersin, a very low vulnerable shore is located according to FCVAM findings, where other methods classified the shore as moderate to high vulnerable. These differences might result from a few factors. Firstly, the map given in the study of Aykut (2021) was formed by CVI analysis on the shoreline divided into cells of 100m x 100m for five different CVI methods. However, the FCVAM application was conducted on shoreline projections of study areas, which means no cells with specific dimensions were used during the calculation process. Thus, only one representative input value was used for each parameter. This has a consequence of the decrease in the ability to reflect sensitivity to parameter changes along the studied shoreline. Secondly, although there are standard parameters between these CVI methods, the number and type of parameters considered vary significantly. For example, factors such as river flow regulation or coastal protection structures are only considered in FCVAM. Moreover, the Total Vulnerability Index and CVI Sub-Index methods are the only methods that include socio-economic parameters (Aykut,2021). On the other hand, the parameters of roads and population are not directly considered in FCVAM. To sum up, despite the slight variations, the general behavior of FCVAM results compared to methods presented in the study of Aykut (2021) demonstrate compatible patterns. The differences are mainly caused by the 100m x 100m unit cell approach used in the study of Aykut (2021), the representative parameter approach used in this study, and the consideration of socioeconomic parameters and their types. This comparison once again highlights the importance of selecting parameters to represent vulnerability and the characteristics of the coastline, as well as the aim of the vulnerability study.

CHAPTER 6

CONCLUSION

Throughout history, coastal areas have been attraction points for humankind because of their economic potential and natural features, which are still valid. As a result, many coastal cultural heritage areas and natural conservation zones are located on Turkish coasts. However, with 8333 km shoreline length, Turkish coasts are threatened by climate change-induced global mean sea level rise. Coastal cultural heritage areas and natural conservation zones are crucial for Turkiye economically and sociologically. Identifying how vulnerable these areas are against sea level rise lies within Turkiye's sustainable development goals. Therefore, in this study, a modified version of FCVAM developed by Gülizar Özyurt Tarakcıoğlu in 2010 was used to calculate the CVI of areas located within 10 m elevation and 1 km inland for all of the IPCC AR6 Shared Socioeconomic Pathways. A modified version of the model requires seven physical and four human input parameters to get impact scores of 3 modules, which would be used to get CVI. The reduction of sediment supply was removed from human parameters, and weights of erosion human inference system input parameters were re-distributed. FCVAM was rewritten in Python using and modifying a fuzzy logic library named Simpful (Spolaor, 2020) since this programming language is open source, contrary to MATLAB. After model modifications and the determination of shorelines to be studied, database pre-processing, which is required to derive input parameters, was initiated. Parameter preprocesses varied from simple spatial join to combining multiple datasets to re-generate the input layer.

The results of the study indicated that since most of the natural conservation zone and cultural heritage sites are located in the Aegean Region, overall, the highest number of least and most vulnerable shores are within this region, both module impact scores and CVI scores, although the only high vulnerable location is located

in Black Sea Region. However, the FCVAM structure enables this model to analyze each module's physical and human impact score and give more detailed results rather than relying solely on CVI for representation. In the module component aspect, human impact scores did not change between SSP sets for the same locations since no human behavior forecast was used for this study. In other words, CVI score variations were related to the adopted SSP. In the case of natural conservation zones, dominant behavior was observed in all ErosionHI, InundationHI, and Storm SurgeHI, which were low-vulnerable. However, the most severe class obtained by all three of them was high vulnerable. In the case of cultural heritage sites, the only difference is that for InundationHI, the most severely obtained class was very high vulnerable. Contrary to human impact scores, physical impact scores depend on SSP. Regarding the natural conservation zone and SSP2-4.5 scenario, for erosionPP and surgePP, the most critical obtained class was medium vulnerable. On the other hand, for InundationPP, one very high vulnerability along with 135 high vulnerable shorelines was detected. This situation also affected the cumulative impact score of inundation as 136 high vulnerable shorelines against inundation were detected, while there were no high vulnerable shorelines against erosion and storm surge. Moreover, shoreline CVI results calculated by aggregating erosion, inundation, and storm surge also indicated that the most critical obtained vulnerability class was moderate. The dominant behavior was low vulnerability, which could be explained by generating FCVAM class limits using global datasets. Thus, to obtain how local results could be grouped, the Jenks Natural Breaks method was applied. New class limits indicated that 136 (11.6%) locations belong to the most vulnerable group. There had been vulnerability class pattern changes when SSP5-8.5 conditions were applied. The highest number of class shift-ups were observed in erosion, with 146 new moderate vulnerable shorelines. However, inundation impact scores were most detrimentally affected since 33 new high vulnerable shorelines and 10 new very high vulnerable shorelines against inundationPP were introduced. As a result, 43 new high vulnerable shorelines in terms of inundation cumulative impact scores were obtained. For storm surge, there were 44 new moderate vulnerable shorelines for both the physical impact

sore and cumulative impact scores. Concerning CVI, because of these changes, the number of moderate vulnerable shorelines increased by 21. However, no high or very high vulnerable shorelines were detected for SSP5-8.5, as observed in the case of SSP2-4.5. To localize the vulnerability class limits, Jenks Natural Breaks were applied, and 216 (18.4%) of the studied locations were denoted as members of the most vulnerable group of Türkiye.

SSP2-4.5 results indicated that like natural conservation zones, the most observed vulnerability class for cultural heritage sites was a low vulnerability for cumulative impact scores and CVI. On the other hand, despite having the same most common vulnerability class, cultural heritage sites are more vulnerable by having one high vulnerable shore and a higher number of moderate vulnerable shorelines compared to natural conservation zones. On the other hand, localization of CVI results using Jenks Natural Breaks indicated that 189 locations (16.1%) belong to the most critical group of Turkish coasts. In terms of impact scores, inundation physical and human impact scores were higher than those of other modules. There were 170 shorelines with high vulnerable inundation physical scores and one with very high vulnerable inundation human impact scores. The effect of these on the cumulative impact score of inundation resulted in 174 high vulnerable locations. In the case of erosion and storm surges, no locations had high vulnerable physical impact scores. At the same time, 1 and 8 locations had high vulnerable human impact scores, respectively, which also affected cumulative impact scores since there were no high vulnerable locations in terms of erosion cumulative impact score and three high vulnerable locations concerning storm surge cumulative impact score.

Adopting SSP5-8.5 instead of SSP2-4.5 resulted in class changes similar to the natural conservation zone but at a larger scale. Physical and cumulative impact scores of erosion demonstrated the highest number of class changes by 265 new moderate vulnerable locations. The most severe class shifts occurred with the inundation of physical and cumulative impact scores. In the case of inundation physical impact scores, 29 and 26 new locations were denoted as high and very high vulnerable, respectively. These changes resulted in 54 new high-vulnerable locations

regarding cumulative impact scores. The storm surge module was the one least affected by adopting a different pathway since the only change was that 1 location became high vulnerable in terms of cumulative impact score. Increases in the class vulnerabilities resulted in 30 new locations being denoted as moderate vulnerable. In other words, a number of high vulnerable locations did not change as well as there were not any locations introduced as very high vulnerable. Localization of results, however, stated that 243 (20.7%) studied shorelines belong to the most critical group of Turkish coasts. In addition to SSP2-4.5 and SSP5-8.5, results of SSP1-1.9, SSP1-2.6, and SSP3-7.0 were also computed and given in the appendix section. The behavior of these three pathways is also in line with explained ones. As the severity of the considered pathway increases, shorelines become more vulnerable.

In order to determine the correlation of physical and human impact scores to cumulative impact scores, scatter diagrams of each module for both natural conservation zones and cultural heritage sites, as well as SSP2-4.5 and SSP5-8.5, were generated. Natural conservation zone and cultural heritage site behavior resembled each other. Thus, diagrams of cultural heritage sites were given in appendices. For both natural conservation zones and cultural heritage sites, patterns indicated that physical impact scores are more effective on cumulative impact scores than human impact scores. This could be explained by the main philosophy of FCVAM, as the basis of natural parameters created the model are determinant on vulnerability. To give an example of this claim, between cumulative impact scores of 2 and 3, after physical impact scores become greater than 2.2, a linear increasing trend between physical impact scores and cumulative impact scores is obtained. However, to occur this trend between human impact scores and cumulative impact scores, the bare minimum human impact score level is around 3.2. This pattern was valid for all considered scenarios and modules. Also, a comparison of scatter diagrams of different scenarios indicated that as the scenario severity increases, overall cumulative impact score nodes shift to higher levels. In addition to module component scatter diagrams, cumulative impact scores versus CVI scatter diagrams were also generated to get insight into how cumulative impact scores are correlated

with CVI results. Storm surge distribution trend concerning CVI indicated storm surge was more correlated compared to other modules if slope of distribution trendline was considered. In the case of inundation, although the highest cumulative impact scores were calculated for this module, their impacts on CVI were less than storm surge. Lastly, erosion cumulative impact scores demonstrated the steepest inclination angle. Thus, this module could be referred to as the least correlated one.

In addition to internal FCVAM-related discussions, the obtained results were compared with one of the previous studies conducted along Turkish coasts. In his master thesis, Aykut (2021) focused on southern parts of Türkiye and applied five different approaches to present the vulnerability of studied locations. Localized SSP2-4.5 FCVAM results were compared to the findings of a study of Aykut (2021) for Mersin province. Overall, vulnerability patterns were coherent with each other. However, the division of study areas into cells in the previous study while assigning one representative parameter input value for each parameter in this study to represent the entire assessed shoreline resulted in some deviations. Moreover, although considered physical parameters are somehow in line with the vulnerability assessment methods, there are disputes about whether consideration of socio-economic parameters or not, and if so, how it would be. Only two methods given in the study of Aykut (2021) considered socio-economic parameters. However, these parameters were not directly correlated with the ones considered in FCVAM. The dispute between different assessment methods was caused by the fundamental limitation of the vulnerability concept as not being an observable phenomenon. Therefore, there has not been a solid or concrete methodology to be agreed on. Nevertheless, the generation of vulnerability maps and assessment of different locations under different circumstances are expected to contribute and very crucial for policymakers during the decision-making process, which will enable them to generate strategies to contribute more to the sustainable development goals of Türkiye.

For further studies, adopting a cell approach instead of a representative parameter approach and comparing the results would be an important indicator of how effective or ineffective using a representative parameter value could be. Moreover, comparing the results of different cell sizes might also be important to determine the ideal cell size by reaching an optimum point that balances computational effort and marginal error. Also, future studies could attempt to minimize one of the main issues regarding vulnerability, which is the subjectivity of models, by trying to reach objectivity by intersubjectivity. To be more specific, new machine learning techniques have been developed and mass application of different already available vulnerability assessment methodologies to generate results that would be used in training them could be an important step to generate models with lower bias and higher consensus. On the other hand, future studies might be focused on resolving issues related to stationary human behavior data while having projections related to physical parameters. To achieve this, either human usage scenarios might be generated by development plans or virtually, or IPCC AR pathways could be turned into a form representing localized potential human behavior. Finally, concerning parameter inputs, impact, and CVI scores, the study could suggest how applicable and effective alternative protection measures would be.

REFERENCES

Anfuso, G., Postacchini, M., Di Luccio, D., & Benassai, G. (2021). Coastal sensitivity/vulnerability characterization and adaptation strategies: A Review. Journal of Marine Science and Engineering, 9(1), 72. https://doi.org/10.3390/jmse9010072

Athanasiou, P., van Dongeren, A., Giardino, A. et al. Uncertainties in projections of sandy beach erosion due to sea level rise: an analysis at the European scale. Sci Rep 10, 11895 (2020). https://doi.org/10.1038/s41598-020-68576-0

Aykut, F. (2021). Coastal vulnerability assessment for Mersin and İskenderun Bays, northeastern Mediterranean (master's thesis, Middle East Technical University).

Aykut, F., Tezcan, D. Evaluating Sea Level Rise Impacts on the Southeastern Türkiye Coastline: A Coastal Vulnerability Perspective. PFG 92, 335–352 (2024). https://doi.org/10.1007/s41064-024-00284-0

Bandh, S. A., Shafi, S., Peerzada, M., Rehman, T., Bashir, S., Wani, S. A., & Dar, R. (2021). Multidimensional Analysis of Global Climate Change: A Review. Environmental Science and Pollution Research, 28(20), 24872–24888. https://doi.org/10.1007/s11356-021-13139-7

Bukvic, A., Rohat, G., Apotsos, A., & de Sherbinin, A. (2020). A systematic review of coastal vulnerability mapping. Sustainability, 12(7), 2822. https://doi.org/10.3390/su12072822

Cetin, M., Sevik, H., Koc, I., & Zeren Cetin, I. (2023). The change in biocomfort zones in the area of Muğla Province in near future due to the global climate change scenarios. Journal of Thermal Biology, 112, 103434. https://doi.org/10.1016/j.jtherbio.2022.103434

de Smith, M. J., Goodchild, M. F., & Longley, P. A. (2018). Geospatial analysis: A comprehensive guide (5th ed.). Sage Publications.

Deb, D., Uddin, M. M., Mahbub-E-Kibria, A. S., Kumar Das, M., & Hasan, M. (2024). Coastal vulnerability assessment to multi hazards in the exposed coast of southeastern coastal region of Bangladesh. Regional Studies in Marine Science, 73, 103484. https://doi.org/10.1016/j.rsma.2024.103484

Dike, E. C., Amaechi, C. V., Beddu, S. B., Weje, I. I., Ameme, B. G., Efeovbokhan, O., & Oyetunji, A. K. (2024). Coastal vulnerability index sensitivity to shoreline position and coastal elevation parameters in the Niger Delta region, Nigeria. Science of The Total Environment, 919, 170830. https://doi.org/10.1016/j.scitotenv.2024.170830

EPA. (2024). Causes of Climate Change. Environmental Protection Agency. https://www.epa.gov/climatechange-science/causes-climate-change#reflectivity

European Environment Agency (2016). EU-DEM (raster) - version 1.0, Apr. 2016. https://sdi.eea.europa.eu/catalogue/srv/api/records/19cff95e-61ac-45ed-8ee3-c43220d709cf

European Marine Observation and Data Network (EMODnet). (2022, January 31). EMODnet Digital Bathymetry (DTM 2022). EMODnet product catalogue. https://emodnet.ec.europa.eu/geonetwork/srv/eng/catalog.search#/metadata/ff3aff8a-cff1-44a3-a2c8-1910bf109f85

European Space Agency (2024). Copernicus Global Digital Elevation Model. Distributed by OpenTopography. https://doi.org/10.5069/G9028PQB. Accessed: 2024-08-01

Fang, J., Wahl, T., Fang, J., Sun, X., Kong, F., & Liu, M. (2021). Compound flood potential from storm surge and heavy precipitation in coastal China: Dependence, drivers, and impacts. Hydrology and Earth System Sciences, 25(8), 4403–4416. https://doi.org/10.5194/hess-25-4403-2021

Fang, J., Wahl, T., Fang, J., Sun, X., Kong, F., and Liu, M.: Compound flood potential from storm surge and heavy precipitation in coastal China: dependence, drivers, and impacts, Hydrol. Earth Syst. Sci., 25, 4403–4416, https://doi.org/10.5194/hess-25-4403-2021, 2021.

Fannassi, Y., Ennouali, Z., Hakkou, M., Benmohammadi, A., Al-Mutiry, M., Elbisy, M. S., & Ali Masria. (2023). Prediction of coastal vulnerability with machine learning techniques, Mediterranean coast of Tangier-Tetouan, Morocco. Estuarine, Coastal and Shelf Science, 291, 108422. https://doi.org/10.1016/j.ecss.2023.108422

Filonchyk, M., Peterson, M. P., Zhang, L., Hurynovich, V., & He, Y. (2024). Greenhouse gases emissions and global climate change: Examining the influence of CO2, ch4, and n2o. Science of The Total Environment, 935, 173359. https://doi.org/10.1016/j.scitotenv.2024.173359

Gazioglu, C., Simav, Ö., Seker, D., & Tanik, A. (2015). Identification of risk areas along the Turkish coasts using the Coastal Vulnerability Index. Harita Dergisi, 153, 1-8.

Gornitz, V.M., 1990. Vulnerability of the East coast, U.S.A. to future sea level rise. J. Coast. Res. Special Issue 9, 201–237.

Gorokhovich, Y., Leiserowitz, A., & Dugan, D. (2014). Integrating coastal vulnerability and community-based subsistence resource mapping in Northwest Alaska. Journal of Coastal Research, 30(1), 158-169. https://doi.org/10.2112/JCOASTRES-D-13-00072.1

Hersbach, H., Bell, B., Berrisford, P., Biavati, G., Horányi, A., Muñoz Sabater, J., Nicolas, J., Peubey, C., Radu, R., Rozum, I., Schepers, D., Simmons, A., Soci, C., Dee, D., Thépaut, J-N. (2023): ERA5 hourly data on single levels from 1940 to present. Copernicus Climate Change Service (C3S) Climate Data Store (CDS), DOI: 10.24381/cds.adbb2d47

Hinkel, J. (2011). "indicators of vulnerability and adaptive capacity": Towards a clarification of the science–policy interface. Global Environmental Change, 21(1), 198–208. https://doi.org/10.1016/j.gloenvcha.2010.08.002

IPCC, 2001: Climate Change 2001: Synthesis Report. A Contribution of Working Groups I, II, and III to the Third Assessment Report of the Integovernmental Panel on Climate Change [Watson, R.T. and the Core Writing Team (eds.)]. Cambridge University Press, Cambridge, United Kingdom, and New York, NY, USA, 398 pp.

IPCC, 2023: Climate Change 2023: Synthesis Report. Contribution of Working Groups I, II and III to the Sixth Assessment Report of the Intergovernmental Panel on Climate Change [Core Writing Team, H. Lee and J. Romero (eds.)]. IPCC, Geneva, Switzerland, 184 pp., doi: 10.59327/IPCC/AR6-9789291691647.

Jenks, G. F. (1967). The data-driven classification of geographic data. Annuals of the Association of American Geographers, 57(3), 153-163.

Kantamaneni, K., Phillips, M., Thomas, T., & Jenkins, R. (2018). Assessing coastal vulnerability: Development of a combined physical and economic index. Ocean & Coastal Management, 158, 164–175. https://doi.org/10.1016/j.ocecoaman.2018.03.039

Kato, F., & Tajima, Y. (2023). Coastal adaptation to climate change in Japan: a review. Coastal Engineering Journal, 65(4), 597–619. https://doi.org/10.1080/21664250.2023.2259187

Koroglu, A., Ranasinghe, R., Jiménez, J. A., & Dastgheib, A. (2019). Comparison of coastal vulnerability index applications for Barcelona Province. Ocean & Coastal Management, 178, 104799. https://doi.org/10.1016/j.ocecoaman.2019.05.001

Kuleli, T., & Bayazıt, Ş. (2023). Site analysis of maritime transportation infrastructures by using the Coastal Vulnerability Index approach: The case of Bodrum Peninsula. Marine Science and Technology Bulletin, 12(2), 142-155. https://doi.org/10.33714/masteb.1260897

López Royo, M., Ranasinghe, R., & Jiménez, J. A. (2016). A rapid, low-cost approach to coastal vulnerability assessment at a national level. Journal of Coastal Research, 320, 932–945. https://doi.org/10.2112/jcoastres-d-14-00217.1

Mazhar, S., Pellegrini, E., Contin, M., Bravo, C., & De Nobili, M. (2022). Impacts of salinization caused by sea level rise on the biological processes of coastal soils - A Review. Frontiers in Environmental Science, 10. https://doi.org/10.3389/fenvs.2022.909415

McLaughlin, S., McKenna, J., & Cooper, J. A. G. (2002). Socio-economic data in coastal vulnerability indices: Constraints and opportunities. Journal of Coastal Research, 36, 487–497. https://doi.org/10.2112/1551-5036-36.sp1.487

NASA. (2023, January 19). NASA Sea Level Change Portal. IPCC 6th Assessment Report Sea Level Projections. https://sealevel.nasa.gov/ipcc-ar6-sea-level-projection-tool

Nguyen, T. T. X., Bonetti, J., Rogers, K., & Woodroffe, C. D. (2016). Indicator-based assessment of climate-change impacts on coasts: A review of concepts, methodological approaches and vulnerability indices. Ocean & Coastal Management, 123, 18–43. https://doi.org/10.1016/j.ocecoaman.2015.11.022

Oppenheimer, M., B.C. Glavovic , J. Hinkel, R. van de Wal, A.K. Magnan, A. Abd-Elgawad, R. Cai, M. Cifuentes-Jara, R.M. DeConto, T. Ghosh, J. Hay, F. Isla, B. Marzeion, B. Meyssignac, and Z. Sebesvari, 2019: Sea Level Rise and Implications for Low-Lying Islands, Coasts and Communities. In: IPCC Special Report on the Ocean and Cryosphere in a Changing Climate [H.-O. Pörtner, D.C. Roberts, V. Masson-Delmotte, P. Zhai, M. Tignor, E. Poloczanska, K. Mintenbeck, A. Alegría, M. Nicolai, A. Okem, J. Petzold, B. Rama, N.M. Weyer (eds.)]. Cambridge University Press, Cambridge, UK and New York, NY, USA, pp. 321–445. https://doi.org/10.1017/9781009157964.006.

Ozsahin E, Ozdes M, Ozturk M, Yang D. Coastal Vulnerability Assessment of Thrace Peninsula: Implications for Climate Change and Sea Level Rise. Remote Sensing. 2023; 15(23):5592. https://doi.org/10.3390/rs15235592

Özyurt, G. and Ergin, A., 2010. Improving coastal vulnerability assessments to sea-level rise: a new indicator based methodology for decision makers. Journal of Coastal Research. March 2010 West Palm Beach (Florida), ISSN0749-0208

Özyurt, G. and Ergin, A., 2010. Improving coastal vulnerability assessments to sea-level rise: a new indicator based methodology for decision makers. Journal of Coastal Research. March 2010 West Palm Beach (Florida), ISSN0749-0208

Özyurt. (2010). Fuzzy Vulnerability Assessment of Coastal Areas to Sea Level Rise. Phd Thesis, Department of Civil Engineering, Middle East Technical University, Ankara, Turkiye

Pramanik, M.K., Dash, P. & Behal, D. Improving outcomes for socioeconomic variables with coastal vulnerability index under significant sea-level rise: an approach from Mumbai coasts. Environ Dev Sustain 23, 13819–13853 (2021). https://doi.org/10.1007/s10668-021-01239-w

Rahimi, R., Tavakol-Davani, H., Graves, C., Gomez, A., & Fazel Valipour, M. (2020). Compound Inundation Impacts of Coastal Climate Change: Sea-Level Rise, Groundwater Rise, and Coastal Precipitation. Water, 12(10), 2776. https://doi.org/10.3390/w12102776

Republic of Turkey, Ministry of Transport and Infrastructure. (n.d.). Nautical charts. SHODB. https://www.shodb.gov.tr/shodb_esas/index.php/tr/urunler/haritalar/seyir-haritalari

Roukounis, C. N., & Tsihrintzis, V. A. (2022). Indices of coastal vulnerability to climate change: A Review. Environmental Processes, 9(2). https://doi.org/10.1007/s40710-022-00577-9

S, S., Alshahrani, H. M., Tamizhselvi, A., & Sujaatha, A. (2024). Assessment of coastal vulnerability using AHP and machine learning techniques. Journal of South American Earth Sciences, 147, 105107. https://doi.org/10.1016/j.jsames.2024.105107

Shadrick, J.R., Rood, D.H., Hurst, M.D. et al. Sea-level rise will likely accelerate rock coast cliff retreat rates. Nat Commun 13, 7005 (2022). https://doi.org/10.1038/s41467-022-34386-3

Simav, Ö., Şeker, D. Z., Tanık, A., & Gazioğlu, C. (n.d.). Determining the endangered fields of Turkish coasts with Coastal Vulnerability Index (Kıyı Etkilenebilirlik Göstergesi ile Türkiye Kıyıları Risk Alanlarının Tespiti). General Command of Mapping, Istanbul Technical University, Istanbul University

Simpson, M.J.R., Bonaduce, A., Borck, H.S., Breili, K., Breivik, Ø., Ravndal, O.R., Richter, K., 2024. Sea-Level Rise and Extremes in Norway: Observations and Projections Based on IPCC AR6. Norwegian Centre for Climate Services report 1/2024, ISSN 2704-1018, Oslo, Norway

Simpson, M.J.R., Bonaduce, A., Borck, H.S., Breili, K., Breivik, Ø., Ravndal, O.R., Richter, K., 2024. Sea-Level Rise and Extremes in Norway: Observations and Projections Based on IPCC AR6. Norwegian Centre for Climate Services report 1/2024, ISSN 2704-1018, Oslo, Norway

Slangen ABA, Palmer MD, Camargo CML, Church JA, Edwards TL, Hermans THJ, Hewitt HT, Garner GG, Gregory JM, Kopp RE, Santos VM and van de Wal RSW (2023). The evolution of 21st century sea-level projections from IPCC AR5 to AR6 and beyond. Cambridge Prisms: Coastal Futures, 1, e7, 1–13 https://doi.org/10.1017/cft.2022.8

Spolaor S., Fuchs C., Cazzaniga P., Kaymak U., Besozzi D., Nobile M.S.: Simpful: a user-friendly Python library for fuzzy logic, International Journal of Computational Intelligence Systems, 13(1):1687–1698, 2020 DOI:10.2991/ijcis.d.201012.002

Thieler, E.R. and Hammer-Klose, E.S. (2000) National Assessment to Coastal Vulnerability to Future Sea-Level Rise: Preliminary Results for the U.S Atlantic Coast. U.S Geological Survey, Open File Report, 99-593. https://doi.org/10.3133/ofr00178

U.S. Environmental Protection Agency. (n.d.). Climate indicators: Greenhouse gases. Retrieved October 31, 2024, from https://www.epa.gov/climate-indicators/greenhouse-gases

United Nations. (2015). The Paris Agreement. United Nations Climate Change. https://unfccc.int/process-and-meetings/the-paris-agreement?gad_source=1&gclid=Cj0KCQjwwae1BhC_ARIsAK4JfrxFxF7tCVmTd727KBrshCgi6rgtbeMANkGr5cl704jDXGCvHzRvqaoaApYeEALw_wcB

United Nations. (n.d.). Coastal Zone Management. United Nations Environment Program. https://www.unep.org/topics/ocean-seas-and-coasts/regional-seas-programme/coastal-zone-management

United Nations. (n.d.). Coastal Zone Management. United Nations Environment Program. https://www.unep.org/topics/ocean-seas-and-coasts/regional-seas-programme/coastal-zone-management

US Department of Commerce, N. O. and A. A. (2019, October 31). What percentage of the American population lives near the coast?. NOAA’s National Ocean Service. https://oceanservice.noaa.gov/facts/population.html

US Department of Commerce, N. O. and A. A. (2019, October 31). What percentage of the American population lives near the coast?. NOAA’s National Ocean Service. https://oceanservice.noaa.gov/facts/population.html

van de Wal, R., Melet, A., Bellafiore, D., Camus, P., Ferrarin, C., Oude Essink, G., Haigh, I. D., Lionello, P., Luijendijk, A., Toimil, A., Staneva, J., and Vousdoukas, M.: Sea Level Rise in Europe: Impacts and consequences, in: Sea Level Rise in Europe: 1st Assessment Report of the Knowledge Hub on Sea Level Rise (SLRE1), edited by: van den Hurk, B., Pinardi, N., Kiefer, T., Larkin, K., Manderscheid, P., and Richter, K., Copernicus Publications, State Planet, 3-slre1, 5, https://doi.org/10.5194/sp-3-slre1-5-2024, 2024.

Vitousek, S., Barnard, P., Fletcher, C. et al. Doubling of coastal flooding frequency within decades due to sea-level rise. Sci Rep 7, 1399 (2017). https://doi.org/10.1038/s41598-017-01362-7

Vousdoukas, Michail; Mentaschi, Lorenzo; Voukouvalas, Evangelos; Verlaan, Martin; Feyen, Luc (2016): Extreme Sea level - RCP45. European Commission, Joint Research Centre (JRC) [Dataset] PID: http://data.europa.eu/89h/e9e42344-119d-479e-9bc7-57400d12a8a2

Zamrsky, D., Oude Essink, G. H., & Bierkens, M. F. (2024). Global impact of sea level rise on Coastal Fresh Groundwater Resources. Earth's Future, 12(1). https://doi.org/10.1029/2023ef003581

APPENDICES

A. Natural Conservation Zones SSP1-1.9

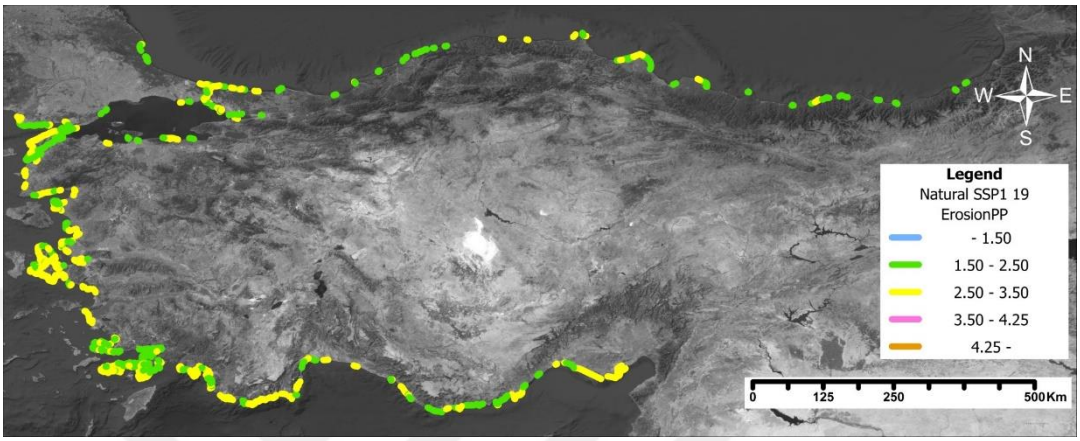


Figure 7.1. SSP1-1.9 Natural Conservation Zone ErosionPP Distribution

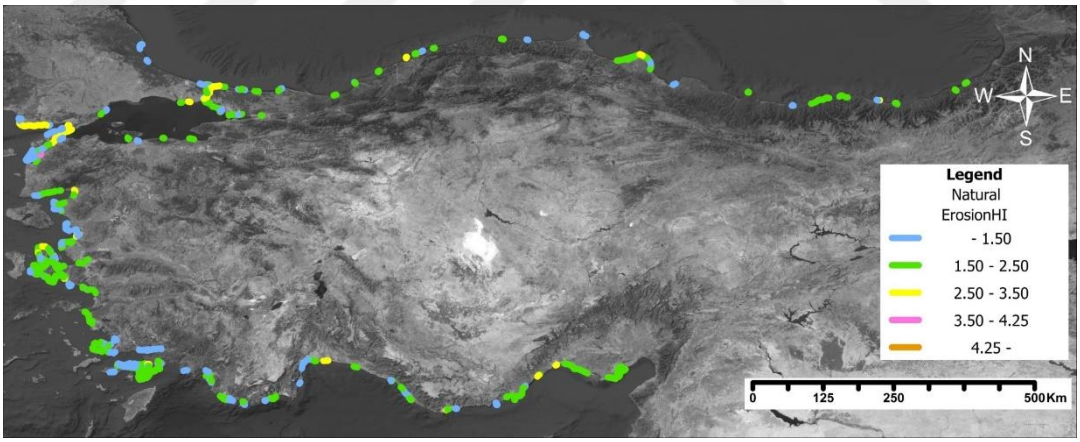


Figure 7.2. SSP1-1.9 Natural Conservation Zone ErosionHI Distribution

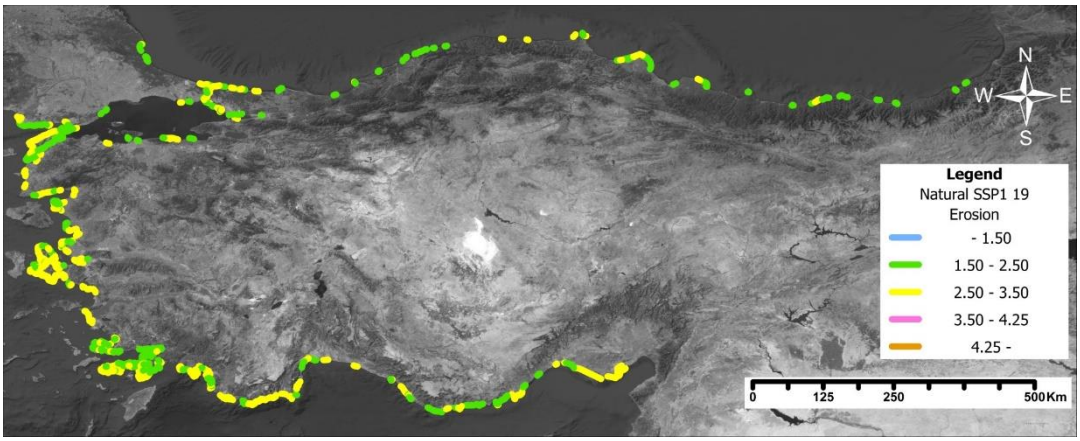


Figure 7.3. SSP1-1.9 Natural Conservation Zone Erosion Distribution

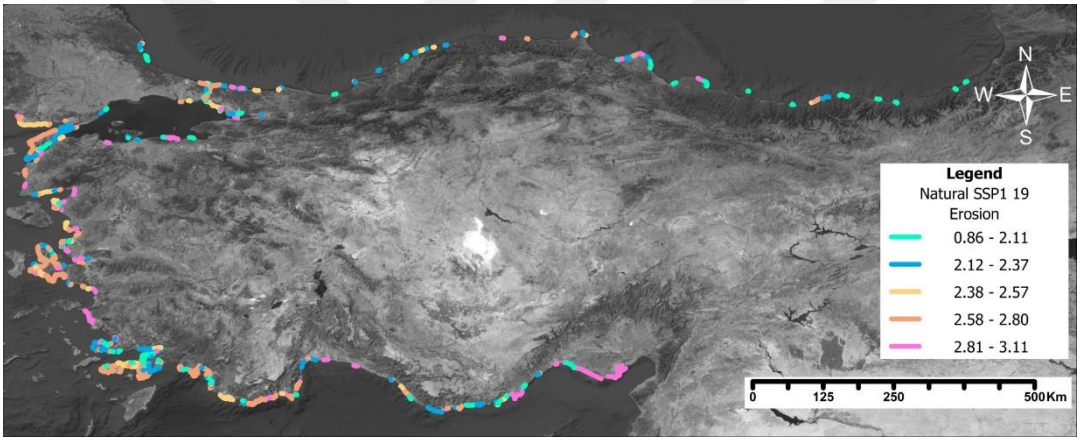


Figure 7.4. SSP1-1.9 Natural Conservation Zone Erosion Jenks Distribution

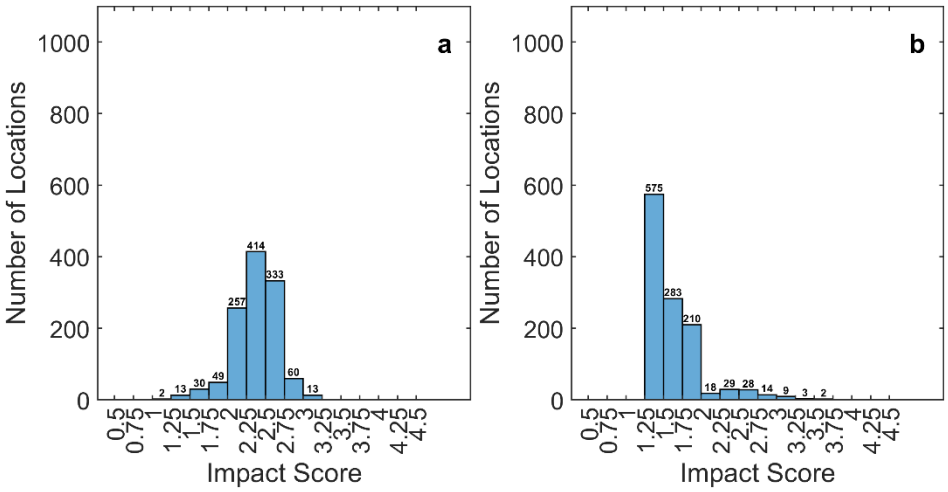


Figure 7.5. SSP1-1.9 Natural Conservation Zone Erosion (a) Physical Impact Score (b) Human Impact Score

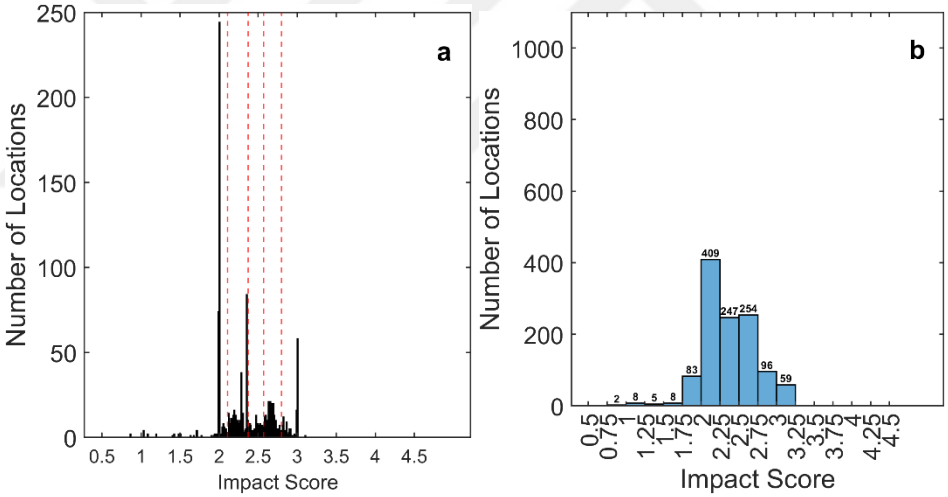


Figure 7.6. SSP1-1.9 Natural Conservation Zone Erosion (a) Jenks (b) FCVAM Histograms

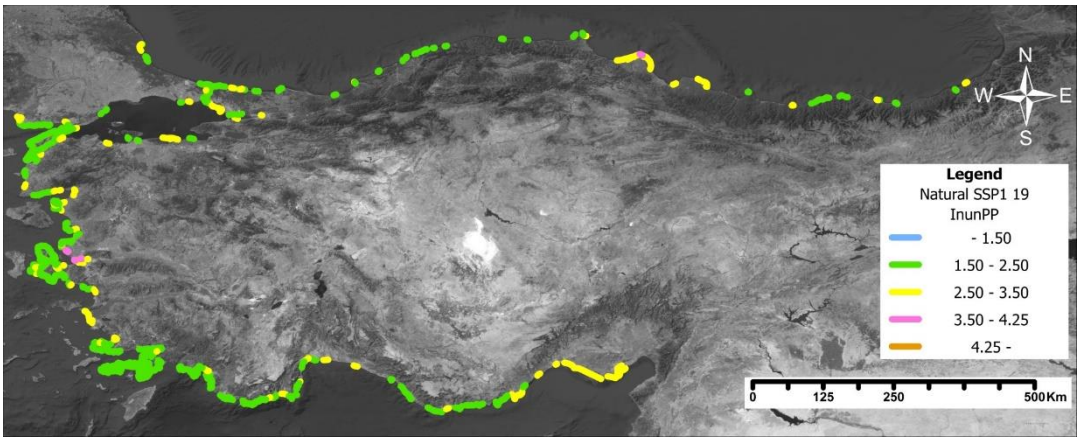


Figure 7.7. SSP1-1.9 Natural Conservation Zone InundationPP Distribution

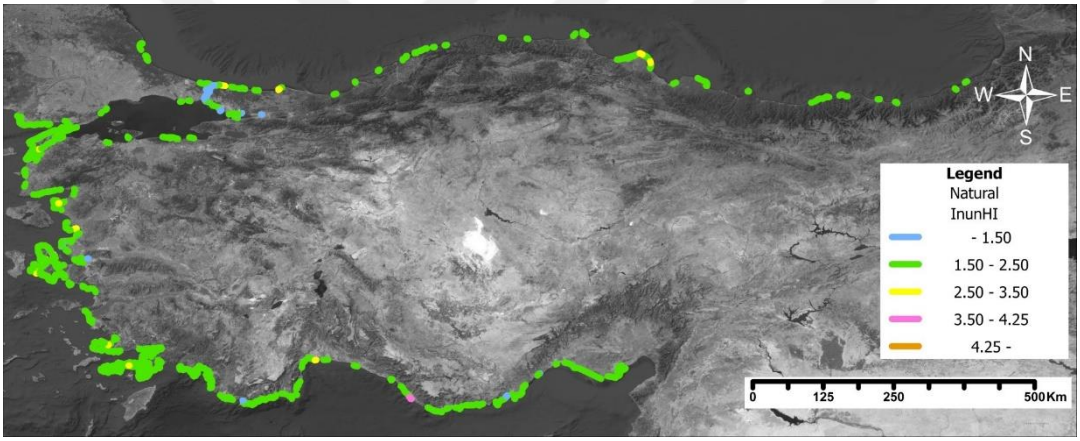


Figure 7.8. SSP1-1.9 Natural Conservation Zone InundationHI Distribution

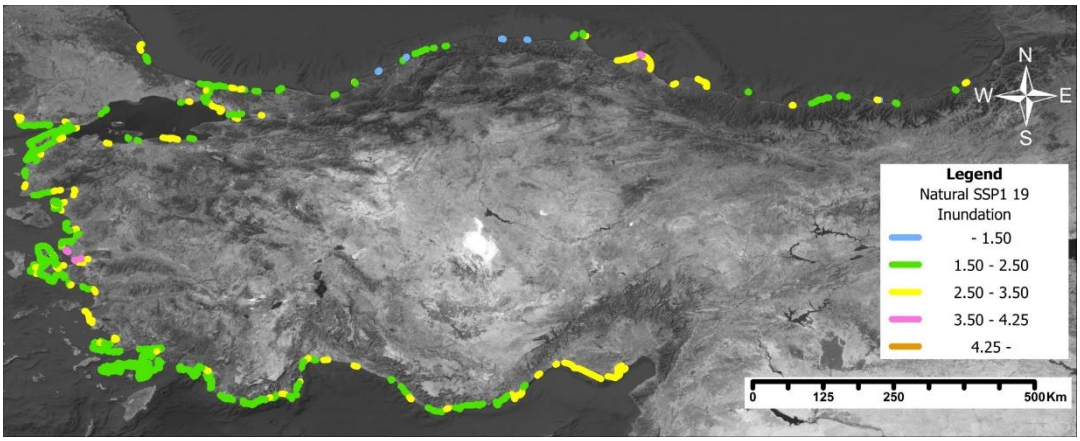


Figure 7.9. SSP1-1.9 Natural Conservation Zone Inundation Distribution

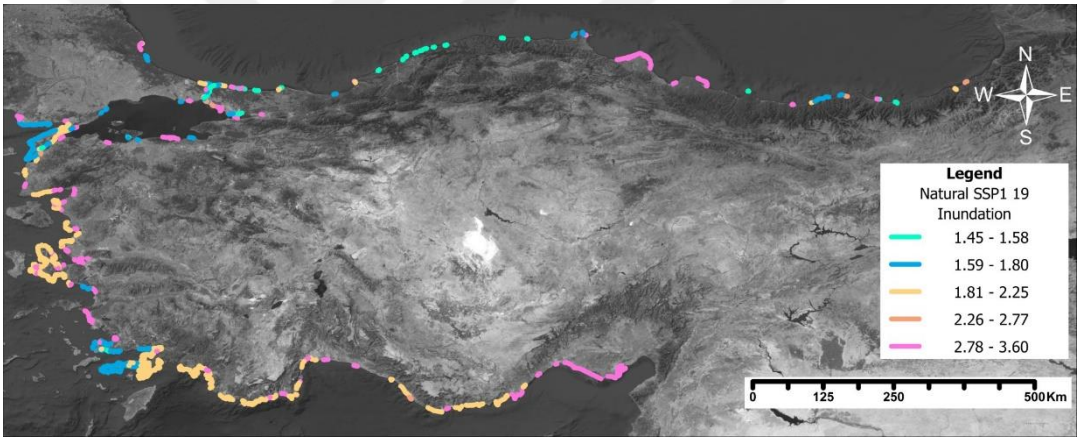


Figure 7.10. SSP1-1.9 Natural Conservation Zone Inundation Jenks Distribution

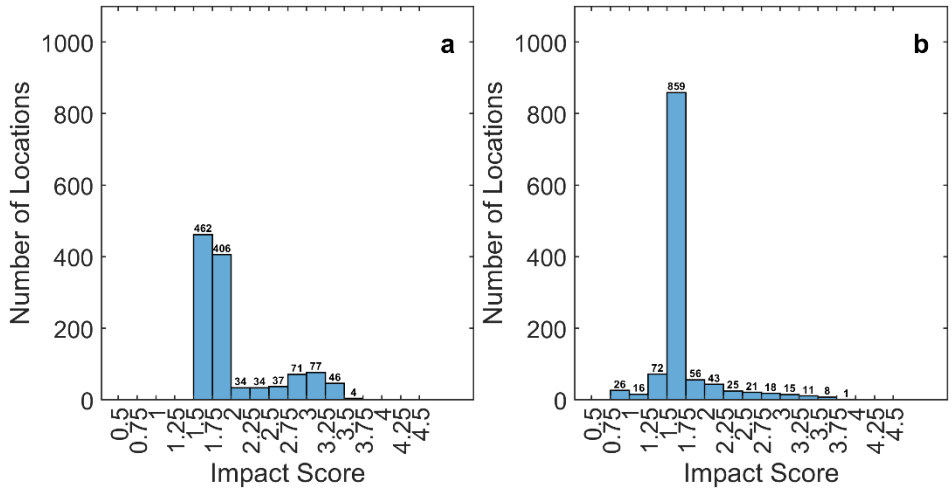


Figure 7.11. SSP1-1.9 Natural Conservation Zone Inundation (a) Physical Impact Score (b) Human Impact Score

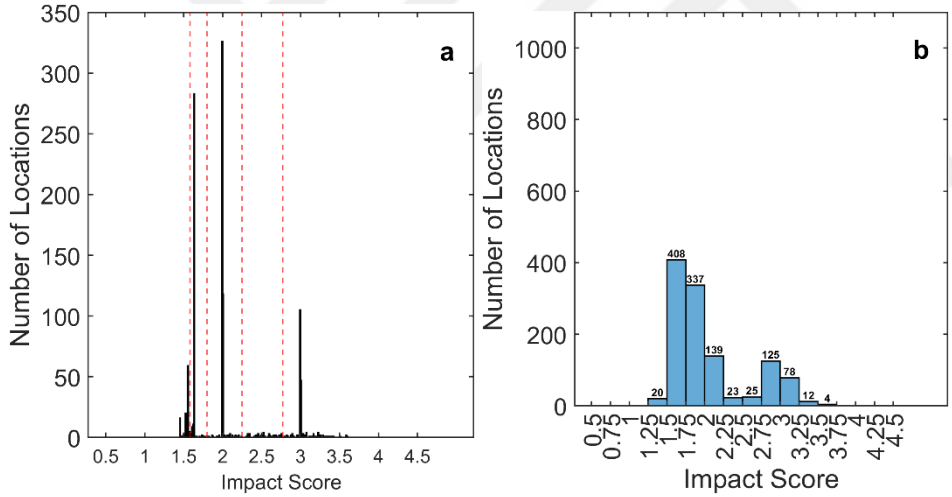


Figure 7.12. SSP1-1.9 Natural Conservation Zone Inundation (a) Jenks (b) FCVAM Histograms

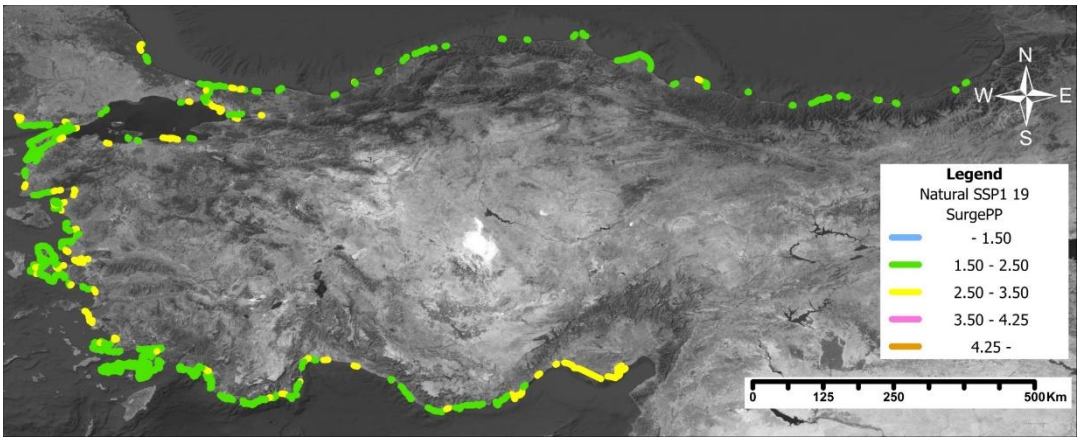


Figure 7.13. SSP1-1.9 Natural Conservation Zone Storm SurgePP Distribution

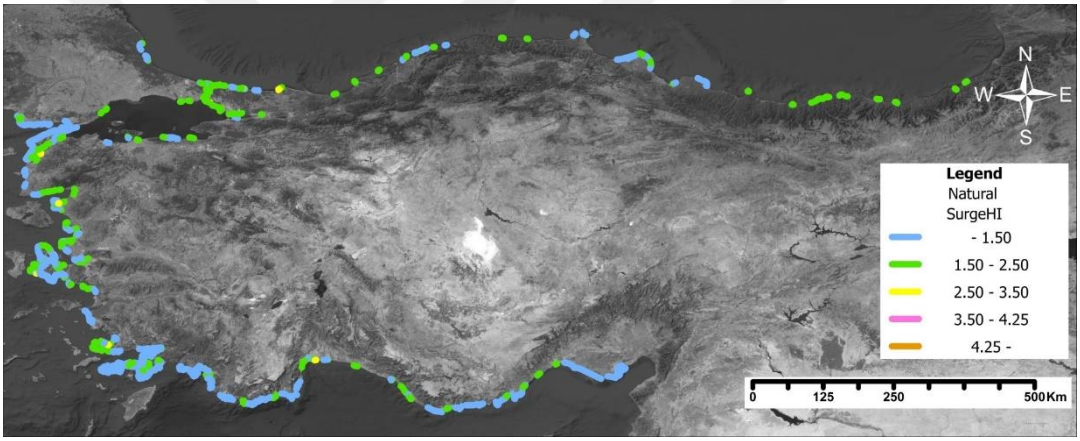


Figure 7.14. SSP1-1.9 Natural Conservation Zone Storm SurgeHI Distribution

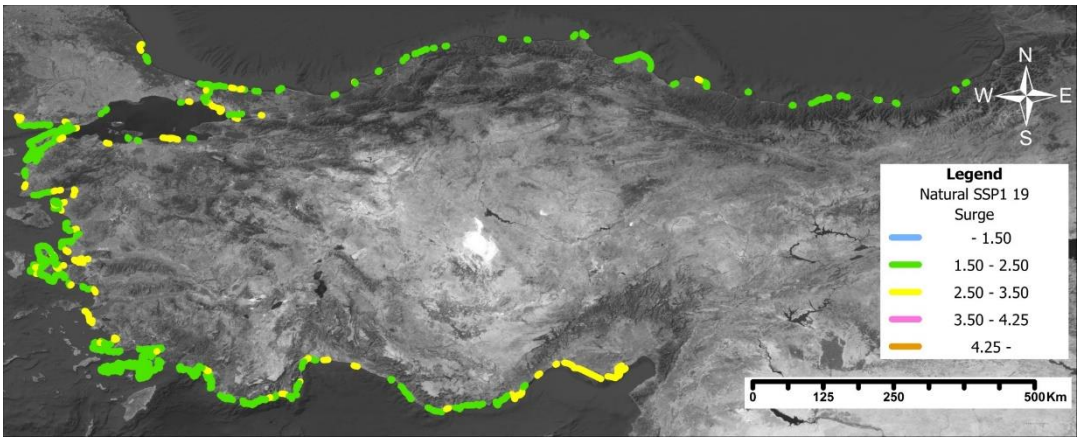


Figure 7.15. SSP1-1.9 Natural Conservation Zone Storm Surge Distribution

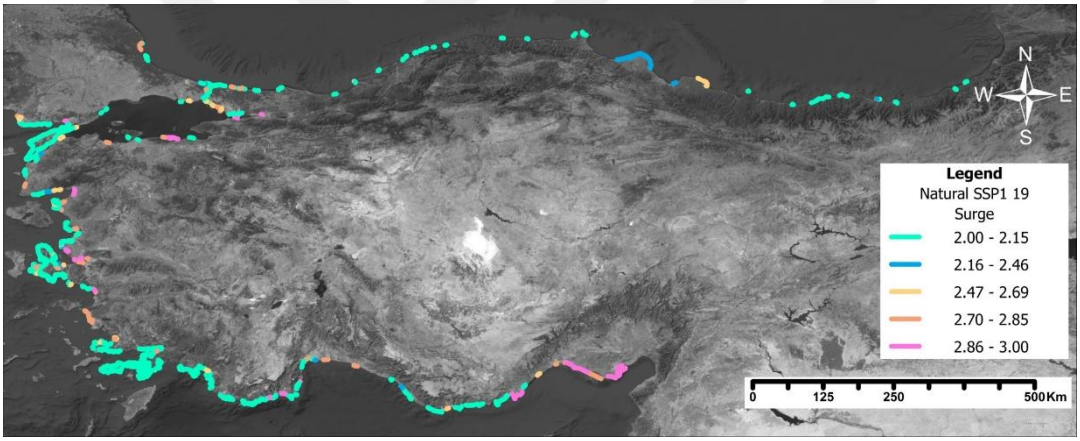


Figure 7.16. SSP1-1.9 Natural Conservation Zone Storm Surge Jenks Distribution

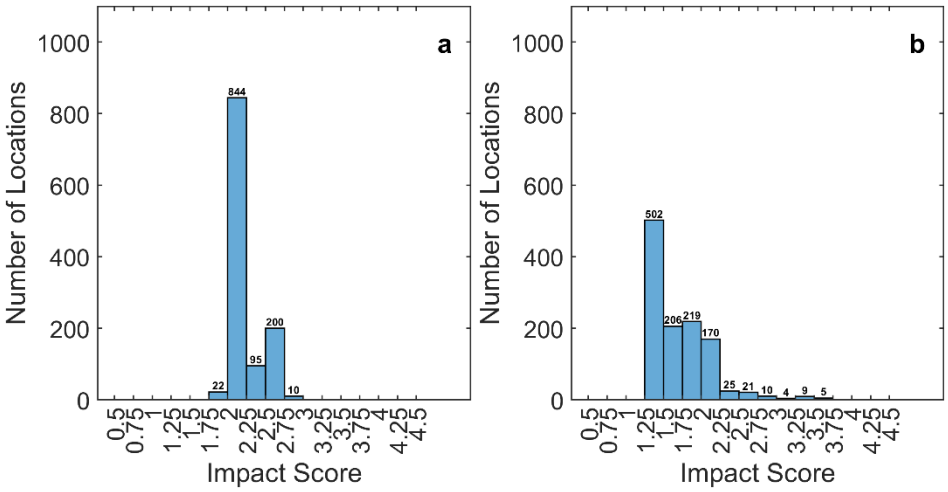


Figure 7.17. SSP1-1.9 Natural Conservation Zone Storm Surge (a) Physical Impact Score (b) Human Impact Score

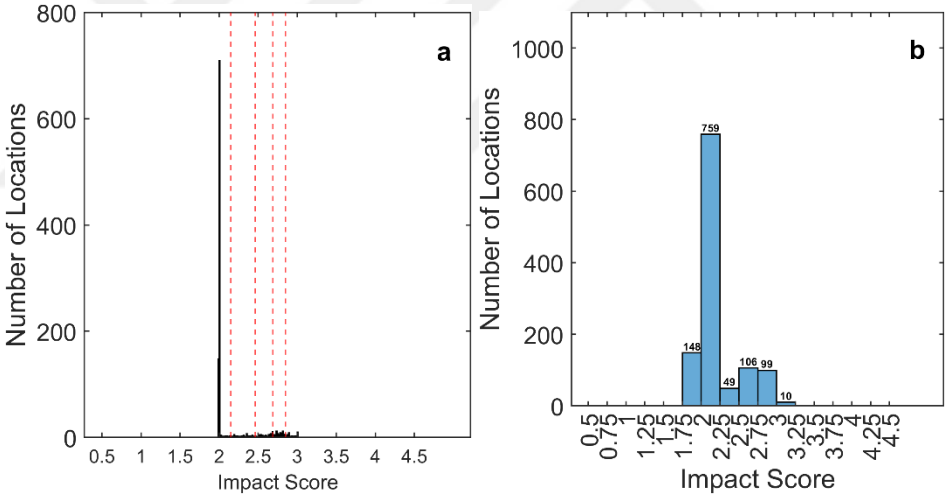


Figure 7.18. SSP1-1.9 Natural Conservation Zone Storm Surge (a) Jenks (b) FCVAM Histograms

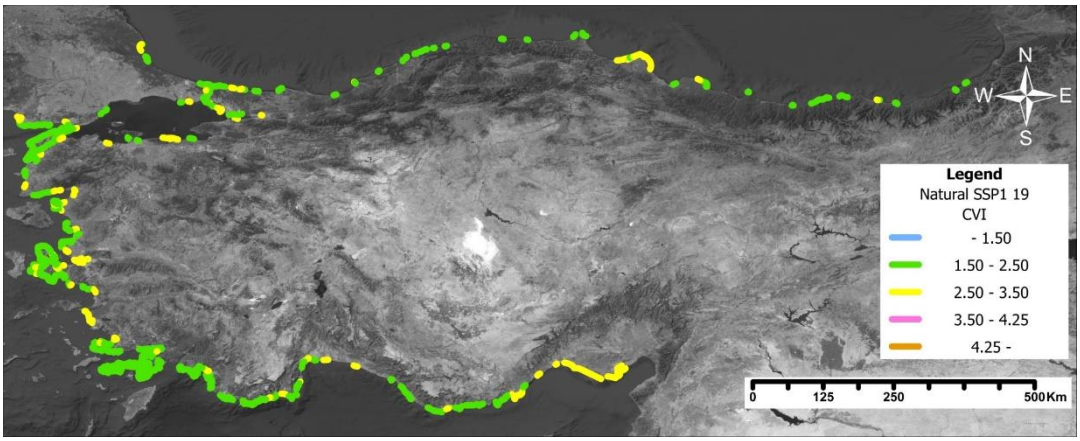


Figure 7.19. SSP1-1.9 Natural Conservation Zone CVI Distribution

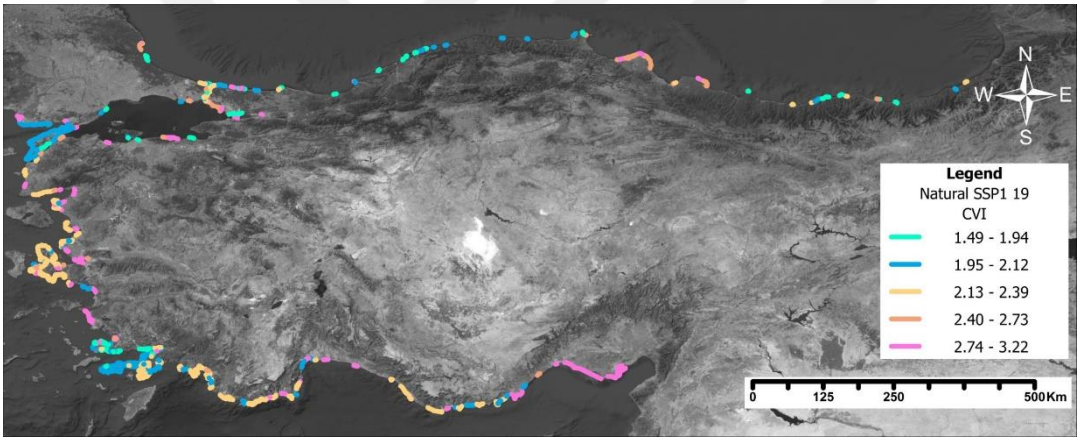


Figure 7.20. SSP1-1.9 Natural Conservation Zone CVI Jenks Distribution

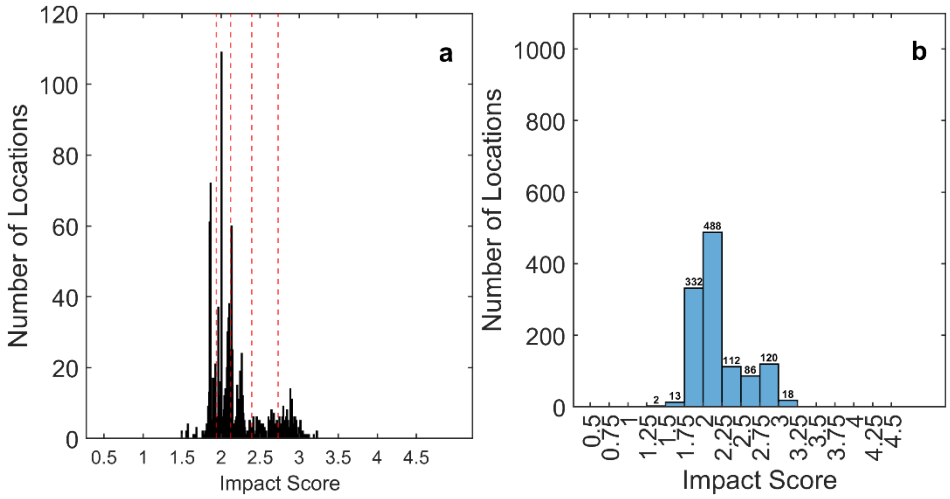


Figure 7.21. SSP1-1.9 Natural Conservation Zone CVI (a) Jenks (b) FCVAM Histograms

Table 7.1 SSP1-1.9 Natural Conservation Zone Impact & CVI Scores

NAT SSP1-19	Erosion			Inundation			Storm Surge			CVI
	PP	HI	Vul	PP	HI	Vul	PP	HI	Vul	
< 1.5 Very Low	16	586	15	0	114	20	0	509	0	2
1.5 – 2.5 Low	746	531	744	933	983	904	959	613	954	942
2.5 – 3.5 Moderate	409	52	412	235	65	244	212	44	217	227
3.5 – 4.25 High	0	2	0	3	9	3	0	5	0	0
4.25 > Very High	0	0	0	0	0	0	0	0	0	0

B. Natural Conservation Zones SSP1-2.6

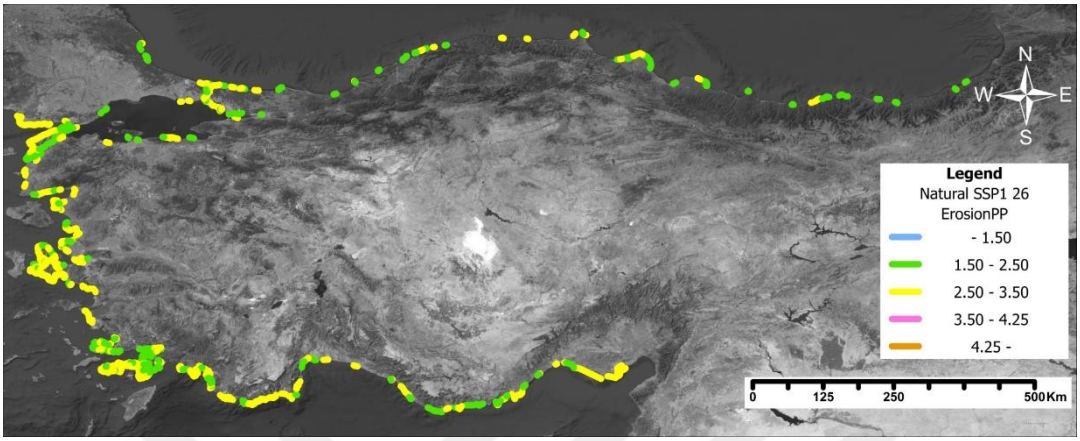


Figure 7.22. SSP1-2.6 Natural Conservation Zone ErosionPP Distribution

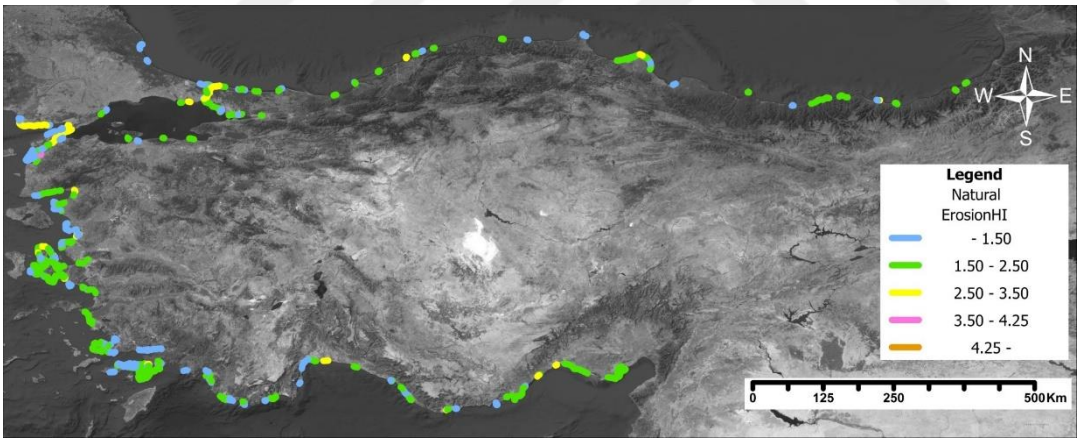


Figure 7.23. SSP1-2.6 Natural Conservation Zone ErosionHI Distribution

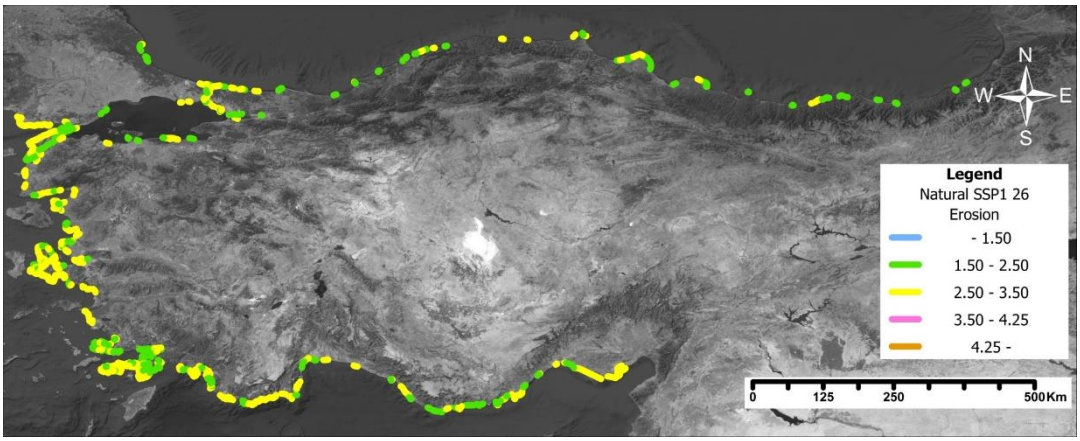


Figure 7.24. SSP1-2.6 Natural Conservation Zone Erosion Distribution

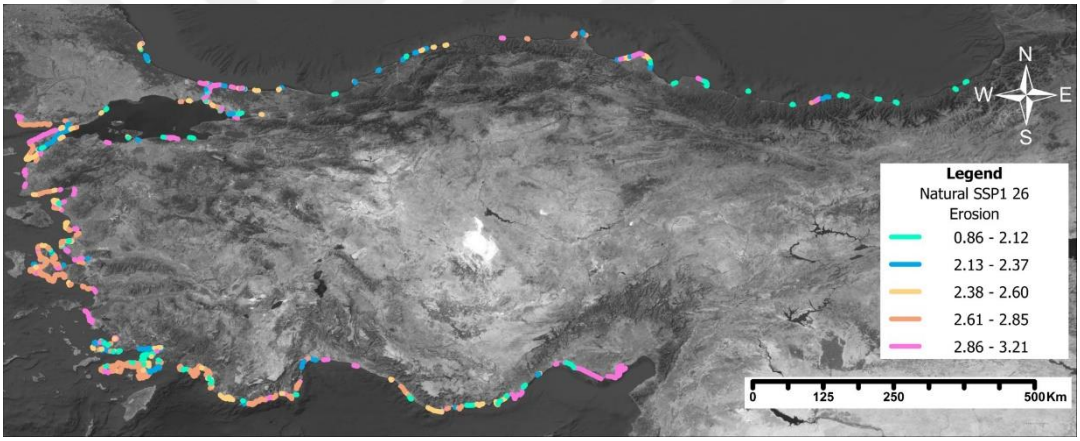


Figure 7.25. SSP1-2.6 Natural Conservation Zone Erosion Jenks Distribution

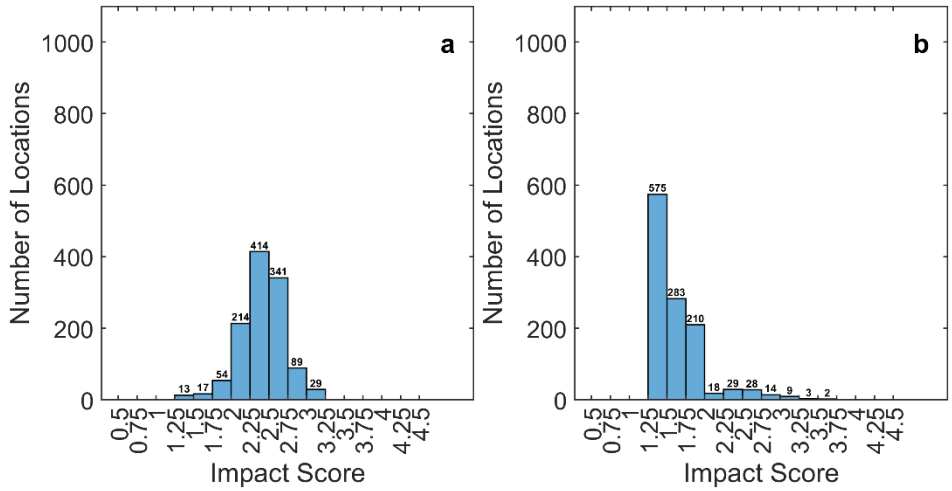


Figure 7.26. SSP1-2.6 Natural Conservation Zone Erosion (a) Physical Impact Score (b) Human Impact Score

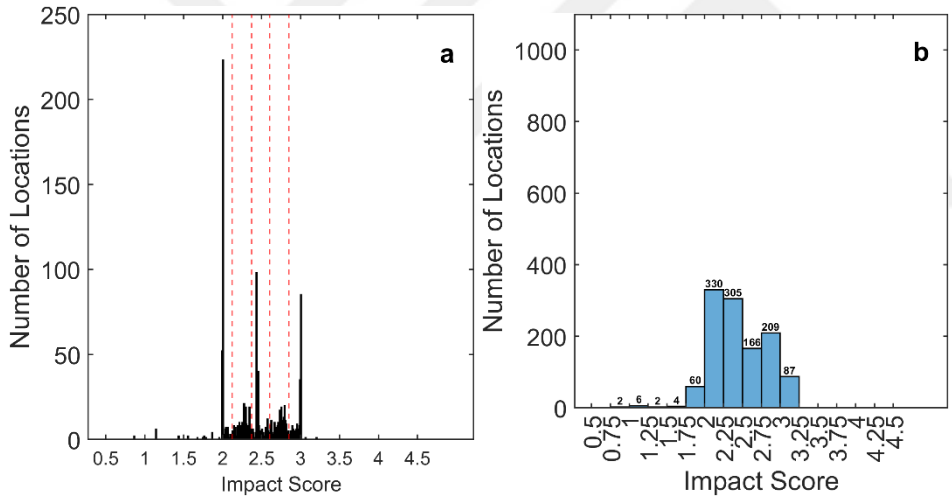


Figure 7.27. SSP1-2.6 Natural Conservation Zone Erosion (a) Jenks (b) FCVAM Histograms

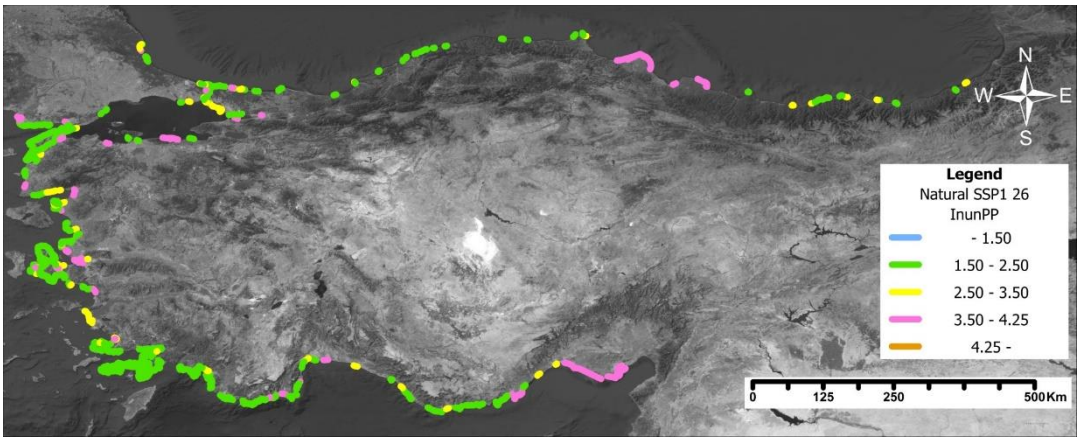


Figure 7.28. SSP1-2.6 Natural Conservation Zone InundationPP Distribution

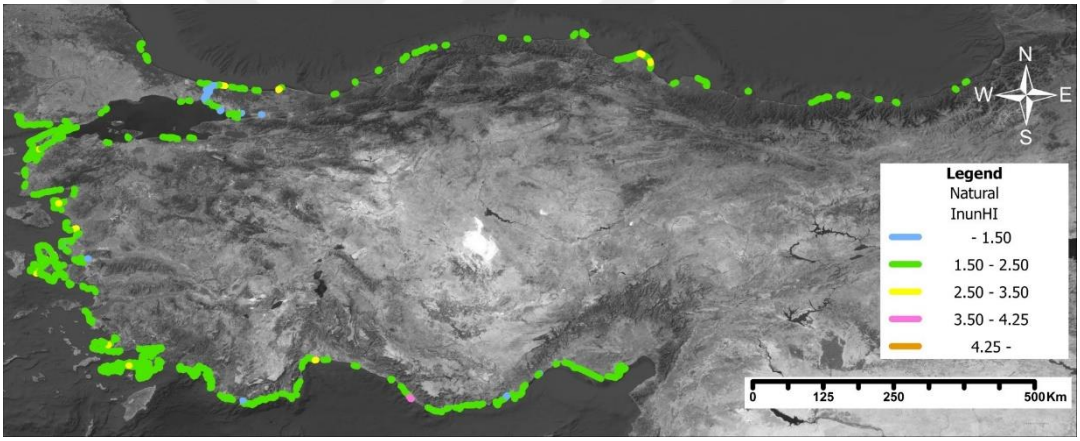


Figure 7.29. SSP1-2.6 Natural Conservation Zone InundationHI Distribution

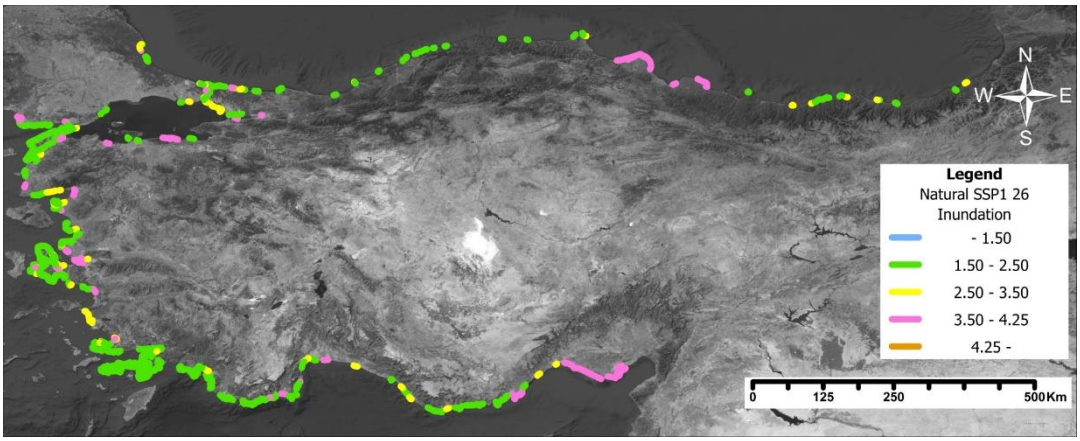


Figure 7.30. SSP1-2.6 Natural Conservation Zone Inundation Distribution

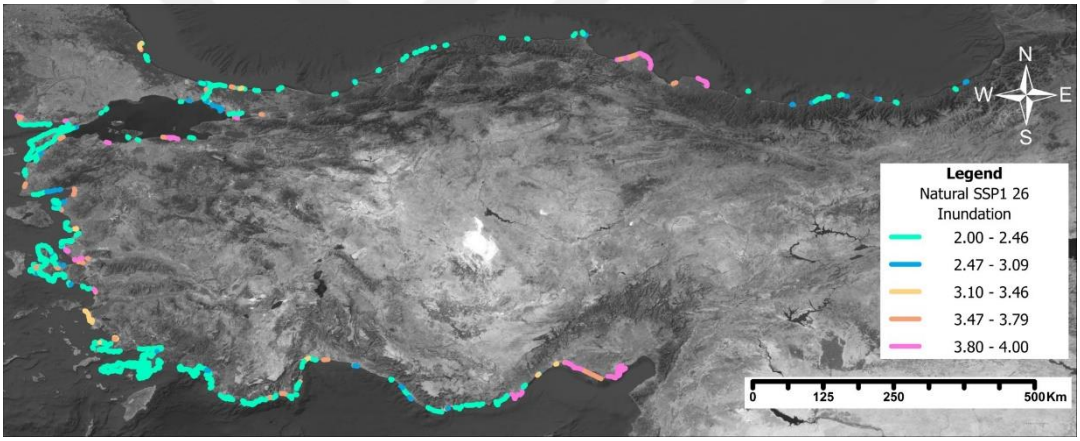


Figure 7.31. SSP1-2.6 Natural Conservation Zone Inundation Jenks Distribution

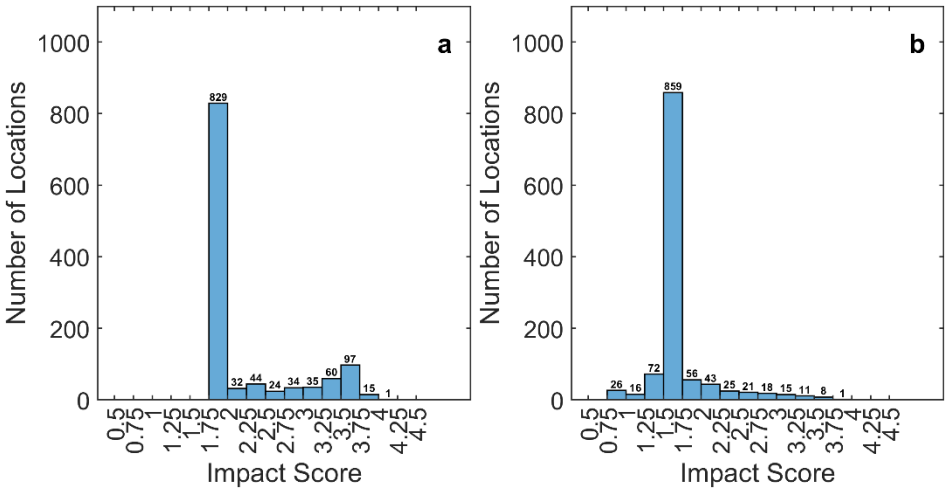


Figure 7.32. SSP1-2.6 Natural Conservation Zone Inundation (a) Physical Impact Score (b) Human Impact Score

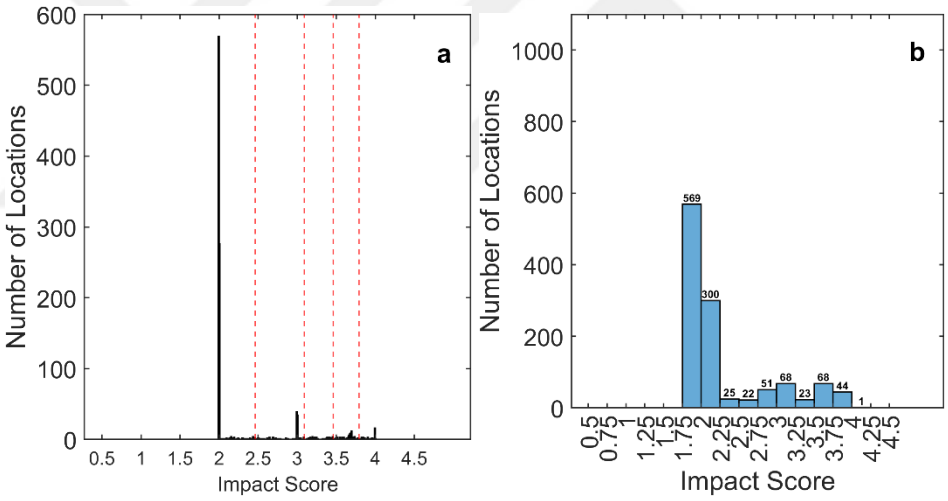


Figure 7.33. SSP1-2.6 Natural Conservation Zone Inundation (a) Jenks (b) FCVAM Histograms

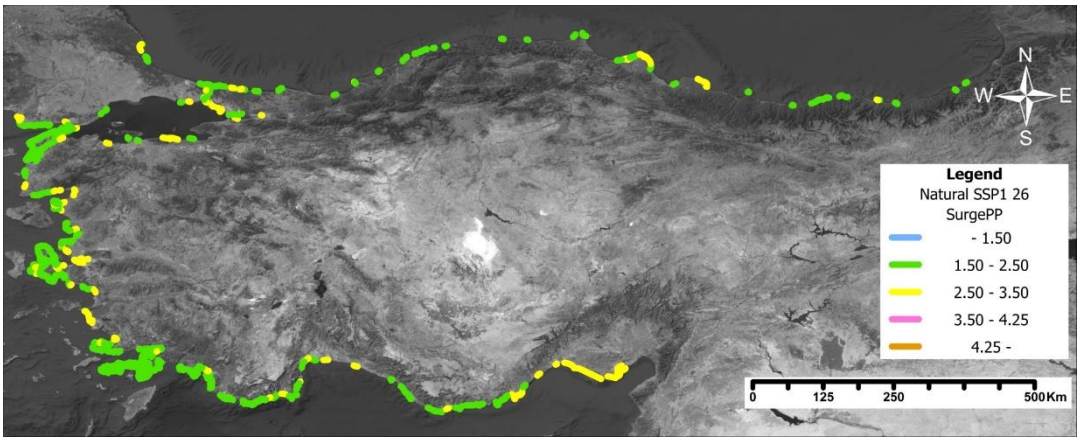


Figure 7.34. SSP1-2.6 Natural Conservation Zone Storm SurgePP Distribution

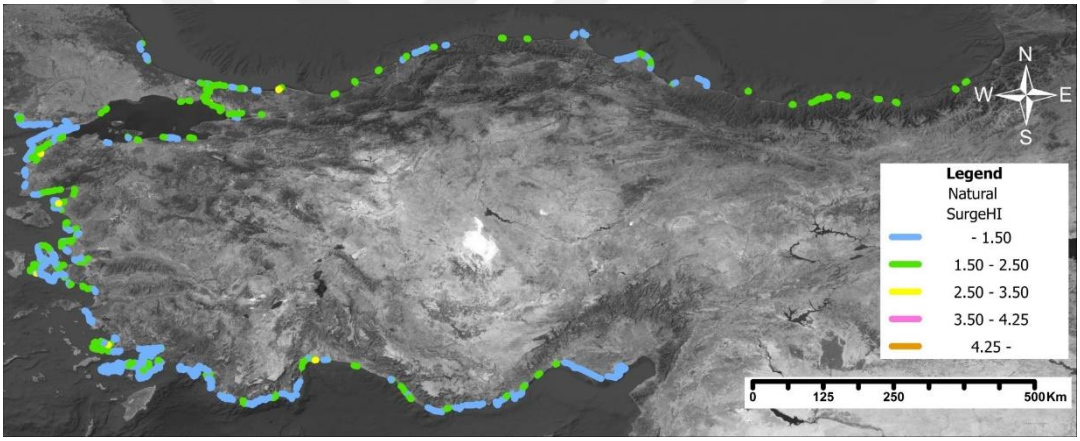


Figure 7.35. SSP1-2.6 Natural Conservation Zone Storm SurgeHI Distribution

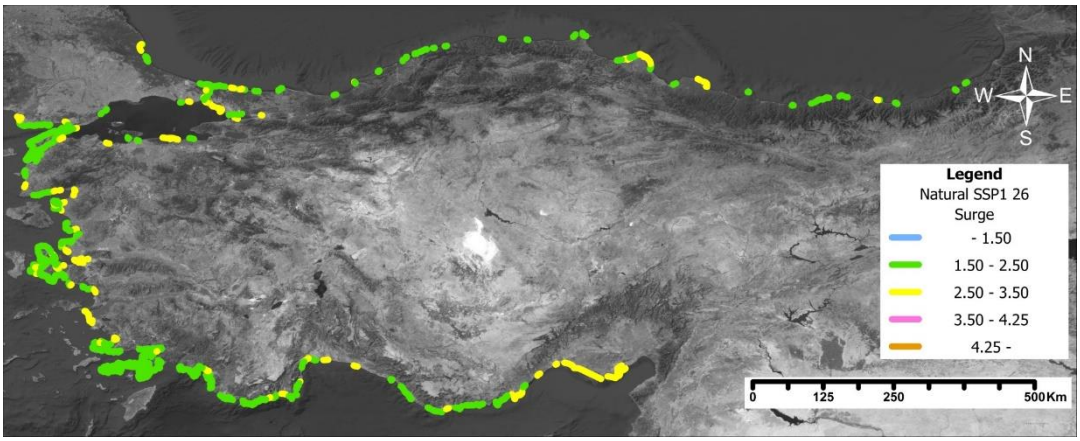


Figure 7.36. SSP1-2.6 Natural Conservation Zone Storm Surge Distribution

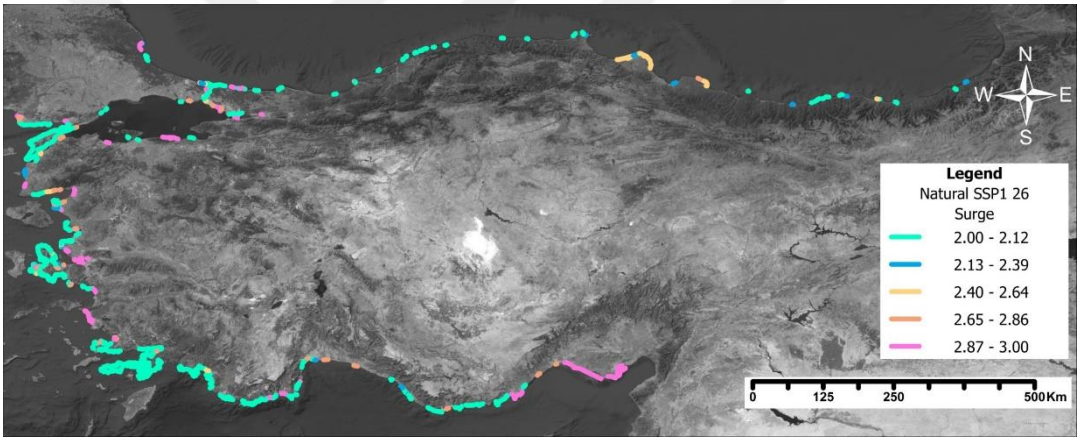


Figure 7.37. SSP1-2.6 Natural Conservation Zone Storm Surge Jenks Distribution

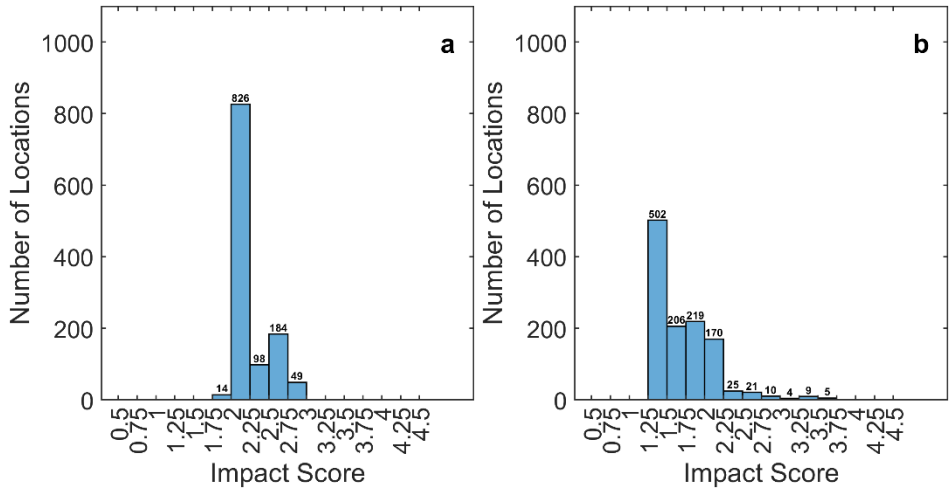


Figure 7.38. SSP1-2.6 Natural Conservation Zone Storm Surge (a) Physical Impact Score (b) Human Impact Score

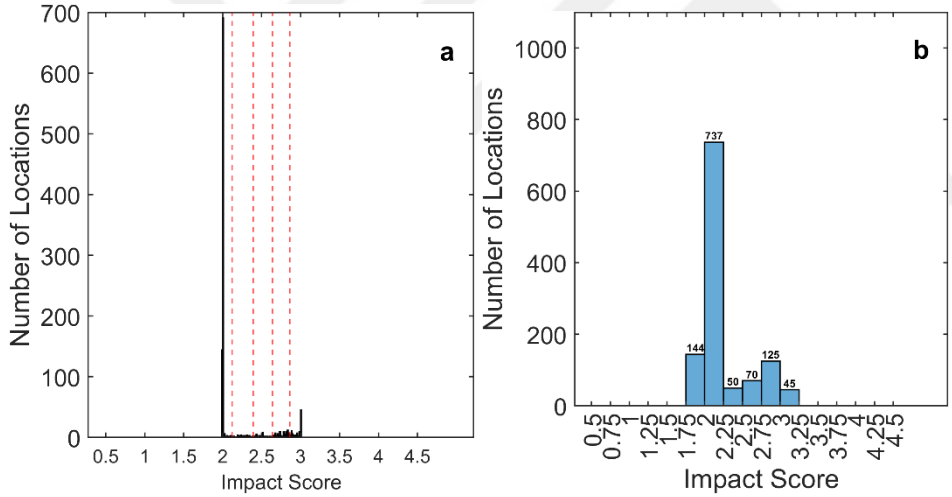


Figure 7.39. SSP1-2.6 Natural Conservation Zone Storm Surge (a) Jenks (b) FCVAM Histograms

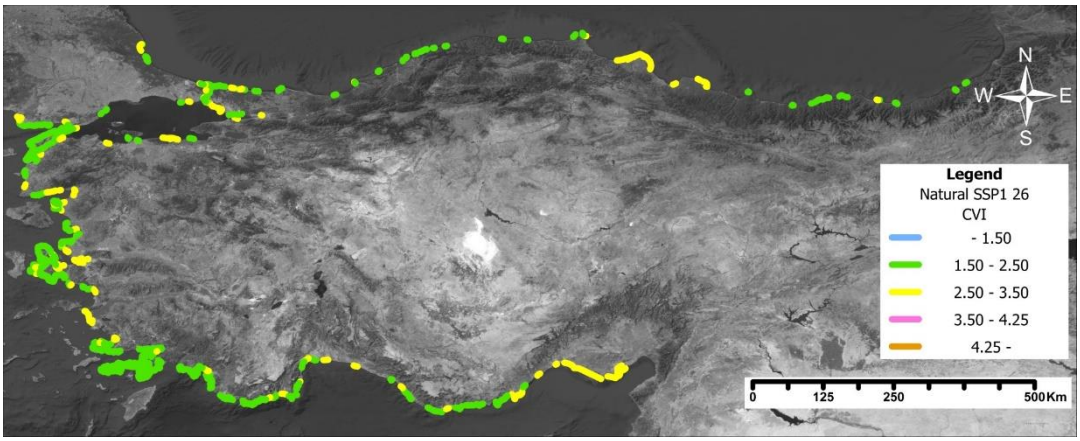


Figure 7.40. SSP1-2.6 Natural Conservation Zone CVI Distribution

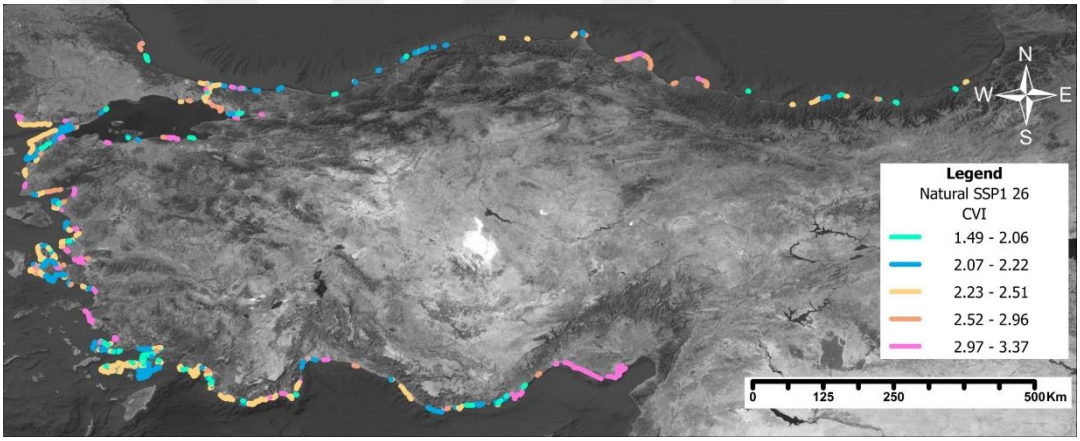


Figure 7.41. SSP1-2.6 Natural Conservation Zone CVI Jenks Distribution

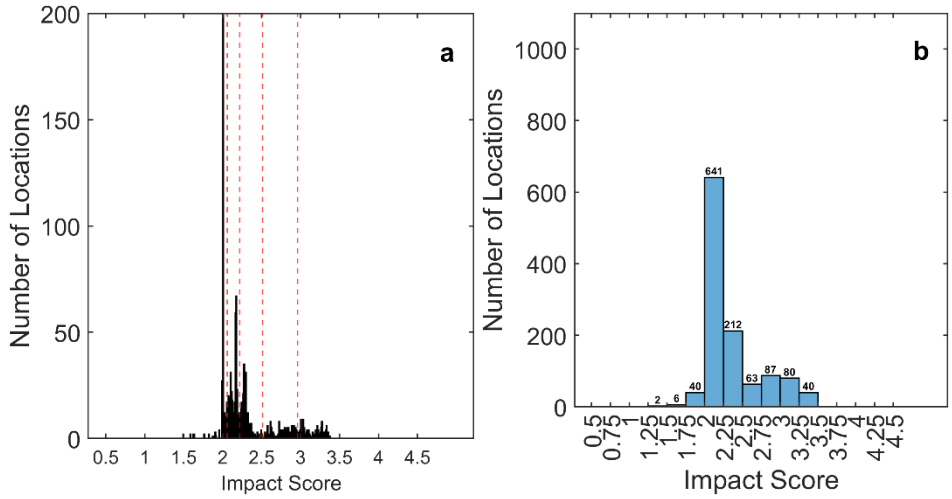


Figure 7.42. SSP1-2.6 Natural Conservation Zone CVI (a) Jenks (b) FCVAM Histograms

Table 7.2 SSP1-2.6 Natural Conservation Zone Impact & CVI Scores

NAT SSP1-26	Erosion			Inundation			Storm Surge			CVI
	PP	HI	Vul	PP	HI	Vul	PP	HI	Vul	
< 1.5 Very Low	14	586	10	0	114	0	0	509	0	2
1.5 – 2.5 Low	696	531	697	903	983	892	934	613	927	898
2.5 – 3.5 Moderate	461	52	464	152	65	163	237	44	244	271
3.5 – 4.25 High	0	2	0	116	9	116	0	5	0	0
4.25 > Very High	0	0	0	0	0	0	0	0	0	0

C. Natural Conservation Zones SSP3-7.0

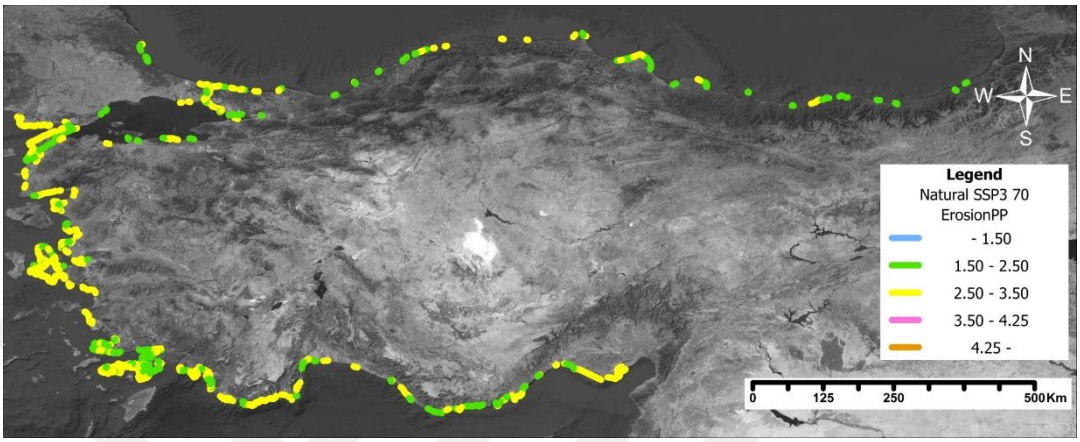


Figure 7.43. SSP3-7.0 Natural Conservation Zone ErosionPP Distribution

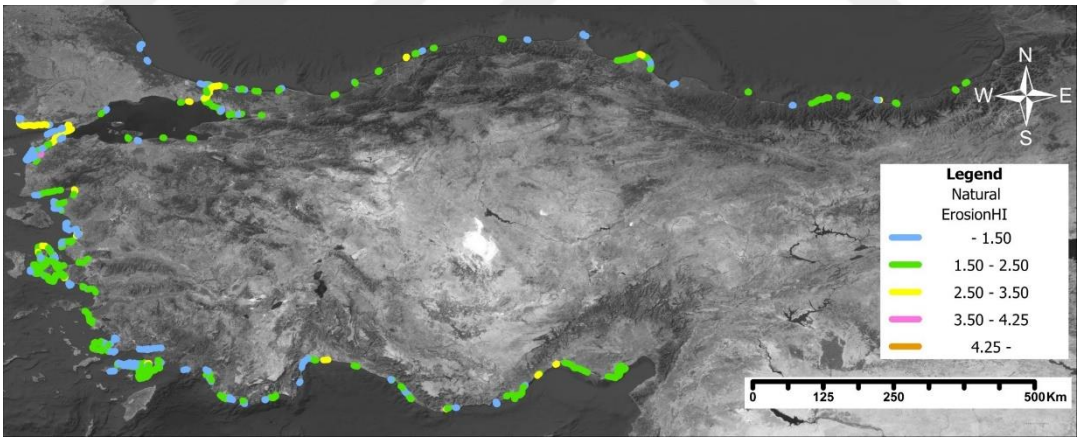


Figure 7.44. SSP3-7.0 Natural Conservation Zone ErosionHI Distribution

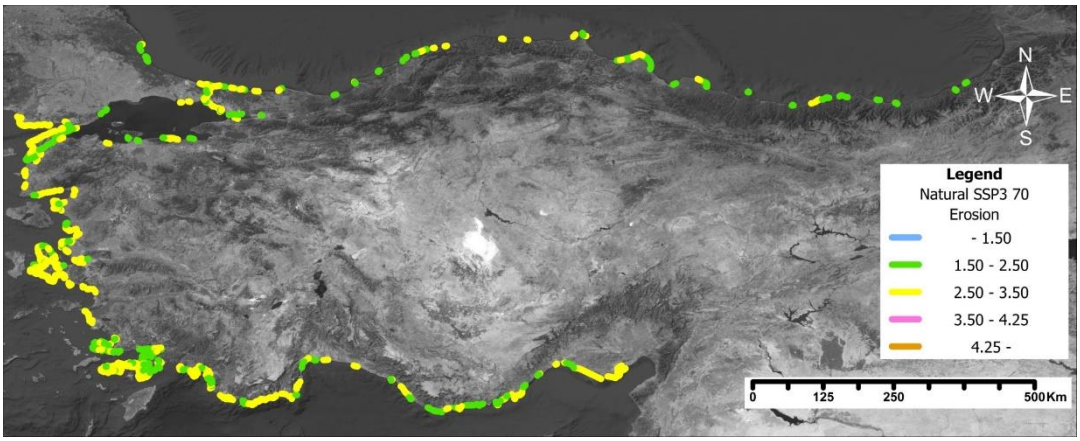


Figure 7.45. SSP3-7.0 Natural Conservation Zone Erosion Distribution

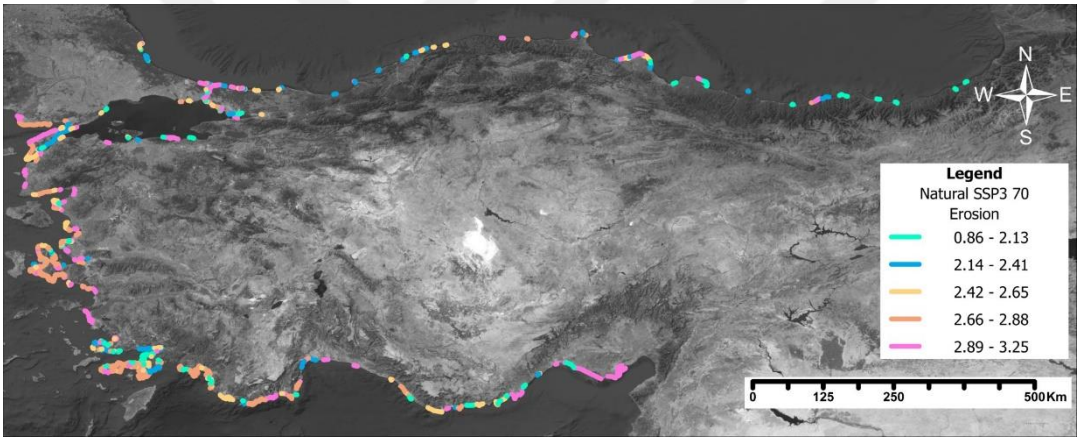


Figure 7.46. SSP3-7.0 Natural Conservation Zone Erosion Jenks Distribution

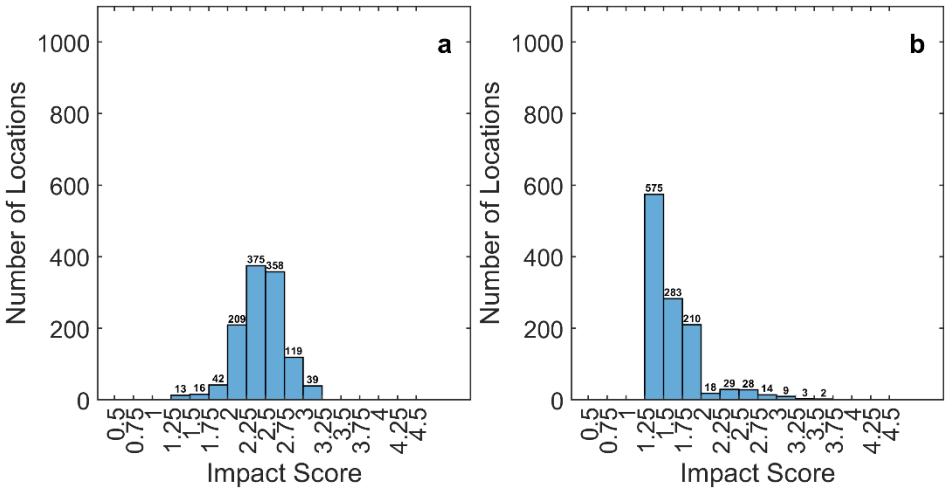


Figure 7.47. SSP3-7.0 Natural Conservation Zone Erosion (a) Physical Impact Score (b) Human Impact Score

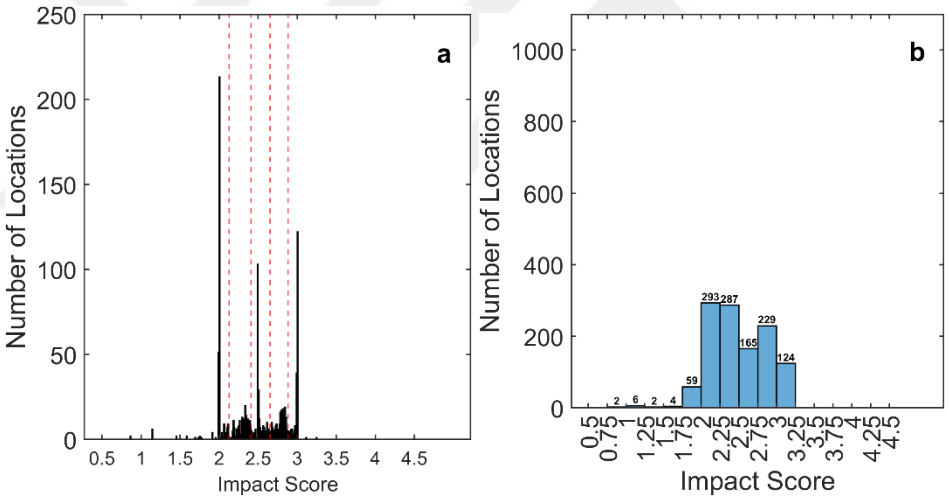


Figure 7.48. SSP3-7.0 Natural Conservation Zone Erosion (a) Jenks (b) FCVAM Histograms

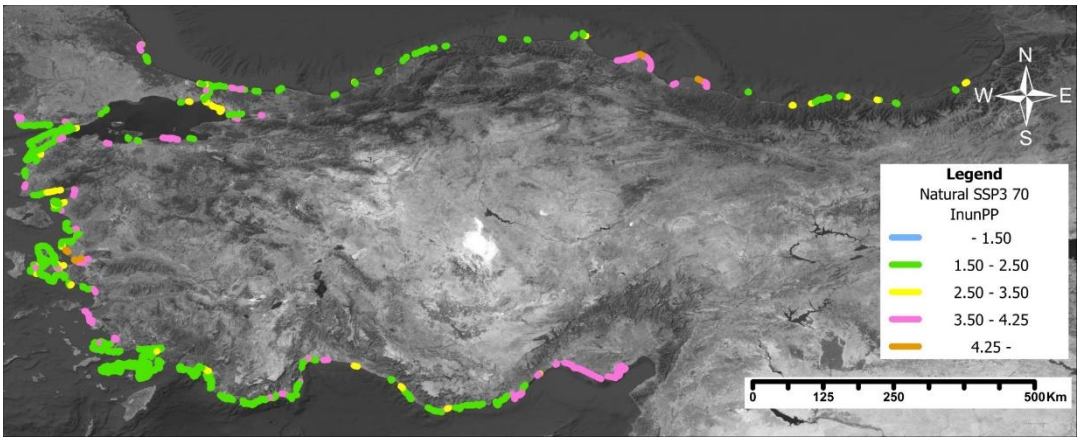


Figure 7.49. SSP3-7.0 Natural Conservation Zone InundationPP Distribution

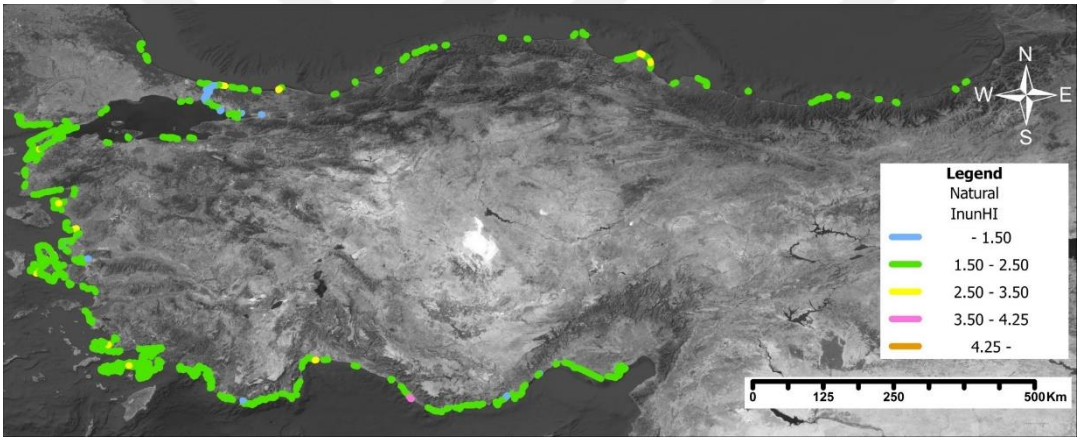


Figure 7.50. SSP3-7.0 Natural Conservation Zone InundationHI Distribution

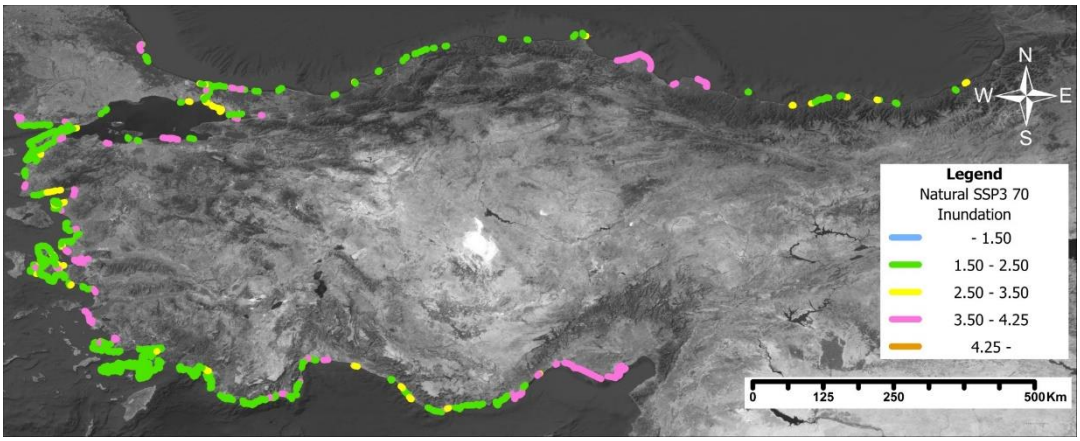


Figure 7.51. SSP3-7.0 Natural Conservation Zone Inundation Distribution

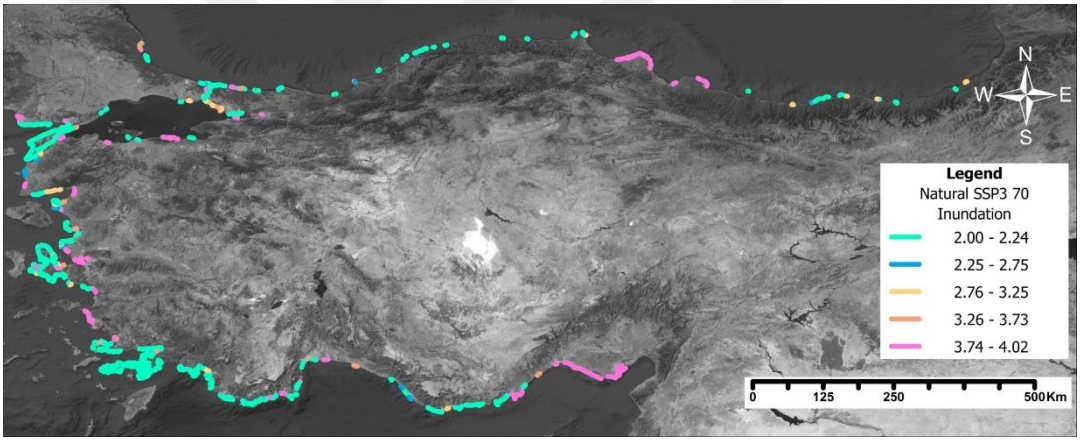


Figure 7.52. SSP3-7.0 Natural Conservation Zone Inundation Jenks Distribution

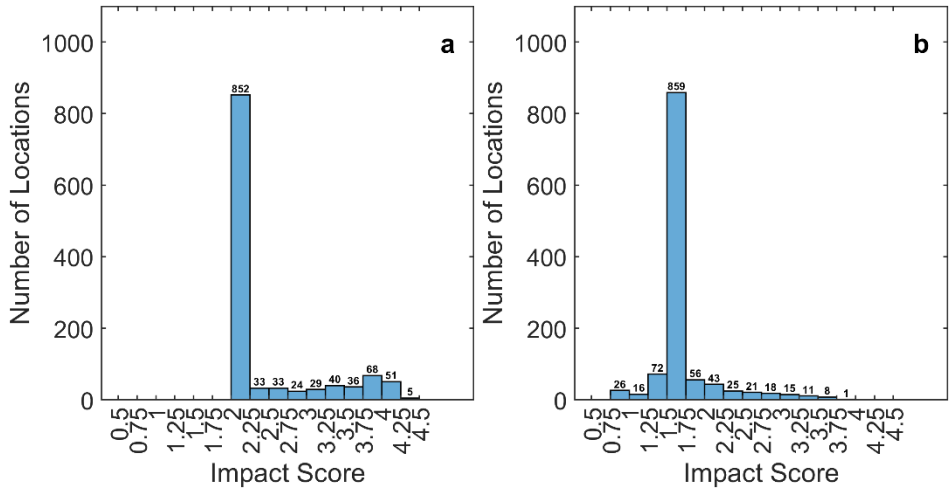


Figure 7.53. SSP3-7.0 Natural Conservation Zone Inundation (a) Physical Impact Score (b) Human Impact Score

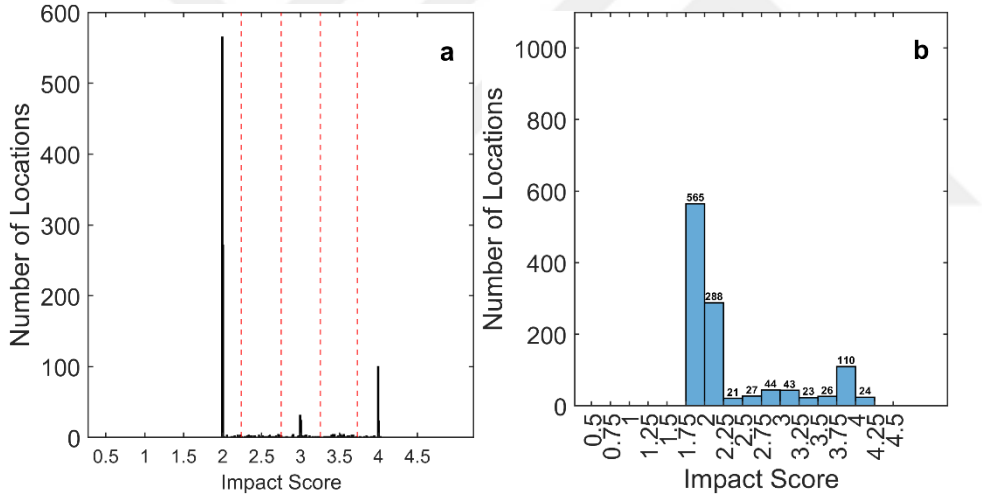


Figure 7.54. SSP3-7.0 Natural Conservation Zone Inundation (a) Jenks (b) FCVAM Histograms

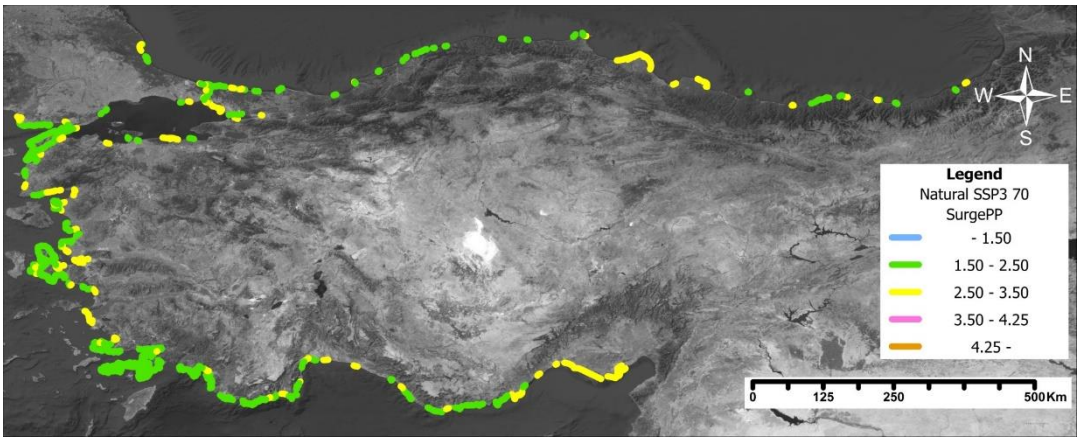


Figure 7.55. SSP3-7.0 Natural Conservation Zone Storm SurgePP Distribution

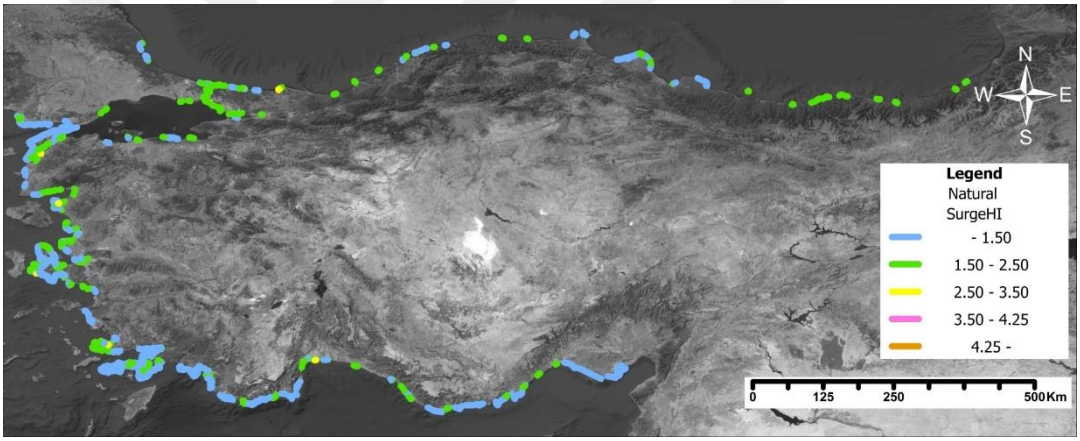


Figure 7.56. SSP3-7.0 Natural Conservation Zone Storm SurgeHI Distribution

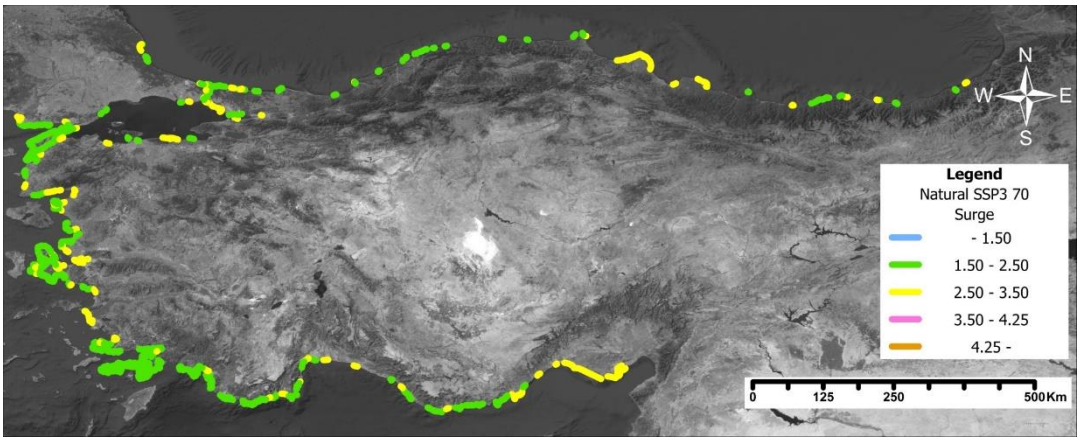


Figure 7.57. SSP3-7.0 Natural Conservation Zone Storm Surge Distribution

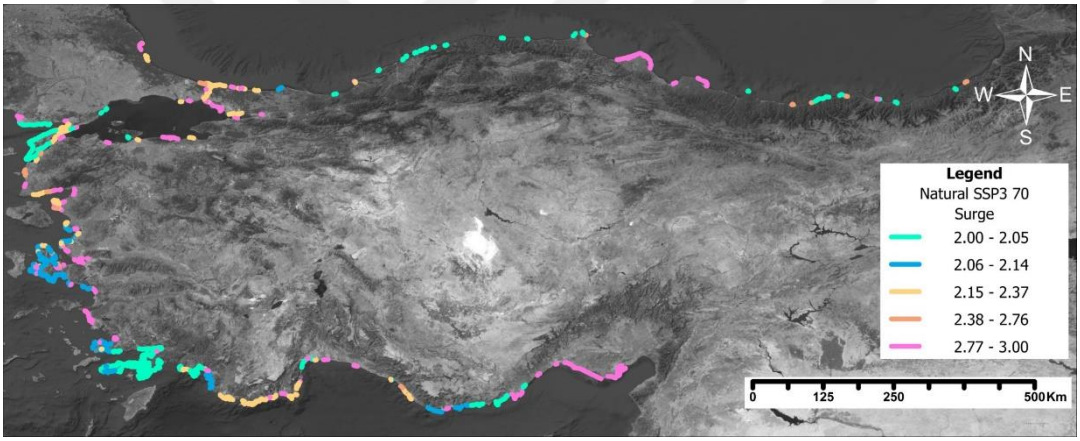


Figure 7.58. SSP3-7.0 Natural Conservation Zone Storm Surge Jenks Distribution

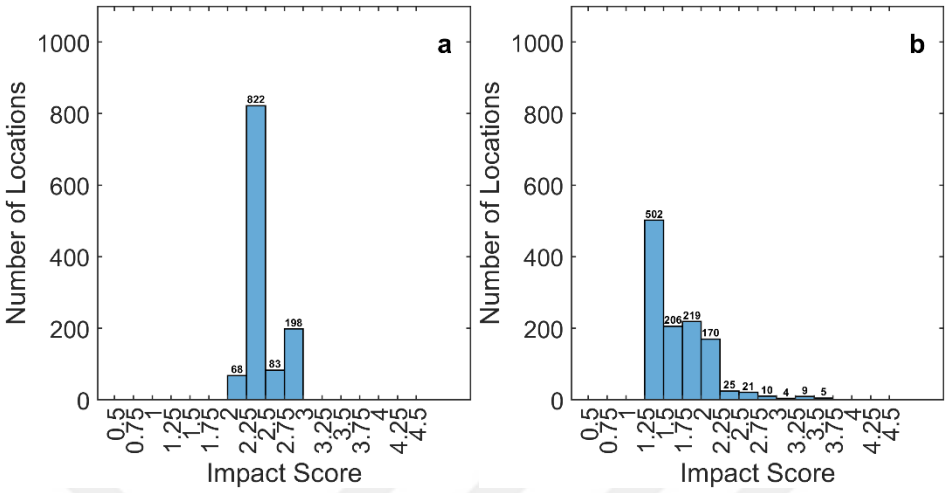


Figure 7.59. SSP3-7.0 Natural Conservation Zone Storm Surge (a) Physical Impact Score (b) Human Impact Score

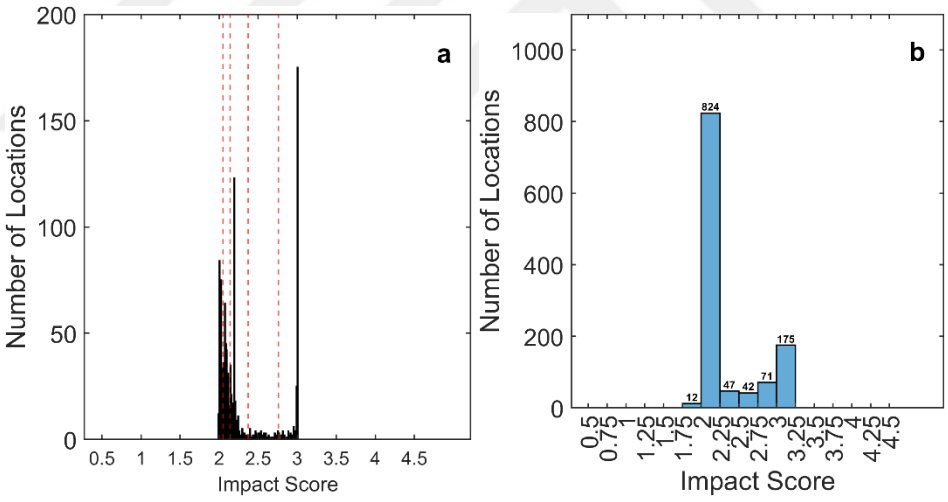


Figure 7.60. SSP3-7.0 Natural Conservation Zone Storm Surge (a) Jenks (b) FCVAM Histograms

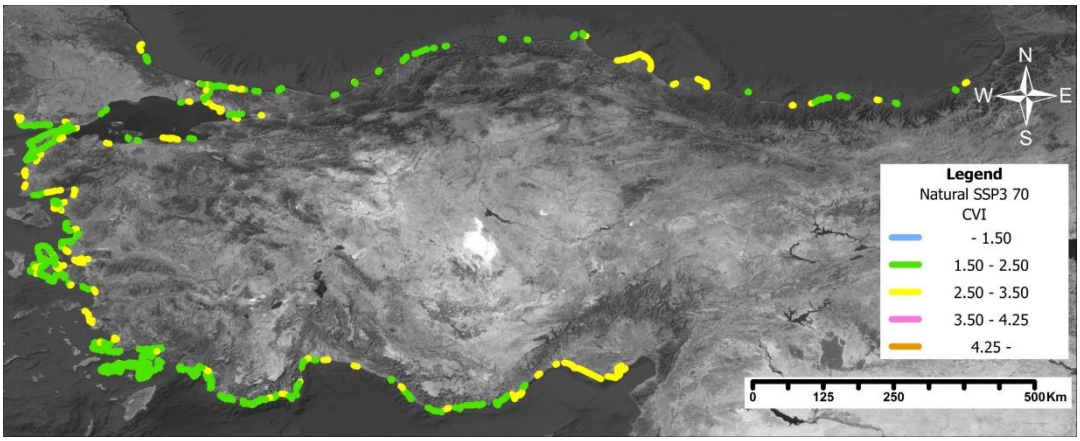


Figure 7.61. SSP3-7.0 Natural Conservation Zone CVI Distribution

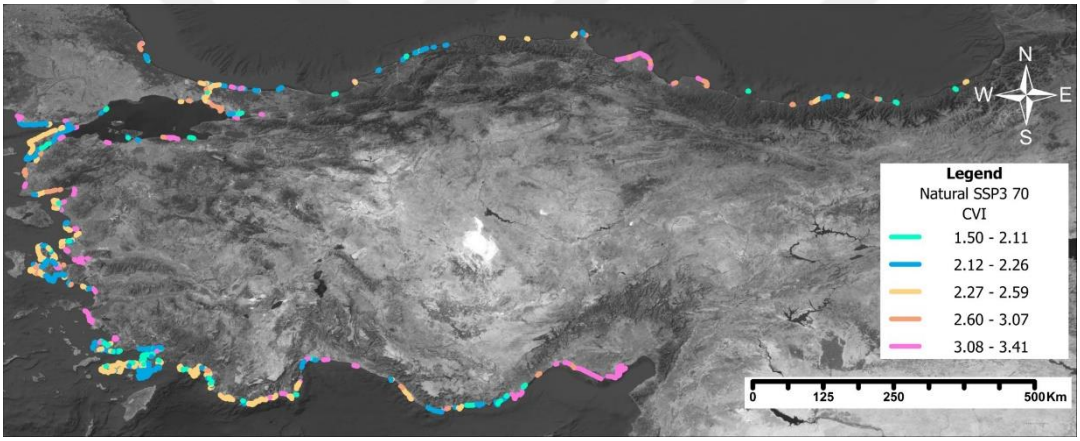


Figure 7.62. SSP3-7.0 Natural Conservation Zone CVI Jenks Distribution

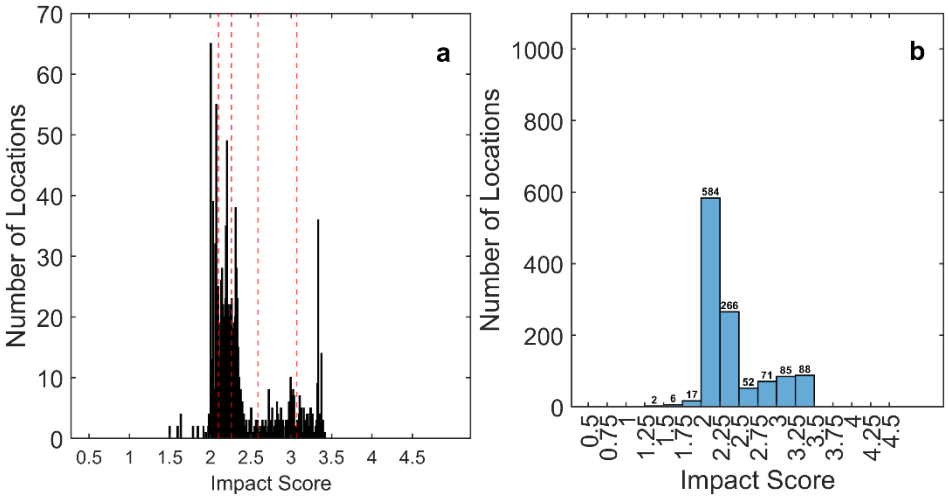


Figure 7.63. SSP3-7.0 Natural Conservation Zone CVI (a) Jenks (b) FCVAM Histograms

Table 7.3 SSP3-7.0 Natural Conservation Zone Impact & CVI Scores

NAT SSP3-70	Erosion			Inundation			Storm Surge			CVI
	PP	HI	Vul	PP	HI	Vul	PP	HI	Vul	
< 1.5 Very Low	14	586	10	0	114	0	0	509	0	2
1.5 – 2.5 Low	638	531	640	885	983	874	889	613	882	874
2.5 – 3.5 Moderate	519	52	521	123	65	134	282	44	289	295
3.5 – 4.25 High	0	2	0	158	9	163	0	5	0	0
4.25 > Very High	0	0	0	5	0	0	0	0	0	0

D. Cultural Heritage Sites SSP1-1.9

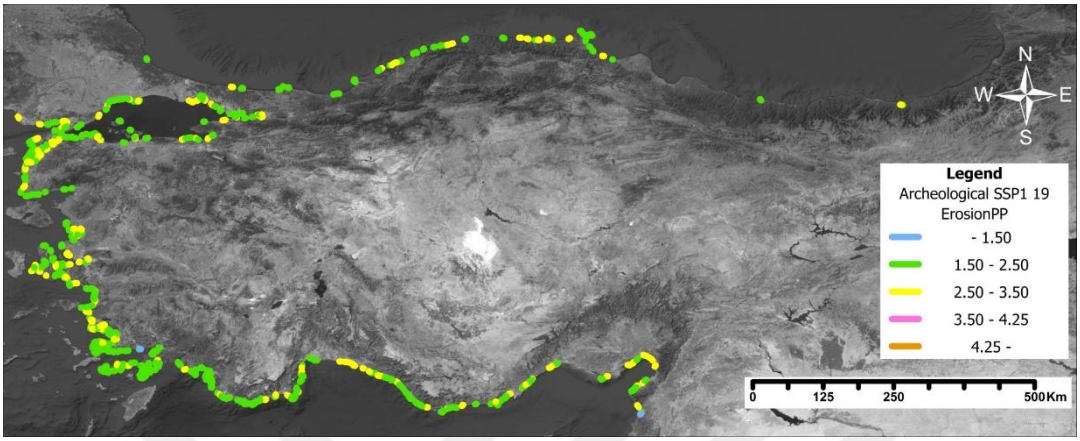


Figure 7.64. SSP1-1.9 Cultural Heritage Site ErosionPP Distribution

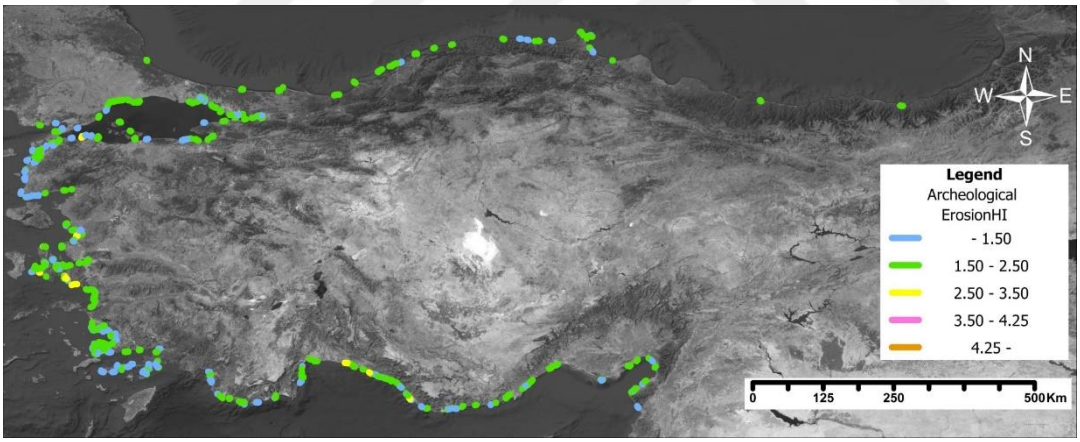


Figure 7.65. SSP1-1.9 Cultural Heritage Site ErosionHI Distribution

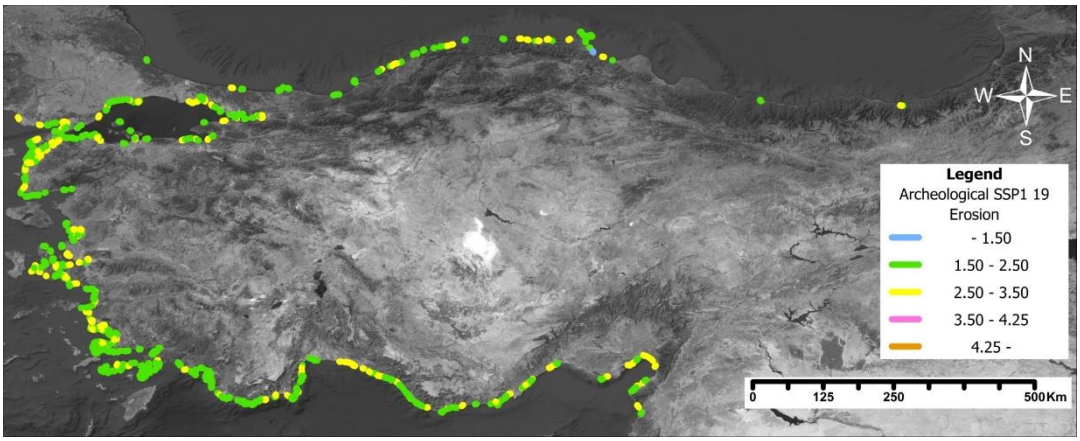


Figure 7.66. SSP1-1.9 Cultural Heritage Site Erosion Distribution

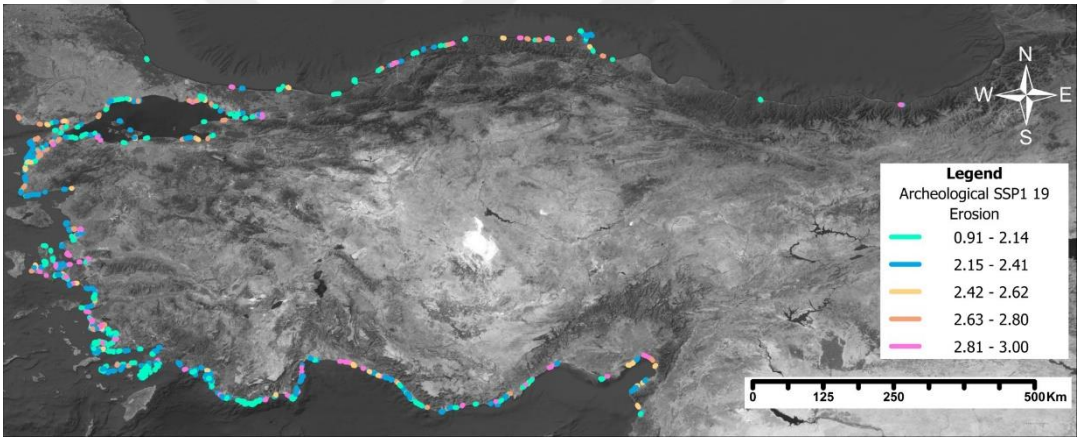


Figure 7.67. SSP1-1.9 Cultural Heritage Site Erosion Jenks Distribution

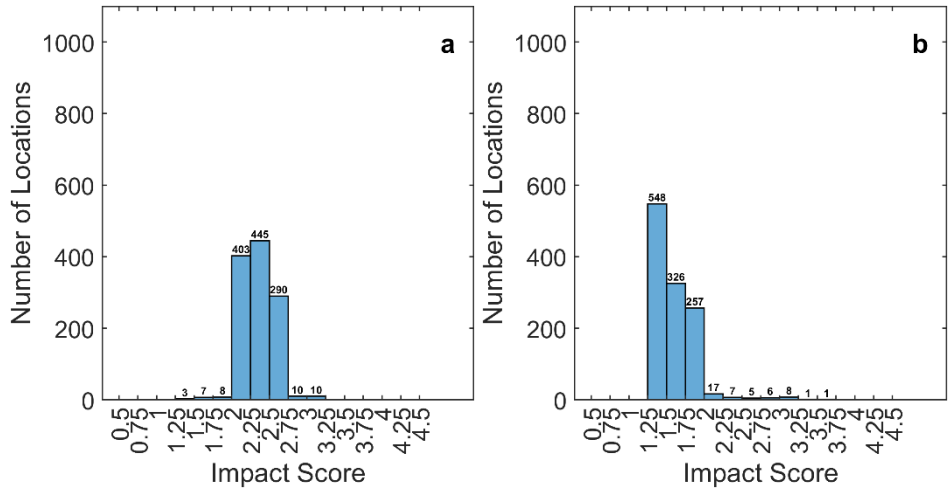


Figure 7.68. SSP1-1.9 Cultural Heritage Site Erosion (a) Physical Impact Score (b) Human Impact Score

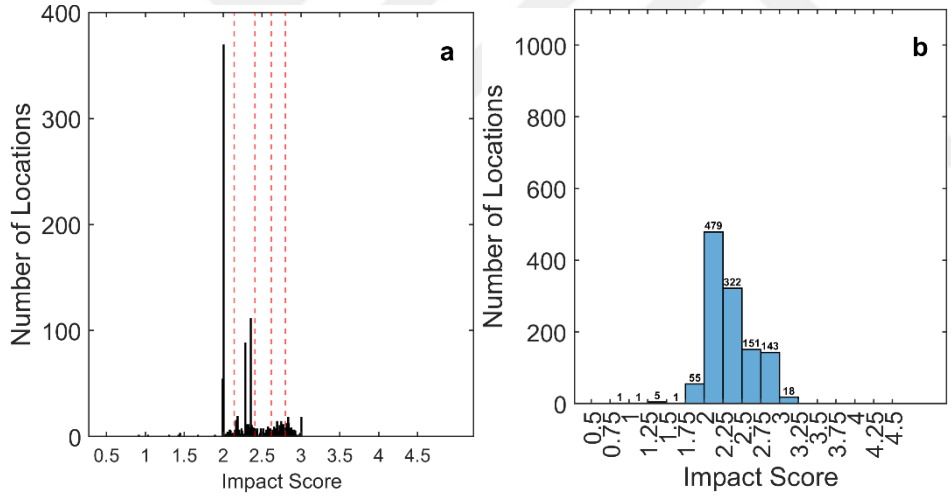


Figure 7.69. SSP1-1.9 Cultural Heritage Site Erosion (a) Jenks (b) FCVAM Histograms

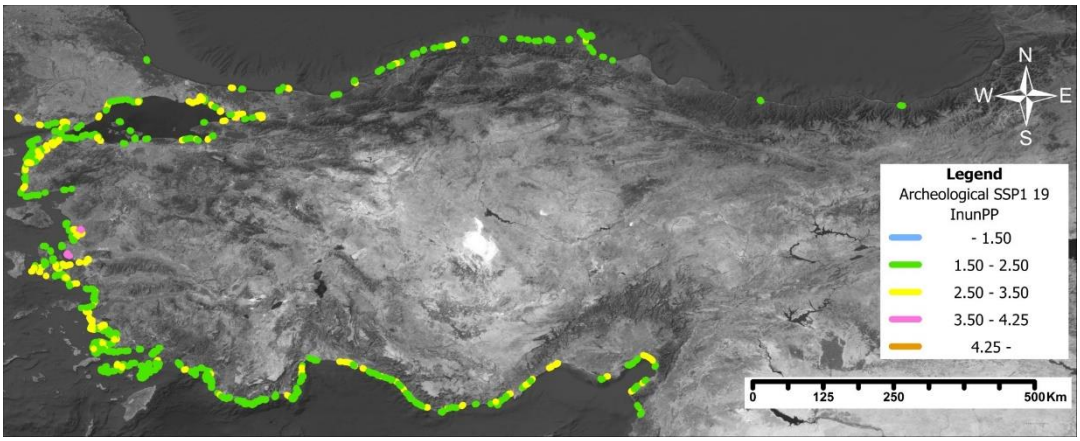


Figure 7.70. SSP1-1.9 Cultural Heritage Site InundationPP Distribution

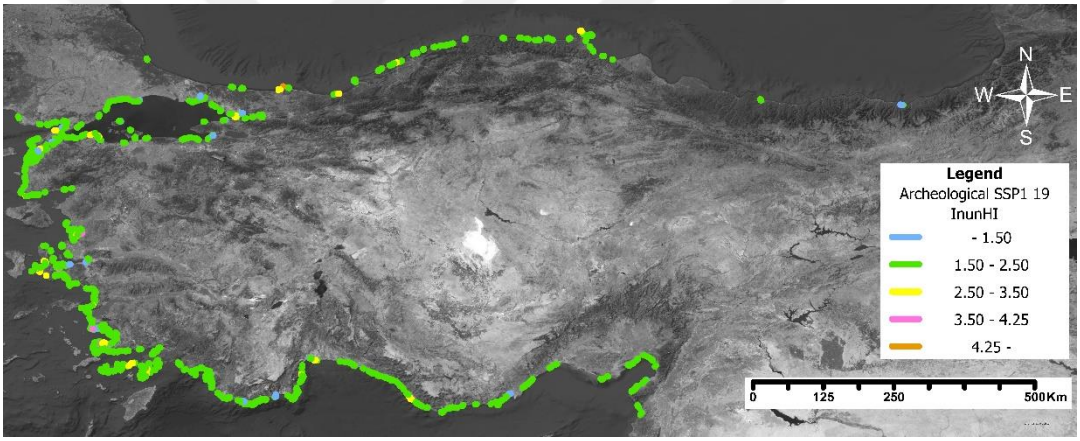


Figure 7.71. SSP1-1.9 Cultural Heritage Site InundationHI Distribution

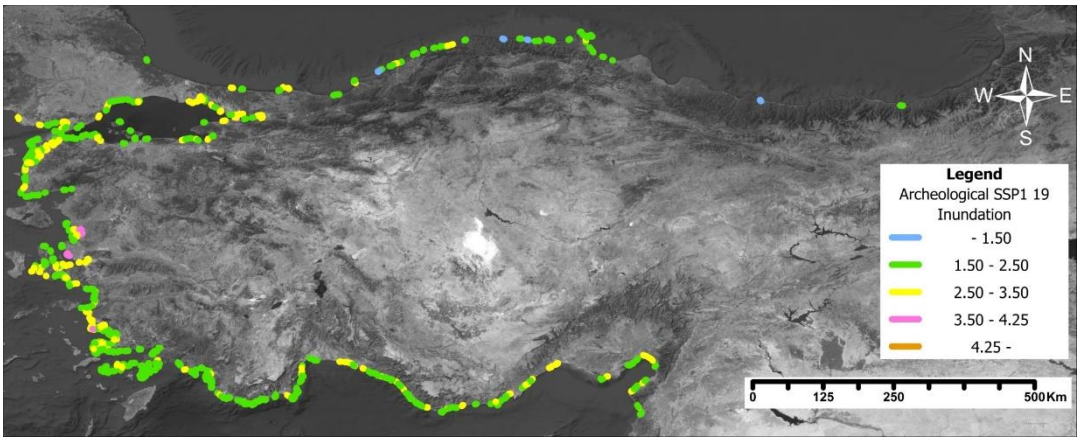


Figure 7.72. SSP1-1.9 Cultural Heritage Site Inundation Distribution

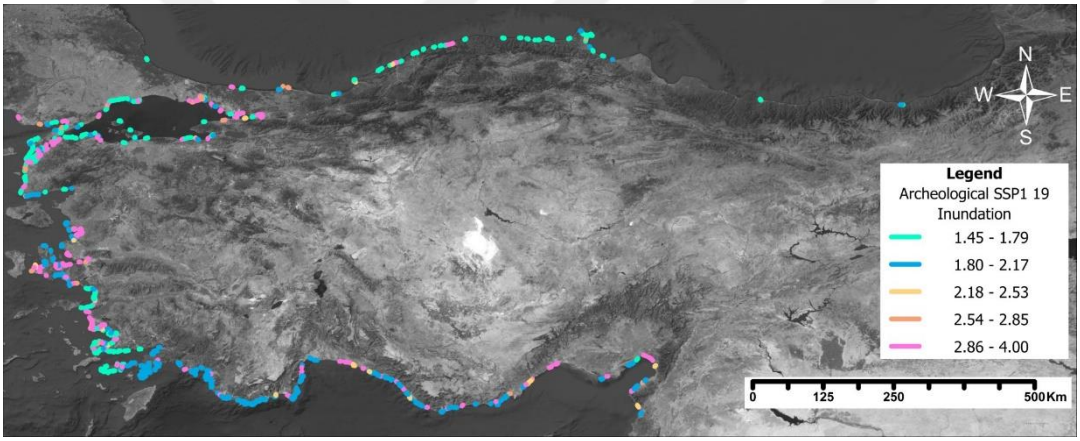


Figure 7.73. SSP1-1.9 Cultural Heritage Site Inundation Jenks Distribution

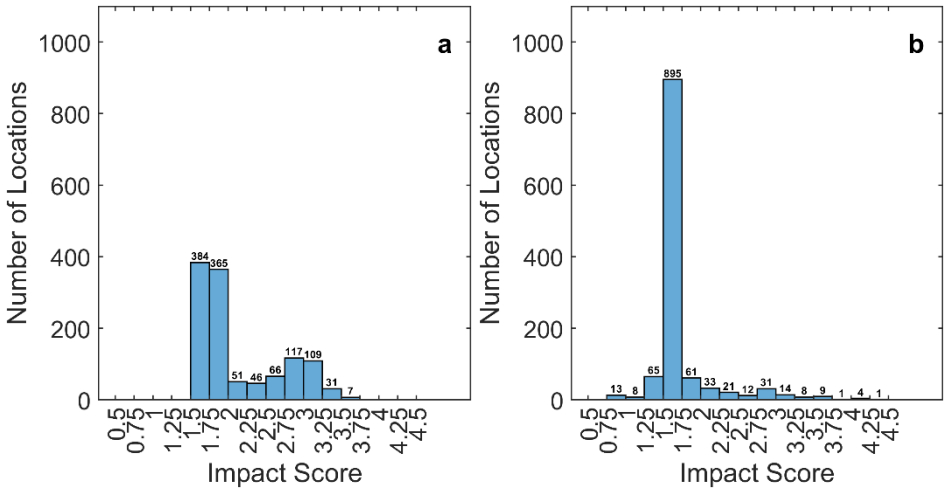


Figure 7.74. SSP1-1.9 Cultural Heritage Site Inundation (a) Physical Impact Score (b) Human Impact Score

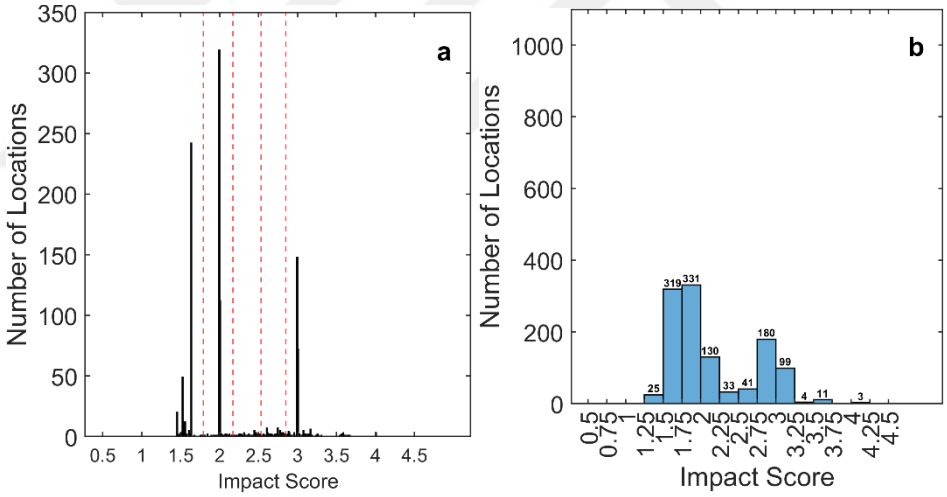


Figure 7.75. SSP1-1.9 Cultural Heritage Site Inundation (a) Jenks (b) FCVAM Histograms

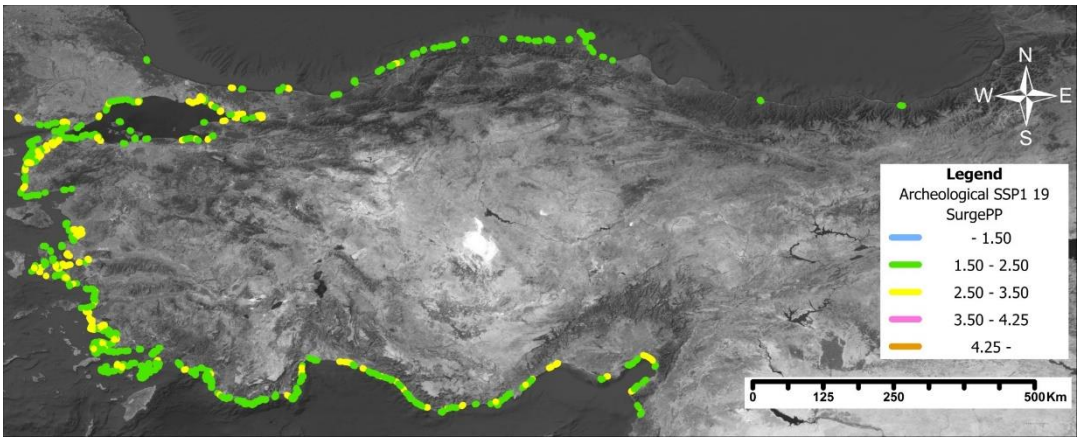


Figure 7.76. SSP1-1.9 Cultural Heritage Site Storm SurgePP Distribution

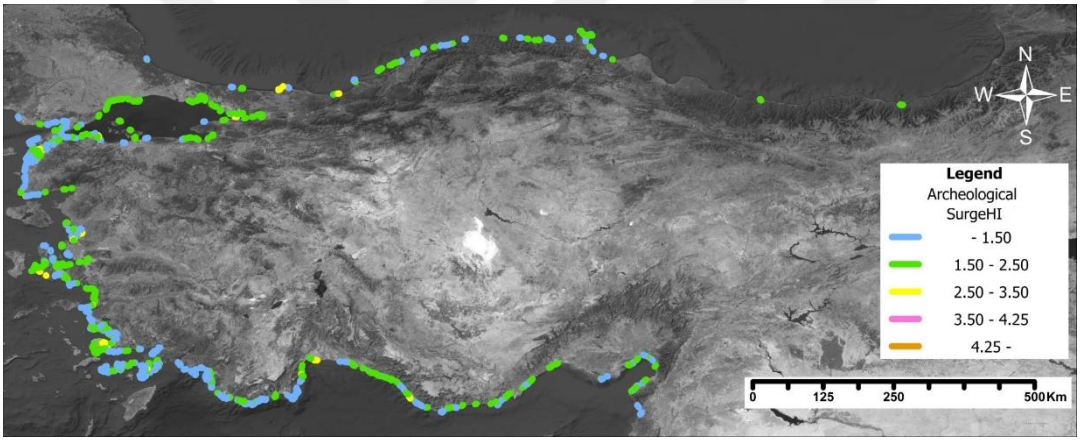


Figure 7.77. SSP1-1.9 Cultural Heritage Site Storm SurgeHI Distribution

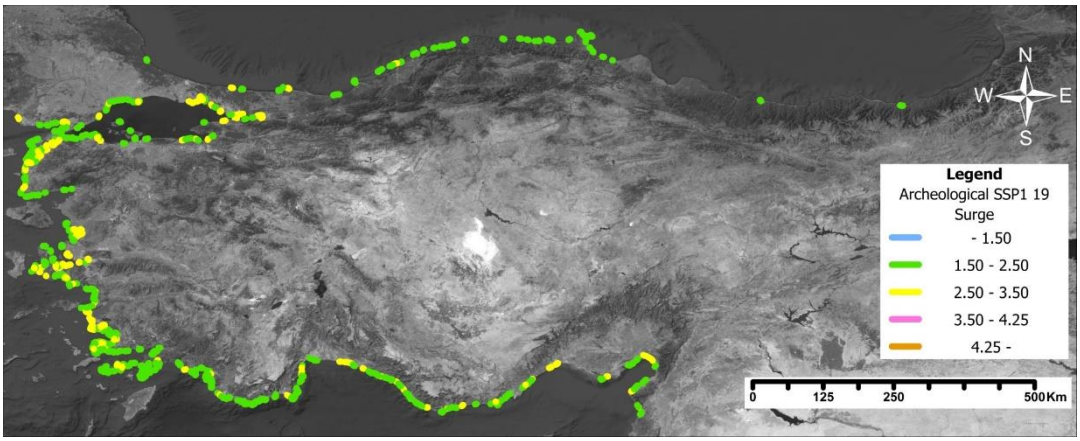


Figure 7.78. SSP1-1.9 Cultural Heritage Site Storm Surge Distribution

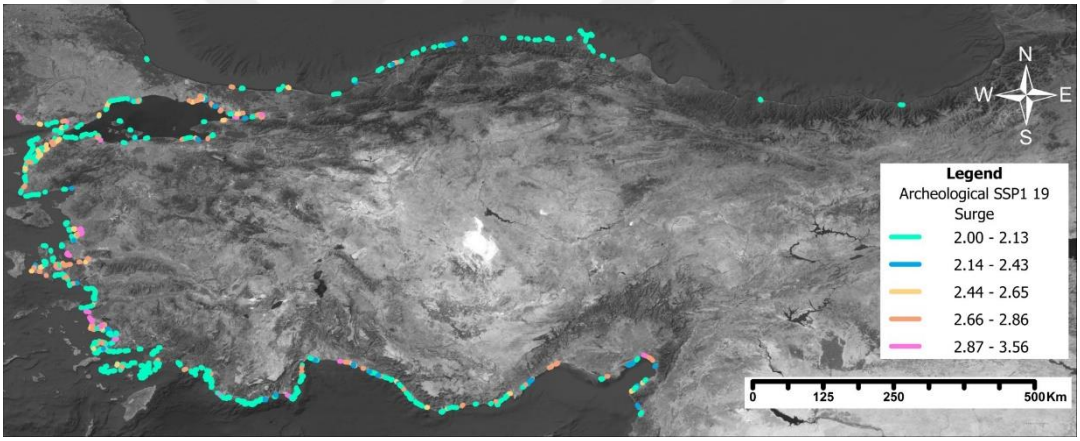


Figure 7.79. SSP1-1.9 Cultural Heritage Site Storm Surge Jenks Distribution

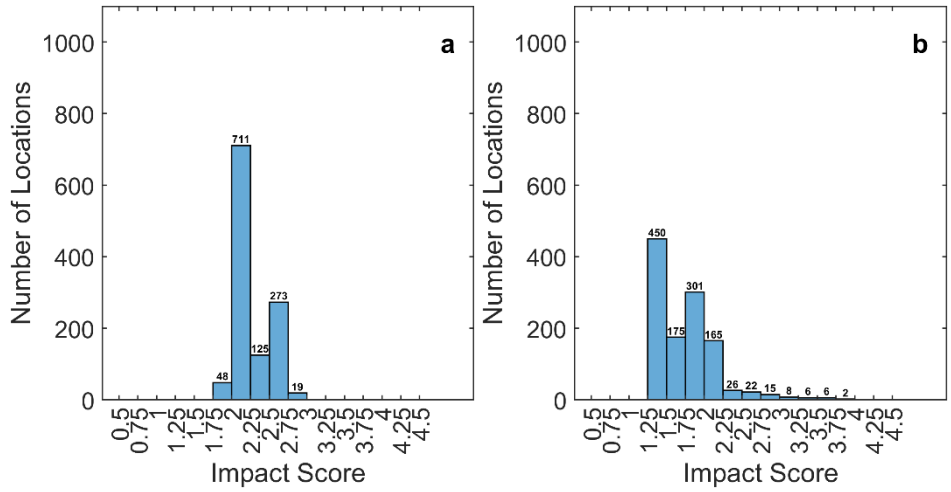


Figure 7.80. SSP1-1.9 Cultural Heritage Site Storm Surge (a) Physical Impact Score (b) Human Impact Score

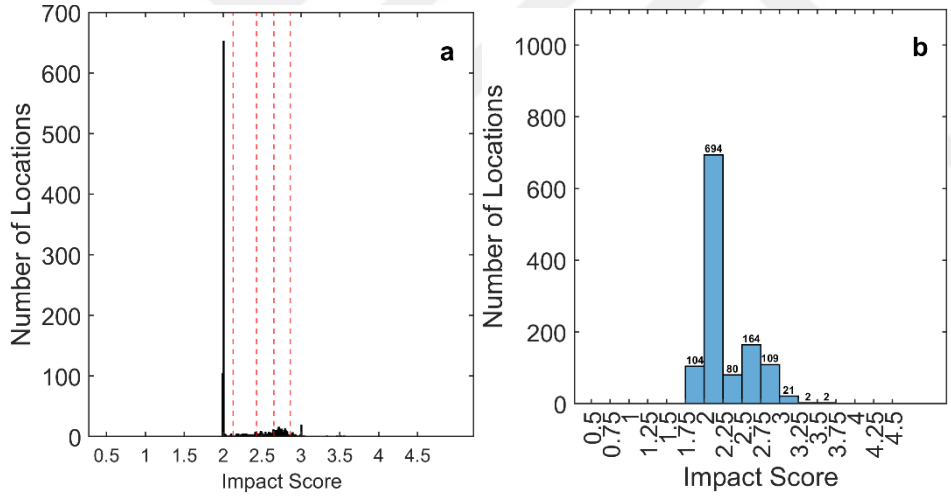


Figure 7.81. SSP1-1.9 Cultural Heritage Site Storm Surge (a) Jenks (b) FCVAM Histograms

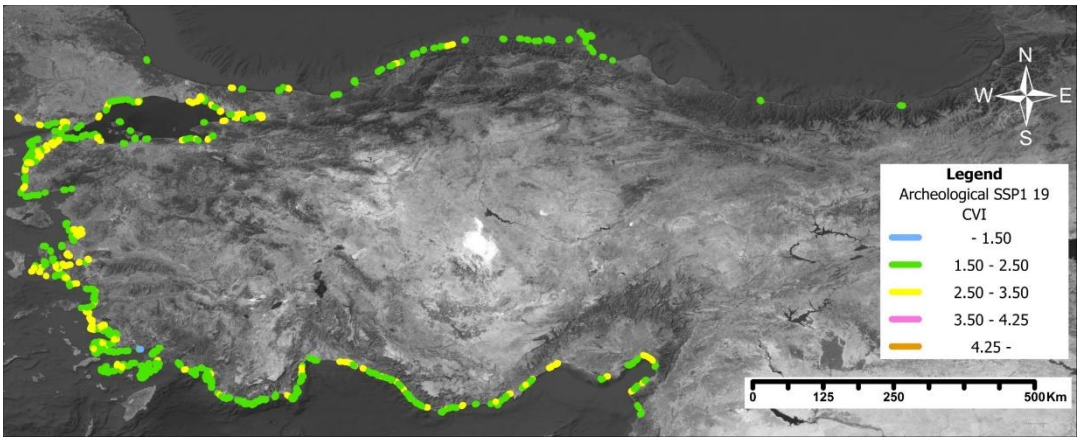


Figure 7.82. SSP1-1.9 Cultural Heritage Site CVI Distribution

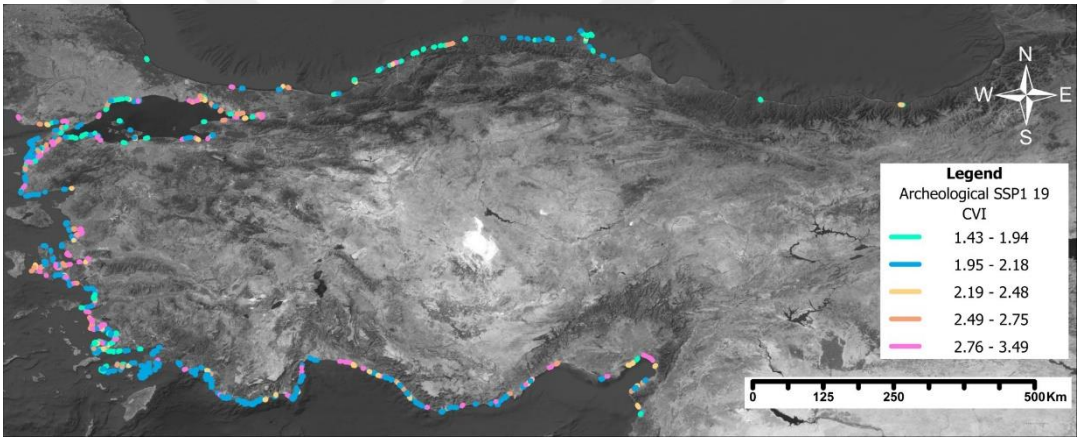


Figure 7.83. SSP1-1.9 Cultural Heritage Site CVI Jenks Distribution

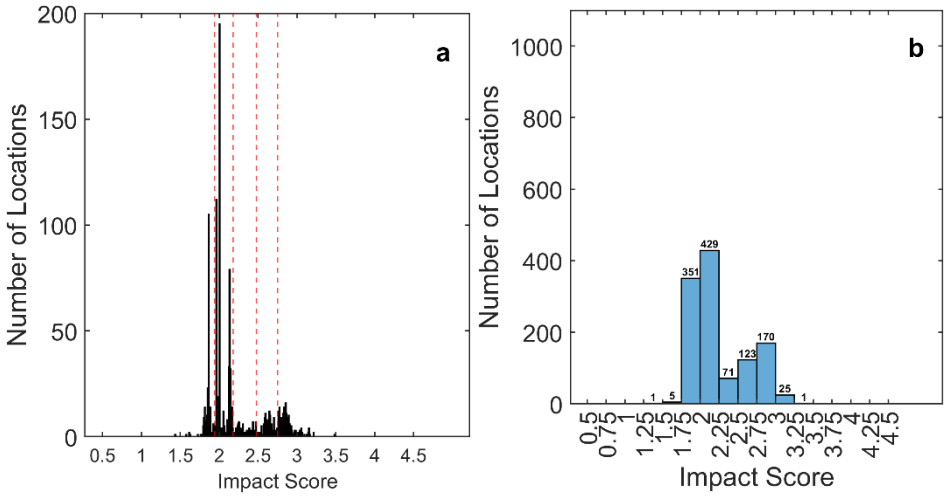


Figure 7.84. SSP1-1.9 Cultural Heritage Site CVI (a) Jenks (b) FCVAM Histograms

Table 7.4 SSP1-1.9 Cultural Heritage Site Impact & CVI Scores

ARC SSP1-19	Erosion			Inundation			Storm Surge			CVI
	PP	HI	Vul	PP	HI	Vul	PP	HI	Vul	
< 1.5 Very Low	3	548	7	0	86	25	0	450	0	1
1.5 – 2.5 Low	863	607	857	846	1010	813	884	667	878	856
2.5 – 3.5 Moderate	310	20	312	323	65	324	292	51	296	319
3.5 – 4.25 High	0	1	0	7	14	14	0	8	2	0
4.25 > Very High	0	0	0	0	1	0	0	0	0	0

E. Cultural Heritage Sites SSP1-2.6

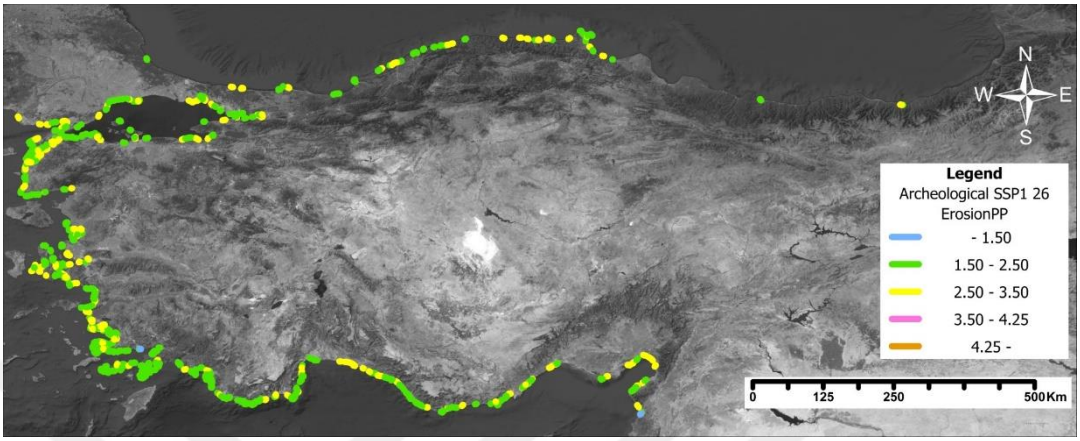


Figure 7.85. SSP1-2.6 Cultural Heritage Site ErosionPP Distribution

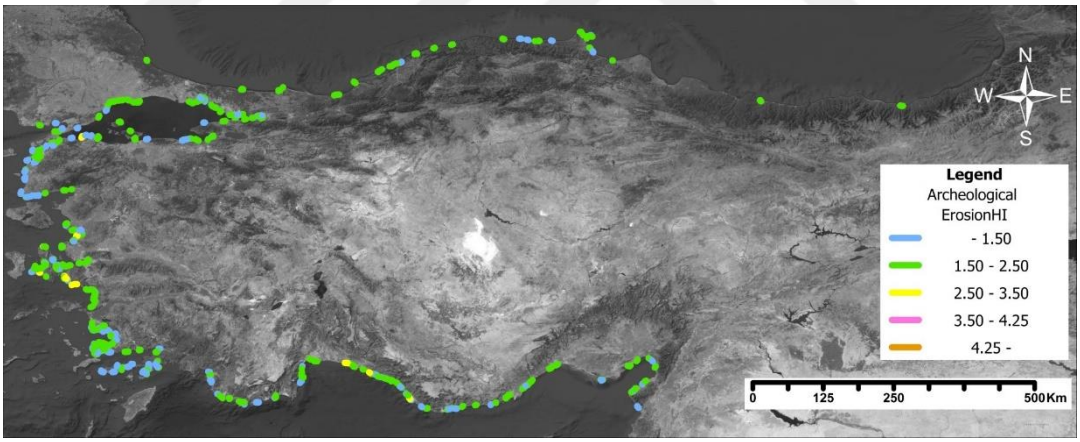


Figure 7.86. SSP1-2.6 Cultural Heritage Site ErosionHI Distribution

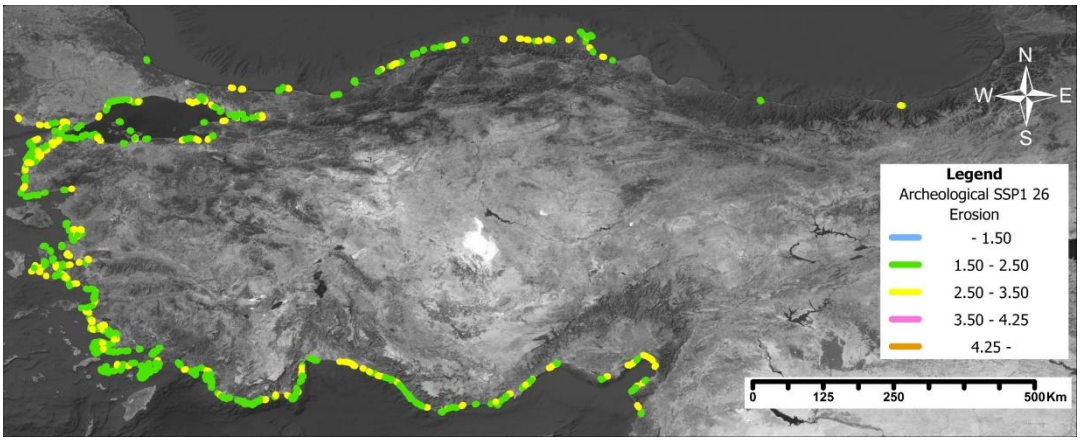


Figure 7.87. SSP1-2.6 Cultural Heritage Site Erosion Distribution

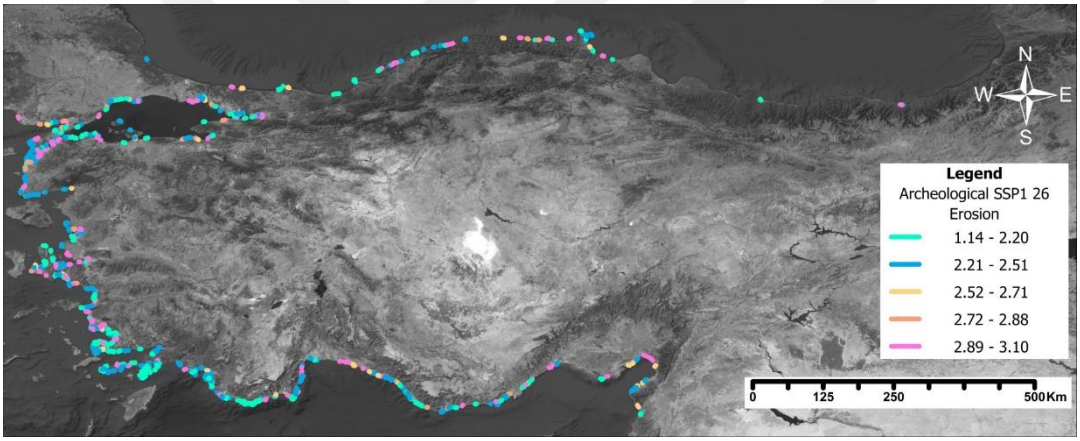


Figure 7.88. SSP1-2.6 Cultural Heritage Site Erosion Jenks Distribution

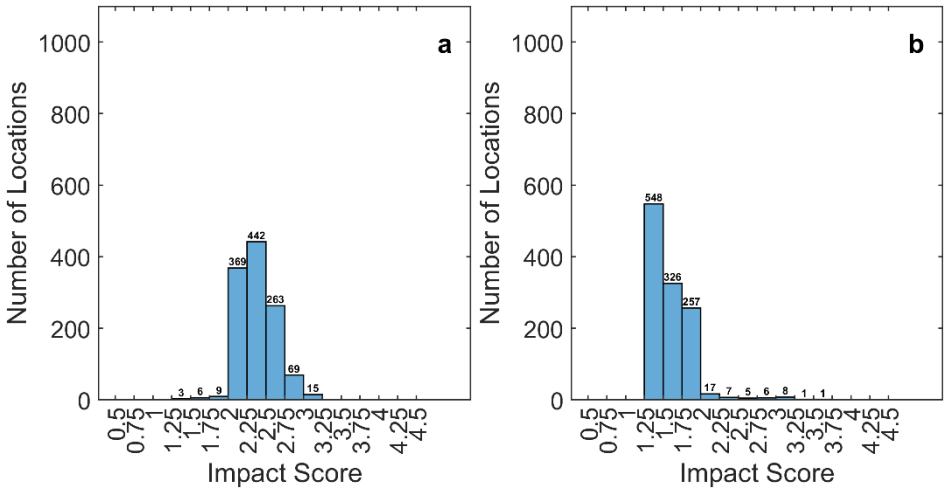


Figure 7.89. SSP1-2.6 Cultural Heritage Site Erosion (a) Physical Impact Score (b) Human Impact Score

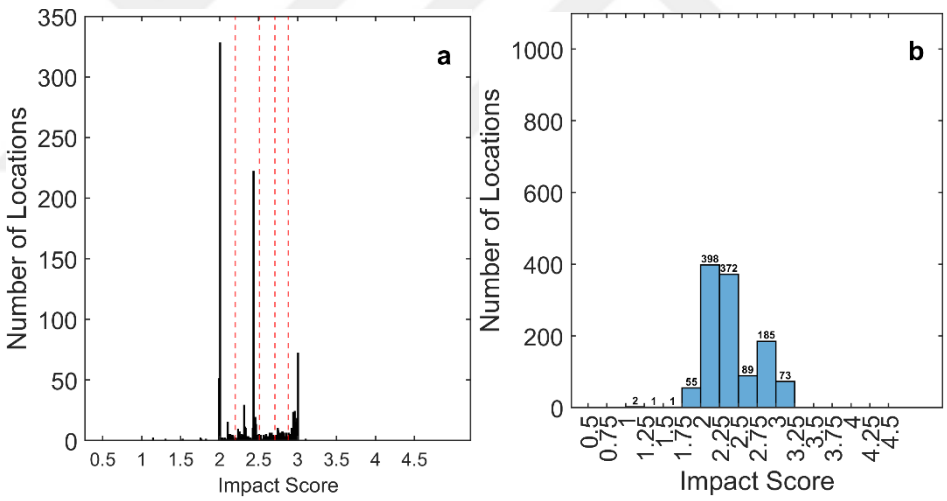


Figure 7.90. SSP1-2.6 Cultural Heritage Site Erosion (a) Jenks (b) FCVAM Histograms

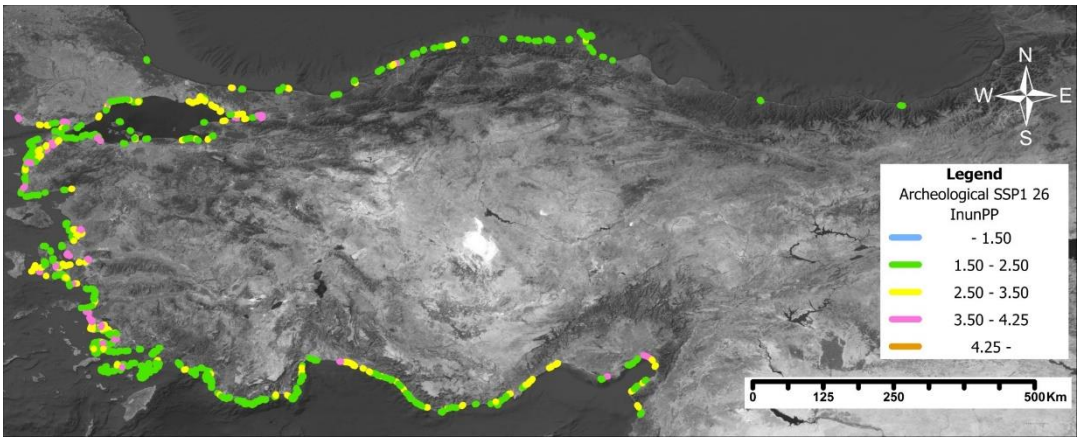


Figure 7.91. SSP1-2.6 Cultural Heritage Site InundationPP Distribution

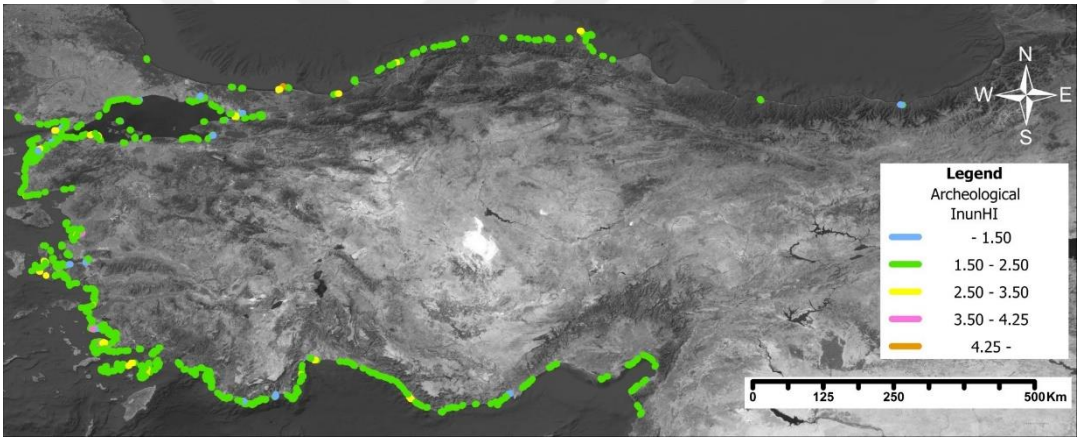


Figure 7.92. SSP1-2.6 Cultural Heritage Site InundationHI Distribution

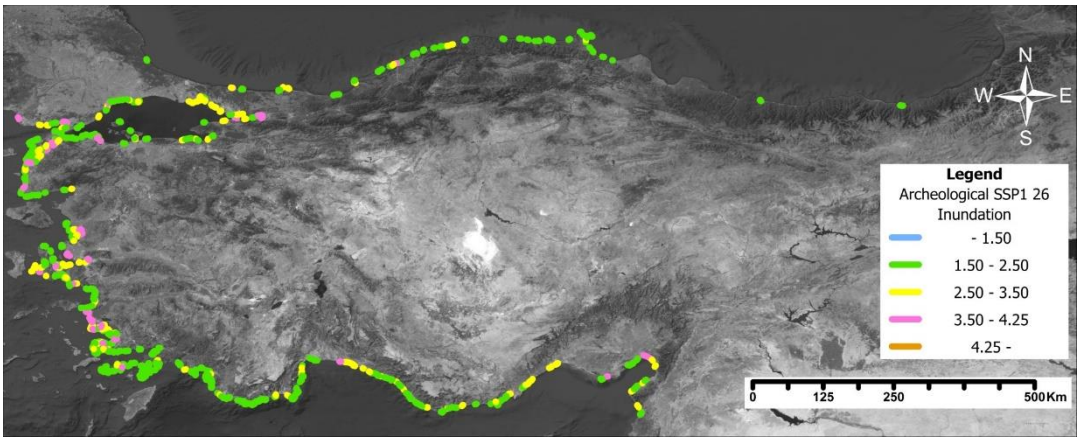


Figure 7.93. SSP1-2.6 Cultural Heritage Site Inundation Distribution

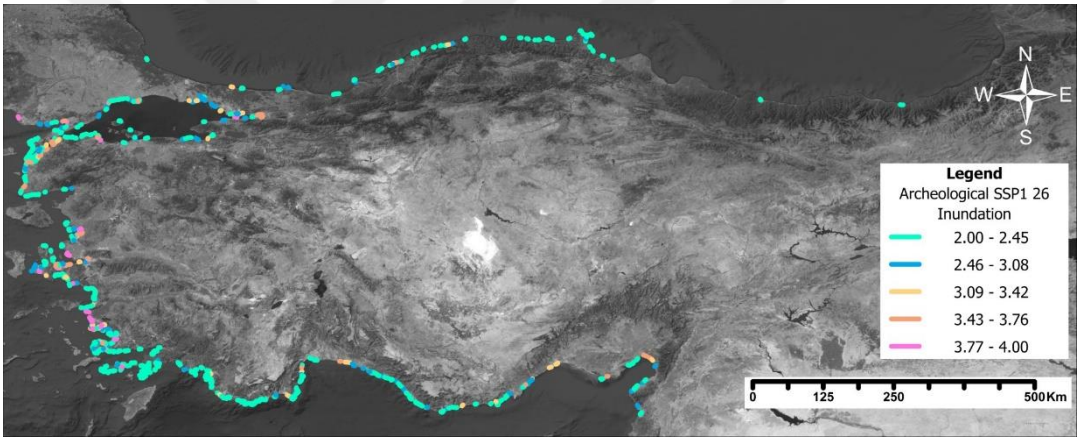


Figure 7.94. SSP1-2.6 Cultural Heritage Site Inundation Jenks Distribution

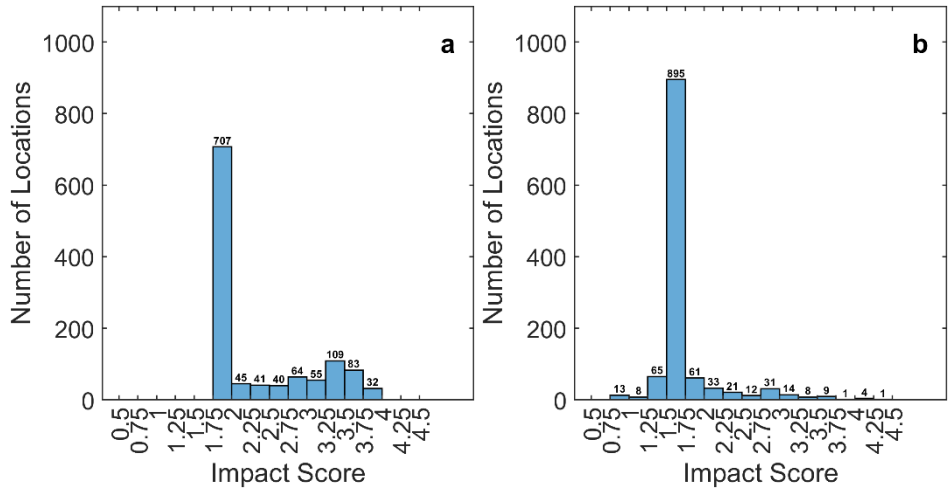


Figure 7.95. SSP1-2.6 Cultural Heritage Site Inundation (a) Physical Impact Score (b) Human Impact Score

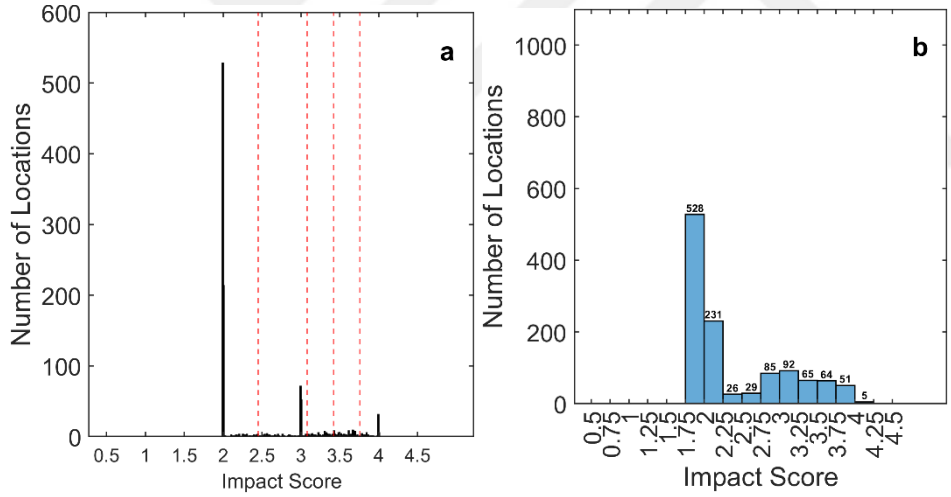


Figure 7.96. SSP1-2.6 Cultural Heritage Site Inundation (a) Jenks (b) FCVAM Histograms

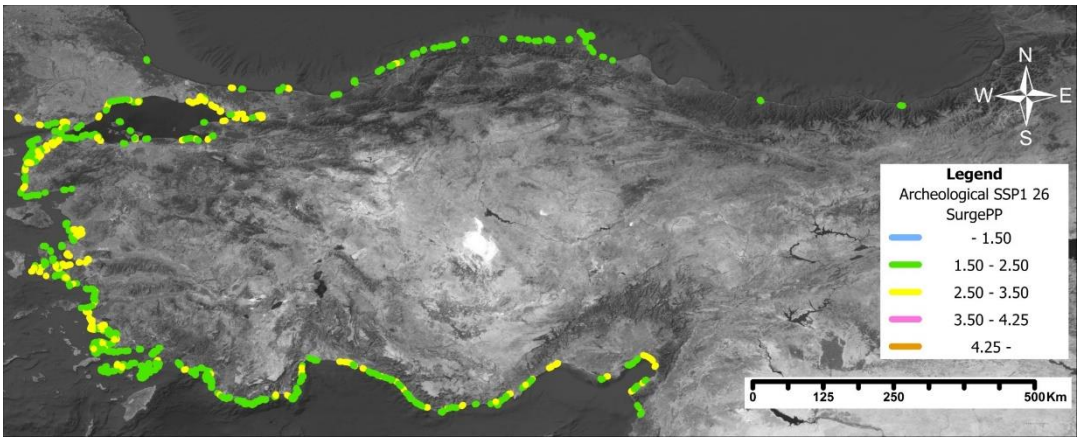


Figure 7.97. SSP1-2.6 Cultural Heritage Site Storm SurgePP Distribution

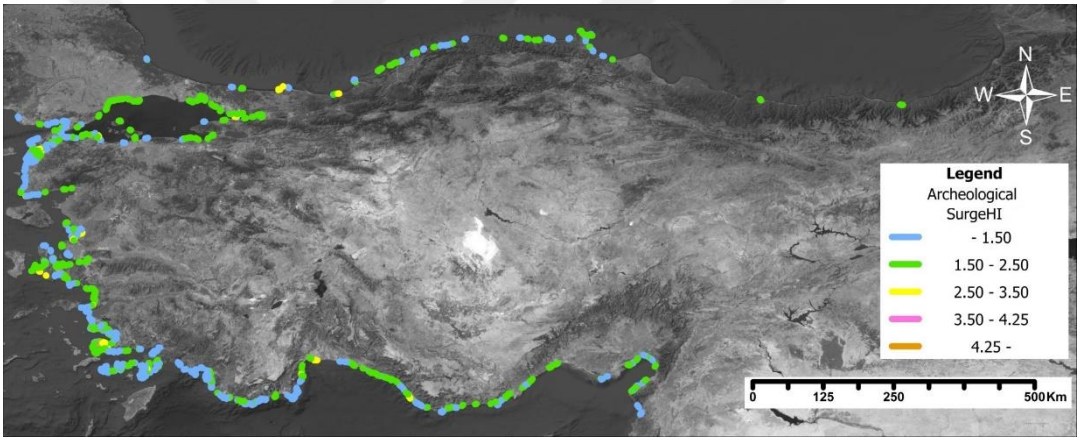


Figure 7.98. SSP1-2.6 Cultural Heritage Site Storm SurgeHI Distribution

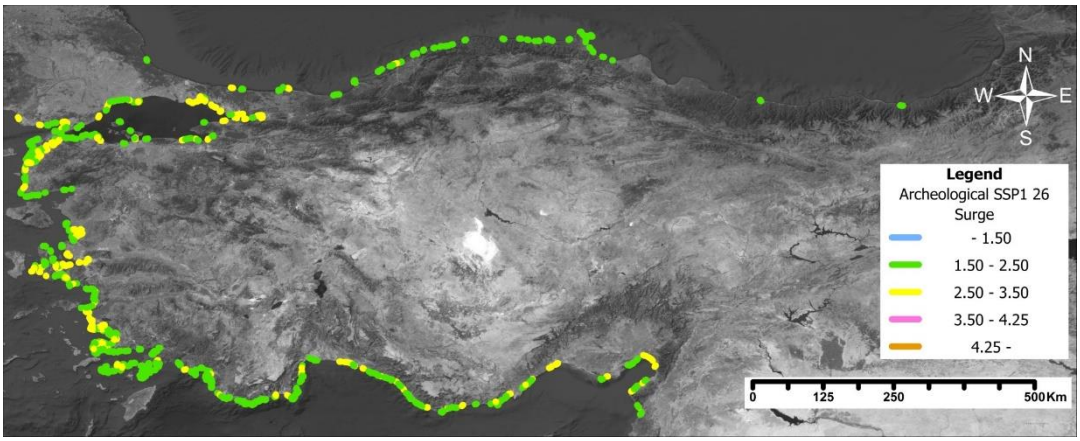


Figure 7.99. SSP1-2.6 Cultural Heritage Site Storm Surge Distribution

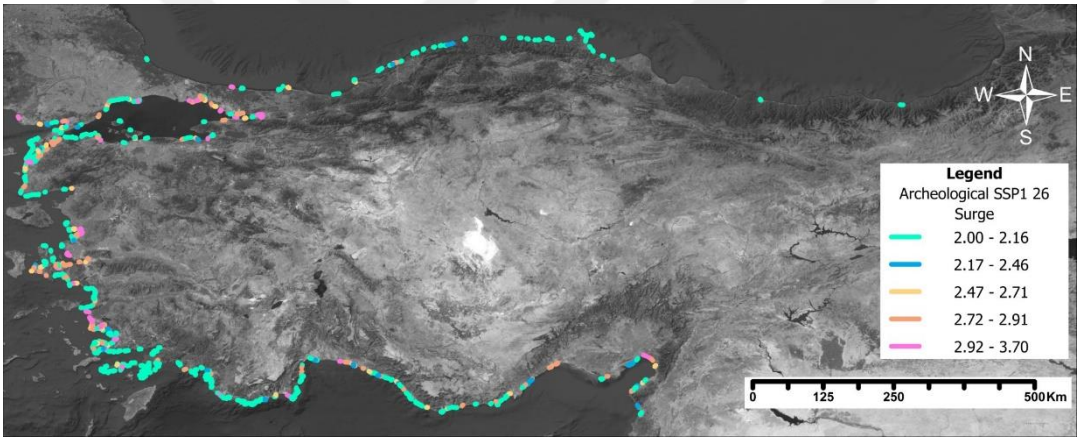


Figure 7.100. SSP1-2.6 Cultural Heritage Site Storm Surge Jenks Distribution

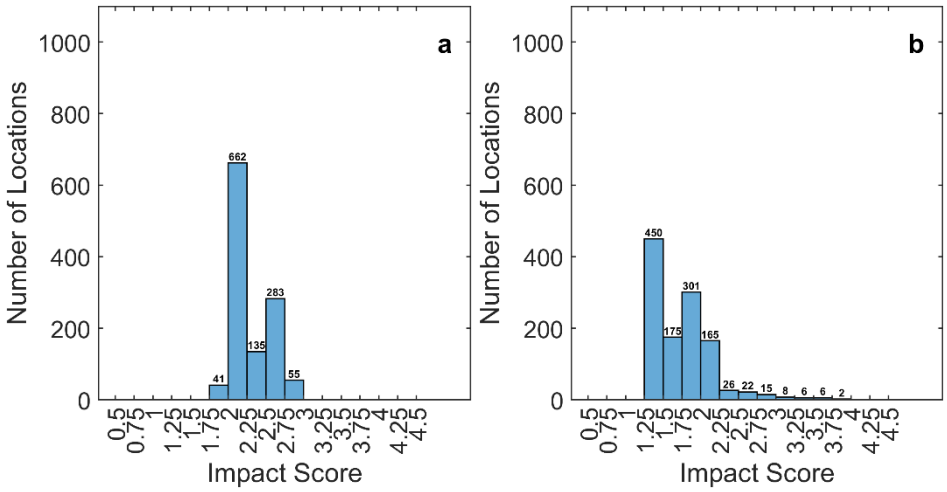


Figure 7.101. SSP1-2.6 Cultural Heritage Site Storm Surge (a) Physical Impact Score (b) Human Impact Score

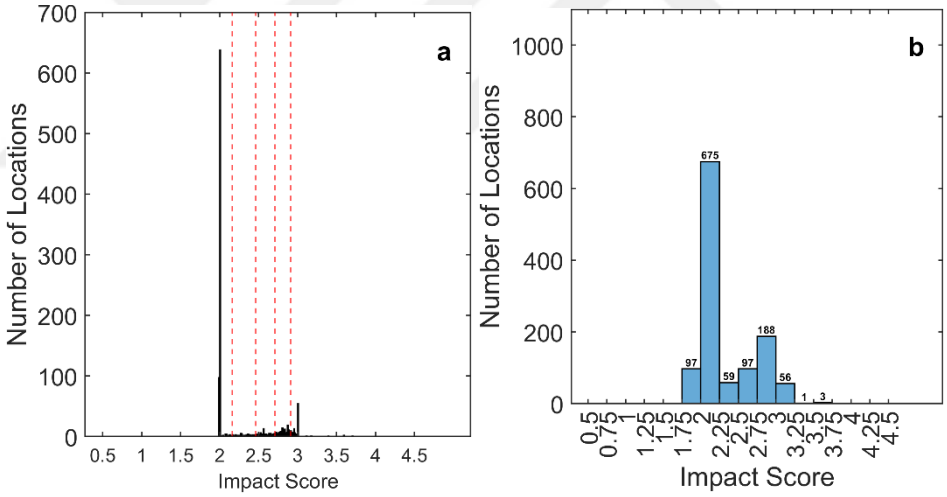


Figure 7.102. SSP1-2.6 Cultural Heritage Site Storm Surge (a) Jenks (b) FCVAM Histograms

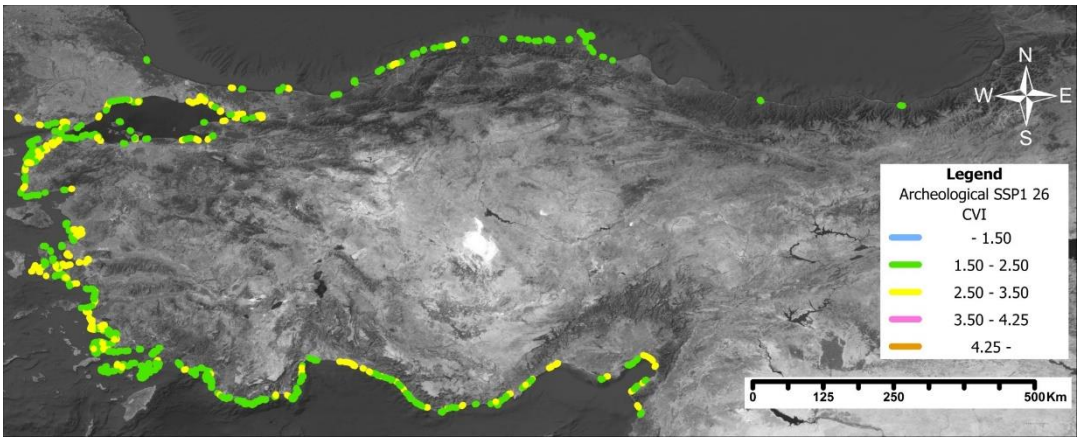


Figure 7.103. SSP1-2.6 Cultural Heritage Site CVI Distribution

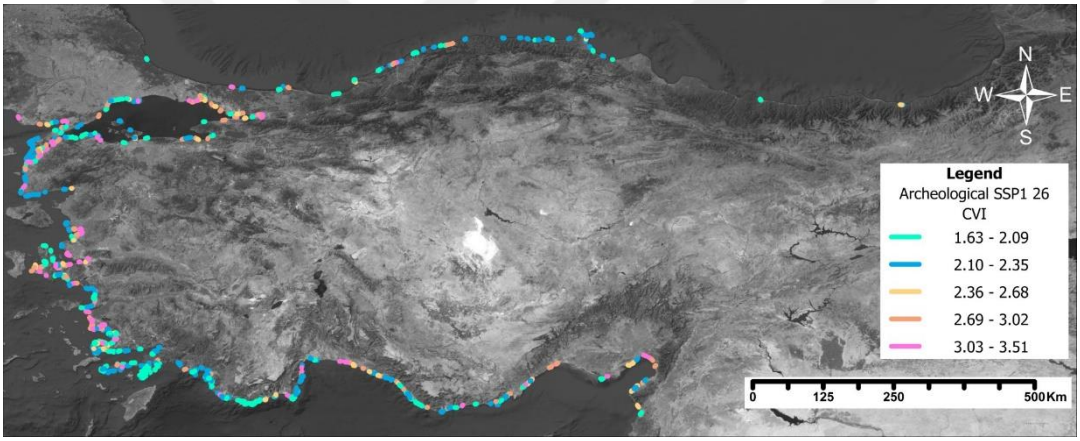


Figure 7.104. SSP1-2.6 Cultural Heritage Site CVI Jenks Distribution

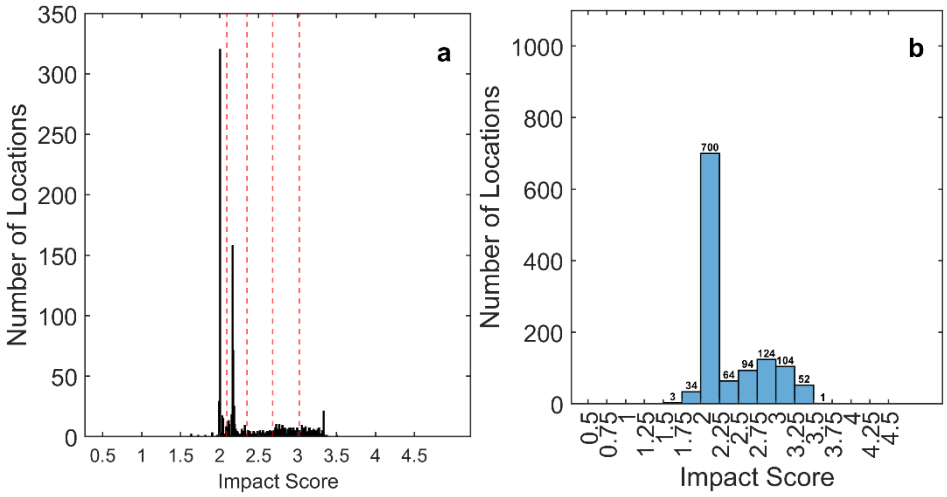


Figure 7.105. SSP1-2.6 Cultural Heritage Site CVI (a) Jenks (b) FCVAM Histograms

Table 7.5 SSP1-2.6 Cultural Heritage Site Impact & CVI Scores

ARC SSP1-26	Erosion			Inundation			Storm Surge			CVI
	PP	HI	Vul	PP	HI	Vul	PP	HI	Vul	
< 1.5 Very Low	3	548	3	0	86	0	0	450	0	0
1.5 – 2.5 Low	826	607	826	793	1010	785	838	667	831	801
2.5 – 3.5 Moderate	347	20	347	268	65	271	338	51	342	374
3.5 – 4.25 High	0	1	0	115	14	120	0	8	3	1
4.25 > Very High	0	0	0	0	1	0	0	0	0	0

F. Cultural Heritage Sites SSP3-7.0

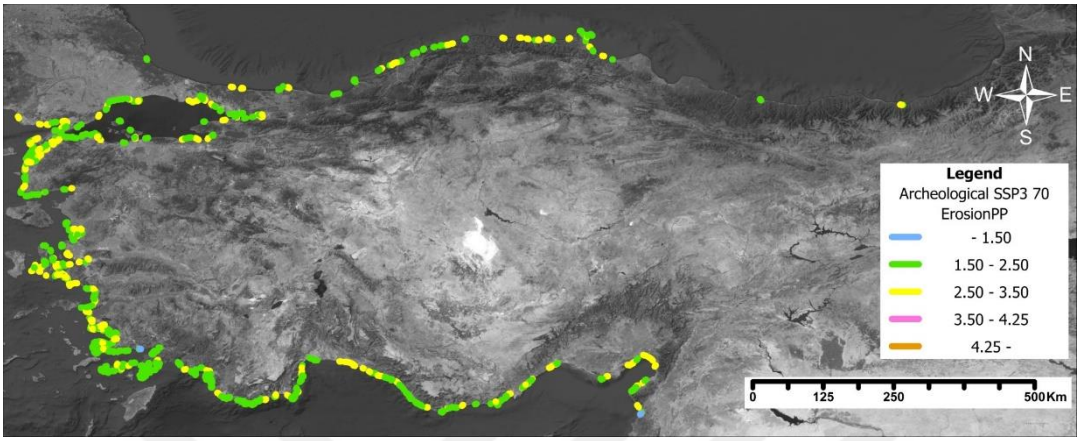


Figure 7.106. SSP3-7.0 Cultural Heritage Site ErosionPP Distribution

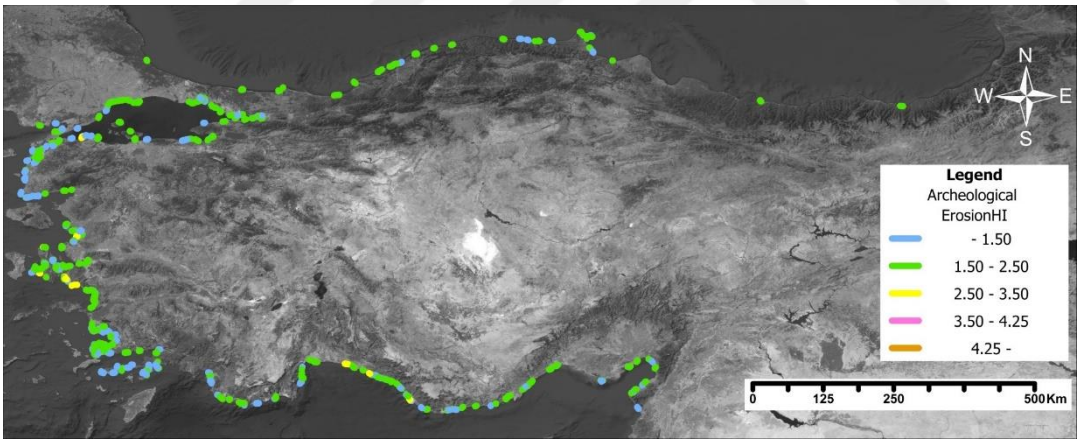


Figure 7.107. SSP3-7.0 Cultural Heritage Site ErosionHI Distribution

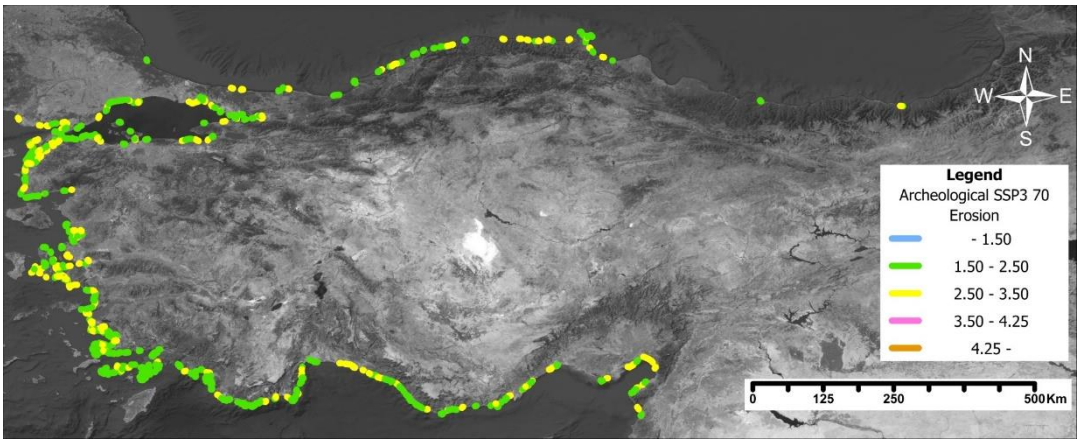


Figure 7.108. SSP3-7.0 Cultural Heritage Site Erosion Distribution

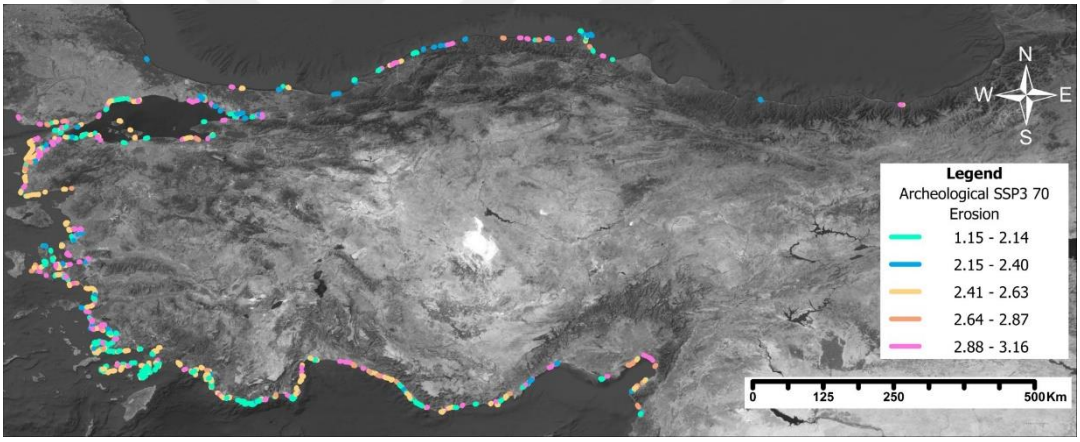


Figure 7.109. SSP3-7.0 Cultural Heritage Site Erosion Jenks Distribution

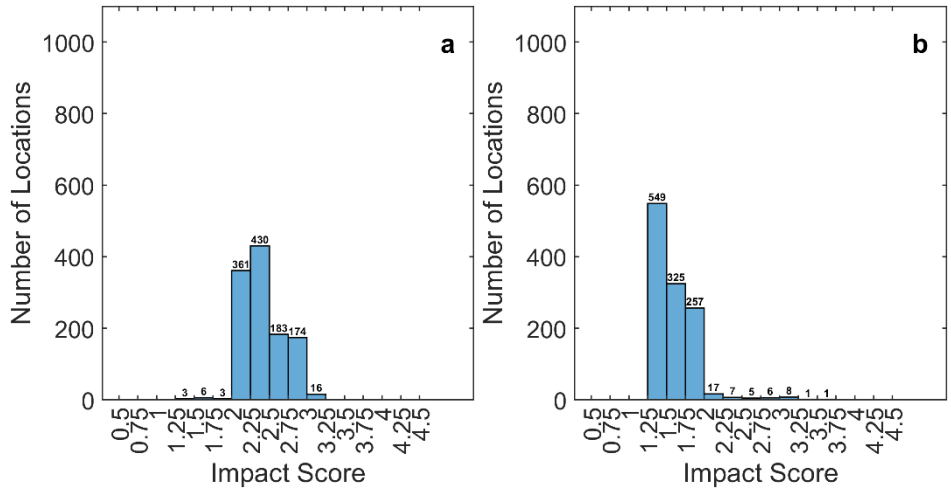


Figure 7.110. SSP3-7.0 Cultural Heritage Site Erosion (a) Physical Impact Score (b) Human Impact Score

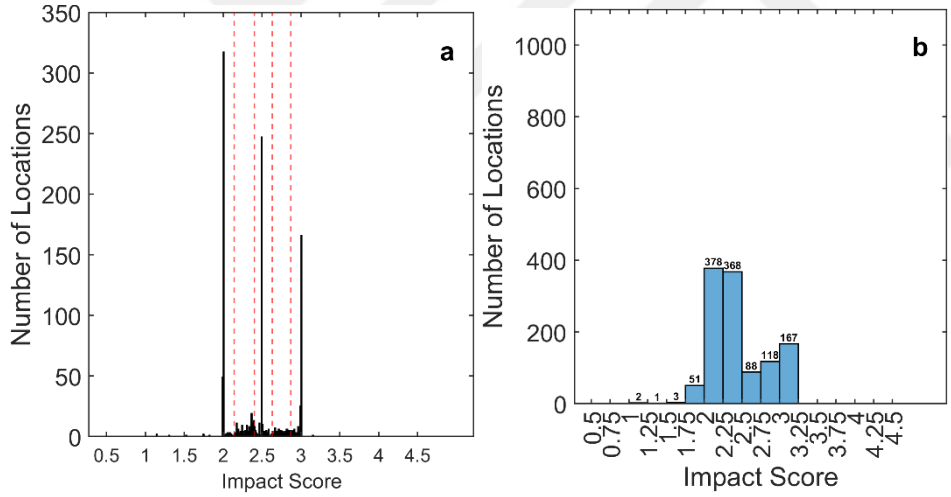


Figure 7.111. SSP3-7.0 Cultural Heritage Site Erosion (a) Jenks (b) FCVAM Histograms

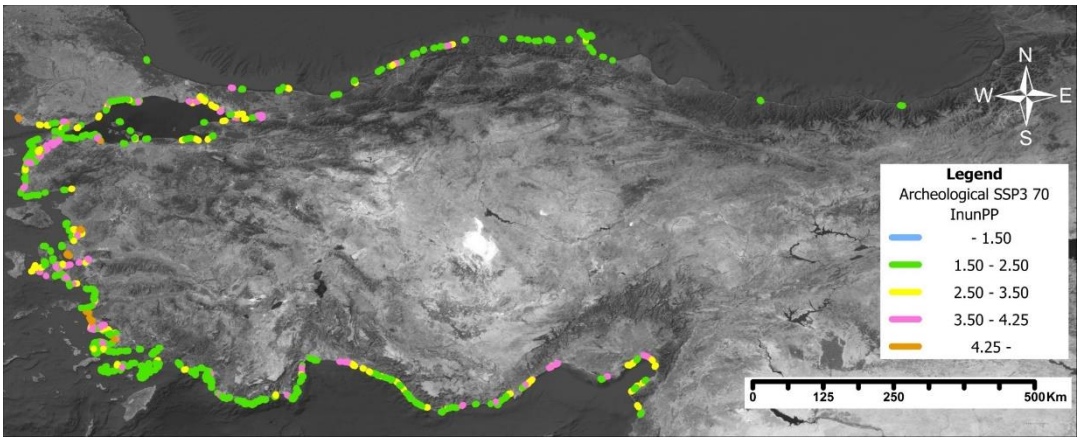


Figure 7.112. SSP3-7.0 Cultural Heritage Site InundationPP Distribution

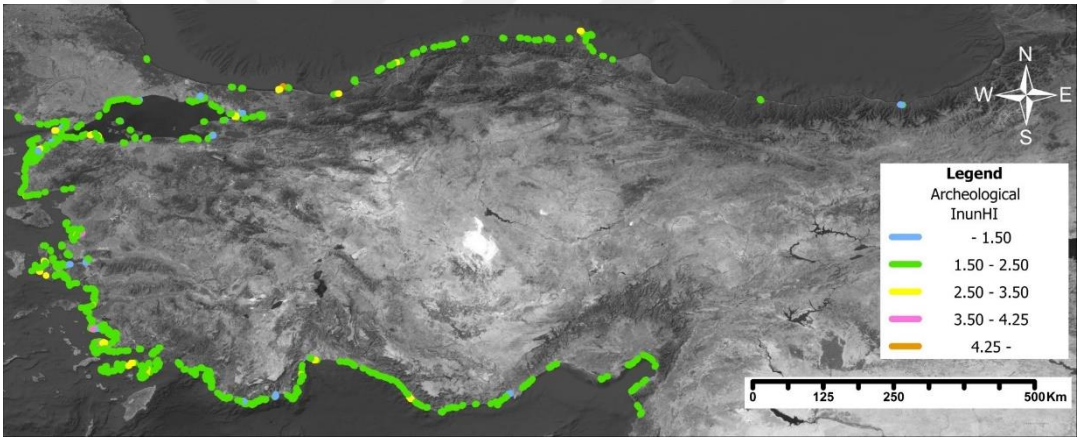


Figure 7.113. SSP3-7.0 Cultural Heritage Site InundationHI Distribution

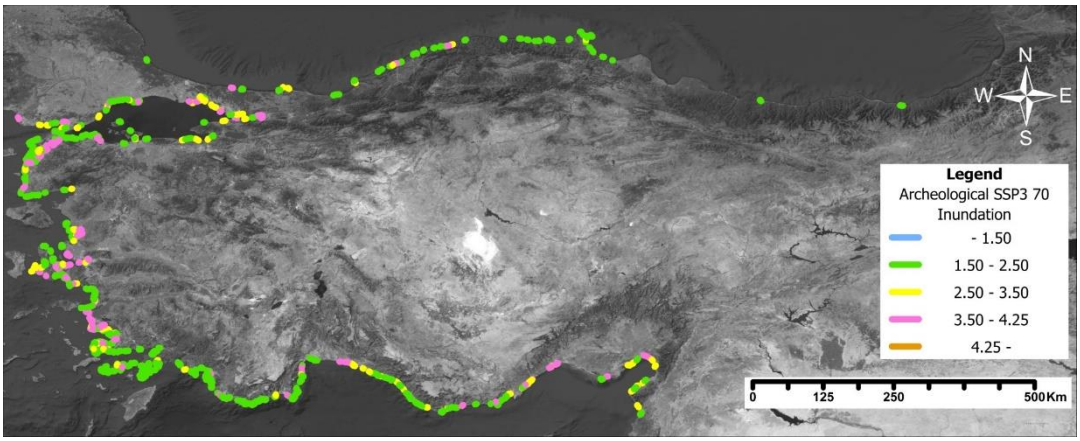


Figure 7.114. SSP3-7.0 Cultural Heritage Site Inundation Distribution

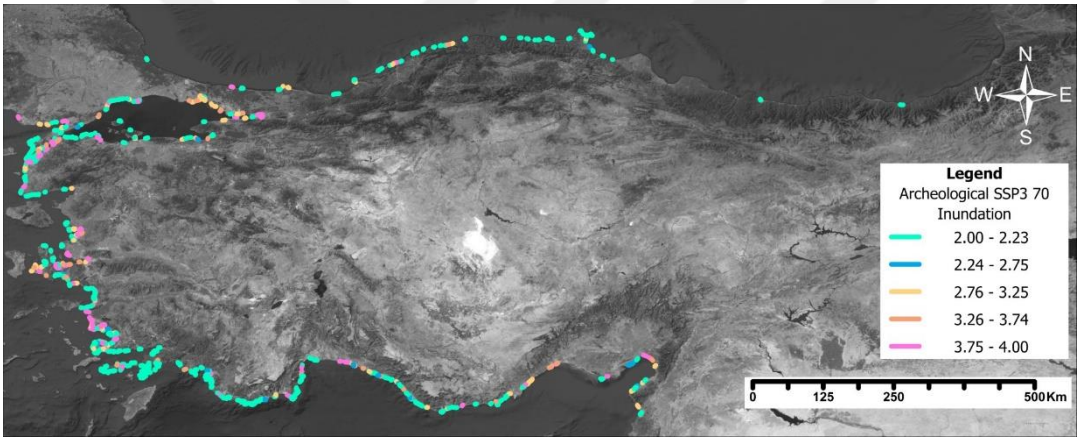


Figure 7.115. SSP3-7.0 Cultural Heritage Site Inundation Jenks Distribution

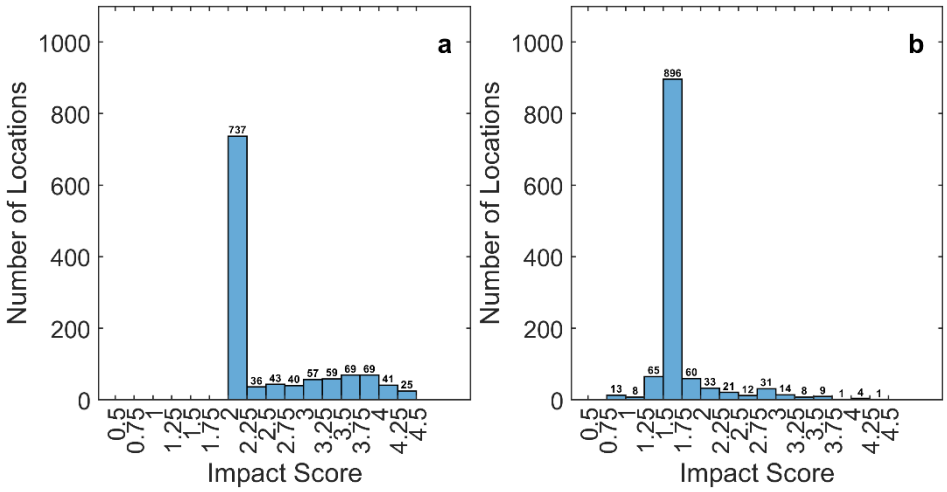


Figure 7.116. SSP3-7.0 Cultural Heritage Site Inundation (a) Physical Impact Score (b) Human Impact Score

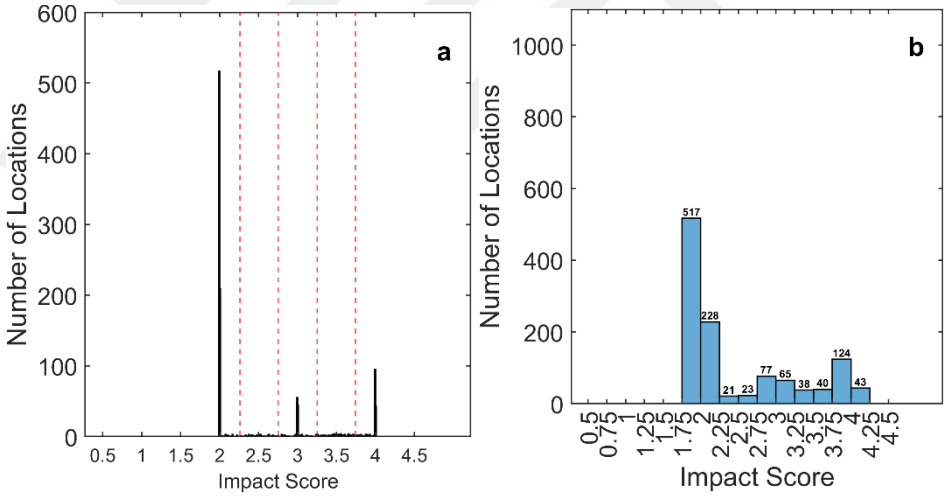


Figure 7.117. SSP3-7.0 Cultural Heritage Site Inundation (a) Jenks (b) FCVAM Histograms

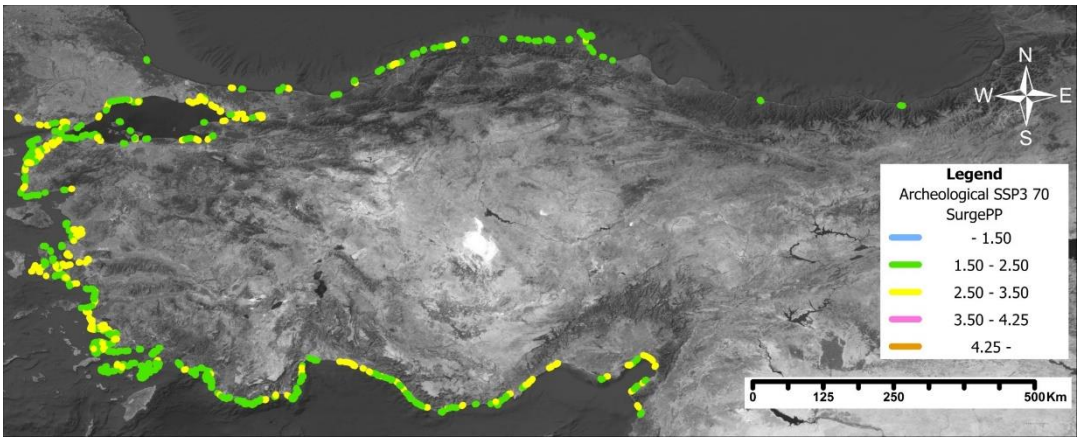


Figure 7.118. SSP3-7.0 Cultural Heritage Site Storm SurgePP Distribution

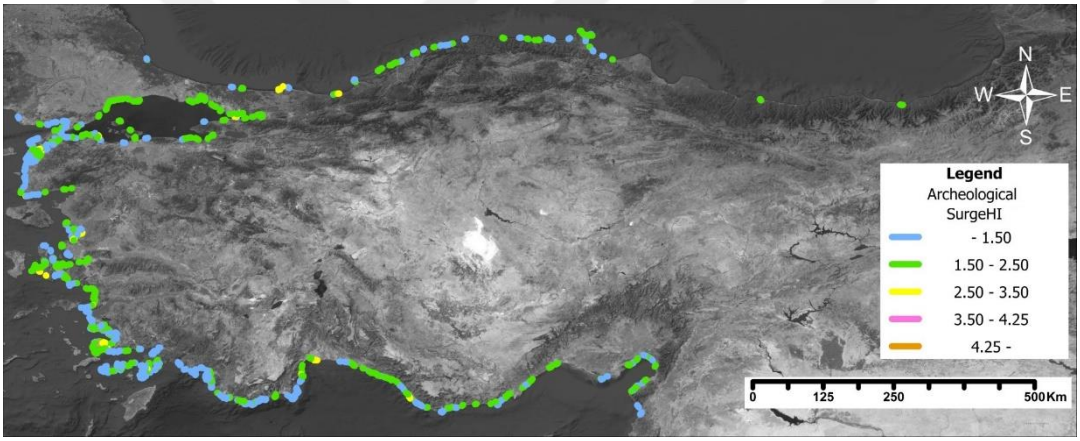


Figure 7.119. SSP3-7.0 Cultural Heritage Site Storm SurgeHI Distribution

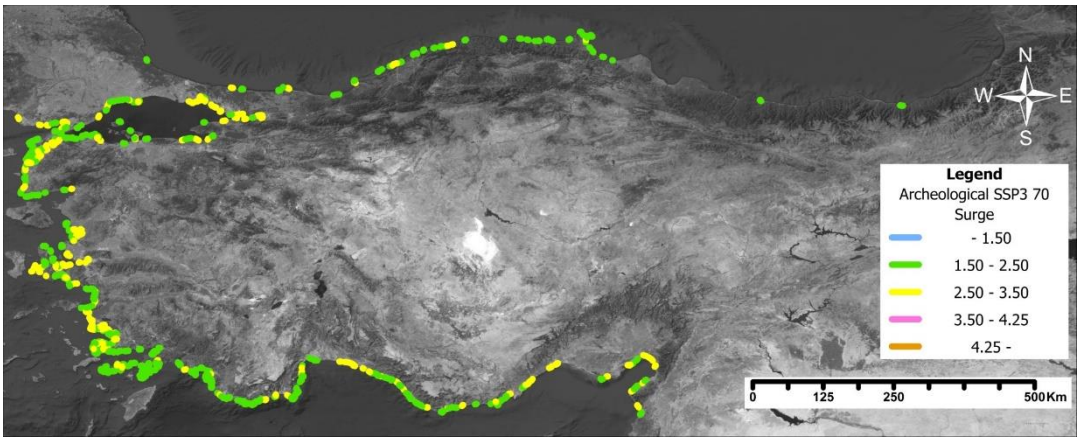


Figure 7.120. SSP3-7.0 Cultural Heritage Site Storm Surge Distribution

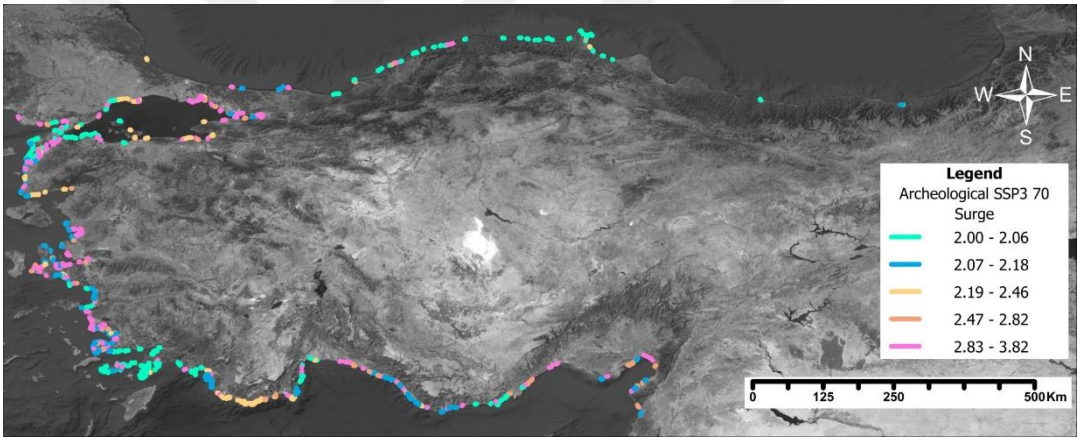


Figure 7.121. SSP3-7.0 Cultural Heritage Site Storm Surge Jenks Distribution

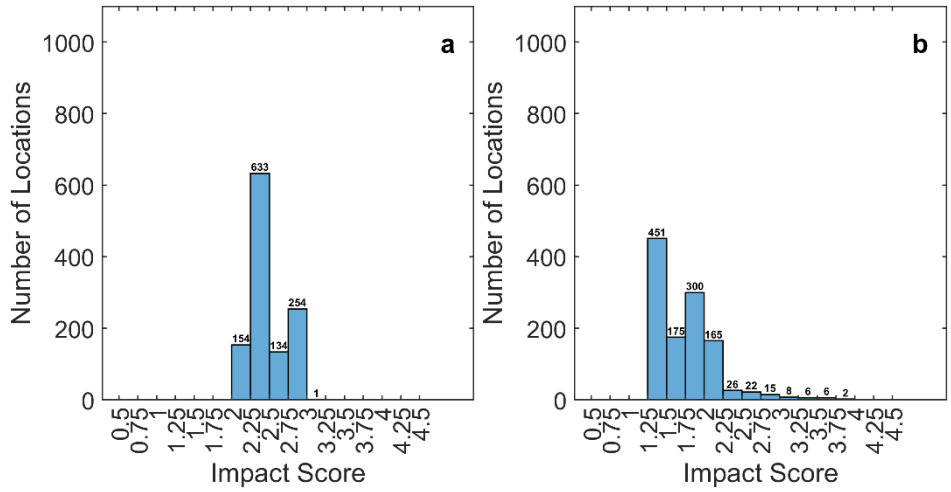


Figure 7.122. SSP3-7.0 Cultural Heritage Site Storm Surge (a) Physical Impact Score (b) Human Impact Score

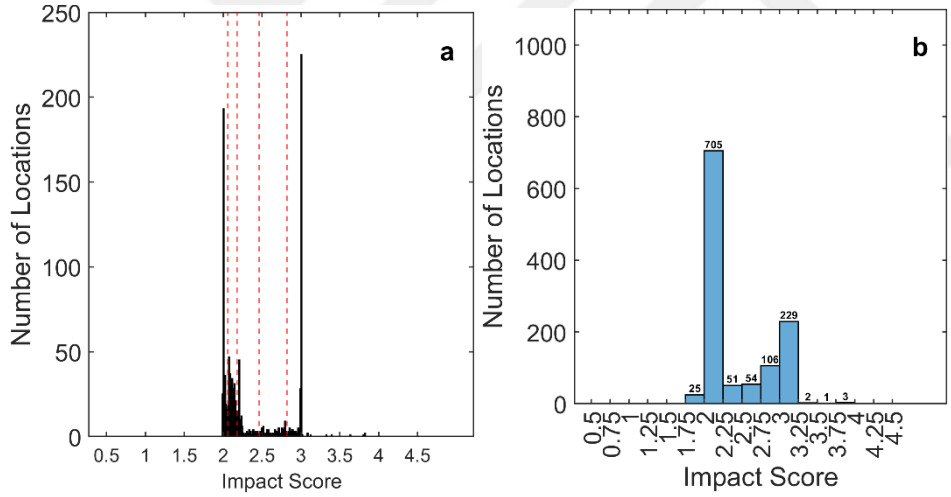


Figure 7.123. SSP3-7.0 Cultural Heritage Site Storm Surge (a) Jenks (b) FCVAM Histograms

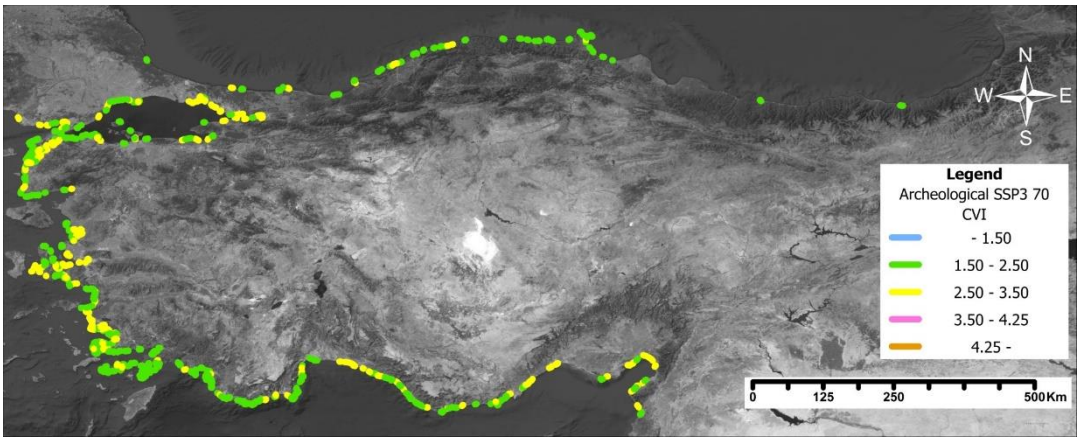


Figure 7.124. SSP3-7.0 Cultural Heritage Site CVI Distribution

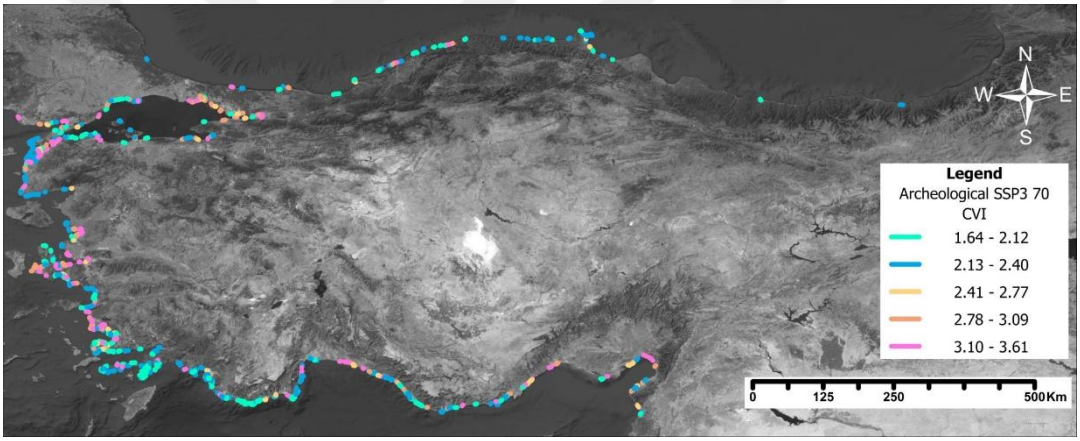


Figure 7.125. SSP3-7.0 Cultural Heritage Site CVI Jenks Distribution

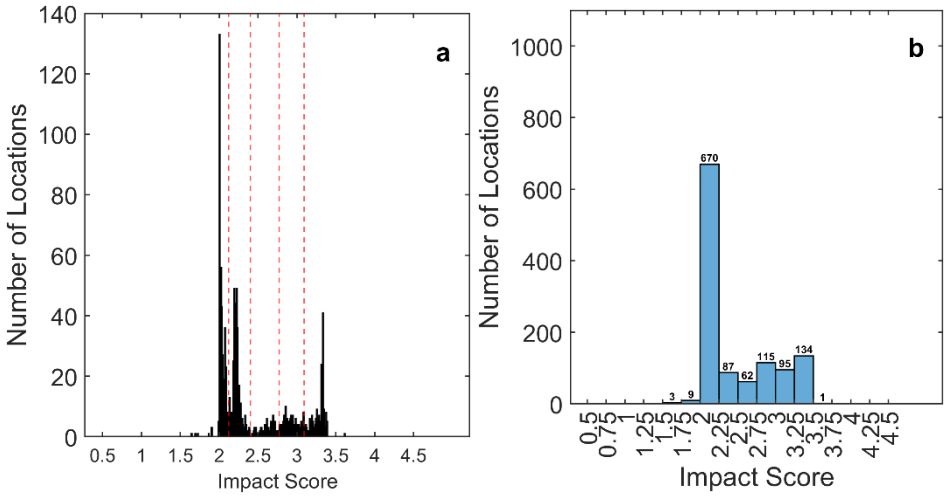


Figure 7.126. SSP3-7.0 Cultural Heritage Site CVI (a) Jenks (b) FCVAM Histograms

Table 7.6 SSP3-7.0 Cultural Heritage Site Impact & CVI Scores

ARC SSP3-70	Erosion			Inundation			Storm Surge			CVI
	PP	HI	Vul	PP	HI	Vul	PP	HI	Vul	
< 1.5 Very Low	3	549	3	0	86	0	0	451	0	0
1.5 – 2.5 Low	800	606	800	773	1010	766	787	666	781	769
2.5 – 3.5 Moderate	373	20	373	199	65	203	389	51	391	406
3.5 – 4.25 High	0	1	0	179	14	207	0	8	4	1
4.25 > Very High	0	0	0	25	1	0	0	0	0	0

G. Cultural Heritage Site SSP2-4.5 & SSP5-8.5 Scatter Diagrams

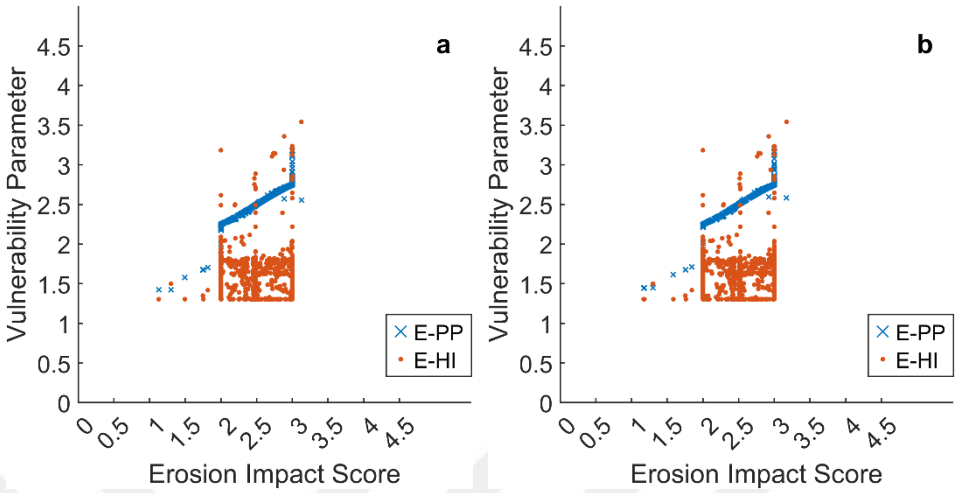


Figure 7.127. SSP2-4.5 & SSP5-8.5 Cultural Heritage Site Erosion Scatter Diagrams (a) SSP2-4.5 (b) SSP-8.5

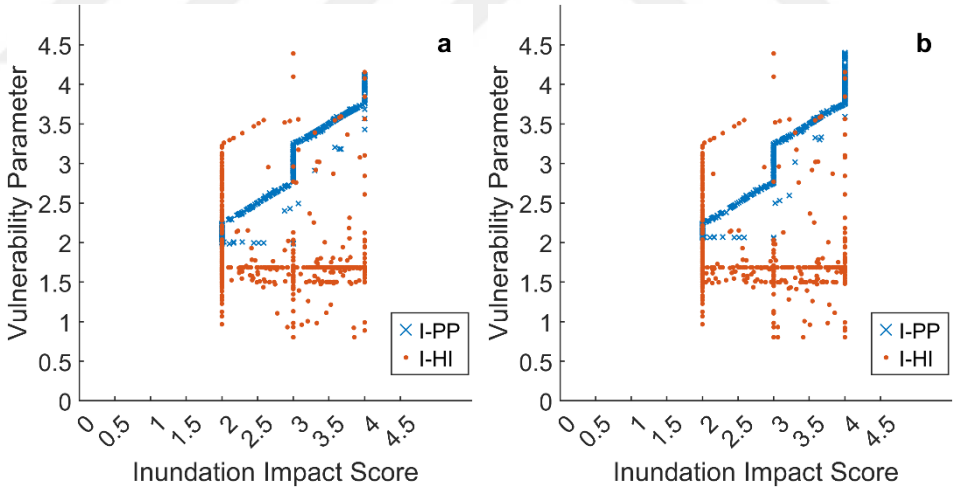


Figure 7.128. SSP2-4.5 & SSP5-8.5 Cultural Heritage Site Inundation Scatter Diagrams (a) SSP2-4.5 (b) SSP-8.5

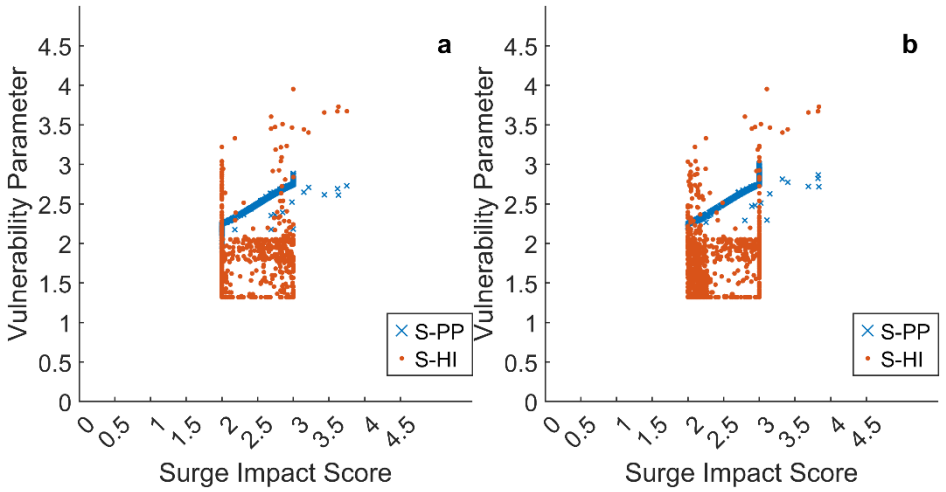


Figure 7.129. SSP2-4.5 & SSP5-8.5 Cultural Heritage Site Storm Surge Scatter Diagrams (a) SSP2-4.5 (b) SSP-8.5

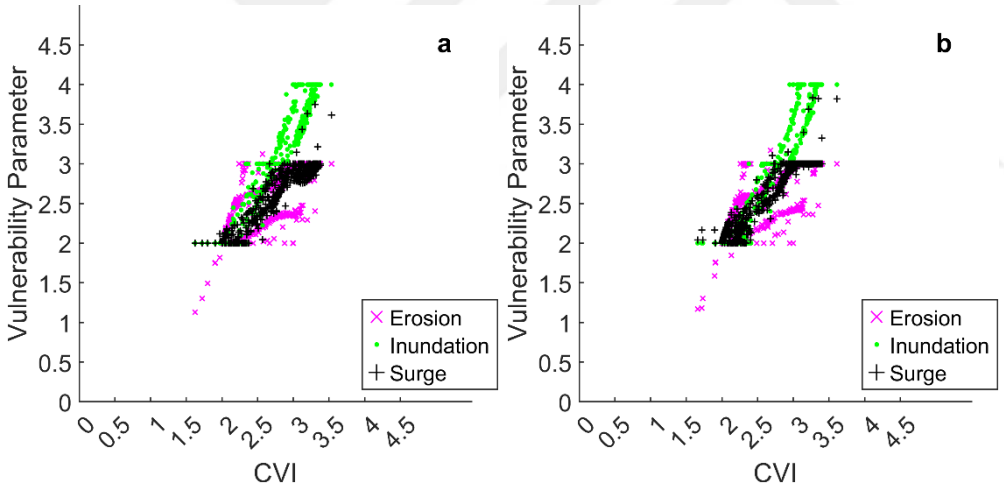


Figure 7.130. SSP2-4.5 & SSP5-8.5 Cultural Heritage Site Cumulative Impact Score Scatter Diagrams (a) SSP2-4.5 (b) SSP-8.5